Université de Montréal

Study of a novel evolutionarily conserved pattern of histone acetylation

par

Roshan Elizabeth Rajan

Programmes de biologie moléculaire
Faculté de médecine

Thèse présentée à la Faculté de médecine
en vue de l'obtention du grade de *Philosophiae Doctor* (Ph.D.)
en biologie moléculaire
option biologie des systèmes

Décembre, 2017

Resumé

Le génome eucaryote est empaqueté dans une structure hautement ordonnée appelée chromatine. Même si la structure de la chromatine est importante pour le maintien de l'intégrité génomique, elle constitue une barrière à de nombreux processus basés sur l'ADN tels que la réplication de l'ADN, la transcription et la réparation de l'ADN. Les histones contiennent une diversité déconcertante de modifications covalentes qui sont concentrées principalement, mais non exclusivement dans leurs queues amino-terminales. Les modifications des histones jouent un rôle central dans la régulation de la structure et de la fonction de la chromatine. Cependant, la détermination de la stoechiométrie des modifications à des sites spécifiques, l'identification des motifs de modifications et l'établissement de leurs rôles physiologiques restent des défis redoutables.

Dans cette étude, nous avons utilisé la spectrométrie de masse pour déterminer la stoechiométrie de l'acétylation de résidus lysine spécifiques des histones. En général, les résidus lysine des histones dépourvus d'acétylation sont dérivatisés pour rendre les peptides résultants chimiquement équivalents à leurs homologues acétylés, mais pouvant être distingués par spectrométrie de masse. Cependant, cette méthode est insuffisante pour étudier les peptides contenant plus d'une lysine acétylable, tels que ceux dérivés de la queue N-terminale des histones H3 et H4. La digestion trypsique de tels peptides génère des «isomères de position», des isomères qui ont la même masse, mais qui portent des groupes acétyle à des positions différentes. La quantification précise de l'acétylation d'un site spécifique dans ces peptides est donc un défi analytique majeur.

Dans le deuxième chapitre, nous décrivons une nouvelle méthode, pour quantifier l'acétylation à un site spécifique dans les peptides co-éluants isomériques et isobariques, qui combine des données LC-MS / MS à haute résolution avec un nouvel algorithme bioinformatique, Iso-PeptidAce. En utilisant des spectres de masse en tandem (MS/MS) de peptides synthétiques, les produits de fragmentation caractéristiques de chaque isomère de position ont été identifiés et utilisés pour déconvoluer des spectres provenant de mélanges d'isomères de position et quantifier l'abondance de chaque isomère. Nous avons ensuite testé l'applicabilité de l'Iso-PeptidAce pour quantifier les augmentations en fonction du temps de l'acétylation des histones des cellules d'érythroleucémie K562 traitées avec des inhibiteurs d'histone déacétylase (HDAC). En utilisant notre méthode, nous avons également trouvé que les histones H3 et H4 associées à CAF-1, un facteur d'assemblage de la chromatine, ont une stoechiométrie élevée d'acétylation sur plusieurs résidus de H3 et H4, par rapport aux histones totales.

Dans le chapitre 3, nous avons appliqué Iso-PeptidAce pour déterminer la stoechiométrie de l'acétylation chez la levure de fission présentant un mutant d'histone désacétylase. Conformément aux études antérieures impliquant Clr3 et Sir2 dans la régulation de l'hétérochromatine, nous avons observé que les cellules dépourvues de ces HDAC présentaient une augmentation de l'acétylation H3-K14 uniquement sur les peptides coexistant avec H3-K9 di / tri méthylé, une marque caractéristique de l'hétérochromatine.

Au chapitre 4, nous décrivons la découverte de très hauts niveaux d'acétylation sur deux résidus de lysine. Nous avons trouvé qu'une stoechiométrie élevée d'acétylation

(20-25%) à H3-K14 et H3-K23 et une faible stoechiométrie d'acétylation à H3-K9 et H3-K18 (<10%) est un profil global de H3 conservé sur le plan évolutif d'acétylation. En utilisant des souches de levures de fission (*S. pombe*) où la seule source de gènes d'histone porte des mutations H3-K14R et / ou H3-K23R qui empêchent l'acétylation, nous avons démontré que H3-K14 et H3-K23 ont des fonctions distinctes. De façon surprenante, nous avons trouvé que les phénotypes observés dans les cellules mutantes H3-K14R sont largement dus à la mutation du résidu lysine, plutôt qu'à la perte d'acétylation. En utilisant des souches de *S. pombe* dépourvues d'histone acétyltransférases (HAT), nous avons identifié Mst2 et Gcn5 comme étant les acétyltransférases qui contribuent à H3-K14ac et à H3-K23ac *in vivo*.

Très peu d'études ont cherché à déterminer spécifiquement les stoechiométries d'acétylation des histones. Nos résultats suggèrent qu'en moyenne, sur l'ensemble du génome, chaque deuxième ou troisième nucléosome contient une molécule H3 avec une acétylation K14 et / ou K23. Cela nous amène à penser que l'acétylation de l'histone H3 à l'échelle du génome peut jouer un rôle important dans la fonction chromosomique. Il est impératif de comprendre la signification fonctionnelle de ce modèle d'acétylation étant donné que la thérapie épigénétique est activement étudiée comme stratégie pour traiter de nombreuses maladies.

Mots-clés

Histones, acétylation, spectrométrie de masse, histone acétyltransférases, histone déacétylases, *Schizosaccharomyces pombe*

Abstract

The eukaryotic genome is packaged into a highly ordered chromatin structure. Even though chromatin structure is important for maintaining genomic integrity, it is a barrier to numerous DNA-based processes such as DNA replication, transcription and DNA repair. Histones contain a bewildering diversity of covalent modifications that are mostly but not exclusively concentrated within their amino-terminal tails. Histone modifications play a central role in regulating chromatin structure and function. However, determining the stoichiometry of site-specific modifications, identifying patterns of modifications and establishing their physiological roles remain formidable challenges.

In this study, we exploited mass spectrometry to determine the stoichiometry of acetylation at specific histone lysine residues. In general, histone lysine residues lacking acetylation are derivatized to render the resulting peptides chemically equivalent but distinguishable by mass from their acetylated counterparts. However, this method is insufficient to study peptides that contain more than one acetylatable lysine, such as those derived from the N-terminal tail of histones H3 and H4. Tryptic digestion of such peptides generates 'positional isomers', isomers that have the same mass but bearing acetyl groups located at different positions. Accurate quantification of site-specific acetylation in those peptides is, therefore, a major analytical challenge.

In the second chapter, we describe a novel method for quantifying site-specific acetylation of co-eluting isomeric and isobaric peptides that combines high-resolution LC-MS/MS data with a novel bioinformatics algorithm, Iso-PeptidAce. Using tandem mass spectra (MS/MS) of synthetic peptides, fragmentation products diagnostic of each positional isomer were identified and were used to deconvolute spectra that arise from mixtures of positional isomers and quantify the abundance of each isomer. We then tested the applicability of Iso-PeptidAce to quantify time-dependent increases in histone acetylation of K562 erythroleukaemia cells treated with histone deacetylase (HDAC) inhibitors. Using our method, we also found that histones H3 and H4 associated with CAF-1, a chromatin assembly factor, have a high stoichiometry of acetylation on multiple residues of H3 and H4, compared with total histones.

In Chapter 3, we applied Iso-PeptidAce to determine the stoichiometry of acetylation in fission yeast histone deacetylase mutants. Consistent with previous reports implicating Clr3 and Sir2 in heterochromatin function, we observed that cells lacking these HDACs showed an increase in H3-K14 acetylation only on those peptides where it co-exists with di/trimethylated H3-K9, a mark of heterochromatin.

In chapter 4, we describe the discovery of very high levels of acetylation on two lysine residues. We found that a high stoichiometry of acetylation (20-25%) at H3-K14 and H3-K23, and low stoichiometry of acetylation at H3-K9 and H3-K18 (<10%), is an evolutionarily conserved global pattern of H3 acetylation. Using fission yeast (*S.*

pombe) strains harboring histone mutations *H3-K14R* and/or *H3-K23R* that prevent acetylation, we demonstrate that H3-K14 and H3-K23 have separable functions. Surprisingly, we found that the phenotypes observed in *H3-K14R* mutant cells are largely due to mutation of the lysine residue, rather than loss of acetylation. Using *S. pombe* strains that lack histone acetyltransferases (HATs) we identified Mst2 and Gcn5 as the acetyltransferases that contribute to H3-K14ac and H3-K23ac *in vivo*.

Very few studies have aimed at specifically determining the acetylation stoichiometries of histones. Our results suggest that, on average, over the entire genome, every second or third nucleosome contains an H3 molecule with K14 and/or K23 acetylation. This leads us to surmise that genome-wide acetylation of histone H3 may have an important role in chromosome function. It is imperative to understand the functional significance of this acetylation pattern given that epigenetic therapy is actively pursued as a strategy to treat many diseases.

Key Words:

Histones, acetylation, mass spectrometry, histone acetyltransferases, histone deacetylases, *Schizosaccharomyces pombe*

Table of Contents

List of tables

List of figures

List of abbreviations

ac	acetyl
Acetyl-CoA	acetyl coenzyme A
ACN	acetonitrile
ADP	adenosine diphosphate
ATP	adenosine 5´-triphosphate
ATRX	α-thalassemia/mental retardation syndrome X-linked
BCA	Bicinchoninic Acid
BET	bromodomain and extra terminal domain
bp	base pair
BRD	bromodomain
CAF-1	Chromatin Assembly Factor 1
CENP-A	centromere protein-A
ChIP	Chromatin immunoprecipitation
CO_2	carbon dioxide
CPT	Camptothecin
C-terminus	carboxyl terminus
DAXX	Death domain–associated protein 6
DDR	DNA damage response
DMSO	dimethylsulphoxide
DNA	deoxyribonucleic acid
dNTP	deoxyribonucleoside triphosphate
DSB	double-strand break
DTT	dithiothreitol
EDTA	Ethylenediaminetetraacetic acid
Esa1	Essential Sas family acetyltransferase 1
FACS	fluorescence-activated cell sorting
FACT	facilitates chromatin transcription
FASTA	FAST-All
fmol	Femtomole

Gcn5	General control non-repressible 5
GNAT	Gcn5-related N-acetyltransferase
H_2SO_4	Sulfuric acid
HAT	histone acetyltransferase
HCD	High-energy collision dissociation
HCl	hydrogen chloride
HDAC	Histone deacetylase
HDACi	Histone deacetylase inhibitor
HEPES	N-(2-hydroxyethyl) piperazine-N´-(2-ethanosulfonic acid)
His	histidine
HJURP	Holliday junction recognition protein
HPLC	High performance liquid chromatography
HR	homologous recombination
HU	hydroxyurea
i.d.	Internal diameter
IPTG	isopropyl-β-D-thiogalactopyranoside
KAT	lysine acetyltransferase
KDAC	lysine deacetylase
KDM	lysine demethylase
LC-MS/MS	Liquid chromatography tandem mass spectrometry
Leu	leucine
LOH	loss of heterozygosity
LRR	Leucine-rich repeat
m/z	mass-to-charge
MgCl2	magnesium chloride
MMS	methyl methanesulfonate
MOZ	Monocytic leukemia Zinc finger
MS/MS	tandem mass spectra
MYST	MOZ, Ybf2/Sas3, Sas2, TIP60

NaCl	sodium chloride
NAD+	nicotinamide adenine dinucleotide
NCP	nucleosome core particle
NHEJ	non-homologous end joining
nLC	Nano-liquid chromatography
N-terminus	amino terminus
NuA3	nucleosomal acetylation of H3
NuA4	nucleosomal acetylation of H4
O.D.	optical density
PCAF	p300/CBP associating factor
PcG	Polycomb group
PCNA	Proliferating Cell Nuclear Antigen
PCR	polymerase chain reaction
PEV	position effect variegation
PH	pleckstrin-homology
PHD	plant homeodomain
PIKK	phosphoinositide 3-kinase related kinase
ppm	parts-per-million
PMSF	phenylmethylsulfonyl fluoride
PRM	parallel reaction monitoring
PRMT	protein arginine methyltransferases
PTM	post translational modification
PSM	peptide spectrum matching
RBBP7	retinoblastoma binding protein 7
RFC	replication factor C
RNA	ribonucleic acid
RNR	ribonucleotide reductase
RP	Reverse phase
RPA	replication protein A
RPMI	Roswell Park Memorial Institute medium

RP-HPLC	reverse phase high performance liquid chromatography
RSC	remodel the structure of chromatin
Rtt109	Ty1 transposition gene product 109
SAGA	Spt-Ada-Gcn5-acetyltransferase
SAHA	suberoylanilide hydroxamic acid
SAS	something about silencing
SC	synthetic complete
SDS	sodium dodecyl sulfate
SDS-PAGE	sodium dodecyl sulfate polyacrylamide gel
SILAC	Stable isotope labeling by amino acid in cell culture
SLIK	SAGA-like
SRM	Single reaction monitoring
ssDNA	single-strand DNA
STAGA	SPT3-TAF$_{II}$31-GCN5L acetylase
SWI/SNF	SWItch/Sucrose NonFermentable
TAP	tandem affinity purification
TCA	Trichloroacetic acid
TEV	tobacco etch virus
TFA	Trifluoroacetic acid
TFTC	TBP-free TAFII complex
TIP60	Tat-interacting protein
Top1	topoisomerase I
TRRAP	Transformation/transcription domain-associated protein
TrxG	Trithorax group
Ts	thermosensitivity
TSA	trichostatin A
URA	uracil
UV	Ultraviolet

WT	wild-type
XIC	Extracted ion chromatogram
YES	yeast extract supplemented
YPD	yeast peptone dextrose
5-FOA	5-Fluoroorotic acid
γ-H2AX	H2AX serine 139 phosphorylation

Acknowledgments

This work could not have been completed without the constant support of my supervisor, family, and friends. Words cannot express my gratitude to you all, but this is a humble attempt.

First, I would like to express my special thanks to my supervisor Dr. Alain Verreault for giving me the opportunity to pursue my Ph.D. under his supervision. Alain has been a wonderful teacher and an excellent mentor. He broadened my horizon of thought by encouraging me to think critically and testing every result with the 'baloney detection kit.' My deepest gratitude to you, Alain, for all the insightful discussions, your unconditional support through the years and especially for not losing faith in me when the going got tough.

I would like to extend my sincere thanks to my co-supervisor Dr. Pierre Thibault who patiently explained the basics of mass spectrometry to me, a novice in this analytical technique. Pierre's ability to think outside his area of expertise and critically question the results have been of tremendous value to my research. He also gave me access to his lab space for work.

The results presented here could not have been made possible without Dr. Nebiyu Abshiru. Nebiyu and I had a fruitful collaboration on all three projects of this thesis, which lean on mass spectrometry-based analyses. Along with Pierre, Nebiyu has given me the ability to appreciate MS-based methods and their applications in biology. Thank you Nebiyu, for all your help and discussions.

Moreover, I would like to thank the members of my Ph.D. committee, Dr. Lea Harrington, and Dr. Jason Tanny, for their valuable advice on my research project. I am hugely grateful to Dr. Richard Bertrand and Dr. Martine Raymond, and for all their support during my Ph.D. Special gratitude to Dr. Julie Mantovani, Suzanne Renaud, Vivianne Jodoin, Pascale Le Therizien, Lucie Yan Liu, Mirela Pascariu and Sandra Weber who have helped me during this journey. I would also like to acknowledge IRIC

Members Ph.D. awards and the Molecular Biology Program of the Université de Montréal for their scholarships recognizing my efforts.

I extend my special thanks to the past and current members of Verreault lab and Thibault lab for all their support. Each one of you who have contributed to my learning experience. I especially acknowledge the students of IRIC, past, and present, who have been an important part of my life at IRIC. Thank you for your smiles, kind words, reagents and help with instruments.

My dear friends, Arun, Simi, Dezi, Becky and Chris who were always there for me, through thick and thin, this would not have been possible without you.

A few years ago, I carried a dream of doing my Ph.D. It came to fruition only because of the continual support of my family. I started my Ph.D. merely two weeks after getting married, something unthinkable for an Indian girl who had an arranged marriage. My family, which includes my husband Bobby, my parents, parents-in-law, my brothers-in-law, their families and my sweet sisters, have been my strength during the last six years. Special thanks to Papa, Mama, Dada and Amma for their unconditional love and encouragement. I owe it to my husband the most for making my dream come true. Thank you beyond words, my beloved Achacha, for all your sacrifices, words of comfort, encouragement, and prayers. You are indeed the greatest blessing in my life! It gives me great pleasure to dedicate this thesis to my family.

To the one who has constantly been with me through it all, thank you Abba!

"We are like dwarfs sitting on the shoulders of giants. We see more, and things that are more distant, than they did, not because our sight is superior or because we are taller than they, but because they raise us up, and by their great stature add to ours."

John of Salisbury

1. Introduction

1.1. Eukaryotic chromatin: an architectural marvel

The eukaryotic genome showcases an elaborate and dynamic architecture. In human cells, roughly two meters of deoxyribonucleic acid (DNA), is packaged into the confines of the cell nucleus which is only a few micrometers wide. This incredible feat is accomplished through hierarchical folding and compaction of DNA into chromatin. The chromatin structure poses challenges to all cellular processes that require access to DNA such as DNA replication, transcription and DNA repair. Cells have evolved to overcome DNA compaction while maintaining regulation of these processes through a myriad of effectors that belong into four broad categories: ATP-dependent chromatin remodelers, DNA and histone modifying enzymes and histone chaperones.

1.1.1. The nucleosome core particle

The ‘quantum’ of chromatin structure is the nucleosome. Major discoveries that led to the elucidation of chromatin structure came in 1973-74 (Olins and Olins, 2003). An insightful proposition by Roger Kornberg that the repeating unit of chromatin has 200 base pairs (bp) of DNA and eight histone molecules lent a new perspective to the puzzling structure of chromatin (Kornberg, 1974; Thomas and Kornberg, 1975). Oudet and colleagues provided the first biochemical and microscopic evidence for a repeating structure in chromatin in 1975, confirming Kornberg’s ideas (Oudet et al., 1975). The 2.8 Å resolution structure of the nucleosome reconstituted with alpha satellite repeat DNA provided intricate details of histone arrangement and histone-DNA interactions (Luger et al., 1997). The nucleosome core particle consists of 147 bp of DNA wrapped around an octameric protein core in 1.65 turns of a left-handed superhelix. The protein

core is composed of two molecules each of four core histone proteins, known as H2A, H2B, H3 and H4, which form a central H3-H4 tetramer $(H3\text{-}H4)_2$ flanked by two H2A-H2B dimers (Fig 1.1). Histone H3 makes additional contacts with histone H2A and with the DNA and plays an important role in the stabilization of NCP.

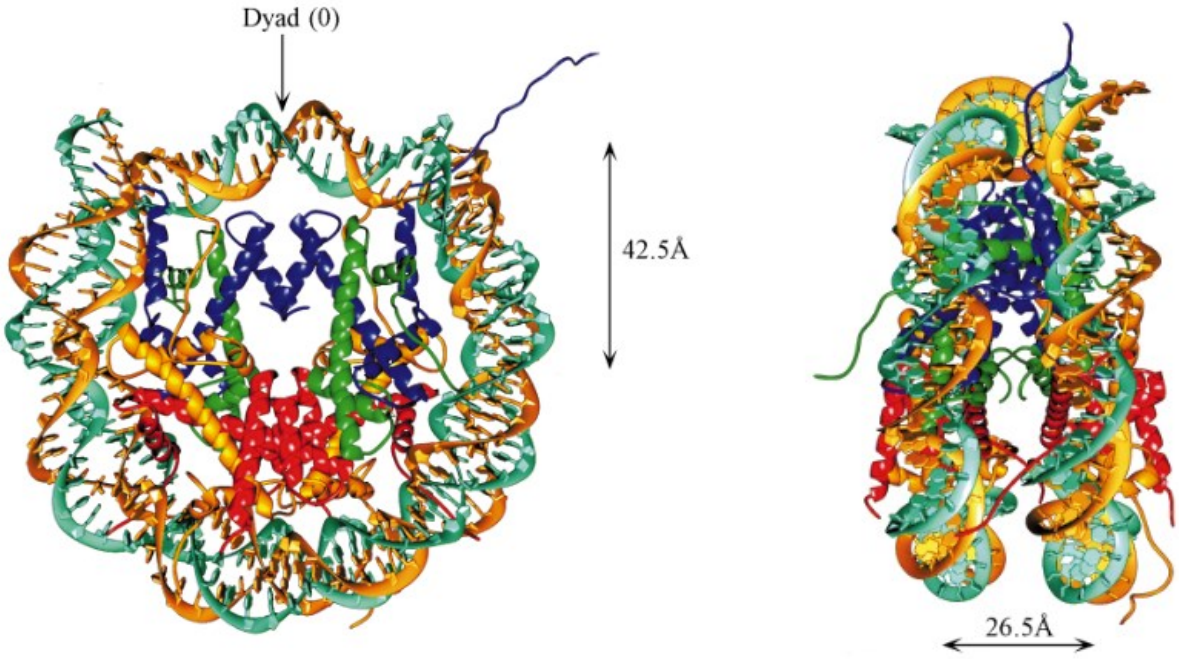

Figure 1.1. Nucleosome core particle: ribbon traces for the 147 bp DNA phosphodiester backbones (brown and turquoise) and eight histone protein main chains (blue: H3; green: H4; yellow: H2A; red: H2B. The views are down the DNA superhelix axis for the left particle and perpendicular to it for the right particle. For both particles, the pseudo-twofold axis of symmetry (shown at the top) is aligned vertically with the center of the 147 bp of nucleosomal DNA (Dutnall and Ramakrishnan, 1997).

1.1.2. Chromatin structure

Chromatin consists of two structural entities: the nucleosome core particle and the 'linker' region: short DNA segments of varying length that connect nucleosome core particles. One molecule of linker histone H1 binds to the linker DNA. Nucleosomes are connected to each other through linker DNA to form linear nucleosomal arrays that have the appearance of 'beads-on-a-string', the primary structure of chromatin. The packaging of DNA with histones yields a chromatin fiber that is approximately 10 nm in diameter and shortens its length approximately six-fold (Fig 1.2). Short-range interactions between neighboring nucleosomes result in a higher-order structure of chromatin, commonly known as the 30 nm fiber (Luger et al., 2012; Woodcock and Dimitrov, 2001). Linker histone H1 plays an important role in stabilizing the 30 nm fiber. However, using ChromEMT, a method combining electron microscopy tomography (EMT) with ChromEM labeling which enhances the contrast of DNA, Ou *et al.* has recently shown that chromatin exists as a flexible 5- to -24 nm diameter chain that can be packed at different densities in interphase cells and in mitotic chromosomes (Ou et al., 2017). Our knowledge of the dynamics and formation of higher-order structures remains limited despite technological advances.

1.1.3. Euchromatin and heterochromatin

One of the earliest observations of distinct chromatin structures was made by German botanist Emil Heitz in 1928 (Straub, 2003). He observed cytologically distinguishable chromosome regions that he called euchromatin and heterochromatin based on differential staining and proposed that the heterochromatin is functionally inactive.

Heterochromatin is highly condensed chromatin characterized by repetitive DNA elements, is gene-poor and less transcribed. Conversely, euchromatin is rich in genes, more accessible to the transcription machinery and hence easily transcribed.

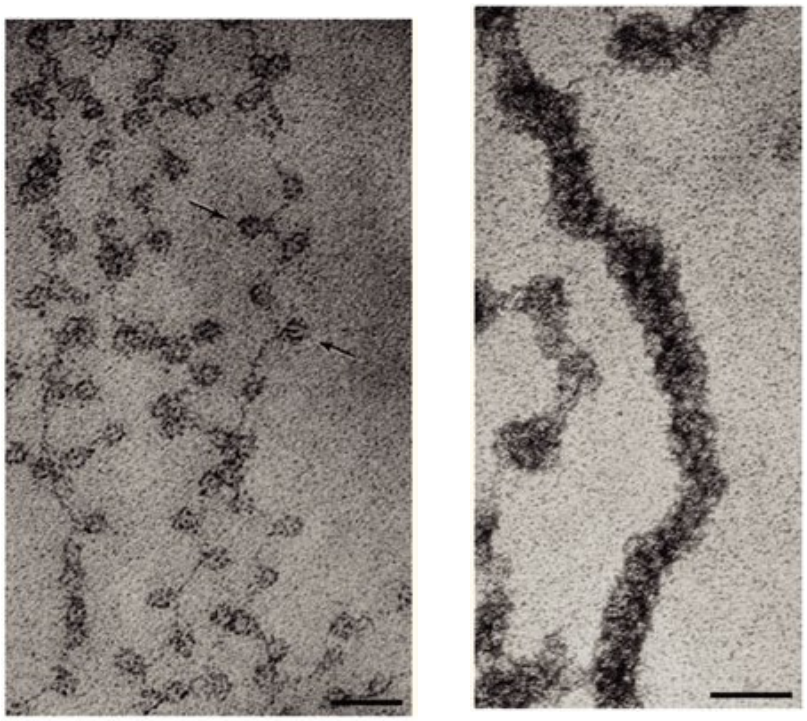

Figure 1.2. Chromatin fibers: A) At low ionic strength chromatin appears as 'beads on a string'. Black bar: 30 nm. B) Moderate ionic strength forms the higher-order 30-nm fiber. Black bar: 50 nm (Olins and Olins, 2003)

Extensive methylation of histone 3 at lysine 9 (H3K9me) is a characteristic of heterochromatin domains shared by most eukaryotes (Huisinga et al., 2006). This posttranslational modification is catalyzed by the evolutionarily conserved H3K9-specific histone methyltransferase SU(VAR)3-9 (Suv39h1&2 in mammals, Clr4 in

fission yeast). Another conserved feature of heterochromatin is the presence of non-histone chromosomal protein heterochromatin protein 1 (HP1, Swi6 in fission yeast). Moreover, heterochromatin regions contain histones that are hypoacetylated on H3 and H4 (Trojer and Reinberg, 2007). Heterochromatin is broadly classified as either Constitutive heterochromatin or Facultative heterochromatin. Constitutive heterochromatin is silenced throughout the cell cycle and occurs at centromeres, telomeres, and transposable elements. Facultative heterochromatin is found at developmentally regulated loci such as the mating type loci and certain meiotic genes in yeast. Facultative heterochromatin can be converted into euchromatin in response to cellular signals. Heterochromatin can propagate in a sequence-independent manner and spread across domains. Heterochromatin structure interferes with recombination (Grewal and Jia, 2007).

1.2. Histones

Histones are highly conserved proteins enriched in the basic amino acids arginine and lysine. They are extremely abundant in eukaryotic cells; their total mass (4 core histones and H1) is roughly equal to that of a cell's DNA. In addition to their role as architectural proteins, histones contribute to chromosome function through three principal mechanisms: ATP-dependent remodeling complexes can alter the properties of nucleosomes or their position relative to specific DNA sequences, variant or 'replacement' histones can alter the composition of nucleosomes by replacing the most abundant forms of the core histones and a rich variety of covalent histone modifications can regulate their function. There are four canonical core histones: H2A, H2B, H3, and H4. Variant histones exist for core histones H3, H2A and H2B and for the linker histone

H1. Intriguingly, no variant of histone H4 seems to exist. All core histones have two structurally and functionally distinct domains, a globular histone-fold domain and a conformationally flexible and highly charged amino-terminal domain, commonly known as the histone tail. The histone-fold domain consists of three α-helices (α1-α3) connected by short loops L1 and L2 (Fig 1.3). The histone-fold domain aids in the assembly of histone dimers through a so-called 'handshake' motif. The histone-fold domains mediate histone-histone and histone-DNA interactions. The N-terminal tails of histones are unstructured and protrude out of the nucleosomal DNA (Luger 2000). A striking feature of the N-terminal tails is that they are the targets of many post-translational modifications, elaborated in section 1.3.

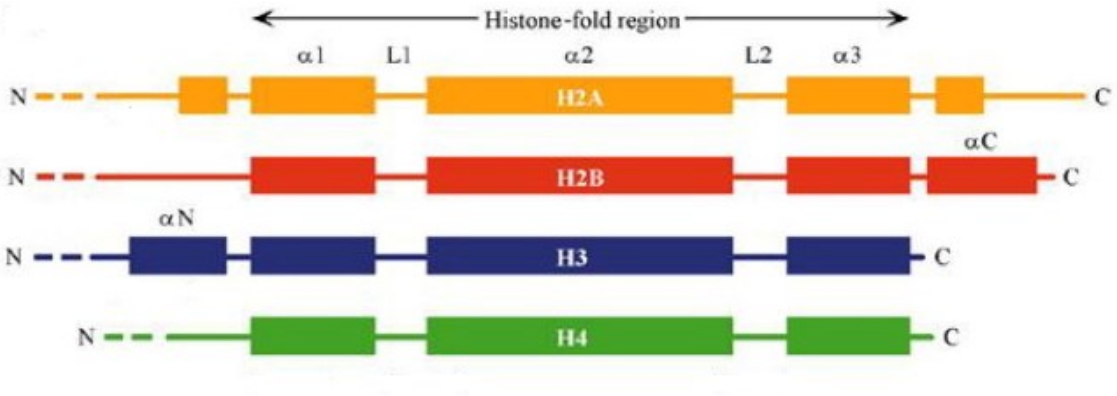

Figure 1.3. The secondary structure of core histones showing the globular histone-fold domain and the unstructured 'tail' domains. α-helices are depicted as solid boxes and are numbered according to Luger et al., 1997 (Dutnall and Ramakrishnan, 1997).

1.2.1. Histone H3 variants

The regulatory repertoire of chromatin structure and function is expanded through the replacement of canonical histones by variants. Variant histones can be incorporated into chromatin throughout the cell cycle, unlike canonical histones that are deposited onto nascent DNA during replication. All core histones except H4 have variants, the H3 variants being the least diverse. In human cells, histone H3 is present as eight different variants: H3.1, H3.2, H3.3, H3.1t (H3.4), H3.3C (H3.5), H3.Y.1 (H3.Y), H3.Y.2 (H3.X) and CenH3 (see Fig. 1.4). H3.4 and H3.5 are testis-specific H3 variants. The H3 variants can be grouped into two classes. Canonical forms of histone H3 provide the supply of H3 molecules needed during replication. In humans, there are two flavors of replicative histone H3, known as H3.1 and H3.2 that differ by a single amino acid (Fig 1.4). Replacement variants are incorporated in a replication-independent manner. H3.3 is the replication-independent histone H3 in humans. CenH3 also known as CENP-A is a centromeric H3 variant exclusively found in the nucleosomes present at centromeres.

The highly basic nature of histones can lead to non-specific interactions between soluble (non-nucleosomal) histones and DNA, generating aggregates. Cells delegate dedicated escort proteins, also known as chaperones, to prevent such non-specific interaction of histones. Chaperones selectively associate with either canonical or variant histone forms. For example, chromatin assembly factor-1 (CAF-1) specifically associates with core histones H3.1 and H3.2, but not with the variant H3.3 (Akiyama

et al., 2011; Latreille et al., 2014; Tagami et al., 2004). There are two H3.3-specific chaperones, the HIRA complex deposits H3.3-H4 complexes at transiently nucleosome-free regions. A protein complex formed by the Death domain-associated protein 6 (DAXX) and the α-thalassemia/mental retardation syndrome X-linked (ATRX), incorporates H3.3-H4 into pericentric heterochromatin and sub-telomeric chromatin regions (Banumathy et al., 2009; Goldberg et al., 2010; Lewis et al., 2010; Rai et al., 2011; Ray-Gallet et al., 2002; Tagami et al., 2004). The Holliday junction recognition protein (HJURP) is a chaperone specific for the centromeric variant CenH3, which it incorporates at centromeres in early G1 (Dunleavy et al., 2009; Foltz et al., 2009; Jansen et al., 2007).

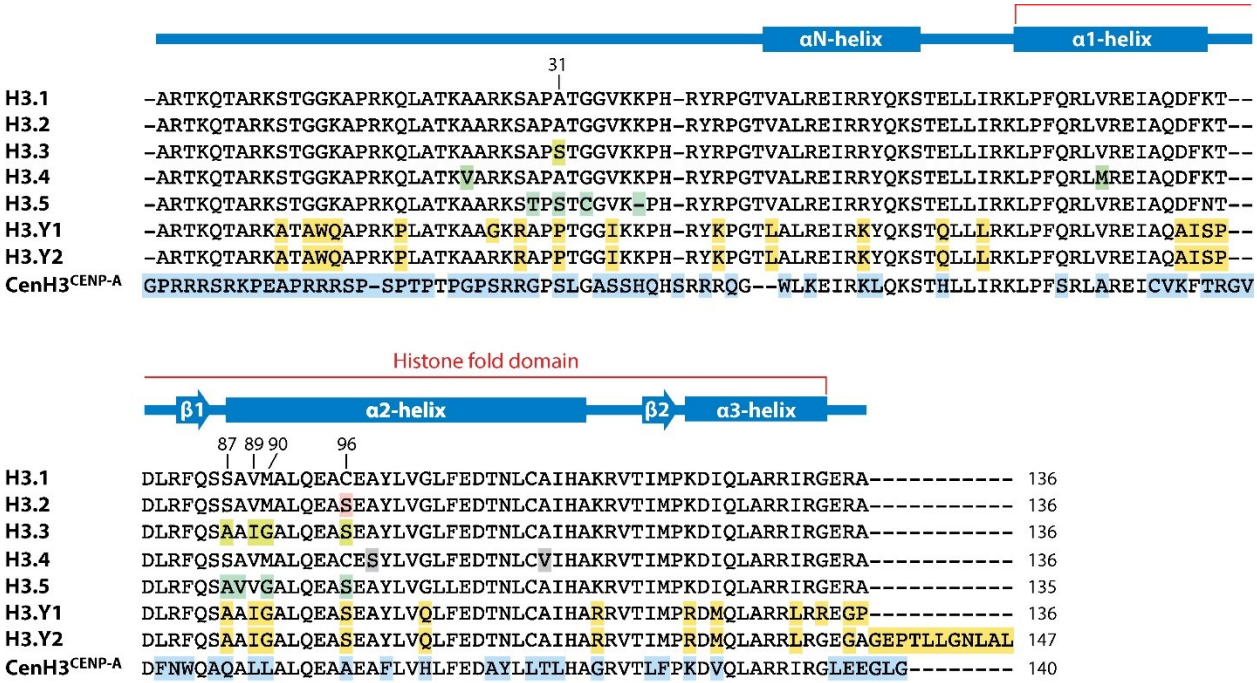

Figure 1.4. Alignment of amino acid sequences of human histone H3 isoforms. The sequences are compared to H3.1 and the differences are highlighted (Filipescu *et al*., 2014)

1.3. Post-translational modifications of histones

In the mid-1960s, seminal work by Allfrey and Murray demonstrated that histones are post-translationally modified (Allfrey, Faulkner, & Mirsky, 1964; Allfrey & Mirsky, 1964; Murray, 1964). The last few decades saw the discovery of a staggering number of histone post-translational modifications (PTMs). Researchers in the field have demonstrated tremendous enthusiasm to identify, catalog, classify and interpret cross-talk between various histone modifications. These include extensively studied PTMs such as acetylation, methylation, phosphorylation, ubiquitination, sumoylation, poly (ADP) ribosylation, deimination and proline isomerization (Kouzarides, 2007). Many newly identified modifications such as butyrylation, crotonylation, malonylation, succinylation, formylation, hydroxylation and O-GlcNAcylation have increased the complexity of studying covalent histone modifications and their functions (Huang, Sabari, Garcia, Allis, & Zhao, 2014). The majority of PTMs are located on the histone tails but the globular domains also carry key modifications. The study of covalent modifications in the N-terminal tail domains dominated research until the early 2000s. This was mainly because the primary method for discovering histone modifications, Edman degradation, permitted the analysis of only 20–30 amino acids from the N-terminus of a protein. Covalent modifications that occur within histone-fold domains were identified with the advent of mass spectrometry.

Histone PTMs have been implicated in the regulation of numerous aspects of chromatin structure and function. The dynamic regulation of chromatin function by histone modifications occurs through two main mechanisms. Many histone

modifications weaken the non-covalent interactions between histones and DNA. For example, acetylation of specific residues reduces the positive charge of histones and their interaction with DNA (Bannister and Kouzarides 2011). Second, PTMs create surfaces that bind to proteins with PTM-specific binding domains. These proteins, collectively known as 'readers' of histone PTMS, in turn, mediate the biological effects that are associated with specific PTMs (Yun *et al.* 2011). Many lines of evidence point towards an active interplay between different histone marks in the regulation of chromatin function. Our current understanding of histone modifications was revolutionized by the 'Histone Code hypothesis' which suggests that distinct histone modifications may form combinational readouts which, in turn, expand the repertoire of chromatin effectors that can act at a given locus (Jenuwein et al., 2001; Strahl and Allis, 2000). Although there are many proponents of 'histone code' hypothesis, there lacks a consensus opinion of exactly what this entails (Rando, 2012).

1.3.1. Are all histone modifications 'epigenetic'?

A brief history of the use of the term 'epigenetics' is given here to illustrate that histone modifications and epigenetic modifications have been used interchangeably in the literature. The term 'epigenetics' was coined by Waddington in 1942 to define 'complex developmental processes that connect phenotypes to genotypes (Waddington, 2012). This term has however generated much controversy in recent years. One of the popular definitions of epigenetics was given by Riggs, Martienssen and Russo as "*The study of mitotically and/or meiotically heritable changes in gene function that cannot be explained by changes in DNA sequence (Riggs et al., 1996)*. Bird defined the term

'epigenetics' as: "*the structural adaptation of chromosomal regions so as to register, signal or perpetuate altered activity states*" (Bird, 2007). According to Mark Ptashne, "*the use of the word epigenetic implies a fundamental property of the system - self-propagation - that is, so far as we now know, not true of nucleosome modifications"* (Ptashne, 2007). A more narrow definition that has been widely accepted defines 'epigenetics' as "*a stably heritable phenotype resulting from changes in a chromosome without alterations in the DNA sequence*" (Berger et al., 2009). Thus, the researchers in the field are divided in their definition of which histone modifications should be considered epigenetic and which should not. In this thesis, histone modifications that are stably inherited across generations are referred to as epigenetic modifications while those that are dynamically regulated during different cellular processes are referred to as histone modifications.

1.3.2. Writers, Readers and Erasers

Regulation of chromatin structure and function is a dynamic and complex process. Extracellular and intracellular cues trigger a cascade of downstream events that result in localized or genome-level alterations in chromatin structure mediated by chromatin modifiers. Chromatin regulators can be broadly classified into: 'writers', 'readers' and 'erasers'. Writers introduce modifications on DNA or histones while erasers, as the name suggests, remove modifications. Histone acetyltransferases (HATs), Histone methyltransferases (HMTs), kinases and protein arginine methyltransferases (PRMTs) are examples of writers. Examples of erasers include histone deacetylases (HDACs),

phosphatases and lysine demethylases (KDMs). See section 1.4.1. and 1.4.2. for a detailed description of 'writers' and 'erases' pertinent to this thesis.

Readers recognize modifications and use them as docking sites through specialized domains. Most often, readers are part of multi-subunit protein complexes. Bromodomains, chromodomains, WD40 repeats, Tudor domains and PHD fingers are all chromatin-binding domains that recognize modified histone tails. Some of the most common histone readers are listed in Table 1.1. Bromodomains recognize and bind acetylated lysine residues. Gcn5 contains a bromodomain that is important for the binding, recognition and retention of the histone acetyltransferase protein complex SAGA on acetylated promoter nucleosomes (See section 1.4.1.). Chromodomains specifically bind methylated lysine tails. In *Drosophila melanogaster* and vertebrates, the chromodomain of heterochromatin protein 1 (HP1) binds methylated H3K9, whereas the chromodomain of Polycomb binds methylated H3K27 (Filippakopoulos and Knapp, 2012; Marmorstein and Zhou, 2014; Patel, 2016; Patel and Wang, 2013).

1.4. Histone acetylation

Histone lysine acetylation discovered in 1964 is one of the best studied post-translational modifications (Allfrey et al., 1964). Acetylation refers to the covalent addition of an acetyl group from acetyl-coenzyme A (acetyl-CoA) to the epsilon (ε) amino group of lysine. This reversible modification is catalyzed by two families of enzymes, histone acetyltransferases (HATs) and histone deacetylases (HDACs). Acetylation removes the positive charge of the ε-amino group of the lysine side chain. Lysine acetylation has been implicated in many cellular processes such as

nucleosome assembly, DNA replication, transcription, DNA damage response (*i.e.* DNA damage signaling) and DNA repair (Bannister and Kouzarides, 2011; Shahbazian and Grunstein, 2007). It is interesting to note that the relationship between histone acetylation and transcription was first observed prior to the discovery of nucleosomes as the building blocks of chromatin.

Table 1.1 Readers of histone modifications

Recognize	Reader domain	Known histone modifications
Methyllysine	ADD	H3K9me3
	Ankyrin	H3K9me2, H3K9me1
	BAH	H4K20me2
	Chromobarrel	H3K36me3, H3K36me2, H4K20me1, H3K4me1
	Chromodomain	H3K9me3, H3K9me2, H3K27me3, H3K27me2
	Double Chromodomain	H3K4me3, H3K4me2, H3K4me1
	MBT	H3Kme1, H3Kme2, H4Kme1, H4Kme2
	PHD	H3K4me3, H3K4me2, H3K9me3
	PWWP	H3K36me3, H4K20me1, H4K20me3, H3K79me3
	TTD	H3K4me3, H3K9me3, H4K20me2
	Tudor	H3K36me3
	WD40	H3K27me3, H3K9me3
	zf-CW	H3K4me
Methylarginine	ADD	H4R3me2s
	Tudor	H3Rme2, H4Rme2
	WD40	H3R2me2
Acetyllysine	Bromodomain	H3Kac, H4Kac, H2AKac, H2BKac
	DBD	H3KacKac, H4KacKac
	DPF	H3Kac
	Double PH	H3K56ac
Phosphoserine or phosphothreonine	14-3-3 pr	H3S10ph, H3S28ph
	BIR	H3T3ph
	Tandem BRCT	H2AXS139ph
Unmodified histone	ADD	H3
	BAH–PHD	H3
	PHD	H3
	PZP	H3
	WD40	H3

1.4.1. Histone acetyltransferases

Histone acetyltransferases catalyze the addition of acetyl groups to lysine side chains. In the early 1990s, two acetyltransferases, Nat1-Ard1, were purified. They acetylated the N-terminal amino group of H2A and H2B and not internal lysines like other HATs do (Park and Szostak, 1992). The first histone acetyltransferase to be purified was *Saccharomyces cerevisiae* Hat1 which acetylates histone H4 molecules at lysine residues 5 and 12 prior to H4 deposition onto DNA (Kleff et al., 1995; Parthun et al., 1996). Most HATs are part of multi-subunit complexes. The combinations of these subunits contribute to the unique features of each HAT complex. HATs are divided into two major classes, type-A and type-B, based on their substrate specificity. Type-A HATs are nuclear HATs that catalyze transcription-related acetylation in the context of chromatin (nucleosomal histones). The first A-type HAT to be purified was Gcn5, a homolog of the yeast transcriptional co-activator Gcn5, from the macronuclei of the ciliate protozoan *Tetrahymena thermophila* (Brownell et al., 1996). The A-type HATs can be classified into at least three subfamilies: GCN5/PCAF, MYST and CBP/p300. The families of nuclear HATs show very high sequence divergence. In addition to the well-characterized nuclear HAT families, there are others that are less studied such as TAF250 (Hodawadekar and Marmorstein, 2007). The type-B HATs are distinguished by the fact that they acetylate histones prior to their deposition into chromatin. Histone acetyltransferase 1 (Hat1) and yeast Rtt109 are examples of B-type HATs. They acetylate new H3 and H4 molecules, a mark important for their deposition onto chromatin. Even though Hat1 was initially thought to be cytoplasmic, evidence shows

that it is also found in the nucleus (Parthun, 2007). Many studies have shown that several HATs also have non-histone substrates (Sterner and Berger, 2000).

1.4.1.1. Gcn5-related N-acetyltransferases

The General control non-repressible 5 (Gcn5)-related N-acetyltransferases (GNATs) belong to a superfamily of enzymes. The Gcn5/PCAF family consists of yeast Gcn5, Hat1, Elp3, metazoan Gcn5, p300/CBP associating factor (PCAF) and related proteins. The metazoan Gcn5 homologs have a metazoan-specific N-terminal PCAF homology domain absent in yeast. HATs of the GNAT family are characterized by four conserved sequence motifs, A-D, of which motif A, which houses the acetyl-CoA binding domain, is the most highly conserved. The A, B and D domains of GNAT HATs form a central core. The N- and C-terminal domains flanking the core confer substrate specificity (Hodawadekar and Marmorstein, 2007; Kimura et al., 2005; Marmorstein and Zhou, 2014; Ud-Din et al., 2016). Denu and coworkers have elucidated the catalytic mechanism of GNAT HATs. They showed that Gcn5 functions through a ternary complex mechanism in which both substrates (i.e., lysine and acetyl-CoA) must be bound to the enzyme before catalysis can occur. This involves deprotonation of the lysine substrate by Glu173 (of yGcn5), facilitating the direct transfer of the acetyl group from acetyl-CoA to the lysine side chain (Tanner et al., 1999).

Gcn5 is the catalytic subunit of several multi-subunit lysine acetyltransferase complexes with well-established roles in gene transcription. In *S. cerevisiae*, these complexes include Spt-Ada-Gcn5-acetyltransferase (SAGA), ADA, and SAGA-like (SLIK) (Grant et al., 1997; Pray-Grant et al., 2002). Orthologous complexes with similar

subunit composition include the SAGA and ATAC complexes in *Drosophila* and the STAGA (SPT3-TAF$_{II}$31-GCN5L acetylase), PCAF and TBP-free TAFII complex (TFTC) complexes in humans (Lee and Workman, 2007; Nagy and Tora, 2007). In *S. cerevisiae,* Gcn5 has been shown to play an important role in replication-coupled nucleosome assembly, in parallel with Rtt109, the HAT that acetylates H3-K56. This study showed that deletion of some subunits common to the various Gcn5-containing HAT complexes (Ada1, Ada2, Ada3, Spt7 or Spt20) phenocopy the deletion of *GCN5* in cells lacking Rtt109 but the authors were not able to ascribe the role of Gcn5 in replication-coupled nucleosome assembly to a well-established protein complex that contains Gcn5 as catalytic subunit (Burgess et al., 2010).

Gcn5 has both histone and non-histone substrates. The substrate specificity is regulated by non-catalytic proteins present in each complex. However, interactions between Gcn5 and side chains in the +2 and +4 positions relative to the substrate lysine is conserved across divergent protein substrates (Clements et al., 2003; Poux and Marmorstein, 2003). Recombinant Gcn5 has little or no activity toward nucleosomal histones but predominantly acetylates lysine 14 of H3 and lysines 8 and 16 of H4 (Kuo et al., 1996). When part of multi-subunit complexes, Gcn5 can acetylate both free and nucleosomal histones. For example, *S. cerevisiae* ADA preferentially acetylates K14 and K18 of nucleosomal H3 whereas SAGA acetylates K14 and K18 and, to a lesser degree, K23 and K9 (Grant et al., 1999).

1.4.1.2. MYST family acetyltransferases

The MYST family acetyltransferases are highly conserved, nuclear HATs that play important roles in DNA replication, transcriptional regulation, the DNA damage response and DNA repair. They always function in multi-subunit complexes that are also evolutionarily conserved. The term MYST family was coined after founding members of the family: **M**OZ (MOnocytic leukemia Zing finger), **Y**bf2-**S**as3, **S**as2 (Something about silencing protein 2) and **T**IP60 (Tat-interacting protein 60). All MYST family HATs contain a highly conserved MYST domain, which consists of an acetyl-CoA binding domain and a zinc finger. In addition, some members also have additional domains such as chromodomain and plant homeodomain (PHD)-linked zinc fingers (Sapountzi and Côté, 2011; Yang, 2015). The MYST acetyltransferases from major model organisms are listed in Table 1.2

Several structural studies of MYST HATs from yeast to humans have been reported. Even though the amino- and carboxy-terminal domains are divergent, MYST family members possess a core region involved in acetyl-CoA binding that is conserved across the members of various acetyltransferase families. The structures of MYST HATs superimpose well with Hat1 and Gcn5/PCAF (Marmorstein and Zhou, 2014). The MYST family HATs have a conserved glutamate residue which overlays with the catalytic glutamate residue of Gcn5/PCAF. In addition, MYST family HATs have a cysteine residue in the active site. MYST HATs have a ping-pong catalytic mechanism, in which the enzyme first forms an acetylated intermediate involving a conserved cysteine in the catalytic site before the formation of an acetylated histone product (Yan

et al., 2000, 2002). Studies of the MYST family enzymes Esa1 and MOZ indicate that efficient acetylation is influenced by interactions with regions of the substrate located at a distance from the lysine to be acetylated. For example, piccolo (Nucleosomal Acetylation of H4) NuA4 is predominantly an H4 N-terminal tail specific enzyme. Full-length histone H4 is acetylated 2000-fold faster than histone tail peptides, indicating that interactions with the histone-fold domain of H4 are critical for the high catalytic efficiency (Bernsden and Denu, 2008).

Table 1.2. MYST acetyltransferases in model organisms

MYST Proteins	KAT5	KAT6	KAT7	KAT8
Saccharomyces cerevisiae	Esa1	Sas3		Sas2
Schizosaccharomyces pombe	Mst1	Mst2		
Caenorhabditis elegans	mys-1	mys-4		mys-2
Drosophila melanogaster	dTIP60	Enok CG1894	CHM	MOF
Arabidopsis thaliana	HAM1, HAM2			
Mus musculus	TIP60	KAT6A/MOZ/MYST3	HBO1/MYST2	MOF/MYST1
		KAT6B/Qkf/MORF/MYST4		
Homo sapiens	TIP60/PLIP	KAT6A/MOZ/MYST3	HBO1/MYST2	MOF/MYST1
		KAT6B/MORF/MYST4		

1.4.2. Histone deacetylases

Histone deacetylases (HDACs) catalyze the removal of acetyl groups from lysine side chains and have been implicated in gene repression. Based on phylogeny histone deacetylases have been classified into two families, the classical HDAC family and the yeast *s*ilent *i*nformation *r*egulator 2 (Sir2)-related deacetylases, commonly known as sirtuins. The classical family can be further sub-divided into three classes of HDACs:

Class I, Class II and Class IV. Class I HDACs are homologous to *S. cerevisiae* Rpd3 and include human HDAC1, HDAC2, HDAC3 and HDAC8. Enzymes that have sequence homology to *S. cerevisiae* Hda1 constitute the Class II HDACs. They can be further divided into two subclasses based on their phylogeny: Class IIa and Class IIb (Frye, 2000; Gregoretti et al., 2004). Class IIa includes human HDAC 4,5, 7 and 9 while Class IIb includes HDAC 6 and 10. Class III HDACs are also called sirtuins after the founding member of the family, the *S. cerevisiae* Sir2 enzyme (Seto and Yoshida, 2014). In *S. cerevisiae*, the class III HDACs include Sirt2, Hst1, Hst2, Hst3 and Hst4 and SIRT1 through SIRT7 in humans. Human HDAC 11 is thus far the sole member of class IV HDACs.

Sirtuins do not share sequence or structural homology to other HDAC families. They use a distinct catalytic mechanism that is dependent on the oxidized form of nicotinamide adenine dinucleotide (NAD+) as a co-substrate. Class I, II and IV HDACs require a zinc ion (Zn), for deacetylase activity. They share structural similarity in their catalytic domains (Hodawadekar and Marmorstein, 2007).

HDACs are also part of multi-subunit complexes. HDACs have been shown to have protein substrates other than histones. Taking into consideration the increasing number of non-histone substrates for HATs and HDACs, a new naming system has been put forward (Allis et al., 2007). These enzymes are now called lysine acetyltransferases (KATs) and lysine deacetylases (KDACs) under the new nomenclature.

1.4.3. Histone deacetylase inhibitors

Chromatin regulators are frequently mutated in cancer, neurological disorders, metabolic disorders and inflammatory diseases. Changes in DNA and histone modifications are reversible and the ability to modulate enzymatic properties and/or structural properties of chromatin modifying enzymes have led to the development of a repertoire of pharmacological inhibitors. The predominant class of these inhibitors target HDACs and are known as histone deacetylase inhibitors (HDACi). Even though most of these inhibitors were originally developed to combat cancers, several of them are being used to treat immune and neurological disorders (Falkenberg and Johnstone, 2014; Marks and Xu, 2009).

The most commonly used HDAC inhibitors are so-called "pan" inhibitors that target multiple HDACs. This broad range of specificity makes it difficult to determine whether the biological consequences of HDAC inhibition are due to inhibition of a specific HDAC, or the combined effect of inhibiting multiple HDACs. HDACi can also inhibit histone deacetylases that are part of multi-protein complexes that incorporate them as key enzymatic components.

Based on their chemical structure, HDACis are classified into the following groups; hydroxamic acids (trichostatin A, vorinostat), carboxylic acids (valproate, butyrate), benzamides (entinostat, mocetinostat), cyclic peptides (apicidin, romidepsin), epoxyketones (trapoxin), and hybrid molecules. Hydroxamate derivatives generally inhibit HDACs from multiple classes whereas benzamide derivatives are generally

restricted to inhibiting class I HDACs. (Falkenberg and Johnstone, 2014; Marks, 2010; West and Johnstone, 2014).

In addition to HDACi, inhibitors of chromatin modulators (*e.g.* small molecules that prevent bromodomains from recognizing acetylated lysine residues), are also in development and clinical trials (Filippakopoulos and Knapp, 2014; Muller et al., 2011). US Food and Drug Administration (FDA)-approved DNA-demethylating agents azacitidine (also known as 5-azacytidine) and decitabine (also known as 5-aza-2′-deoxycytidine) which are used to treat myelodysplastic syndromes (MDS) and a range of other malignancies are by far the most successful and long-standing inhibitors of epigenetic processes. Inhibitors of histone methyltransferases such as DOT1L and EZH2 as well as inhibitors of protein arginine methyltransferase (PRMT) show promise for the treatment of cancer and immune disorders (Falkenberg and Johnstone, 2014 and references within).

Table 1.3 Histone deacetylase inhibitors

Group	Compound	Use	Disease
Hydroxamic acid	Vorinostat (SAHA, Zolinza)	FDA approved	Cutaneous T-cell lyphoma (CTCL)
	Panobinostat (LBH589)	phase III clinical trial	CTCL
	Belinostat (PXD101)	phase II clinical trial	Thymoma
	Belinostat (PXD101)	FDA approved	Peripheral T-cell lymphoma (PTCL)
	Abexinostat (PCI24781)	phase II clinical trial	follicular lymphoma
	Givinostat (ITF2357)	phase II clinical trial	JAK2V617F-expressing myeloproliferative neoplasms
	Dacinostat (LAQ824, NVP-LAQ824)	phase I clinical trial	solid and hematological malignancies
	Quisinostat (JNJ-26481585)	phase II clinical trial	CTCL
	CHR-3996	phase I clinical trial	solid tumors
	Pracinostat (SB939)	phase II clinical trial	prostrate cancer
Cyclic peptides	Romidepsin (Depsipeptide, FK228)	FDA approved	CTCL, PTCL
Benzamide	Mocetinostat (MGCD0103)	phase II clinical trial	B cell malignancies
	Entinostat (MS-275, SNDX-275)	phase II clinical trial	melanoma
	Chidamide	phase II clinical trial	solid tumors and lymphomas
	AR-42	phase I clinical trial	hematological malignancies
Aliphatic acid	Valproic acid (VPA)	FDA-approved	neurological disorders
	Pivanex (AN-9)	phase II clinical trial	small cell lung cancer
	Butyrate	FDA-approved	neurological disorders

1.4.4. Cellular functions of histone acetylation

Histone acetylation has been implicated in several important cellular functions including replication-coupled nucleosome assembly, DNA damage response, DNA repair and regulation of gene expression. In this section, evidence that supports the role of histone acetylation in these processes is discussed.

1.4.4.1. Chromatin assembly

During DNA replication, duplication of DNA is accompanied by a transient disruption of chromatin structure and concomitant histone synthesis. The chromatin structure is rapidly re-established in a step-wise manner through two key steps. First, pre-existing or parental histones located ahead of replication forks are distributed among the two nascent sister chromatids. Parental histone segregation is followed by deposition of newly synthesized histones, a process called replication-coupled (DNA synthesis-coupled or *de novo*) nucleosome assembly (Verreault, 2000). In addition to chromatin assembly that occurs throughout the genome during S-phase, chromatin structure is dynamically transformed during transcription. This constitutes the replication-independent or DNA synthesis-independent chromatin assembly. In addition, at sites of DNA repair, a PCNA-dependent chromatin assembly occurs.

One question that has been of interest to early researchers was the timing of nucleosome assembly with respect to DNA synthesis. Using a very short pulse-labeling time of 1 min with tritiated thymidine, Seale showed that newly replicated chromatin is sensitive to digestion by DNase I, but recovers its resistance characteristic of mature

chromatin after about 15 min (Seale, 1975). However, electron microscopic observations showed that both arms of the replication fork contained nucleosomes and lacked stretches of nucleosome-free DNA, implying that chromatin maturation continues even after *de novo* nucleosome assembly (reviewed in Annunziato, 2012). A likely explanation for the gradual maturation came with the identification of acetylation on newly synthesized histones (Jackson et al., 1976; Ruiz-Carrillo et al., 1975). Acetylation of new H4 molecules was shown to have a half-life of 20-30 min suggesting that acetylation was partly responsible for the increased DNase I sensitivity of new chromatin (Cousens and Alberts, 1982; Jackson et al., 1976; Ruiz-Carrillo et al., 1975). It was later demonstrated that chromatin replicated in the presence of sodium butyrate had higher magnesium-solubility, characteristic of acetylated chromatin, compared to bulk chromatin. The increased solubility in magnesium coincided with a five to six-fold decrease in linker histone H1, thus establishing that deacetylation of new histones is necessary for chromatin maturation (Annunziato and Seale, 1983; Perry and Annunziato, 1989).

Pioneering studies in the mid-70s showed that new histone H4 is acetylated in the cytoplasm based on biochemical fractionation of cytosolic and nuclear proteins. One caveat of this approach is that numerous proteins that are soluble in the nucleus end up in the "cytosolic" extract. In a nutshell, these authors could not conclude that the acetylation of new histone molecules took place in the cytoplasm based on the fractionation experiments that they conducted at the time (Jackson et al., 1976; Louie et al., 1974; Ruiz-Carrillo et al., 1975). There are four lysine residues in the amino-terminal tail of H4 that can be acetylated: lysine 5, 8, 12 and 16. Using Edman

sequencing of newly synthesized H4 pulse-labeled with tritiated lysine, the sites of acetylation were found to be H4K5 and H4K12 in yeast, flies and mammalian (HeLa) cells (Benson et al., 2006; Sobel et al., 1995). In *Tetrahymena*, H4K4 and H4K11 are the deposition-related acetylation sites, due to a deletion of arginine at position 3 (Chicoine et al., 1986). Even though specific functions of H4K5 and H4K12 acetylation remain enigmatic, this evolutionarily conserved pattern of H4 diacetylation is considered a hallmark of replication-coupled chromatin assembly.

Histone H3 is also acetylated rapidly after synthesis (Jackson et al., 1976). The pattern and sites of acetylation in new H3 molecules have been less conserved than those of H4. For example, in the fruit fly, newly synthesized H3 is acetylated on lysine 14 and 23 while in the ciliate *Tetrahymena*, lysine 9 and 14 are acetylated (Sobel et al., 1995). In budding yeast, *Saccharomyces cerevisiae*, four of the five N-terminal tail lysine residues (K9, K14, K23 and K27) are acetylated, with H3K9 showing the highest level of acetylation, followed by H3K27 (Kuo et al., 1996). In mammalian cells, about ten percent of new histone H3 molecules are acetylated at lysine residues 14, 18 and 23 (Benson et al., 2006). Unlike H4 which is predominantly acetylated on lysines K5 and K12, a large proportion of new H3 molecules are nonmodified, particularly in mammalian cells (Benson et al., 2006; Sobel et al., 1995).

The N-terminal tail acetylations of H3 and H4 are important for nucleosome assembly. In *S. cerevisiae*, the N-terminal tails of H3 and H4 have redundant functions in nucleosome assembly both *in vitro* and *in vivo*. In addition, cells lacking N-terminal tail acetylation of both H3 and H4, through mutation of multiple lysine residues to arginine, are not viable. The extracts from these cells are defective in chromatin assembly *in*

vitro. (Ling et al., 1996; Ma et al., 1998). Surprisingly, in *S.cerevisiae* cells lacking the N-terminal of H3, the conserved deposition-related H4-K5, K12 acetylation is not required for histone deposition *in vitro* and *in vivo*, as long as H4 lysine 8 is intact (Ma et al., 1998). It has been demonstrated that the N-terminal tails of H3 and H4 are not necessary for CAF-1 dependent chromatin assembly *in vitro* (Shibahara et al., 2000). The presence of multiple copies of histone genes makes it difficult to perform comprehensive studies in *S. pombe* and higher eukaryotes. Using fluorescent protein-tagged histones under the control of heat shock inducible promoters, Ahmed and Henikoff showed that the N-terminal tail of H3.3, but not that of H3.1, is dispensable for its deposition onto DNA (Ahmad and Henikoff, 2002). However, it is unclear whether post-translational modifications of H3.1 are necessary for its assembly into chromatin in higher eukaryotes.

In addition to the acetylation that occurs on the N-terminal tails, new histones are also acetylated in the globular domain prior to their deposition into chromatin. The best well-characterized globular domain acetylation occurs on lysine 56 of histone H3. H3K56 acetylation is found in yeast (budding yeast, fission yeast and *Candida albicans*) and *Drosophila* (Masumoto et al., 2005; Recht et al., 2006; Wurtele et al., 2010; Xu et al., 2005). Even though H3 lysine 56 acetylation has been detected in humans, the abundance is very low (Drogaris et al., 2012; Jasencakova et al., 2010). Lysine 56 is the last residue of the α-N helix of histone H3 and the non-acetylated form interacts with DNA at the entry/exit point of the nucleosome (Masumoto et al., 2005; Ozdemir et al., 2005; Xu et al., 2005).The acetylation of K56 is thought to weaken the histone-DNA interactions by neutralizing the positive charge of lysine (Bernier et al., 2015; Neumann

et al., 2009; Su et al., 2012). H3 lysine 56 acetylation occurs predominantly on newly synthesized histones, peaks during S-phase and, in the absence of DNA lesions, is removed from histones in G2/M (Celic et al., 2006; Maas et al., 2006; Masumoto et al., 2005). Evidence suggests that H3K56 acetylation plays an important role in both replication-coupled and replication-independent chromatin assembly. A critical function of H3 lysine 56 acetylation in these processes may be to regulate interactions with histone chaperones as this modification has been shown to promote the association of new H3 molecules with histone chaperones CAF-1 and Rtt106 (Li et al., 2008). H3 molecules bound to CAF-1 and Rtt106 during S-phase are acetylated at H3K56 (Li et al., 2008; Masumoto et al., 2005). In cells lacking H3K56ac, the amounts of new H3 molecules bound to CAF-1 and Rtt106 are considerably reduced which, in turn, delays the deposition of new histones behind replication forks (Li et al., 2008). The reduced amounts of histones bound to Rtt106 when H3-K56 cannot be acetylated can be, at least partially explained by the fact that Rtt106 binds with higher affinity to H3 molecules that are K56-acetylated. Together, these results indicate that the acetylation of new histone H3 at K56 promotes H3-H4 deposition by CAF-1 and Rtt106 onto nascent chromatin during S phase. Mutations that abolish H3K56ac show synthetic lethality with mutation of lysine residues in the N-terminal tails of H3 or H4 in the presence of genotoxic agents that cause DNA damage during S phase (Li et al., 2008). It could be possible that new histone deposition behind replication forks which is important for DNA damage survival is partially compromised when mutations that abolish K56 acetylation or H3 N-terminal tail acetylations are present but more severely compromised when both forms of acetylations are compromised.

Histone H4 lysine 91 is another site of histone core domain acetylation (Ye et al., 2005). Lysine 91 residues from the two H4 molecules lie along the interfaces between the central H3/H4 tetramer and the two H2A/H2B dimers. The non-acetylated side chain of lysine 91 forms a salt bridge with a glutamic acid residue in histone H2B (Cosgrove et al., 2004) thus, arguably, H4K91 acetylation could weaken the interaction between the central H3/H4 tetramer and the H2A/H2B dimers. H4K91 acetylation is found in yeast, bovine and human cells. H4K91 acetylation is found on H3 molecules associated with nuclear Hat1, a HAT known to selectively acetylate new histones prior to their deposition into chromatin. This observation suggests that H4 lysine 91 acetylation is a PTM found on newly synthesized histones. However, it is not known what fraction of new histones carries this modification. Genetic analysis of mutants shows that this modification functions with histone chaperones Asf1 and CAF-1(Ye et al., 2005). In Ye et al, they show that when mutations of H4K91 are combined with the loss of DNA damage response proteins such as Mec1, Mec3, yKu70 or Rad52, there is increased sensitivity to DNA alkylating agent methyl methanesulfonate (MMS). The authors demonstrate that when strains lack chromatin assembly proteins such as Asf1 or Cac1 and also have an H4K91A mutation, they are more sensitive to MMS or UV radiation respectively. However, the increase in sensitivity for double mutants is substantially small.

1.4.4.2. DNA damage response

In eukaryotic and prokaryotic cells, genomic integrity is constantly challenged by exogenous and endogenous sources of DNA lesions. For instance, a human cell must repair over 10,000 DNA lesions per day to counteract hydrolytic depurination, an

endogenous source of DNA damage (Lindahl 1993). Failure to repair DNA lesions can lead to deleterious mutations, genetic instability, cell death, and in humans a strong predisposition to cancer. Cells have evolved elaborate mechanisms to combat the onslaught of DNA lesions. These include surveillance mechanisms known as checkpoints. The main cell cycle checkpoints are the DNA replication checkpoint or S-phase checkpoint, the G1 checkpoint which is very weak in budding yeast and the G2/M checkpoint (Nyberg et al., 2002). In addition to checkpoints, there exist repair pathways that repair different types of DNA lesions such as modified bases, DNA adducts, cross links and double strand breaks (Sancar, 1995). Hence, the DNA damage response (DDR) is a coordinated action of checkpoint pathways and DNA repair pathways.

The DNA replication checkpoint or S-M checkpoint senses blocks encountered by replication forks. These barriers to replication fork progression include endogenous DNA lesions such as oxidized and alkylated DNA bases or DNA lesions caused by external agents such as ultraviolet radiation and hydroxyurea, which depletes the deoxyribonucleotide triphosphate (dNTP) pool by inhibiting ribonucleotide reductase. The checkpoint response which, in effect, is a signaling cascade that slows down DNA replication by preventing the firing of new replication origins, protects stalled replication forks until DNA synthesis can resume and delays the onset of mitosis (M) until replication is completed. Moreover, the S phase checkpoint recruits the DNA repair machinery to sights of DNA damage (Boddy and Russell, 1999; Nyberg et al., 2002).

The key components of the S phase checkpoint and their overall mode of action are evolutionarily conserved (Figure 1.6). Checkpoint pathways include sensor proteins, which recognize damaged DNA directly or indirectly, transducers, generally protein kinases that transmit the signal and effectors, the downstream proteins which prevent cell cycle progression. Central to this signalling pathway are the transducers, members of the phosphoinositide 3-kinase related family of protein kinases (PIKKs), Ataxia telangiectasia mutated (Human ATM/ *S. pombe* Tel1/ *S. cerevisiae* Tel1), ATM-and Rad3-related (Human ATR/ *S. pombe* Rad3/ *S. cerevisiae* Mec1) and DNA-dependent protein kinase-like family (DNA-PKcs). ATM and ATR activate the serine/threonine kinases CHK1 and CHK2 (*S. pombe* Cds1/ *S. cerevisiae* Rad53) that in turn phosphorylate numerous downstream effectors (Nyberg 2002, Boddy and Russell 2001).

One of the most harmful lesions is the DNA double-strand break (DSB). DSBs are naturally formed during processes such as meiotic recombination and the assembly of the T-cell receptor and immunoglobulin genes via V(D)J recombination, in T cells and B cells respectively. They can also be formed by free radicals, ionizing radiations and due to defects in replication. DSBs are repaired by two major pathways. Non-homologous end-joining (NHEJ) involves processing and religation of broken DNA ends. Homologous recombination (HR) takes advantage of homologous templates from an undamaged sister chromatid or homologous chromosome to repair the lesion with high fidelity (Shiloh, 2003; Shiloh and Ziv, 2013).

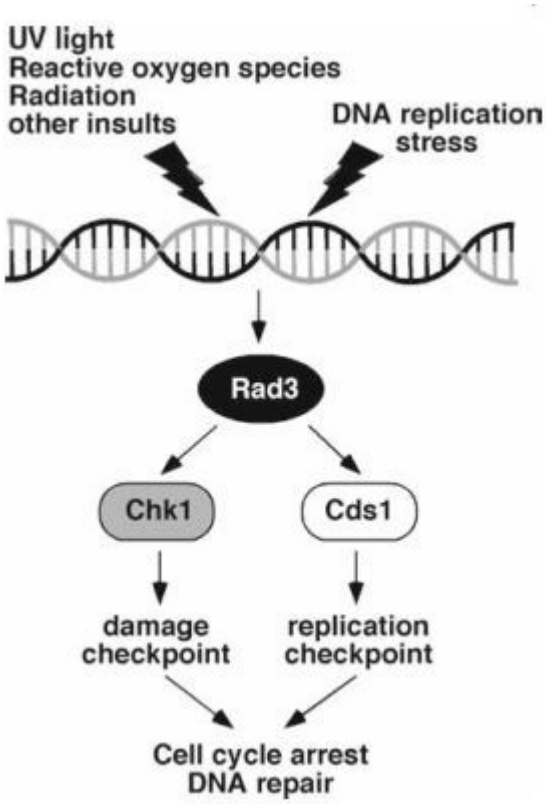

Figure 1.5. Simplified checkpoint activation pathway in fission yeast (Noguchi et al., 2009)

Timely repair of lethal mutations is challenged by chromatin structure, which entails remodeling to permit access of repair machinery to damaged DNA. This concept is highlighted in the “Access-Repair-Restore” model according to which, the initial steps permit access of the repair machinery to DNA damage while the later steps faithfully restore the original nucleosomal organization (Green and Almouzni, 2002; Smerdon, 1991). Since post-translational modifications (PTMs) are known to affect many aspects of chromatin structure and function, it is not surprising that they also play important roles in several forms of DNA repair. There are two changes in PTM patterns in

response to DNA damage or more specifically to DSBs. Global changes in PTM patterns which, for example, reflect the transcriptional activation of repair genes or local changes in the vicinity of DSBs which might contribute as platforms for DNA damage response proteins.

One of the best-established DNA damage-associated chromatin modifications is the phosphorylation of the SQ motif near the C-terminus of mammalian histone variant H2AX, known as γ-H2AX (Rogaku 1998). In budding and fission yeasts, the homologs of mammalian H2AX are the major histone H2A proteins which also undergo phosphorylation in response to DNA damage (Downs et al., 2000; Nakamura et al., 2004). γ-H2AX and γ-H2A are generated by ATM, ATR, and DNA-PK or their homologs in yeast. Using chromatin immunoprecipitation (ChIP) assays it has been shown that γ-H2AX can be detected up to 50Kb on either side of the site of DSB in *S. cerevisiae* and ~2 Mb in human cells (van Attikum and Gasser, 2005; Wurtele and Verreault, 2006).

Histone acetylation has been implicated in the DNA damage response. One of the first reports of the role of histone acetylation in DNA repair came from studies in budding yeast. Esa1 (the catalytic subunit of nucleosomal acetyltransferase of H4 (NuA4) complex) -mediated acetylation of H4 was shown to be important for the repair of DNA double-strand breaks through NHEJ and the repair of DSBs caused by camptothecin-induced damage at the replication fork (Bird et al., 2002). It was subsequently shown that the NuA4 complex is recruited to DSBs relatively early after DSB induction. In

chromatin immediately flanking the DSB, enrichment of NuA4-mediated H4 K8ac was visible at early time points (Downs et al., 2004). Strikingly, the mammalian Esa1 homolog TIP60 is also required for DNA double-strand break repair. Ectopic expression of a catalytic activity deficient TIP60 mutant resulted in cells defective in DNA double-strand break repair and DNA damage-induced apoptotic competence (Ikura et al., 2000). The NuA4 subunit Yng2 was reported to be required in response to DNA damage during S phase, suggesting a role for NuA4 in genome maintenance during DNA replication (Choy and Kron, 2002). Moreover, TIP60 and a co-factor of its catalytic activity Transformation/transcription domain-associated protein (TRRAP) were shown to be recruited to chromatin surrounding DSBs *in vivo*. The authors demonstrate that the TRRAP–TIP60 complex directly acetylates nucleosomes in the vicinity of a site-specific DSB and is needed for recruitment of HR proteins and efficient HR-mediated repair in mouse and human cells. Depletion of TRRAP impaired DNA damage-induced histone H4 hyperacetylation and accumulation of repair molecules at sites of DSBs (Murr et al., 2006). Acetylation of H4 at lysines 5 and 12 is a hallmark of newly synthesized histones. In vertebrates, HAT1-RbAp46/RBBP7 catalyzes this diacetylation and its absence was shown to confer sensitivity MMS and the DNA topoisomerase I inhibitor camptothecin (Barman et al., 2006). In budding yeast, Hat1, a homolog of the vertebrate HAT1-RbAp46/RBBP7, works redundantly with acetylatable lysine residues in the N-terminal tail of H3 to promote homologous recombination repair of DNA double-strand breaks (Qin and Parthun, 2002).

A transient increase in the acetylation of several lysine residues in the N-terminal tails of histone H3 and H4 occurs at DSBs introduced by HO endonuclease in *S. cerevisiae*. The authors used a system where an HO-induced site-specific DSB at the *MAT* locus is repaired by HR-driven mating-type switching. They demonstrated that both HATs (NuA4 and Gcn5) and HDACs (Rpd3, Sir2 and Hst1) associated with regions close to the DSB, but the association of HATs preceded those of HDACs, consistent with the 'Access-repair-restore' model (Tamburini and Tyler, 2005). Congruent with the temporal association of HATs and HDACs, the histone deacetylase complex Sin3/Rpd3-mediated deacetylation of H4K16 was monitored very late after DSB induction (Jazayeri et al., 2004). In *S. pombe*, acetylation of H3-K14 has been reported to be important for DNA damage checkpoint activation. Upon induction of HO endonuclease activity, the authors showed that H3-K14 acetylation increased at 2 Kb from the damage sites but not further away (Reddy et al., 2011).

Two sites of acetylation on new H3 molecules, H3K56 and H4K91 have also been implicated in DNA repair. Mutations that abolish H3K56 acetylation (*rtt109*Δ, *asf1*Δ or *H3K56R* mutants) cause hypersensitivity to genotoxic agents that interfere with DNA replication (Celic et al., 2006; Masumoto et al., 2005). In budding yeast, double mutants that carried H3K56R mutation and also lacked Asf1 (*Δasf1*) exhibited sensitivity to hydroxyurea similar to that of each of the single mutants suggesting an epistatic relationship (Recht et al., 2006). Two genes are said to have an epistatic relationship when a mutation in one gene suppresses or masks the phenotypes in the second gene. In such a case, both genes are considered to be in the same genetic pathway (Roth et

al., 2009). Transient exposure of *rtt109*Δ cells to MMS in the S-phase impedes DNA replication and leads to persistent checkpoint activation (Wurtele et al., 2012). H3K56ac occurs preferentially during S phase in the fission yeast *S. pombe* where it is important for cell survival in response to genotoxic agents that interfere with DNA replication (Haldar and Kamakaka, 2008; Recht et al., 2006; Xhemalce et al., 2007). H4 lysine 91 mutations also cause sensitivity to genotoxic agents (Ye et al., 2005).

Histone acetylation may also play a role in the DNA damage response by recruiting chromatin remodeling complexes to restore the original chromatin organization following repair. For example, the Arp4 subunit of NuA4 has been shown to bind γ-H2A (Downs et al., 2004). Arp4 is also a subunit of two ATP-dependent chromatin remodeling complexes INO80 and SWR1, which are recruited to DSBs in a γ-H2A-dependent manner (van Attikum et al., 2004; Kobor et al., 2004; Morrison et al., 2004). In another study, both NuA4 and GCN5 were shown to be required for the recruitment of the SWI/SNF chromatin remodeling complex, resection of DNA ends and H2A phosphorylation. The data suggest that the acetylation is bound by the bromodomain of the Swi2 subunit of SWI/SNF since the removal of the bromodomain results in loss of SWI/SNF accumulation and H2A phosphorylation (Bennett and Peterson, 2015).

1.4.4.3. Regulation of gene expression

The functional association linking enhanced histone acetylation and transcription in eukaryotic cells was proposed by Allfrey and colleagues more than 50 years ago

(Allfrey and Mirsky, 1964; Allfrey et al., 1964). They showed that radio-labeled acetate was rapidly taken up and incorporated into histones in isolated nuclei. Allfrey further demonstrated that acetylation of histones lowered their ability to inhibit RNA synthesis. This led him to put forward a daring hypothesis: “the dynamic and reversible mechanism for activation as well as repression of RNA synthesis” by reversible post-translational histone acetylation (Allfrey et al., 1964). Subsequently, using biochemical fractionation, acetylated histones were shown to be preferentially associated with active chromatin (Sealy and Chalkley, 1978; Vidali et al., 1978). Many studies have broadly supported this hypothesis over the years thus leading the researchers to come to a general understanding that highly acetylated histones are a hallmark of actively transcribed genes whereas genes that are repressed or inactive are hypoacetylated. Purification of HATs and HDACs strengthened the causal relationship between histone acetylation and gene expression (Brownell et al., 1996; Taunton et al., 1996). Acetylation is proposed to alter gene expression either through altering chromatin packaging directly (by changes in inter-nucleosomal contacts or changes in electrostatic charge) or by acting as a platform for the recruitment of chromatin binding proteins (Berger, 2007).

Chromatin immunoprecipitation (ChIP) or related techniques that can be applied to the entire genome such as ChIP-CHIP (ChIP data analyzed by DNA hybridization to microarrays) and ChIP-Seq (ChIP data analyzed by high-throughput DNA sequencing) are powerful methods to study DNA-protein interactions *in vivo*. Studies using these techniques have shown strong correlations between patterns of histone modifications and transcriptional activity (Li et al., 2007). In ChIP, chromosomal proteins are

selectively isolated along with the DNA that they are associated with *in vivo*. However, one important factor is generally overlooked while interpreting the results of studies associating histone acetylation with gene transcription or other processes such as DNA repair. In ChIP experiments, antibodies that, under a certain range of conditions, preferentially recognize histones acetylated at specific lysine residues, are used to immunoprecipitate chromatin fragments that are chemically modified with formaldehyde which, among other chemical adducts, generates covalent bonds between proteins located in close proximity to the DNA. If there is a high recovery of fragments from a chromosomal region or specific gene(s), that region is termed ‘hyperacetylated’ and generally assumed to be 'hyperacetylated' in the majority of cells in the starting population. However, this assumption is not necessarily correct. One can readily imagine scenarios where the specific gene of interest is only hyperacetylated in a small subset of the starting cell population (*e.g.* <5%). In such cases, small decreases in acetylation of the gene of interest observed in ChIP assays performed with wild-type cells and a mutant strain lacking a given HAT cannot be accepted as strong evidence that transcription of that gene of interest is genuinely regulated by this specific HAT. In addition, the last few years have revealed that a considerable number of antibodies against a plethora of histone modifications lack the high degree of specificity desired of these reagents (Egelhofer et al., 2011; Fuchs et al., 2011; Nishikori et al., 2012). The frequent lack of specificity of antibodies against histone modification is particularly alarming when these antibodies are used to study mammalian cells where, unlike yeast and other model organisms, it is impossible to mutate histone residues in order to confirm antibody specificity. Another important

factor to consider is the ‘control’ used in the immunoprecipitation. Some of the negative controls routinely used include no antibody or ‘bead-only’, use of an isotype control for the antibody, or immunoprecipitation from an isogenic non-tagged strain or vector-transfected cells.

Despite these challenges, in conjunction with other lines of evidence, ChIP assays have proven extremely valuable in establishing solid functional links between histone acetylation with transcription. The most incisive studies were conducted in model organisms where histone residues whose acetylation is suspected to play a role in transcription can be mutated to assess the consequences on transcription itself or transcription-related processes. Genome-wide studies in S. *cerevisiae* have identified the localization of distinct histone modifications on canonical histones as well as histone variants. Many of these modifications have also been identified in *Schizosaccharomyces pombe*, *Drosophila melanogaster*, *Mus musculus*, *Arabidopsis thaliana* and *Homo sapiens* (Rando, 2007). Most modifications formed distinct localized patterns within the upstream region, the core promoter, the 5' end of the open reading frame (ORF) and the 3' end of the ORF (Li et al., 2007; Rando, 2007). The acetylation of most individual lysines in the histone H3 and H4 tails correlates positively with gene transcription (Kurdistani et al., 2004; Liu et al., 2005; Pokholok et al., 2005; Sinha et al., 2006; Wirén et al., 2005). The acetylation of H3 and H4 at active genes has been associated with the activity of HATs, such as Gcn5 that acetylates H3 and H2B sites and, Esa1, that preferentially acetylates H4 and H2A sites (Allard et al., 1999; Kuo et al., 2000; Suka et al., 2001).

In addition to genome-wide studies of multiple modifications, the role of individual modifications on gene expression has also been studied. A group of studies has implicated H3K56ac in the regulation of gene expression. Cells in which H3 lysine 56 has been mutated into a non-acetylatable arginine (*H3K56R* mutants) have decreased expression of genes encoding histones H2A and H2B. It has been proposed that reduced transcription in *H3K56R* mutants results from diminished recruitment of the SWI/SNF chromatin remodeling complex to the promoter and the coding region of histone genes in the absence of H3K56ac (Xu et al., 2005). Consistently, another group demonstrated that *rtt109*Δ cells have reduced expression of the histone gene *HTA1* encoding histone H2A (Fillingham et al., 2009). Moreover, it has been suggested that Asf1 and H3K56ac promote transcription of the model gene *PHO5* by driving chromatin disassembly at its promoter region (Williams et al., 2008). In support of these experiments, global levels of H3K56ac correlate with RNA polymerase II occupancy at the promoter region and along the open reading frame of transcribed genes (Rufiange et al., 2007). These results suggest that the incorporation of K56-acetylated histone H3 at transcribed loci might further enhance gene expression by facilitating recruitment or progression of the transcription machinery at active genomic regions.

1.5. Studying histone modifications in model organisms

Good experimental models are key to studying cellular processes. Model organisms have been pivotal in addressing and solving many questions raised in the field of chromatin research. Historically, *Saccharomyces cerevisiae* (budding yeast), *Schizosaccharomyces pombe* (fission yeast), *Neurospora crassa, Tetrahymena*

thermophila, Caenorhabditis elegans (worm), *Drosophila melanogaster* (fruit fly), *Arabidopsis thaliana*, *Zea mays* (maize), mouse and mammalian cells have been used to study chromatin.

Unicellular and 'lower' eukaryotes like *S. cerevisiae*, *S. pombe* and *N. crassa* permit powerful genetic analyses partly owing to their short lifespan. The budding yeast *S. cerevisiae* has been an invaluable model in understanding chromatin structure associated with both euchromatic regions and heterochromatic regions. *In S. cerevisiae*, the unique silent information regulator (SIR) proteins were shown to be associated with heterochromatin (Grunstein and Gasser, 2013). *S. pombe* and *N. crassa* have been instrumental in studying silencing mechanisms that also exist in higher eukaryotes such as RNA interference (RNAi)-mediated silencing and heterochromatin formation dependent on H3-K9 methylation and heterochromatin protein (HP1) (Allshire and Ekwall, 2015; Aramayo and Selker, 2013; Martienssen and Moazed, 2015). A genome defense mechanism called repeat-induced point mutation (RIP) was discovered in *N. crassa*, in which repeat sequences are prone to induce G:C to A:T mutations (Aramayo and Selker, 2013).

The protozoan *Tetrahymena thermophila* has also contributed to significant discoveries, primarily due to their nuclear dimorphism. Ciliates have two nuclei, the somatic macronucleus, which is transcriptionally active and the germ-line micronucleus which is inactive throughout the life cycle except during reproduction. Examining the differences in the active and silent nuclei in *T. thermophila* enabled the identification of histone variants. The first histone acetyltransferase was purified from this ciliate. *T. thermophila* is also an interesting organism for the study of RNAi. Ciliates have a

peculiar phenomenon of DNA elimination during their sexual cycle, which is mediated by small non-coding RNAs and histone modifications (Chalker et al., 2013). Using reverse genetics studies with RNAi libraries, the nematode *C. elegans* has been a valuable organism to study epigenetic control of events that also occur during metazoan development (Kyriakakis et al., 2016).

The fruit fly *Drosophila melanogaster* has been a classic genetic model organism. It has also been central to many discoveries in chromatin structure and function. Position effect variegation (PEV), in which gene activity is governed by the surrounding chromatin structure and not the DNA sequence, was first described in the 1930s in *Drosophila* through observations of eye color. Research of suppressors and enhancers of position effect variegation have laid the foundation for discovering chromatin remodeling proteins and histone modifying proteins. Histone methyltransferases, Polycomb group (PcG) proteins and Trithorax group (TrxG) proteins, all originally discovered through genetic screens in *Drosophila*, are now the subject of intense research (Elgin and Reuter, 2013).

Plants, such as *Arabidopsis thaliana* have been pivotal in epigenetic research. They formed the source of many discoveries such as transposable elements, non-coding RNAs in transcriptional silencing, links between DNA methylation, histone modification and components of the RNAi machinery (Pikaard and Mittelsten Scheid, 2014).

1.5.1 *Schizosaccharomyces pombe* as a model for studying histone modifications

The fission yeast *Schizosaccharomyces pombe* is an important model organism for investigating cellular and molecular processes. Studies in this single-celled eukaryote have improved our understanding of the eukaryotic cell cycle, RNA interference pathway (RNAi), DNA damage response, meiotic differentiation, cell polarity, stress response mechanisms and heterochromatin structure and function. First described in 1893 by Paul Lindner, fission yeast was first isolated from East African millet beer and the name *pombe* comes from the Swahili word for beer (Hayles and Nurse, 2016).

S. pombe began to be used as a model organism in the 1950s by two eminent scientists, Urs Leopold and Murdoch Mitchison. Urs Leopold used *S. pombe* to study the basic mechanisms of genetics in eukaryotes. Murdoch Mitchison was interested in studying the mechanisms and kinetics of cell growth between two successive divisions. A giant leap for the *S. pombe* research came when Paul Nurse combined the genetic tools developed by Leopold with the cell cycle studies of Mitchison. Following the pioneering work of Lee Hartwell on *S. cerevisiae*, Nurse isolated cell division cycle (*cdc*) mutants in *S. pombe*. This led to the identification of cyclin-dependent kinases as key players in driving the cell cycle across major transition points - from G1 into S-phase and from G2 into mitosis (Hayles and Nurse, 2016; Hoffman et al.). Paul Nurse was awarded the 2001 Nobel Prize in Physiology or Medicine, together with Tim Hunt and Lee Hartwell. Another important landmark in *S. pombe* research came with its genome sequencing in 2002.

S. pombe haploid cells are rod-shaped ascomycete yeast that is ~7–14 μm in length and ~4 μm wide. The diploids are longer and wider than haploids. *S. pombe* grows by tip elongation and divides by medial fission on attaining a critical cell length. It has a rapid life cycle with a generation time in the vegetative growth of 2.5 h at 30°C in rich media. Cells continue to undergo mitotic cell cycles until nutrients become limiting and, as proliferation ceases, they enter the stationary phase. *S. pombe* is normally a haploid organism, however, at the diploid zygote stage, if cells are not committed to the meiotic program and nitrogen levels are increased, they reenter vegetative growth as diploids. Thus, *S. pombe* offers the advantage of a model organism that can be studied either as haploid or diploid. The *S. pombe* genome consists of three linear chromosomes of 5.6, 4.8, and 3.6 Mbp, respectively, for chromosomes I, II, and III. The telomeres, centromeres, and origins of replication are more similar to those of complex eukaryotes than that is in budding yeast (Wood et al. 2002) and heterochromatin can be formed by both RNAi-dependent and RNAi-independent pathways (Reyes-Turcu and Grewal, 2012). The RNAi machinery does not exist in *S. cerevisiae*. The process of mRNA splicing also appears to be more similar to splicing in human cells. Nearly 50% of fission yeast genes have at least one intron, and in total there are 5300 introns in 2510 protein-coding genes.

S. pombe has a typical eukaryotic cell cycle in that the mitotic cell cycle is divided into G1, S, G2 and M phases (Figure 1.6). Nuclear division is followed by cell division during which a septum divides each cell into two equal-sized daughter cells. However, unlike

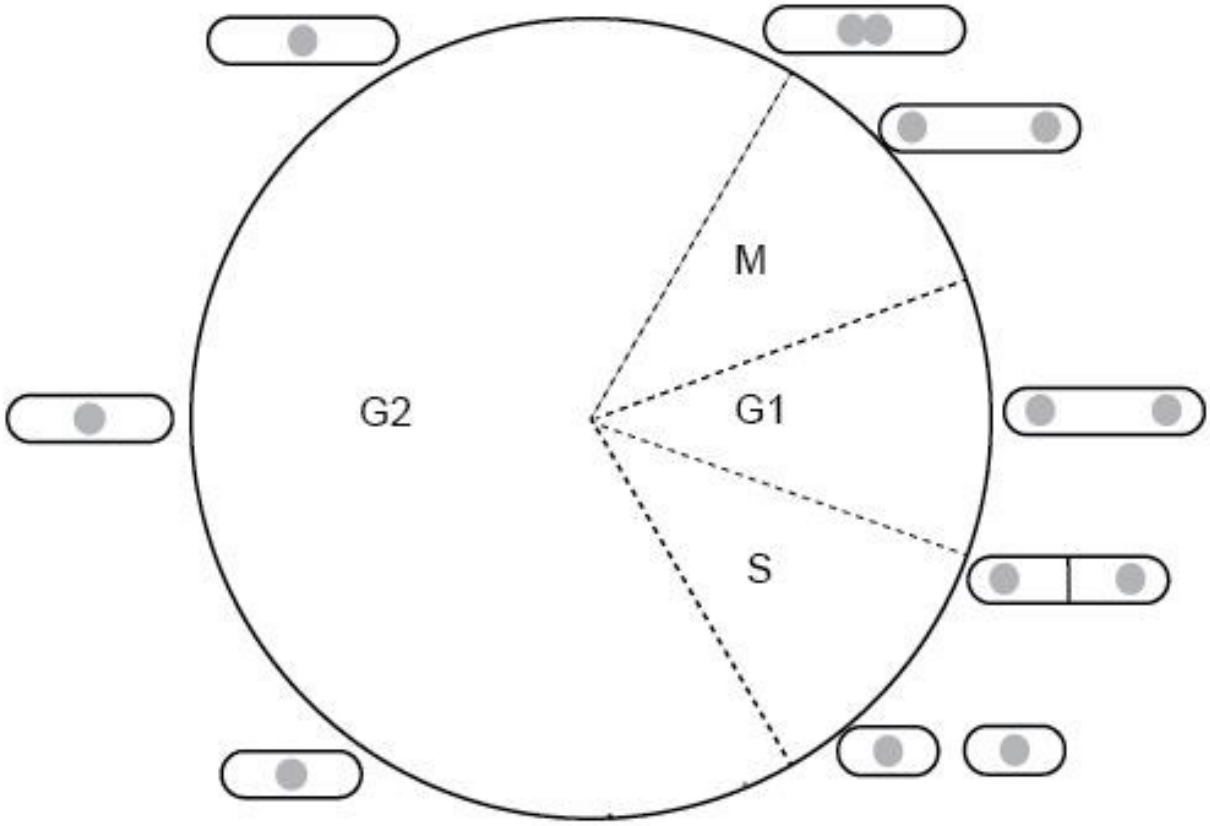

Figure 1.6. Fission yeast mitotic cell cycle

other eukaryotic cell cycles, in exponentially proliferating fission yeast cells, the nuclear division is offset or delayed relative to cell division. Consequently, cells with newly divided nuclei enter the next cell cycle and undergo G1 and S phases prior to cytokinesis. Thus, upon completion of cytokinesis, the newborn cell is already in G2 phase. Length of the cell is an effective metric for understanding its position in the cell cycle because of the strict control of cell size (Forsburg, 2003).

The fission yeast is a great model organism to study epigenetic regulation due to its highly conserved histone modifications (some of which such as histone H3K9 methylation and H4K20 methylation are absent in *S. cerevisiae*), simple genome organization, and amenability to genetic and biochemical manipulations. One of the most important chromatin-related discoveries made in *S. pombe* was in understanding the roles of epigenetic marks and the RNA interference machinery in pericentric heterochromatin structure and function.

1.6. Replication-dependent nucleosome assembly

Faithful duplication of the entire genome is an essential process for all cells. This arduous task is complicated by the existence of chromatin structures that pose a barrier to the replication machinery. An additional level of complexity arises when the local chromatin structure of a given locus, defined by the presence or absence of different post-translational modifications, must be faithfully propagated following replication. Histones, the architectural proteins of chromatin should also be doubled to restore a normal nucleosome density on newly replicated DNA. Eukaryotic cells have evolved molecular mechanisms to ensure a close coordination between the machinery involved in DNA replication and those responsible for chromatin assembly.

Maintenance of chromatin structure following DNA replication is achieved by two concerted processes. First, the progression of the replication fork is associated with a transient disruption of nucleosomes. Parental histones (also known pre-existing histones) derived from nucleosomes ahead of the replication forks are randomly segregated among the two nascent sister chromatids. Parental histone segregation

occurs contemporaneously with the incorporation of newly synthesized histones to fill gaps in the nucleosome arrays, a process called replication-coupled nucleosome assembly (Verreault, 2000).

Under physiological conditions, positively charged histones form insoluble aggregates with negatively charged DNA *in vitro*. Non-specific binding of histones to DNA is prevented by a variety of histone chaperones. They contribute to chromatin assembly *in vivo* by shielding the positive charge of histones and escorting them to sites of nucleosome assembly at the replication fork. One chaperone that plays a significant role in *de novo* nucleosome assembly is Chromatin Assembly Factor 1 (CAF-1). CAF-1 was originally identified as a protein that promoted the incorporation of new H3/H4 molecules onto nascent DNA during *in vitro* SV40 DNA replication (Smith and Stillman 1989). The human CAF1 protein consists of three subunits: p150, p60 and p48. Functional homologs of CAF1 have been found in mouse, *Drosophila*, budding and fission yeast.

CAF-1 is recruited to the replication fork through its interaction with the DNA polymerase processivity clamp PCNA and mediates deposition of two H3-H4 dimers onto nascent DNA. The chaperone Asf1 likely functions as a donor of H3-H4 dimers to CAF-1. Two H2A-H2B dimers then associate with the $(H3\text{-}H4)_2$ heterotetramer to complete nucleosome formation. The assembly factors that directly deposit H2A-H2B dimers onto chromatin remain unidentified (Annunziato 2012). In *S. cerevisiae*, the histone chaperone Rtt106 also interacts with the large subunit of CAF-1 and binds to

$(H3\text{-}H4)_2$ heterotetramers *in vivo*. This has led to the proposition that Rtt106 assembles H3-H4 dimers into tetramers before their deposition onto chromatin by CAF-1 (Fazly *et al.* 2012, Huang *et al.* 2005). In addition to histone chaperones, acetylation of multiple lysines on the N-terminal tails of both H3 and H4 function in *de novo* nucleosome assembly (See section 1.4.4.1)

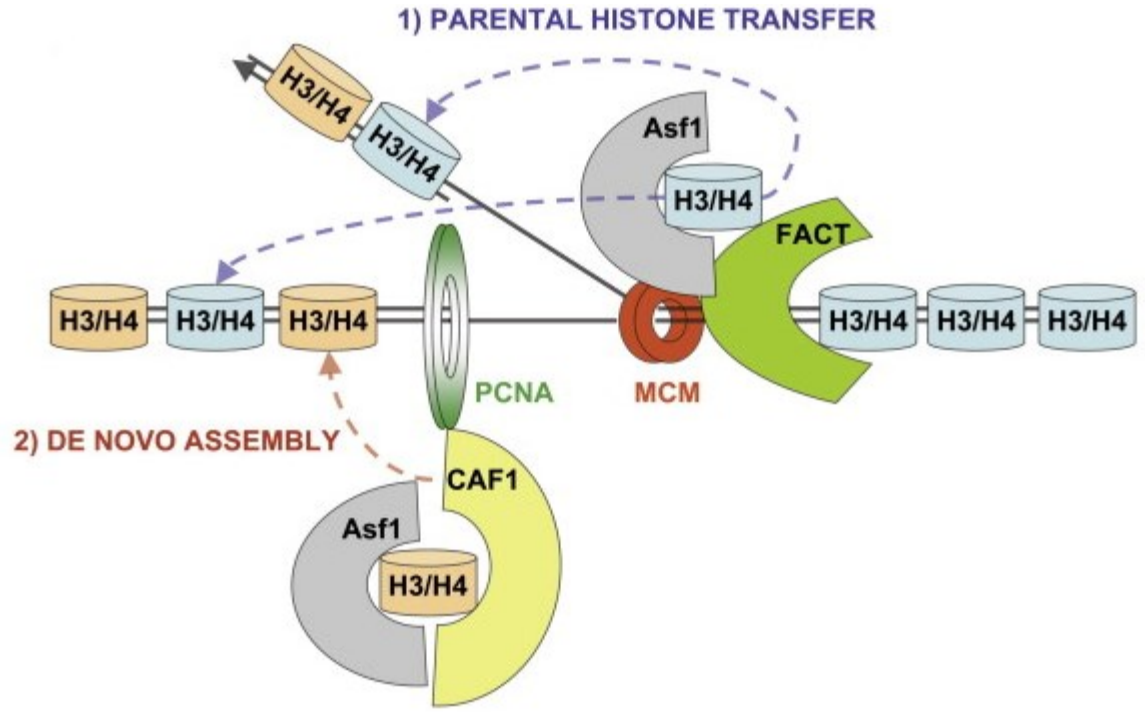

Figure 1.7 Replication-coupled nucleosome assembly. The duplication of chromatin structures involves two concerted steps that occur rapidly during the passage of DNA replication forks. The first process is the transfer of parental or pre-existing histones (pale blue disks) behind replication forks which, in general, can take place onto the DNA duplexes generated through either leading or lagging strand DNA synthesis. The gaps in nucleosome arrays created by DNA duplication are filled-in by deposition of newly synthesized histones (orange disks) that are acetylated at several distinct lysine residues (Rocha and Verreault, 2008).

1.7 Quantifying histone modifications

There exists a plethora of histone modifications and more are being identified thanks to high-resolution mass spectrometry methods. A recent survey has tallied 519 modifications occurring on 237 sites in core and linker histones (Zhao and Garcia, 2015). Many of the identified modifications have physiological functions making them important targets in both academic and clinical studies. Studying histone modifications is made difficult because of at least two of their properties: 1) More than one modification can occur at a given residue. For example, lysine 9 of histone H3 can be acetylated, mono, di, or tri-methylated. 2) More than one type of modification can be present at the same time over a short histone peptide. This is the case, for instance, for with H3K14 acetylation and H3S10 phosphorylation. 3) Histone modifications are dynamic. For example, histone H3 serine 10 and serine 28 are phosphorylated during the early stages of mitosis, concomitant with chromosome condensation, and both residues are dephosphorylated after the onset of anaphase. Despite these challenges, studies of histone modifications have provided a wealth of information on their role in regulating many cellular processes.

Researchers employ two main methods to study histone modifications. For many years, assays that rely on modification-specific antibodies have been the gold standard for identifying histone modifications. These assays include immunoblotting and Chromatin Immunoprecipitation (ChIP). However, several studies in recent years have shown that modification-specific antibodies exhibit cross-reactivity (Egelhofer et al., 2011; Fuchs et al., 2011; Nishikori et al., 2012) Amino acid sequences neighboring the

target residue, modifications on neighboring residues and chemical similarities of different modifications contribute toward antibody cross-reactivity (Drogaris et al., 2012; Fuchs et al., 2011; Rothbart et al., 2012; Zheng et al., 2016). Moreover, antibody-based detection methods cannot reveal the fraction of histone molecules that carry a specific modification. Although this has been achieved, the development of antibodies that specifically recognize combinatorial patterns of histone marks is far from trivial.

Liquid chromatography coupled with mass spectrometry (LC-MS) is a powerful technique that has enabled researchers to identify and validate histone post-translational modifications, quantitatively assess the changes in abundance of histone modifications during various physiological processes and to study combinatorial marks. Mass spectrometry is an analytical technique that measures the mass-to-charge (*m/z*) ratio of ions in the gas phase. A mass spectrometer has three main components, an ion source, a mass analyzer and a detector. The sample is ionized into the gas phase in the ion source. The ions are then introduced into a vacuum environment and guided through the mass analyzer where ions with different m/z ratios are filtered and separated. The ions finally reach the detector that converts the signals into the digital output plot of different *m/z* ratios and their intensities called a mass spectrum (Huang et al., 2015).

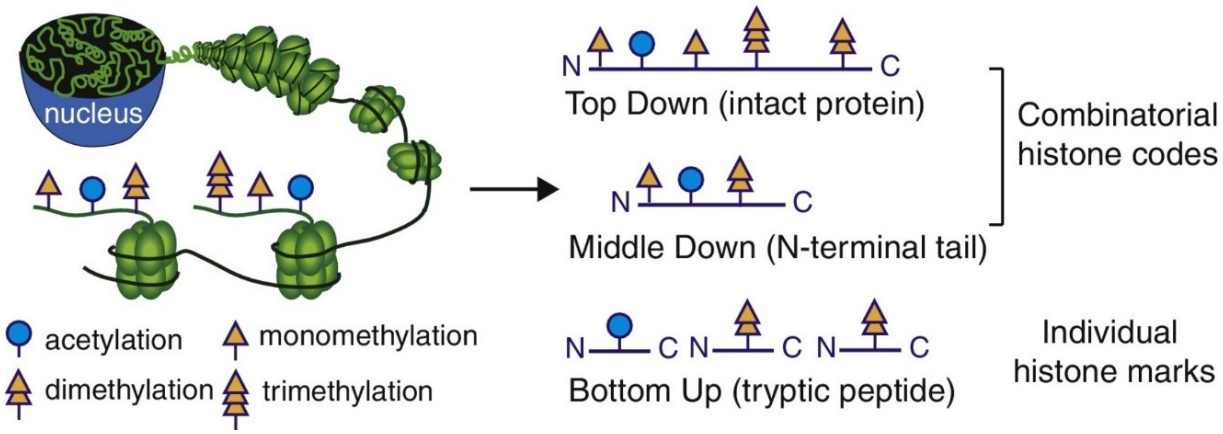

Figure 1.8. Summary of methods used for mass spectrometric analysis of histone modifications (Zheng et al. 2016).

Three analytical modes are generally used for studying histone modifications: Bottom Up, Middle Down and Top Down (Fig 1.7). In the Bottom-up analysis, histones are digested by a protease such as trypsin to generate short peptides that are then separated by reverse-phase high performance liquid chromatography (RP-HPLC), sequenced and quantified (Chait, 2006). In Bottom-up studies of histones, trypsin is the protease of choice due to its high efficiency and specificity for lysines and arginines (Olsen et al., 2004). However, the use of trypsin is not without its pitfalls. Histones are rich in lysines and arginines, and trypsin digestion, therefore, results in numerous extremely short peptides that are not retained by RP-HPLC columns. Furthermore, histones contain several adjacent lysines and arginines, a sequence feature that can lead to missed-cleavage events because trypsin will, in many cases, cleave at random after one of the adjacent lysine or arginine residues. Trypsin also fails to cleave the

peptide bond on the C-terminal side of modified lysines or arginines (with the notable exception of mono-methyl lysine). All these make quantitation of modifications on trypsin-generated peptides very difficult. These problems are, to some extent, overcome by chemical derivatization of histone samples prior to protease digestion (Garcia et al., 2007). Propionic anhydride is most commonly used for derivatization. In this method, the protein's N-terminal amino group and the ε-amino groups of unmodified and monomethylated lysines are propionylated, which imparts an increase in mass of 14 Da relative to the mass of an acetyl group. In addition, propionyl groups increase the hydrophobicity of the peptides leading to better retention and resolution during RP-HPLC (Karch et al., 2013; Zheng et al., 2016). It is crucial that propionylation of free lysines go to completion to accurately estimate stoichiometries of acetylation.

Middle-down and Top-down approaches involve the analysis of larger peptides or entire proteins, respectively, and are therefore more useful to study combinatorial patterns of histone modifications. Bottom-up MS has limited use in this approach because the tryptic peptides are small and, thus, may not contain all the PTMs that are part of a given pattern. In middle-down, the proteases commonly used are AspN for histone H4 and GluC for histone H3. Decreased sensitivity is a major caveat of middle-down and top-down MS. Larger peptides result in dilution of signal compared to smaller peptides. In addition, the larger number of PTMs increases the number of modified forms, which in turn weakens the signal for any combination of PTMs (Zheng et al., 2016). In both the middle-down and top-down approaches the types of chromatography required are very different. They are beyond the scope of this thesis

and are not discussed but for those interested the following review is insightful (Sidoli and Garcia, 2017).

There are many mass spectrometry-based proteomic studies published every year identifying histone modifications. Even though indirect approaches like Stable Isotope Labeling of Amino acids in Cell culture (SILAC) have been used to compare relative changes across conditions, very few studies have focused on the stoichiometry of histone marks. It is imperative to study the stoichiometry of histone acetylation to accurately interpret the biological significance of modification of individual sites. An interesting example is illustrated in *Candida albicans*, a fungal pathogen. Doxycycline-induced repression of *HST3*, the gene encoding the enzyme that deacetylates H3K56, increased the stoichiometry of H3K56 acetylation from 48% to 87%. Even though this increase was less than two-fold, the cellular phenotypes were dramatic (Wurtele et al., 2010). It is important to note that even though studying stoichiometric changes is critical, it presents the researcher with many technical challenges. One central issue is that post-translationally modified peptides and their corresponding unmodified counterparts have varying detection efficiencies. This necessitates that synthetic peptides for each of the modifications are analyzed for their ionization efficiencies. For example, to compare the stoichiometric changes of acetylation for a given tryptic peptide -$_{9}$KSTGGKAPR$_{17}$-, one should ideally analyze the detection efficiencies of synthetic peptides for the nine proteoforms illustrated below. This complexity is

proportional to the number of internal lysines and the combinatorial modifications of a given peptide.

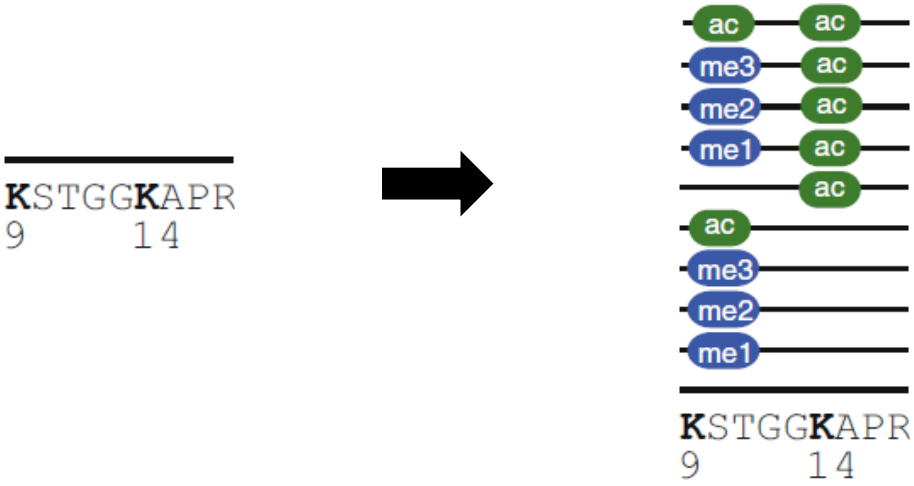

Figure 1.9. Proteoforms of the H3 tryptic peptide -$_{9}$KSTGGKAPR$_{17}$-

1.8. Thesis Objectives

Histone post-translational modifications, and particularly histone acetylation have been extensively studied. However, there have been very few attempts to study stoichiometries or abundance of modifications, and even fewer studies have tried to link histone stoichiometries to physiological relevance. Studies from our laboratory have shown that less than a two-fold increase (from 48% to 87%) in the acetylation stoichiometry of H3K56 in *C. albicans* is sufficient to cause catastrophic chromosome damage and loss of cell viability (Wurtele et al., 2010). I was interested in understanding the stoichiometries of acetylation on the N-terminal tail of histone H3 using mass spectrometry. The rationale for this was that a previous study from our lab

showed that treating mammalian cells with clinically-relevant histone deacetylase (HDAC) inhibitors such as SAHA and MS-275, substantially increased N-terminal tail acetylation of H3 and H4 (Drogaris et al., 2012). Nonetheless, this study did not determine stoichiometries of site-specific acetylation prior to and after exposure of cells to these HDAC inhibitors. Studying N-terminal tail acetylations of H3 and H4 proved difficult because of the amino acid sequence of histones. Trypsin is the preferred protease for bottom-up analysis, the most commonly used MS strategy for studying individual histone marks. Trypsin digestion of the N-terminal tails of histones generates some peptides that have more than one internal lysine. For instance, upon trypsin digestion, the N-terminal tail of H3 produces three peptides that have more than one internal lysine. This is further complicated in histone H4, which gives rise to a tryptic peptide with four internal lysines. Often, a modification such as acetylation can occur on different lysines on the same peptide thereby forming positional isomers (isomeric peptides). In conventional RP-LC/MS, positional isomers that have the same *m/z* ratio cannot be efficiently resolved and often elute as a single chromatographic peak. Some positional isomers, upon fragmentation of the intact tryptic peptide, produce isomer-specific fragments, which enable the quantification of acetylation site occupancy. However, there also exists, peptides which do not generate isomer-specific fragments. Consequently, the stoichiometries of acetylation cannot be accurately determined for these lysines.

In Chapter 2, we describe the development of mass spectrometry tools and an algorithm, known as Iso-PeptidAce, to determine the relative abundance of isomeric histone peptides. Iso-PeptidAce was built based on information garnered from the time

of elution during RP-HPLC and the fragmentation properties of synthetic peptides corresponding to positional isomers that contain two or more internal lysines that are potentially acetylated. The Iso-PeptidAce algorithm deconvolutes composite MS/MS spectra that arise from mixtures of two or more positional isomers. We also demonstrated that Iso-PeptidAce can be successfully applied to analyze biological samples such as affinity-purified histones bound to CAF1 or histones isolated from cells treated with HDAC inhibitors.

In Chapter 3, we further establish the suitability of Iso-PeptidAce to study histone deacetylase mutants in fission yeast. Histone deacetylases regulate key cellular processes by site-specific deacetylation of a subset of non-histone and histone proteins. Altered expression of HDAC genes and/or perturbation of their catalytic activity have been frequently correlated to the onset and progression of a variety of diseases including cancer. Even though many studies have reported the functions of HDACs using ChIP, our analyses provide molecular-level insights into site-specific acetylation in HDAC mutants of the fission yeast model organism.

In Chapter 4, we illustrate the identification of a novel pattern of histone acetylation based on the *in vivo* abundance of histone H3-K14 acetylation H3-K23 acetylation. We show that about 20-25% of histone H3 molecules are acetylated on lysine residues K14 and K23 in a variety of human cell types, *Drosophila* S2 cells and fission yeast. We have endeavored to identify the physiological roles of this pattern of acetylation using histone and HAT mutants in fission yeast. Our results suggest that the severe phenotypes that we observed with one of the mutants are likely due to a change in the amino acid lysine, and not necessarily due to a lack of acetylation of the same lysine.

1.9 References

Ahmad, K., and Henikoff, S. (2002). The histone variant H3.3 marks active chromatin by replication-independent nucleosome assembly. Mol. Cell *9*, 1191–1200.

Akiyama, T., Suzuki, O., Matsuda, J., and Fugaku, A. (2011). Dynamic replacement of histone H3 variants reprograms epigenetic marks in early mouse embryos. PLoS Genet. e1002279.

Allard, S., Utley, R.T., Savard, J., Clarke, A., Grant, P., Brandl, C.J., Pillus, L., Workman, J.L., and Côté, J. (1999). The NuA4 transcription activation/histone H4 acetyltransferase complex contains the essential Esa1 protein as the catalytic subunit and the essential ATM-related cofactor Tra1p. Biochem. Cell Biol. *77*, 383.

Allfrey, V.G., and Mirsky, A.E. (1964). Structural modifications of histones and their possible role in the regulation of RNA synthesis. Science *144*, 559.

Allfrey, V.G., Faulkner, R., and Mirsky, A.E. (1964). Acetylation and methylation of histones and their possible role in the regulation of RNA synthesis. Proc. Natl. Acad. Sci. *51*, 786–794.

Allis, C.D., Berger, S.L., Cote, J., Dent, S., Jenuwien, T., Kouzarides, T., Pillus, L., Reinberg, D., Shi, Y., Shiekhattar, R., et al. (2007). New nomenclature for chromatin-modifying enzymes. Cell *131*, 633–636.

Allshire, R.C., and Ekwall, K. (2015). Epigenetic regulation of chromatin states in Schizosaccharomyces pombe. Cold Spring Harb. Perspect. Biol. *7*, a018770.

Annunziato, A.T. (2012). Assembling chromatin: the long winding road. Biochim. Biophys. Acta Gene Structure Expr. *1819*, 196–210.

Annunziato, A.T., and Seale, R.L. (1983). Histone deacetylation is required for the maturation of newly replicated chromatin. J. Biol. Chem. *258*, 12675–12684.

Aramayo, R., and Selker, E.U. (2013). Neurospora crassa, a model system for epigenetics research. Cold Spring Harb. Perspect. Biol. *5*, 1–18.

van Attikum, H., and Gasser, S.M. (2005). The histone code at DNA breaks: a guide to repair? Nat. Rev. Mol. Cell Biol. *6*, 757–765.

van Attikum, H., Fritsch, O., Hohn, B., and Gasser, S.M. (2004). Recruitment of the INO80 Complex by H2A Phosphorylation Links ATP-Dependent Chromatin Remodeling with DNA Double-Strand Break Repair. Cell *119*, 777–788.

Bannister, A.J., and Kouzarides, T. (2011). Regulation of chromatin by histone modifications. Cell Res. *21*, 381–395.

Banumathy, G., Somaiah, N., Zhang, R., Tang, Y., Hoffmann, J., Andrake, M., Ceulemans, H., Schultz, D., Marmorstein, R., and Adams, P.D. (2009). Human UBN1 is an ortholog of yeast Hpc2p and has an essential role in the HIRA/ASF1a chromatin-remodeling pathway in senescent cells. Mol. Cell. Biol. *29*, 758–770.

Barman, H.K., Takami, Y., Ono, T., Nishijima, H., Sanematsu, F., Shibahara, K-Ichi, and Nakayama, T. (2006). Histone acetyltransferase 1 is dispensable for replication-coupled chromatin assembly but contributes to recover DNA damages created following replication blockage in vertebrate cells. Biochem. Biophys. Res. Commun. *345*, 1547–1557.

Bennett, G., and Peterson, C.L. (2015). SWI/SNF recruitment to a DNA double-strand break by the NuA4 and Gcn5 histone acetyltransferases. DNA Repair (Amst). *30*, 38–45.

Benson, L.J., Gu, Y., Yakovleva, T., Tong, K., Barrows, C., Strack, C.L., Cook, R.G., Mizzen, C.A., and Annunziato, A.T. (2006). Modifications of H3 and H4 during chromatin replication, nucleosome assembly, and histone exchange. J. Biol. Chem. *281*, 9287–9296.

Berger, S.L. (2007). The complex language of chromatin regulation during transcription. Nature *447*, 407–412.

Berger, S.L., Kouzarides, T., Shiekhattar, R., and Shilatifard, A. (2009). An operational definition of epigenetics An operational definition of epigenetics. 781–783.

Bernier, M., Luo, Y., Nwokelo, K.C., Goodwin, M., Dreher, S.J., Zhang, P., Parthun, M.R., Fondufe-Mittendorf, Y., Ottesen, J.J., and Poirier, M.G. (2015). Linker histone H1 and H3K56 acetylation are antagonistic regulators of nucleosome dynamics. Nat. Commun. *6*, 10152.

Bernsden, C.E., and Denu, J.M. (2008). Catalysis and substrate selection by histone/protein lysine acetyltransferases. Curr. Opin. Struct. Biol. *18*, 682–689.

Bird, A. (2007). Perceptions of epigenetics. Nature *447*, 396–398.

Bird, A.W., Yu, D.Y., Pray-Grant, M.G., Qiu, Q., and Christman, M.F. (2002). Acetylation of histone H4 by Esa1 is required for DNA double-strand break repair. Nature *419*, 411–415.

Boddy, M.N., and Russell, P. (1999). DNA replication checkpoint control. Front. Biosci. *4*, D841–D848.

Brownell, J.E., Zhou, J., Ranalli, T., Kobayashi, R., Edmondson, D.G., Roth, S.Y., and Allis, C.D. (1996). Tetrahymena histone acetyltransferase A: a homolog to yeast Gcn5p linking histone acetylation to gene activation. Cell *84*, 843–851.

Burgess, R.J., Zhou, H., Han, J., and Zhang, Z. (2010). A role for Gcn5 in replication-coupled nucleosome assembly. Mol. Cell *37*, 469–480.

Celic, I., Masumoto, H., Griffith, W.P., Meluh, P., Cotter, R.J., Boeke, J.D., and Verreault, A. (2006). The sirtuins Hst3 and Hst4p preserve genome integrity by controlling histone H3 lysine 56 deacetylation. Curr. Biol. *16*, 1280–1289.

Chait, B.T. (2006). Mass Spectrometry : Bottom-Up or Top-down? October *314*, 65–66.

Chalker, D.L., Meyer, E., and Mochizuki, K. (2013). Epigenetics of ciliates. Cold Spring Harb. Perspect. Biol. *5*, a017764.

Chicoine, L.G., Schulman, I.G., Richman, R., Cook, R.G., and Allis, C.D. (1986). Nonrandom utilization of acetylation sites in histones isolated from Tetrahymena. Evidence for functionally distinct H4 acetylation sites. J. Biol. Chem. *261*, 1071–1076.

Choy, J.S., and Kron, S.J. (2002). NuA4 subunit Yng2 function in intra-S-phase DNA damage response. Mol. Cell. Biol. *22*, 8215–8225.

Clements, A., Poux, A.N., Lo, W.-S., Pillus, L., Berger, S.L., and Marmorstein, R. (2003). Structural basis for histone and phosphohistone binding by the GCN5 histone acetyltransferase. Mol. Cell *12*, 461–473.

Cosgrove, M.S., Boeke, J.D., and Wolberger, C. (2004). Regulated nucleosome mobility and the histone code. Nat. Struct. Mol. Biol. *11*, 1037–1043.

Cousens, L.S., and Alberts, B.M. (1982). Accessibility of newly synthesized chromatin to histone acetylase. J. Biol. Chem. *257*, 3945–3949.

Downs, J.A., Allard, S., Jobin-Robitaille, O., Javaheri, A., Auger, A., Bouchard, N., Kron, S.J., Jackson, S.P., and Côté, J. (2004). Binding of chromatin-modifying activities to phosphorylated histone H2A at DNA damage sites. Mol. Cell *16*, 979–990.

Downs, J. a, Lowndes, N.F., and Jackson, S.P. (2000). A role for Saccharomyces cerevisiae histone H2A in DNA repair. Nature *408*, 1001–1004.

Drogaris, P., Villeneuve, V., Pomiès, C., Lee, E.-H., Bourdeau, V., Bonneil, É., Ferbeyre, G., Verreault, A., and Thibault, P. (2012). Histone deacetylase inhibitors globally enhance H3/H4 tail acetylation without affecting H3 lysine 56 acetylation. Sci. Rep. *2*, 1–12.

Dunleavy, E.M., Roche, D., Tagami, H., Lacoste, N., Ray-Gallet, D., Nakamura, Y., Daigo, Y., Nakatani, Y., and Almouzni-Pettinotti, G. (2009). HJURP Is a cell-cycle-dependent maintenance and deposition factor of CENP-A at centromeres. Cell *137*, 485–497.

Dutnall, R.N., and Ramakrishnan, V. (1997). Twists and turns of the nucleosome: tails without ends. Structure *5*, 1255–1259.

Egelhofer, T. a, Minoda, A., Klugman, S., Lee, K., Kolasinska-Zwierz, P., Alekseyenko, A. a, Cheung, M.-S., Day, D.S., Gadel, S., Gorchakov, A. a, et al. (2011). An assessment of histone-modification antibody quality. Nat. Struct. Mol. Biol. *18*, 91–93.

Elgin, S.C.R., and Reuter, G. (2013). Position-effect variegation, heterochromatin formation, and gene silencing in Drosophila. Cold Spring Harb. Perspect. Biol. *5*, a017780.

Falkenberg, K.J., and Johnstone, R.W. (2014). Histone deacetylases and their inhibitors in cancer, neurological diseases and immune disorders. Nat. Rev. Drug Discov. *13*, 673–691.

Filipescu, D., Müller, S., and Almouzni, G. (2014). Histone H3 variants and their chaperones during development and disease: contributing to epigenetic control. Annu. Rev. Cell Dev. Biol. *30*, 615–646.

Filippakopoulos, P., and Knapp, S. (2012). The bromodomain interaction module. FEBS Lett. *586*, 2692–2704.

Filippakopoulos, P., and Knapp, S. (2014). Targeting bromodomains: epigenetic readers of lysine acetylation. Nat. Rev. Drug Discov. *13*, 337–356.

Fillingham, J., Kainth, P., Lambert, J.P., van Bakel, H., Tsui, K., Peña-Castillo, L., Nislow, C., Figeys, D., Hughes, T.R., Greenblatt, J., et al. (2009). Two-color cell array screen reveals interdependent roles for histone chaperones and a chromatin boundary regulator in histone gene repression. Mol. Cell *35*, 340–351.

Foltz, D.R., Jansen, L.E.T., Bailey, A.O., Yates, J.R., Bassett, E.A., Wood, S., Black, B.E., and Cleveland, D.W. (2009). Centromere-specific assembly of CENP-A nucleosomes is mediated by HJURP. Cell *137*, 472–484.

Forsburg, S.L. (2003). Growth and manipulation of S. pombe. Curr. Protoc. Mol. Biol. *Chapter 13*, Unit 13.16.

Frye, R.A. (2000). Phylogenetic classification of prokaryotic and eukaryotic Sir2-like proteins. Biochem. Biophys. Res. Commun. *273*, 793–798.

Fuchs, S.M., Krajewski, K., Baker, R.W., Miller, V.L., and Strahl, B.D. (2011). Influence of combinatorial histone modifications on antibody and effector protein recognition. Curr. Biol. *21*, 53–58.

Garcia, B.A., Mollah, S., Ueberheide, B.M., Busby, S.A., Shabanowitz, J., and Hunt, D.F. (2007). Chemical derivatization of histones for facilitated analysis by mass spectrometry. Nat. Protoc. *2*, 933–938.

Goldberg, A.D., Banaszynski, L.A., Noh, K.-M.M., Lewis, P.W., Elsaesser, S.J., Stadler, S., Dewell, S., Law, M., Guo, X., Li, X., et al. (2010). Distinct factors control histone variant H3.3 localization at specific genomic regions. Cell *140*, 678–691.

Grant, P.A., Duggan, L., Côté, J., Roberts, S.M., Brownell, J.E., Candau, R., Ohba, R., Owen-Hughes, T., Allis, C.D., Winston, F., et al. (1997). Yeast Gcn5 functions in two multisubunit complexes to acetylate nucleosomal histones: Characterization of an Ada complex and the SAGA (Spt/Ada) complex. Genes Dev. *11*, 1640–1650.

Grant, P.A., Eberharter, A., John, S., Cook, R.G., Turner, B.M., and Workman, J.L. (1999). Expanded lysine acetylation specificity of Gcn5 in native complexes. J. Biol. Chem. *274*, 5895–5900.

Green, C.M., and Almouzni, G. (2002). When repair meets chromatin. EMBO Rep. *3*, 28–33.

Gregoretti, I., Lee, Y.-M., and Goodson, H. V (2004). Molecular evolution of the Histone deacetylase family: functional implications of phylogenetic analysis. J. Mol. Biol. *338*, 17–31.

Grewal, S.I.S., and Jia, S. (2007). Heterochromatin revisited. Nat. Rev. Genet. *8*, 35–46.

Grunstein, M., and Gasser, S.M. (2013). Chapter 4 Epigenetics in Saccharomyces Cerevisiae. In Cold Spring Harbor Perspectives in Biology, p. a017491.

Haldar, D., and Kamakaka, R.T. (2008). Schizosaccharomyces pombe Hst4 functions in DNA damage response by regulating histone H3 K56 acetylation. Eukaryot. Cell *7*, 800–813.

Hayles, J., and Nurse, P. (2016). Introduction to Fission Yeast as a Model System. In Fission Yeast: A Laboratory Manual, I. Hagan, A.M. Carr, A. Grallert, and P. Nurse, eds. (Cold Spring Harbor Laboratory Press), pp. 1–11.

Hodawadekar, S.C., and Marmorstein, R. (2007). Chemistry of acetyl transfer by histone modifying enzymes: structure, mechanism and implications for effector design. Oncogene *26*, 5528–5540.

Hoffman, C.S., Wood, V., and Fantes, P.A. An ancient yeast for young geneticists: A primer on the Schizosaccharomyces pombe Model System.

Huang, H., Sabari, B.R., Garcia, B.A., David Allis, C., and Zhao, Y. (2014). SnapShot: Histone modifications. Cell *159*, 458–458.e1.

Huang, H., Lin, S., Garcia, B.A., and Zhao, Y. (2015). Quantitative proteomic analysis of histone modifications. Chem. Rev. *115*, 2376–2418.

Huisinga, K.L., Brower-Toland, B., and Elgin, S.C.R. (2006). The contradictory definitions of heterochromatin: Transcription and silencing. Chromosoma *115*, 110–122.

Ikura, T., Ogryzko, V. V, Grigoriev, M., Groisman, R., Wang, J., Horikoshi, M., Scully, R., Qin, J., and Nakatani, Y. (2000). Involvement of the TIP60 histone acetylase complex in DNA repair and apoptosis. Cell *102*, 463–473.

Jackson, V., Shires, A., Tanphaichitr, N., and Chalkley, R. (1976). Modifications to histones immediately after synthesis. J. Mol. Biol. *104*, 471–483.

Jansen, L.E.T., Black, B.E., Foltz, D.R., and Cleveland, D.W. (2007). Propagation of centromeric chromatin requires exit from mitosis. J. Cell Biol. *176*, 795–805.

Jasencakova, Z., Scharf, A.N.D., Ask, K., Corpet, A., Imhof, A., Almouzni, G., and Groth, A. (2010). Replication stress interferes with histone recycling and predeposition marking of new histones. Mol. Cell *37*, 736–743.

Jazayeri, A., McAinsh, A.D., and Jackson, S.P. (2004). Saccharomyces cerevisiae Sin3p facilitates DNA double-strand break repair. Proc. Natl. Acad. Sci. U. S. A. *101*, 1644–1649.

Jenuwein, T., Allis, C.D., and Allis, D.C. (2001). Translating the histone code. Science (80-.). *293*, 1074–1080.

Karch, K.R., DeNizio, J.E., Black, B.E., and Garcia, B.A. (2013). Identification and interrogation of combinatorial histone modifications. Front. Genet. *4*, 1–15.

Kimura, A., Matsubara, K., and Horikoshi, M. (2005). A decade of histone acetylation: Marking eukaryotic chromosomes with specific codes. J. Biochem. *138*, 647–662.

Kleff, S., Andrulis, E.D., Anderson, C.W., and Sternglanz, R. (1995). Identification of a gene encoding a yeast histone H4 acetyltransferase. J. Biol. Chem. *270*, 24674–24677.

Kobor, M.S., Venkatasubrahmanyam, S., Meneghini, M.D., Gin, J.W., Jennings, J.L., Link, A.J., Madhani, H.D., and Rine, J. (2004). A protein complex containing the conserved Swi2/Snf2-related ATPase Swr1p deposits histone variant H2A.Z into euchromatin. PLoS Biol. *2*.

Kornberg, R.D. (1974). Chromatin structure: a repeating unit of histones and DNA. Science *184*, 868–871.

Kouzarides, T. (2007). Chromatin modifications and their function. Cell *128*, 693–705.

Kuo, M.H., Brownell, J.E., Sobel, R.E., Ranalli, T.A., Cook, R.G., Edmondson, D.G., Roth, S.Y., and Allis, C.D. (1996). Transcription-linked acetylation by Gcn5p of histones H3 and H4 at specific lysines. Nature *383*, 269–272.

Kuo, M.H., Vom Baur, E., Struhl, K., and Allis, C.D. (2000). Gcn4 activator targets Gcn5 histone acetyltransferase to specific promoters independently of transcription. Mol. Cell *6*, 1309–1320.

Kurdistani, S.K., Tavazoie, S., and Grunstein, M. (2004). Mapping global histone acetylation patterns to gene expression. Cell *117*, 721–733.

Kyriakakis, E., Markaki, M., and Tavernarakis, N. (2016). Caenorhabditis elegans as a model for cancer research. Mol. Cell. Oncol. e975027-1-11.

Latreille, D., Bluy, L., Benkirane, M., and Kiernan, R.E. (2014). Identification of histone 3 variant 2 interacting factors. Nucleic Acids Res. *42*, 3542–3550.

Lee, K.K., and Workman, J.L. (2007). Histone acetyltransferase complexes: one size doesn't fit all. Nat. Rev. Mol. Cell Biol. *8*, 284–295.

Lewis, P.W., Elsaesser, S.J., Noh, K.-M., Stadler, S.C., and Allis, C.D. (2010). Daxx is an H3.3-specific histone chaperone and cooperates with ATRX in replication-independent chromatin assembly at telomeres. Proc. Natl. Acad. Sci. U. S. A. *107*, 14075–14080.

Li, B., Carey, M., and Workman, J.L. (2007). The Role of chromatin during transcription. Cell *128*, 707–719.

Li, Q., Zhou, H., Wurtele, H., Davies, B., Horazdovsky, B., Verreault, A., and Zhang, Z. (2008). Acetylation of histone H3 lysine 56 regulates replication-coupled nucleosome assembly. Cell *134*, 244–255.

Ling, X., Harkness, T.A., Schultz, M.C., Fisher-Adams, G., and Grunstein, M. (1996). Yeast histone H3 and H4 amino termini are important for nucleosome assembly in vivo and in vitro: redundant and position-independent functions in assembly but not in gene regulation. Genes Dev. *10*, 686–699.

Liu, C.L., Kaplan, T., Kim, M., Buratowski, S., Schreiber, S.L., Friedman, N., and Rando, O.J. (2005). Single-nucleosome mapping of histone modifications in S. cerevisiae. PLoS Biol. *3*.

Louie, A.J., Candido, E.P., and Dixon, G.H. (1974). Enzymatic modifications and their possible roles in regulating the binding of basic proteins to DNA and in controlling chromosomal structure. Cold Spring Harb. Symp. Quant. Biol. *38*, 803–819.

Luger, K., Mäder, A.W., Richmond, R.K., Sargent, D.F., Richmond, T.J., and Mä, A.W. (1997). Crystal structure of the nucleosome core particle at 2.8 A resolution. Nature *389*, 251–260.

Luger, K., Dechassa, M.L., and Tremethick, D.J. (2012). New insights into nucleosome and chromatin structure: an ordered state or a disordered affair? Nat. Rev. Mol. Cell Biol. *13*, 436–447.

Ma, X.J., Wu, J., Altheim, B. a, Schultz, M.C., and Grunstein, M. (1998). Deposition-related sites K5/K12 in histone H4 are not required for nucleosome deposition in yeast. Proc. Natl. Acad. Sci. U. S. A. *95*, 6693–6698.

Maas, N.L., Miller, K.M., DeFazio, L.G., and Toczyski, D.P. (2006). Cell cycle and checkpoint regulation of histone H3 K56 acetylation by Hst3 and Hst4. Mol. Cell *23*, 109–119.

Marks, P. a (2010). Histone deacetylase inhibitors: a chemical genetics approach to understanding cellular functions. Biochim. Biophys. Acta *1799*, 717–725.

Marks, P.A., and Xu, W.-S. (2009). Histone deacetylase inhibitors: Potential in cancer therapy. Expert Opin. Investig. Drugs *107*, 600–608.

Marmorstein, R., and Zhou, M.-M. (2014). Writers and readers of histone acetylation: structure, mechanism, and inhibition. Cold Spring Harb. Perspect. Biol. *6*, a0187762.

Martienssen, R., and Moazed, D. (2015). RNAi and heterochromatin assembly. Cold Spring Harb. Perspect. Biol. *7*, a019323.

Masumoto, H., Hawke, D., Kobayashi, R., and Verreault, A. (2005). A role for cell-cycle-regulated histone H3 lysine 56 acetylation in the DNA damage response. Nature *436*, 294–298.

Morrison, A.J., Highland, J., Krogan, N.J., Arbel-Eden, A., Greenblatt, J.F., Haber, J.E., and Shen, X. (2004). INO80 and γ-H2AX interaction link ATP-dependent chromatin remodeling to DNA damage repair. Cell *119*, 767–775.

Muller, S., Filippakopoulos, P., and Knapp, S. (2011). Bromodomains as therapeutic targets. Expert Rev. Mol. Med. *13*, e29.

Murr, R., Loizou, J.I., Yang, Y.-G., Cuenin, C., Li, H., Wang, Z.-Q., and Herceg, Z. (2006). Histone acetylation by Trrap–Tip60 modulates loading of repair proteins and repair of DNA double-strand breaks. Nat. Cell Biol. *8*, 91–99.

Murray, K. (1964). The occurrence of epsilon-N-methyl lysine in histones. Biochemistry *3*, 10–15.

Nagy, Z., and Tora, L. (2007). Distinct GCN5/PCAF-containing complexes function as co-activators and are involved in transcription factor and global histone acetylation. Oncogene *26*, 5341–5357.

Nakamura, T.M., Du, L.-L., Redon, C., and Russell, P. (2004). Histone H2A phosphorylation controls Crb2 recruitment at DNA breaks, maintains checkpoint arrest, and influences DNA repair in fission yeast. Mol. Cell. Biol. *24*, 6215–6230.

Neumann, H., Hancock, S.M., Buning, R., Routh, A., Chapman, L., Somers, J., Owen-Hughes, T., van Noort, J., Rhodes, D., and Chin, J.W. (2009). A method for genetically installing site-specific acetylation in recombinant histones defines the effects of H3 K56 acetylation. Mol. Cell *36*, 153–163.

Nishikori, S., Hattori, T., Fuchs, S.M., Yasui, N., Wojcik, J., Koide, A., Strahl, B.D., and Koide, S. (2012). Broad ranges of affinity and specificity of anti-histone antibodies revealed by a quantitative peptide immunoprecipitation assay. J. Mol. Biol. *424*, 391–399.

Noguchi, E., Ansbach, A.B., Noguchi, C., and Russell, P. (2009). Assays used to study the DNA replication checkpoint in fission yeast. Methods Mol. Biol. *521*, 493–507.

Nyberg, K.A., Michelson, R.J., Putnam, C.W., and Weinert, T.A. (2002). Toward Maintaining the Genome: DNA damage and replication checkpoints. Annu. Rev. Genet. *36*, 617–656.

Olins, D.E., and Olins, A.L. (2003). Chromatin history: our view from the bridge. Nat. Rev. Mol. Cell Biol. *4*, 809–814.

Olsen, J. V., Ong, S.-E., and Mann, M. (2004). Trypsin cleaves exclusively C-terminal to arginine and lysine Residues. Mol. Cell. Proteomics *3*, 608–614.

Ou, H.D., Phan, S., Deerinck, T.J., Thor, A., Ellisman, M.H., and O'Shea, C.C. (2017). ChromEMT: Visualizing 3D chromatin structure and compaction in interphase and mitotic cells. Science (80-.). *357*.

Oudet, P., Gross-Bellard, M., and Chambon, P. (1975). Electron microscopic and biochemical evidence that chromatin structure is a repeating unit. Cell *4*, 281–300.

Ozdemir, A., Spicuglia, S., Lasonder, E., Vermeulen, M., Campsteijn, C., Stunnenberg, H.G., and Logie, C. (2005). Characterization of lysine 56 of histone H3 as an acetylation site in Saccharomyces cerevisiae. J. Biol. Chem. *280*, 25949–25952.

Park, E.C., and Szostak, J.W. (1992). ARD1 and NAT1 proteins form a complex that has N-terminal acetyltransferase activity. EMBO J. *11*, 2087–2093.

Parthun, M.R. (2007). Hat1: the emerging cellular roles of a type B histone acetyltransferase. Oncogene *26*, 5319–5328.

Parthun, M.R., Widom, J., and Gottschling, D.E. (1996). The major cytoplasmic histone acetyltransferase in yeast: Links to chromatin replication and histone metabolism. Cell *87*, 85–94.

Patel, D.J. (2016). A structural perspective on the readout of epigenetic histone and DNA methylation marks. Cold Spring Harb. Perspect. Biol. *8*, 1–48.

Patel, D.J., and Wang, Z. (2013). Readout of epigenetic modifications. Annu. Rev. Biochem. *82*, 81–118.

Perry, C.A., and Annunziato, A.T. (1989). Influence of histone acetylation on the solubility, H1 content and DNase I sensitivity of newly assembled chromatin. Nucleic Acids Res. *17*, 4275–4291.

Pikaard, C.S., and Mittelsten Scheid, O. (2014). Epigenetic regulation in plants. Cold Spring Harb. Perspect. Biol. *6*, a019315.

Pokholok, D.K., Harbison, C.T., Levine, S., Cole, M., Hannett, N.M., Lee, T.I., Bell, G.W., Walker, K., Rolfe, P.A., Herbolsheimer, E., et al. (2005). Genome-wide map of nucleosome acetylation and methylation in yeast. Cell *122*, 517–527.

Poux, A.N., and Marmorstein, R. (2003). Molecular Basis for Gcn5 / PCAF Histone Acetyltransferase Selectivity for Histone. Biochemistry *42*, 14366–14374.

Pray-Grant, M.G., Schieltz, D., McMahon, S.J., Wood, J.M., Kennedy, E.L., Cook, R.G., Workman, J.L., Yates, J.R., and Grant, P.A. (2002). The novel SLIK histone acetyltransferase complex functions in the yeast retrograde response pathway. Mol. Cell. Biol. *22*, 8774–8786.

Ptashne, M. (2007). On the use of the word epigenetic. Curr. Biol. *17*, R233–R236.

Qin, S., and Parthun, M.R. (2002). Histone H3 and the histone acetyltransferase Hat1p contribute to DNA double-strand break repair. Mol. Cell. Biol. *22*, 8353–8365.

Rai, T.S., Puri, A., McBryan, T., Hoffman, J., Tang, Y., Pchelintsev, N.A., van Tuyn, J., Marmorstein, R., Schultz, D.C., and Adams, P.D. (2011). Human CABIN1 is a functional member of the human HIRA/UBN1/ASF1a histone H3.3 chaperone complex. Mol. Cell. Biol. *31*, 4107–4118.

Rando, O.J. (2007). Global patterns of histone modifications. Curr. Opin. Genet. Dev. *17*, 94–99.

Rando, O.J. (2012). Combinatorial complexity in chromatin structure and function: revisiting the histone code. Curr. Opin. Genet. Dev. *22*, 148–155.

Ray-Gallet, D., Quivy, J.-P., Scamps, C., Martini, E.M.-D., Lipinski, M., and Almouzni, G. (2002). HIRA is critical for a nucleosome assembly pathway independent of DNA synthesis. Mol. Cell *9*, 1091–1100.

Recht, J., Tsubota, T., Tanny, J.C., Diaz, R.L., Berger, J.M., Zhang, X., Garcia, B.A., Shabanowitz, J., Burlingame, A.L., Hunt, D.F., et al. (2006). Histone chaperone Asf1 is required for histone H3 lysine 56 acetylation, a modification associated with S phase in mitosis and meiosis. Proc. Natl. Acad. Sci. *103*, 6988–6993.

Reddy, B.D., Wang, Y., Niu, L., Higuchi, E.C., Marguerat, S.B., Bähler, J., Smith, G.R., and Jia, S. (2011). Elimination of a specific histone H3K14 acetyltransferase complex bypasses the RNAi pathway to regulate pericentric heterochromatin functions. Genes Dev. *25*, 214–219.

Reyes-Turcu, F.E., and Grewal, S.I.S. (2012). Different means, same end-heterochromatin formation by RNAi and RNAi-independent RNA processing factors in fission yeast. Curr. Opin. Genet. Dev. *22*, 156–163.

Riggs, A.D., Martienssen, R.A., and Russo, V.E. (1996). Introduction (Cold Spring Harbor Laboratory Press).

Rocha, W., and Verreault, A. (2008). Clothing up DNA for all seasons: Histone chaperones and nucleosome assembly pathways. FEBS Lett. *582*, 1938–1949.

Roth, F.P., Lipshitz, H.D., and Andrews, B.J. (2009). Q&A: epistasis. J. Biol. *8*, 35.

Rothbart, S.B., Lin, S., Britton, L.-M., Krajewski, K., Keogh, M.-C., Garcia, B. a, and Strahl, B.D. (2012). Poly-acetylated chromatin signatures are preferred epitopes for site-specific histone H4 acetyl antibodies. Sci. Rep. *2*, 489.

Rufiange, A., Jacques, P.É., Bhat, W., Robert, F., and Nourani, A. (2007). Genome-wide replication-independent histone H3 exchange occurs predominantly at promoters and implicates H3 K56 acetylation and Asf1. Mol. Cell *27*, 393–405.

Ruiz-Carrillo, A., Wangh, L.J., and Allfrey, V.G. (1975). Processing of newly synthesized histone molecules. Science *190*, 117–128.

Sancar, a (1995). DNA repair in humans. Annu. Rev. Genet. *29*, 69–105.

Sapountzi, V., and Côté, J. (2011). MYST-family histone acetyltransferases: Beyond chromatin. Cell. Mol. Life Sci. *68*, 1147–1156.

Seale, R.L. (1975). Assembly of DNA and protein during replication in HeLa cells. Nature *255*, 247–249.

Sealy, L., and Chalkley, R. (1978). DNA associated with hyperacetylated histone is preferentially digested by DNase I. Nucleic Acids Res. *5*, 1863–1876.

Seto, E., and Yoshida, M. (2014). Erasers of histone acetylation: the histone deacetylase enzymes. Cold Spring Harb. Perspect. Biol. *6*, a018713.

Shahbazian, M.D., and Grunstein, M. (2007). Functions of site-specific histone acetylation and deacetylation. Annu. Rev. Biochem. *76*, 75–100.

Shibahara, K., Verreault, A., and Stillman, B. (2000). The N-terminal domains of histones H3 and H4 are not necessary for chromatin assembly factor-1- mediated nucleosome assembly onto replicated DNA in vitro. Proc. Natl. Acad. Sci. U. S. A. *97*, 7766–7771.

Shiloh, Y. (2003). ATM and related protein kinases : safeguarding genome. Nat. Rev. Cancer *3*, 155–168.

Shiloh, Y., and Ziv, Y. (2013). The ATM protein kinase: regulating the cellular response to genotoxic stress, and more. Nat. Rev. Mol. Cell Biol. *14*, 197–210.

Sidoli, S., and Garcia, B.A. (2017). Middle-down proteomics: a still unexploited resource for chromatin biology. Expert Rev. Proteomics *14*, 617–626.

Sinha, I., Wiren, M., and Ekwall, K. (2006). Genome-wide patterns of histone modifications in fission yeast. Chromosom. Res. *14*, 95–105.

Smerdon, M.J. (1991). DNA repair and the role of chromatin structure. Curr. Opin. Cell Biol. *3*, 422–428.

Sobel, R.E., Cook, R.G., Perry, C.A., Annunziato, A.T., and Allis, C.D. (1995). Conservation of deposition-related acetylation sites in newly synthesized histones H3 and H4. Proc. Natl. Acad. Sci. U. S. A. *92*, 1237–1241.

Sterner, D.E., and Berger, S.L. (2000). Acetylation of histones and transcription-related factors. Microbiol. Mol. Biol. Rev. *64*, 435–459.

Strahl, B.D., and Allis, C.D. (2000). The language of covalent histone modifications. Nature *403*, 41–45.

Straub, T. (2003). Heterochromatin dynamics. PLoS Biol. *1*, 23–24.

Su, D., Hu, Q., Li, Q., Thompson, J.R., Cui, G., Fazly, A., Davies, B.A., Botuyan, M.V., Zhang, Z., and Mer, G. (2012). Structural basis for recognition of H3K56-acetylated histone H3-H4 by the chaperone Rtt106. Nature *483*, 104–107.

Suka, N., Suka, Y., Carmen, A.A., Wu, J., and Grunstein, M. (2001). Highly specific antibodies determine histone acetylation site usage in yeast heterochromatin and euchromatin. Mol. Cell *8*, 473–479.

Tagami, H., Ray-Gallet, D., Almouzni, G., and Nakatani, Y. (2004). Histone H3.1 and H3.3 Complexes Mediate Nucleosome Assembly Pathways Dependent or Independent of DNA Synthesis. Cell *116*, 51–61.

Tamburini, B. A, and Tyler, J.K. (2005). Localized histone acetylation and deacetylation triggered by the homologous recombination pathway of double-strand DNA repair localized histone acetylation and deacetylation triggered by the Homologous recombination pathway of double-strand DNA repair. Mol. Cell Biol. *25*, 4903–4913.

Tanner, K.G., Trievel, R.C., Kuo, M.H., Howard, R.M., Berger, S.L., Allis, C.D., Marmorstein, R., and Denut, J.M. (1999). Catalytic mechanism and function of invariant glutamic acid 173 from the histone acetyltransferase GCN5 transcriptional coactivator. J. Biol. Chem. *274*, 18157–18160.

Taunton, J., Hassig, C.A., and Schreiber, S.L. (1996). A mammalian histone deacetylase related to the yeast transcriptional regulator Rpd3p. Science *272*, 408–411.

Thomas, J.O., and Kornberg, R.D. (1975). An octamer of histones in chromatin and free in solution. Proc. Natl. Acad. Sci. U. S. A. *72*, 2626–2630.

Trojer, P., and Reinberg, D. (2007). Facultative Heterochromatin: is there a distinctive molecular signature? Mol. Cell *28*, 1–13.

Ud-Din, A.I.M.S., Tikhomirova, A., and Roujeinikova, A. (2016). Structure and functional diversity of GCN5-related n-acetyltransferases (GNAT). Int. J. Mol. Sci. *17*.

Verreault, A. (2000). De novo nucleosome assembly: new pieces in an old puzzle. Genes Dev. *14*, 1430–1438.

Vidali, G., Boffa, L.C., Bradbury, E.M., and Allfrey, V.G. (1978). Butyrate suppression of histone deacetylation leads to accumulation of multiacetylated forms of histones H3 and H4 and increased DNase I sensitivity of the associated DNA sequences. Proc. Natl. Acad. Sci. U. S. A. *75*, 2239–2243.

Waddington, C.H. (2012). The Epigenotype. Int. J. Epidemiol. *41*, 10–13.

West, A.C., and Johnstone, R.W. (2014). New and emerging HDAC inhibitors for cancer treatment. J Clin Invest. *124*, 30–39.

Williams, S.K., Truong, D., and Tyler, J.K. (2008). Acetylation in the globular core of histone H3 on lysine-56 promotes chromatin disassembly during transcriptional activation. Proc. Natl. Acad. Sci. *105*, 9000–9005.

Wirén, M., Silverstein, R. a, Sinha, I., Walfridsson, J., Lee, H.-M., Laurenson, P., Pillus, L., Robyr, D., Grunstein, M., and Ekwall, K. (2005). Genomewide analysis of nucleosome density histone acetylation and HDAC function in fission yeast. EMBO J. *24*, 2906–2918.

Woodcock, C.L., and Dimitrov, S. (2001). Higher-order structure of chromatin and chromosomes. Curr. Opin. Genet. Dev. *11*, 130–135.

Wurtele, H., and Verreault, A. (2006). Histone post-translational modifications and the response to DNA double-strand breaks. Curr. Opin. Cell Biol. *18*, 137–144.

Wurtele, H., Tsao, S., Lépine, G., Mullick, A., Tremblay, J., Drogaris, P., Lee, E.-H., Thibault, P., Verreault, A., and Raymond, M. (2010). Modulation of histone H3 lysine 56 acetylation as an antifungal therapeutic strategy. Nat. Med. *16*, 774–780.

Wurtele, H., Kaiser, G.S., Bacal, J., St-Hilaire, E., Lee, E.-H., Tsao, S., Dorn, J., Maddox, P., Lisby, M., Pasero, P., et al. (2012). Histone H3 lysine 56 acetylation and the response to DNA replication fork damage. Mol. Cell. Biol. *32*, 154–172.

Xhemalce, B., Miller, K.M., Driscoll, R., Masumoto, H., Jackson, S.P., Kouzarides, T., Verreault, A., and Arcangioli, B. (2007). Regulation of histone H3 lysine 56 acetylation in Schizosaccharomyces pombe. J. Biol. Chem. *282*, 15040–15047.

Xu, F., Zhang, K., and Grunstein, M. (2005). Acetylation in histone H3 globular domain regulates gene expression in yeast. Cell *121*, 375–385.

Yan, Y., Barlev, N. a, Haley, R.H., Berger, S.L., and Marmorstein, R. (2000). Crystal structure of yeast Esa1 suggests a unified mechanism for catalysis and substrate binding by histone acetyltransferases. Mol. Cell *6*, 1195–1205.

Yan, Y., Harper, S., Speicher, D.W., and Marmorstein, R. (2002). The catalytic mechanism of the ESA1 histone acetyltransferase involves a self-acetylated intermediate. Nat. Struct. Biol. *9*, 862–869.

Yang, X.-J. (2015). MOZ and MORF acetyltransferases: Molecular interaction, animal development and human disease. Biochim. Biophys. Acta - Mol. Cell Res. *1853*, 1818–1826.

Ye, J., Ai, X., Eugeni, E.E., Zhang, L., Carpenter, L.R., Jelinek, M.A., Freitas, M.A., and Parthun, M.R. (2005). Histone H4 lysine 91 acetylation a core domain modification associated with chromatin assembly. Mol. Cell *18*, 123–130.

Zhao, Y., and Garcia, B.A. (2015). Comprehensive catalog of currently documented histone modifications. Cold Spring Harb. Perspect. Biol. *7*.

Zheng, Y., Huang, X., and Kelleher, N.L. (2016). Epiproteomics: Quantitative analysis of histone marks and codes by mass spectrometry. Curr. Opin. Chem. Biol. *33*, 142–150.

2. Discovery of protein acetylation patterns by deconvolution of peptide isomer mass spectra

Nebiyu Abshiru*, Olivier Caron-Lizotte*, Roshan Elizabeth Rajan*, Adil Jamai, Christelle Pomies, Alain Verreault & Pierre Thibault

This chapter corresponds to a published article
Nature Communications 2015 **6**:8648

*These authors contributed equally to this work

Olivier Caron-Lizotte built and tested the Iso-PeptidAce deconvolution software. Nebiyu Abshiru designed and carried out the proteomics experiments and prepared the first draft of the manuscript. Christelle Pomies performed the pilot study with HDAC inhibitors. Adil Jamai purified histones associated with CAF-1. Roshan Elizabeth Rajan performed HDAC inhibitor treatment of K562 cells and prepared histones from HDACi-treated cells (Fig 2) and isolated total histones from Cac2-TAP strains (Fig 3).

2.1. Abstract

Protein post-translational modifications (PTMs) play important roles in the control of various biological processes including protein-protein interactions, epigenetics and cell cycle regulation. Mass spectrometry-based proteomics approaches enable comprehensive identification and quantitation of numerous types of PTMs. However, the analysis of PTMs is complicated by the presence of indistinguishable co-eluting isomeric peptides that result in composite spectra with overlapping features that prevent the identification of individual components. In this study, we present Iso-PeptidAce, a novel software tool that enables deconvolution of composite MS/MS spectra of isomeric peptides based on features associated with their characteristic fragment ion patterns. We benchmark Iso-PeptidAce using dilution series prepared from mixtures of known amounts of synthetic acetylated isomers. We also demonstrate its applicability to different biological problems such as the identification of site-specific acetylation patterns in histones bound to chromatin assembly factor-1 and profiling of histone acetylation in cells treated with different classes of HDAC inhibitors.

2.2. Introduction

Histone post-translational modifications (PTMs) control access to genetic information and, consequently, participate in several important cellular processes such as DNA repair and replication, nucleosome assembly and transcriptional regulation (Unnikrishnan et al., 2010; Zentner and Henikoff, 2013). It is now clear that many chromatin-modifying enzymes and enzymes that act on non-histone proteins, recognize 'combinatorial patterns of PTMs', rather than single protein modifications. For instance, ATP-dependent chromatin remodelers often recognize histones that contain more than one acetylated lysine residue that is located in close proximity of each other (Filippakopoulos and Knapp, 2012; Filippakopoulos et al., 2012). Although valuable to infer the functions of PTMs, accurately determining patterns and stoichiometries of PTMs located in isomeric and isobaric peptides remains extremely difficult to achieve even by mass spectrometry (MS). This is because isomeric peptides, which are identical except for the position of the PTMs along the peptide chain, often co-elute during liquid chromatography and generate composite tandem mass spectra (MS/MS) containing indistinguishable fragment ions derived from two or more peptide isomers.

A few MS/MS methods were previously developed to quantify co-eluting isobaric histone peptides. Smith et al. (Smith et al., 2003) were first to use a fragment ion-based approach to determine the fraction of histone H4 molecules acetylated at specific residues based on the normalized intensity ratio of peptide fragment ions containing either protiated or deuterated acetyl groups to distinguish lysine residues that were, respectively, acetylated or free in vivo. However, this approach was limited by the lack of automated data analysis

software and the difficulty to deconvolute co-eluting isomers. Recently, Feller et al. (Feller et al., 2015) described a similar approach in which second generation fragment ions (known as MS^3) were necessary to obtain diagnostic fragment ions that can be used to estimate the abundance of each isomer by solving a set of linear equations. A limitation of this approach is that singly charged MS^2 fragments, and particularly those with a nonmobile proton, fragment poorly and generate MS^3 spectra that are impossible to assign to specific isomers (Huang et al., 2005; Kapp et al., 2003). Sidoli et al. designed a software known as isoScale that can be used to determine the relative abundance of isobaric peptides, based on intensity ratios of fragment ions unique to each isomer (Sidoli et al., 2014). isoScale relies on search engine outputs (for example, Mascot.csv result files) to select isomer-specific fragments used in this analysis. The algorithm EpiProfile recently described by Yuan et al. quantifies isomeric histone peptides by solving a series of linear equations derived from peak heights of unique fragments representative of each isomeric species (Yuan et al., 2015). Several other approaches have also been proposed to deconvolute composite MS/MS spectra of peptide ions with different sequences (Bern et al., 2010; Wang et al., 2014; Zhang et al., 2014), however, their application is limited when analyzing MS/MS spectra of co-fragmented isomeric ions that contain the same modification at different sites.

In this study, we present Iso-PeptidAce, a novel software tool that exploits high-resolution LC-MS/MS data for deconvolution of composite spectra and quantification of site-specific acetylation. The resolution of composite MS/MS spectra derived from isomeric peptides is based on features associated with their characteristic fragment ion patterns obtained

from the corresponding synthetic peptides and, importantly, does not rely on unique fragment ions to distinguish isomers. The application of Iso-PeptidAce is presented here for peptide isomers that contain multiple acetylated lysine residues but can also be applied to other types of modifications such as isomeric phosphopeptides (Courcelles et al., 2012). The use of Iso-PeptidAce is demonstrated by monitoring temporal changes in acetylation patterns of histones H3 and H4 from human erythroleukemic (K562) cells treated with different classes of histone deacetylase inhibitors (HDACi), and by determining acetylation patterns in histones bound to *Saccharomyces cerevisiae* chromatin assembly factor-1 (CAF1).

2.3. Materials and Methods

2.3.1. Synthetic peptide preparations

Synthetic histone H3 and H4 peptides were purchased from GenScript and include four variants of the H3 peptide 17-RKQLATKAAR-26: one with unmodified lysines, two peptides with one acetylated lysine and one peptide with both lysines acetylated (Supplementary Table 1A). A total of 16 H4 peptides were purchased. These included one unmodified, four mono-acetylated, six di-acetylated, four tri-acetylated and one tetra-acetylated form of peptide 1-SGRGKGGKGLGKGGAKRHR-19 (Supplementary Table 1B). The concentration of each peptide was determined based on triplicate ultraviolet absorbance measurements at 205 nm using an Ultraspec 2100 Pro spectrophotometer (GE Healthcare). Each peptide solution was nominally in 1 mg ml^{-1} range. We verified the purity and identity of each peptide by injecting directly 1 pmol of each peptide on a Q-Exactive mass spectrometer (Thermo Scientific). All MS files will be publicly available

from PeptideAtlas database (data identifier: PASS00658, http://www.peptideatlas.org/PASS/PASS00658) For convenience MS/MS spectra of isomeric peptides are provided as Supplementary Fig. 7.

2.3.2. Synthetic peptide mixtures

Standard curves were prepared for seven mixtures of H4 peptides with amounts of specific peptides ranging from 5 to 320 fmol (Supplementary Table 2A–C). Two or three peptides from each group of isomers were selected and added to the mixtures at a fixed amount of 80 fmols. The peptide mixtures were subjected to propionylation, tryptic digestion and LC-MS/MS analysis on a Q-Exactive mass spectrometer coupled to an EASY nLC II system (Thermo scientific).

2.3.3. Detection efficiency of H3 and H4 acetylated peptides

We prepared five mixtures of H3 or H4 synthetic peptides. The amount of each peptide in mixtures 1, 2, 3, 4 and 5 are 25, 50, 100, 200 and 400 fmols, respectively. These samples were subjected to propionylation, tryptic digestion and LC-MS/MS analysis on a Q-Exactive Plus instrument. The signal intensity of each peptide was plotted against the amount of peptide injected as shown in Supplementary Fig. 2 A, B.

2.3.4. Cell treatment with HDAC inhibitors

Suspension cultures of K562 (human erythroleukemic) cells were grown in T-75 flasks at 37°C and 5% CO_2 in RPMI-1640 medium (Gibco) supplemented with 10% fetal bovine serum (Wisent) and 1% penicillin/streptomycin. Asynchronously growing cells were

treated with 1 μM of SAHA, MS-275 or JNJ-26481585 (Selleck Chemicals) for 1, 6 and 24 h. Control cells were treated with DMSO. Two biological replicates were prepared for each condition. After treatment, the cells were collected, centrifuged at 1,000 r.p.m. at room temperature, washed with PBS, and flash frozen in liquid nitrogen. Histones were isolated using acid extraction as previously described (Shechter et al., 2007). Briefly, nuclei from 10^7 cells were isolated with a hypotonic lysis buffer, followed by histone extraction using 0.2 M H_2SO_4 and TCA precipitation. The concentration of histone samples was determined by a Micro-BCA assay (Pierce). Further purification of core histones was performed by reverse-phase HPLC.

2.3.5. Purification of yeast CAF1

The Cac2–TAP purification was adapted from Zhou et. al. (Zhou et al., 2006). Briefly, exponentially growing yeast cells (4 L at ~1.8 X 10^7 cells per ml in YPD medium) were collected by centrifugation and washed twice with ice-cold water. All further steps were carried out on ice. The pellet was resuspended in an equal volume of lysis buffer (25 mM Tris-HCl pH 7.5, 100 mM NaCl, 10 mM $MgCl_2$, 0.1% NP-40, 1 mM EDTA, 10% glycerol, 1 mM DTT and 1 mM PMSF) containing a cocktails of protease inhibitors (5 mM Leupeptin, 25 mM Aprotinin and 5 mM Pepstatin A) and HDAC inhibitors (10 mM nicotinamide, 10 mM sodium butyrate, 10 mM trichostatin A and 100 mM SAHA). Cell suspensions were frozen in liquid nitrogen and lysed in a freezer mill (Spex Certiprep) using two repeats of four cycles with 2 min of grinding (15 impacts per second) and 2 min of cooling per cycle. The resulting cell lysate powder was thawed out on ice. Ethidium bromide (75 mg ml^{-1}) was added and the lysate was incubated on ice for 1 h with

benzonase (25U ml^{-1}). The extract was clarified by centrifugation at 25,000 r.p.m. for 30 min. The supernatant was then incubated with 200 ml of IgG-Agarose beads (Sigma) for 2 h at 4°C. The beads were recovered by centrifugation, extensively washed with lysis buffer followed by several washes with TEV cleavage buffer (10 mM Tris-HCl pH 8, 100 mM NaCl, 1 mM DTT and 0.5 mM EDTA) containing the protease inhibitor and HDAC inhibitor cocktails. To elute Cac2–TAP, the beads were incubated with TEV protease at 4°C overnight in TEV cleavage buffer. A portion of the TEV eluate (30 µl) was resolved by SDS–PAGE and the presence of Cac2-CBP and histones H3 and H4 was confirmed by immunoblotting. The remainder of the TEV eluate (170 µl) was dried in a Speed-Vac, resuspended in 1 ml H_2O and applied to a C18 column equilibrated with 0.1% trifluoroacetic acid (TFA) in water. The C18 column was washed twice with 1 ml of 0.1% TFA in 5% methanol and eluted with 1ml of 70% acetonitrile (ACN). The eluate was dried in a Speed-Vac and resuspended in 0.1% TFA for purification of intact histones by offline HPLC.

2.3.6. Fractionation of core histones by RP-HPLC

Separation of intact core histones was achieved using a narrow-bore Zorbax C8 reverse-phase column (2.1 X150 mm, 5 mm, 300Å) on an Agilent 1200 HPLC system. Solvent A was aqueous 0.1% TFA (Sigma) and solvent B was 0.1% TFA in 100% acetonitrile (ACN). Approximately 2 mg of acid extracted histones were loaded onto the C8 column at a flow rate of 150 ml min^{-1}. Histones were eluted from the column using a gradient of 5–80% solvent B in 60 min. Fractions were collected in a 96-well plate at a rate of one fraction

per minute. Fractions containing histones H3 or H4 were pooled and dried completely in a Speed-vac concentrator.

2.3.7. Propionylation and trypsin digestion of histones

In-solution tryptic digestion of synthetic peptides or core histones was performed as previously described (Abshiru et al., 2013). Briefly, a total of 2 mg of HPLC purified histones H3 and H4 were subjected to propionylation by adding 200 ml of freshly prepared 2:1 (v/v) water: propionic anhydride (Sigma) mixture and vortexing the mixture for 1 h at room temperature. The samples were then dried in a Speed-vac at 4°C. The dried samples were resuspended in 50 mM ammonium bicarbonate, vortexed for 2 min and subjected to a second round of evaporation at 4°C. The samples were collected and resuspended in 100 ml of 50 mM ammonium bicarbonate and vortexed for 5 min to re-dissolve the proteins. Our digestion solution was prepared by adding 200 ml of 50 mM ammonium bicarbonate in a vial containing 20 mg of lyophilized trypsin (Promega). Roughly 0.5 ml of this solution was added to each histone sample and digested overnight at 37°C. After digestion, samples were dried completely in a Speed-vac and then resuspended in 0.2% formic acid before LC-MS/MS analyses.

2.3.8. LC-MS/MS analyses of histone digests

MS data were acquired in duplicates on a Q-Exactive Plus mass spectrometer (Thermo Scientific) coupled to an EASY nLC II system (Thermo scientific). A total of 1 mg of histone H3 and H4 digests generated from the control or HDACi-treated cells were first desalted on a Jupiter C18 (3 mm particles, Phenomenex) trap column (4mm length, 360 mm i.d.)

for 5min at 10 ml min^{-1}, before their elution onto a C18 analytical column (18 cm length, 150 mm i.d.). A linear gradient from 5 to 60% ACN (containing 0.2% formic acid) at 600 nl min^{-1} over 60 min was used for peptide elution. The MS instrument was operated in positive ion mode and capillary voltage of 1.6 kV. MS scans were acquired in the Orbitrap analyzer over the range of 300–1,500 *m/z* at a resolution of 70,000 and automatic gain control target value of 1.0 $X10^6$. An inclusion list containing *m/z*, charge state and collision energy values of H3 and H4 peptides was used to trigger MS/MS acquisition. Every precursor ion found in the inclusion list was automatically selected for fragmentation in the HCD cell at a normalized collision energy setting of 27. The fragments were analyzed in the Orbitrap at a resolution of 35,000 and a target value of 5.5 $X10^5$. The dynamic exclusion setting was disabled to acquire multiple MS/MS spectra per peptide.

2.3.9. Data analysis

Data analysis was performed using the Iso-PeptidAce software. Raw MS and MS/MS files of individual synthetic peptides, mixtures of isomeric peptides or histone digests and FASTA files with H3 and H4 protein sequences were submitted to Iso-PeptidAce. The default settings for deconvolution of composite MS/MS spectra are: precursor mass tolerance: 8 p.p.m., fragment mass tolerance: 0.05 Da, the minimum number of fragment ions (per isomer) considered for deconvolution: 5, types of fragment ions considered: b and y, digestion enzyme: trypsin, missed cleavages: Iso-PeptidAce uses a no-enzyme in silico protein digestion routine to parse the provided FASTA files for potential matches. PTMs included in peptide-spectrum matching: carbamidomethylation of cysteine (C,57.0215 Da), oxidation of methionine (M, 15.9949), phosphorylation of serine,

threonine or tyrosine (S/T/Y, 79.9663), deamidation of asparagine and glutamine (N/Q 0.9840/0.9847), acetylation of lysine (K, 42.0106), propionylation of lysine (K, 56.0262), mono-methylation of lysine (K, 14.0157), di-methylation of lysine (K, 28.0313), tri-methylation of lysine (K, 42.0470), acetylation of protein N-terminus (42.0106). All the PTMs were considered as variable modifications. The output from Iso-PeptidAce is a combined result file (spreadsheet) containing intensity values for all the acetylated and non-acetylated forms of the H3 and H4 peptides obtained after deconvolution. A representative result file for the H4 peptide GKGGKGLGKGGAKR is shown in Supplementary Table 7. A total of 16 different isoforms of this peptide were detected (shown in each column in Supplementary Table 7). These peptides are divided into five groups (per sample) based on their m/z values (shown in each row in Supplementary Table 7): one un-acetylated (0Ac, m/z 747.94), four mono-acetylated (1Ac, m/z 740.93), six di-acetylated (2Ac, 733.93), four tri-acetylated (3Ac, m/z 726.92) and one tetra-acetylated (4Ac, m/z 719.91). Each intensity value in Supplementary Table 7 is normalized based on the peptide's response factor, which is determined from the slope of the lines shown in Supplementary Fig. 2 A, B. The slope of each line was determined from the linear equations that best fit the MS signal responses. Acetylation site occupancy at a specific lysine residue was determined from the ratio of the sum of intensities of peptides bearing the ac-Lys to the sum of intensities of all the 16 peptide isoforms. Iso-PeptidAce can be downloaded from the website: http://proteomics.iric.ca/tools/Iso-PeptidAce. Detailed information on Iso-PeptidAce is also provided as Supplementary Methods.

2.4. Results

2.4.1. Deconvolution of mixed MS/MS spectra by Iso-PeptidAce

We designed a new software tool named Iso-PeptidAce that deconvolutes composite MS/MS spectra of known isomeric peptides. The software takes as input raw MS and MS/MS files of the individual and the mixed isomers, the FASTA sequence file of the protein of interest, and a set of parameters for peptide spectrum matching (PSM) such as modifications, precursor and fragment ion tolerances (see Data analysis under the Methods section). The raw files are processed to extract precursor intensity, MS1 and MS2 injection times, and MS2 peak lists containing *m/z* and intensity values (see Supplementary Methods for a detailed section on spectral deconvolution and normalization of MS signal intensities). Iso-PeptidAce computes the proportion of individual isomers in composite MS/MS spectra based on fragment ion patterns that uniquely identify each isomer. In Iso-PeptidAce, fragment ion patterns are reduced to a set of maximum network flow problems, for which a number of efficient algorithms are known (Ahuja et al., 1993). This approach has previously been used in a wide range of complex problems, such as predicting molecular pathways in complex diseases or selecting single nucleotide polymorphisms and their associated alleles in patient and control groups (Albert, 2005; Cho et al., 2012; Dutt et al., 2009). In our study, we implemented the network flow approach to deconvolute composite fragment spectra of acetylated isomers. Although these isomers share multiple fragment ions, they produce distinct fragment ion patterns that can be transformed into a set of network flow problems. Figure 2.1a shows a schematic overview of the deconvolution conducted by Iso-PeptidAce for a composite MS/MS spectrum generated from two hypothetical co-eluting

isomeric peptides labeled X and Y. For every composite spectrum acquired across the elution curve, fragment ion intensities (Fig. 2.1 a, step 1) are modeled into maximum network flow problems (flow capacity shown as empty bar charts, Fig. 2.1 a, step 2). The networks are filled with fragment ion patterns for isomers X and Y (Fig. 2.1 a, step 3) and merged into a single network with the excess flow (represented as overrunning color bars in Fig. 2.1 a, step 4). The resulting network is processed iteratively by a multivariate optimization technique known as Gradient Descent (Snyman, 2005) (Fig. 2.1 a, step 5), to remove the excess flow in the network. Each iteration step converges towards the maximum flow, which refers to the optimal ratio of X and Y compatible with the composite spectrum (Fig. 2.1 a, left inner circle). Finally, individual elution curves for each isomer are generated based on the abundance ratios of MS/MS spectra (Fig. 2.1 a, right inner circle) and the peak intensity or peak area of the precursor ions.

2.4.2. Extraction of elution profiles and fragment ion patterns

We first used Iso-PeptidAce for MS/MS spectra of synthetic peptides from acetylated isomers of histones H3 and H4 (Supplementary Tables 1 and 2). All possible non-acetylated and acetylated forms of H4 peptide 1-SGRGKGGKGLGKGGAKRHR-19 were synthesized, and the purity of each peptide was confirmed by MS analyses. These peptides were propionylated, digested with trypsin and subjected to LC-MS/MS analysis on a Q-Exactive Plus instrument. We obtained three isomeric groups of H4 peptides acetylated at one, two or three lysine residues, and members of each group generally have very narrow retention time differences (Supplementary Fig. 1). To normalize precursor intensity, we determined the signal intensity response for each peptide as a

function of the amount injected. We observed that mono- or multiply-acetylated isomers yielded a higher response than their propionylated counterparts (Supplementary Fig. 2 A, B). We then prepared equimolar mixtures of peptides for each group of isomers and analyzed them by LC-MS/MS. Although propionylated H4 peptides were readily separated into non-acetylated, mono-, di-, tri- and tetra-acetylated peaks (denoted as Ac0, 1, 2, 3 and 4 in Supplementary Fig. 3 A, top panel), we observed that peptides within the same isomeric group co-eluted and produced mixed MS/MS spectra (Supplementary Fig. 3 A, B). In addition, isomeric peptides shared multiple fragment ions (Supplementary Fig. 4 A–E). Supplementary Fig. 4 E shows a three-dimensional view of the abundance distribution of fragment ions derived from the four mono-acetylated isomers. H4K5ac and H4K16ac are the only mono-acetylated H4 peptide isomers that produced unique fragment ions at *m/z* 1253.7 and 530.3, respectively (Supplementary Fig. 4 E, blue and purple bars). The peak intensities of these fragments can be used to infer the relative abundances of H4K5ac and H4K16ac in a given sample. This approach was previously implemented in existing software tools such as IsoScale (Sidoli et al., 2014). Importantly, the two-other mono-acetylated isomers, H4K8ac and H4K12ac did not produce any isomer-specific fragment ions (Supplementary Fig. 4 E, red and green bars). These peptides share all of their fragments with either H4K5ac or H4K16ac (Supplementary Fig. 4 E, blue and purple bars), and, as a result, fragment ion ratios cannot be used directly to measure the relative proportions of individual peptide isomers. In Iso-PeptidAce, deconvolution of composite MS/MS spectra containing fragments of the four mono-acetylated isomers is achieved by exploiting the distinguishing features associated with isomer-specific fragment ion patterns. Here the fragment ion pattern of a given isomer is

defined by the retention time at which the peptide was eluted and selected for fragmentation, the peak height and m/z of each fragment ion, and the sites of modification. For example, the fragment ion pattern for H4K8ac is different from that of H4K12ac by the presence of additional fragment ions at *m/z* 785.5 and 955.6, and the absence of y-ion fragments at *m/z* 771.4 and 941.6 (Supplementary Fig.4 C, D) and b-ion at *m/z* 299.2. In addition, their shared fragments (for example, *m/z* 242.1, 544.3 and 1239.7) differ slightly in peak intensities (Supplementary Fig. 4 C, D). Thus, by exploiting such isomer-specific differences, Iso-PeptidAce deconvoluted the coeluting mono-acetylated peptides into four distinct elution profiles where the apex of individual isomer peaks was separated by a few seconds (Fig. 2.1 b, left panel, colored solid lines). The elution curve before the deconvolution is shown in Fig. 2.1 b (grey dashed line). Using Iso-PeptidAce, we were able to determine the relative contribution of each isomer to the abundance of selected fragment ions (Fig. 2.1 b, right panel). Most of these fragments are shared between the different isomers, but their distribution and proportion vary across peptides. Fragmentation patterns representative of H4K8ac and H4K12ac were more prominent at the beginning of elution profiles, whereas those of H4K5ac and H4K16ac were observed at later time points. Similarly, deconvolution of the di- and tri-acetylated isomers by Iso-PeptidAce enabled resolution of each isomeric peptide (Supplementary Fig. 5).

We then assessed the performance of Iso-PeptidAce using seven mixtures of peptides for each group of isomers (mono-, di-, tri-acetylated). Each peptide mixture contained known amounts of propionylated and acetylated isomeric H4 peptides each ranging from 5 to 320 fmols. Within each peptide mixture, two to three peptides were selected and

added to each mixture at a fixed amount of 80 fmols (Supplementary Table 2A–C). Raw MS and MS/MS files from these samples were submitted to Iso-PeptidAce for deconvolution. The amount of peptide determined by Iso-PeptideAce as a function of amount injected (in fmol) for the mono-, di- and tri-acetylated groups of isomers is shown in Fig. 2.1 c (see Supplementary Table 3A–C for the mean values and error bars). We used the signal intensity observed at 80 fmols for normalization. In the seven mixtures of mono-acetylated peptides, we observed an increase in the relative proportion of peptides H4K5ac and H4K12ac whereas peptides H4K8ac and H4K16ac (injected at a constant amount of 80 fmol in each mixture) remained unchanged in each mixture (Fig. 2.1 c, upper panel and Supplementary Table 3A). Similarly, we observed increasing levels of H4K5ac/K8ac, H4K5ac/K16ac and H4K8ac/K16ac among the seven mixtures of di-acetylated peptides (Fig. 2.1 c, middle panel and Supplementary Table 3C) and of H4K5ac/K8ac/ K12ac and H4K5ac/K12ac/K16ac in the tri-acetylated mixtures (Fig. 2.1 c, bottom panel and Supplementary Table 3B) in accordance to their expected abundance. Thus, Iso-PeptidAce successfully deconvoluted the composite spectra generated from different co-eluting acetylated isomers present at concentrations ranging over almost two orders of magnitude.

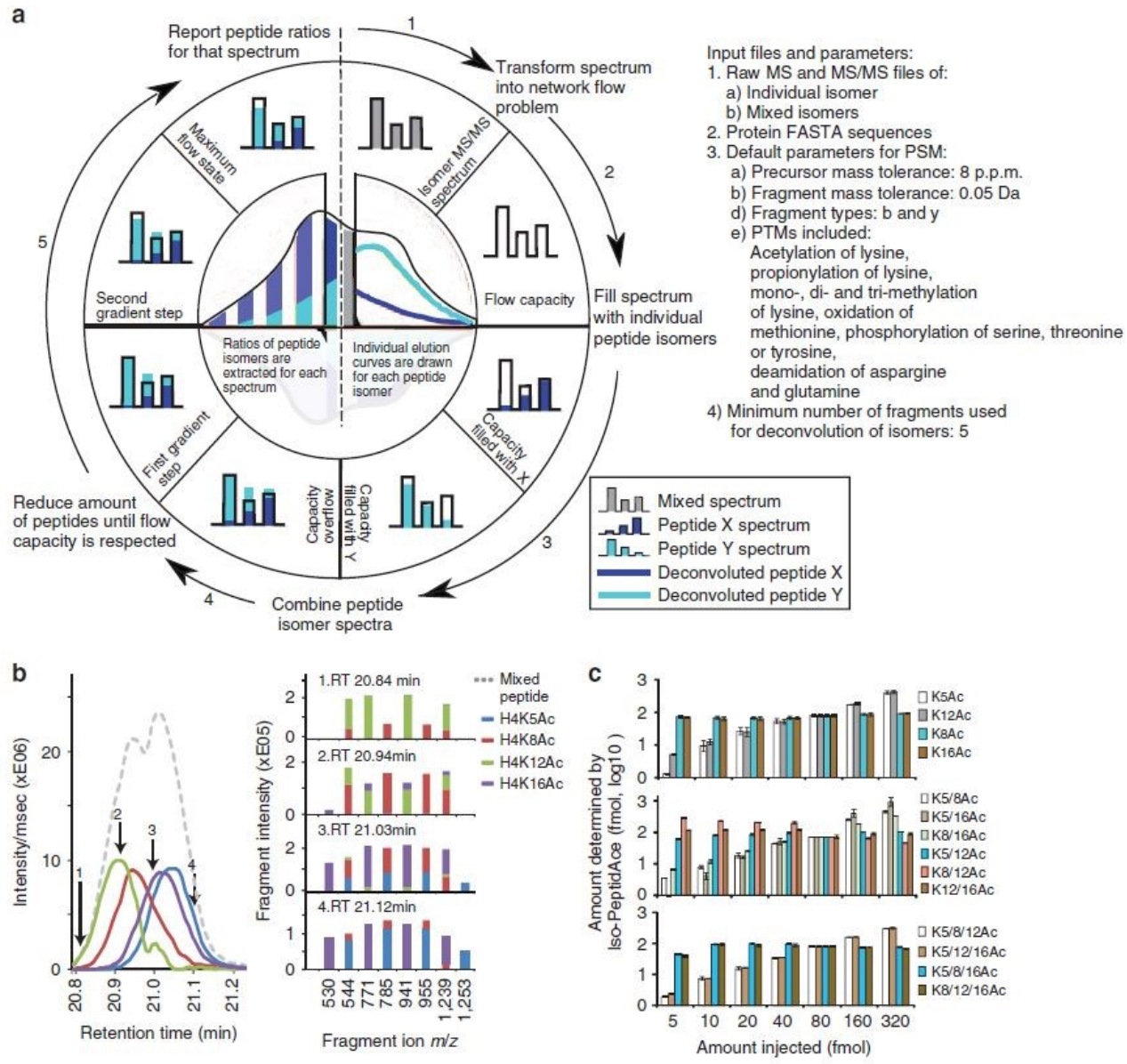

Figure 2.1. Deconvolution of co-eluting acetylated isomers by Iso-PeptidAce

(a) Schematic showing the process of spectral deconvolution by Iso-PeptidAce. The input files and parameters used for deconvolution of mixtures of isomers are listed on the right side of the panel. The process involves building an individual elution curve for X and for Y based on ratios computed for each MS/MS event. Isomeric peptide ratios are computed in five steps: (1) acquire and normalize fragment intensities of a composite spectrum; (2) model fragment intensities as a

network flow with fixed capacities; (3) find the maximum flow for peptide X and for peptide Y; (4) combine both X and Y network flow capacities into the same network flow model; and (5) iteratively reduce the ratio of X and Y until the maximum flow is reached. (b) Left panel: elution profiles of a mixture of mono-acetylated isomers before (dashed line) or after (colored lines) deconvolution. Right panel: the relative intensity of representative fragment ions extracted after isomer deconvolution at four different retention times, RT 20.84, 20.94, 21.03 and 21.12 min. (c) Bar graphs showing the amount of each peptide isomer determined by Iso-PeptidAce as a function of the amount of the same peptide injected as part of seven mixtures, each containing known amounts of the mono-, di- or tri-acetylated groups of isomers (from top to bottom). The mean value and the s.d. for each dilution point are shown in Supplementary Table 3A–C. The amount of peptide determined by Iso-PeptidAce in each mixture was normalized to the 80 fmol signal response. The amounts of peptides K5ac and K12ac (upper panel); K5_8ac, K5_16ac and K8_16ac (middle panel); K5_8_12ac and K5_12_16ac (lower panel) were varied from 5 to 320 fmol. Peptides K8ac and K16ac (upper panel); K5_12ac, K8_12ac and K12_16ac (middle panel); K5_8_16ac and K8_12_16ac (lower panel) were added to each of the seven mixtures at a fixed amount of 80 fmol. Each bar graph represents the mean of two technical replicates with error bars showing the relative distance of the maximum and the minimum values from the mean.

2.4.3. Histone acetylation following HDAC inhibition

We tested our software using tryptic digests of histones isolated from human K562 cells treated with HDAC inhibitors (Fig. 2.2 a). Cells were treated in duplicate for 1, 6 or 24 h with dimethylsulphoxide (DMSO) as solvent control or with the HDAC inhibitors (HDACi) MS-275, SAHA and JNJ-26481585. Histones were isolated by acid extraction and fractionated by reverse phase liquid chromatography (Supplementary Fig. 6). Fractions containing histone H3 or H4 were subjected to propionylation, tryptic digestion and LC-

MS/MS analysis before data deconvolution using Iso-PeptidAce (Fig. 2.2 a). Our results show that 24 h after treatment with SAHA or JNJ-26481585, ~ 50% of H4 peptides 4-GKGGKGLGKGGAKR-17 were acetylated at the four available lysines, whereas only 20% of H4 molecules were tetra-acetylated in cells treated with MS-275 (Fig. 2.2 b). Using Iso-PeptidAce we then determined acetylation site occupancies at H3K18, H3K23, H4K5, H4K8, H4K12 and H4K16 (Supplementary Table 4A, B). The abundance of H3K23ac is higher than that of H3K18ac in both untreated and HDACi-treated samples (Fig. 2.2 c and Supplementary Table 4A). Although previous studies reported trace amounts of H3K18 methylation in mammalian cells (Tang et al., 2014), we did not detect this modification in our samples. Cells treated with all three HDACi demonstrated similar increases in H4 acetylation as a function of time. We observed at least an eightfold increase in acetylation at H4K5, H4K8 or H4K12 after a 24 h treatment with MS-275, SAHA or JNJ (Fig. 2.2 d and Supplementary Table 4B). Up to threefold increase in acetylation was observed at H4K16.

Although a number of studies have previously shown that the HDACi MS-275 and SAHA induce global increases in H3 and H4 acetylation, there was no efficient technique to measure site-specific acetylation stoichiometries of lysines in the N-terminal tail of H4 because some of the acetylated isomers cannot be resolved by nano-LC and do not generate isomer-specific fragments. In our study, we observed that both MS-275 and SAHA caused a major increase in acetylation of the four lysines in the N-terminal tail of H4. In addition, for the first time, we report site-specific changes in histone acetylation caused by the more recently characterized pan-HDACi JNJ-26481585 (Arts et al., 2009).

This drug, also known as Quisinostat, is currently in phase II clinical trial and exhibits antitumor activity in human multiple myeloma and leukemic cells (Deleu et al., 2009; Stühmer et al., 2010; Tong et al., 2010; Venugopal et al., 2013), and recent studies have shown that JNJ-26481585 elicits global increases in acetylation of histones H3 and H4 (Hernan et al., 2014; Venugopal et al., 2013). However, owing to the inherent limitations of immunoassays, these studies did not report the specific lysine residues affected or the stoichiometries of acetylation. Our approach allowed identification of several H3 and H4 sites that increased in acetylation after JNJ-26481585 treatment. When compared with MS-275 and SAHA, JNJ-26481585 caused a more rapid and higher fold increase in acetylation at all the sites that we investigated (Fig. 2.2 b–d). Consistent with these results, JNJ-26481585 has been reported to be 500-fold more potent than SAHA at inhibiting HDAC1 (Arts et al., 2009). These examples illustrate how Iso-PeptidAce provides an automated and rapid approach to quantify global changes in acetylation site occupancies on histone lysine residues. Our method is implemented as a software tool that deconvolutes composite spectra derived from two or more co-eluting isomeric acetylated peptides. In turn, this enables an accurate assessment of acetylation site occupancies at each of the lysines within tryptic peptides.

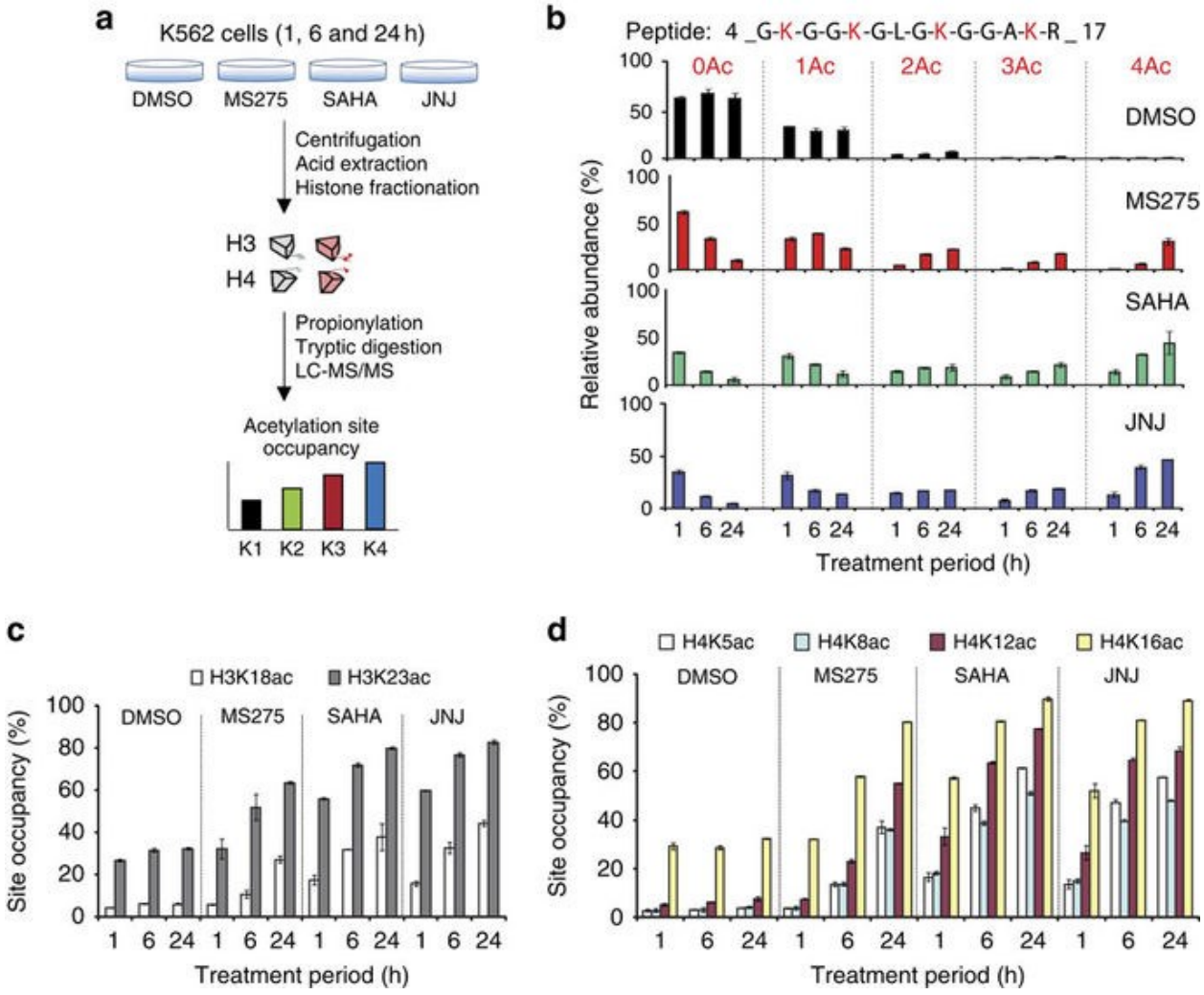

Figure 2.2. Analysis of acetylation site occupancies in histones H3 and H4 following HDACi treatment (a) Histone isolation and MS analysis workflow. Total histones were isolated from human erythroleukemic (K562) cells treated for 1, 6 or 24 h with DMSO (control) or with the HDACi MS-275, SAHA and JNJ-26481585. Total histones were fractionated into individual core histones via offline RP-HPLC. Fractions containing histones H3 and H4 were subjected to propionylation, tryptic digestion and LC-MS/MS analysis. Acetylation site occupancy for each lysine residue was determined based on Iso-PeptidAce reported peptide intensities. (b) Relative abundance of unmodified (0Ac), mono- (1Ac), di- (2Ac), tri- (3Ac) and tetra-acetylated (Ac) peptide 4-GKGGKGLGKGGAKR-17 before (DMSO) or after treatment with MS-275, SAHA

or JNJ-26481585. (c) Acetylation site occupancies of histone H3 at positions K18 and K23 and (d) histone H4 at positions K5, K8, K12 and K16. Each bar graph represents the mean of two technical replicates with error bars showing the relative distance from the mean of the maximum and minimum values.

2.4.4. Acetylation patterns in CAF1-bound histones

Acetylation of multiple residues in newly synthesized histones has been implicated in nucleosome assembly (Li et al., 2012). However, the molecular function and the biological implications of this acetylation have remained unclear because of redundancy among several acetylation sites in new H3 and H4 molecules. The capability of Iso-PeptidAce to determine acetylation patterns in situations where samples are limiting was evaluated for affinity-purified histones bound to CAF1, a protein complex that deposits new histone H3/H4 molecules onto nascent DNA during replication (Zhou et al., 2006). As previously described, we purified the CAF1 complex from asynchronously growing yeast cells via a tandem affinity purification (TAP)-tagged Cac2 subunit (Zhou et al., 2006). We also purified total histones from the same culture to compare their acetylation patterns with those of histones bound to CAF1 (Fig. 2.3 a). The occupancies of H3/H4 acetylation sites were clearly different in CAF1-bound versus total histones (Fig. 2.3 b–d and Supplementary Table 5). We also detected mono-, di- and tri-methylation of H3K36 in the total histones, but these PTMs were absent in CAF1-bound histones (Supplementary Table 5). These results argue that CAF1-bound histones did not dissociate and mix with other histones during our affinity purification procedure. Otherwise, the H3 and H4 acetylation patterns in CAF1-bound and total histones would be identical. In CAF1-bound H3 molecules, we found a high acetylation site occupancy (between 49 and 79%) at each

of the five lysine residues previously known to be acetylated in new histones from S. cerevisiae: H3-K56, K9, K14, K23 and K27, but not at K18 (Fig. 2.3 b). This high degree of acetylation at multiple sites demonstrates that essentially all the H3 molecules bound to CAF1 are acetylated.

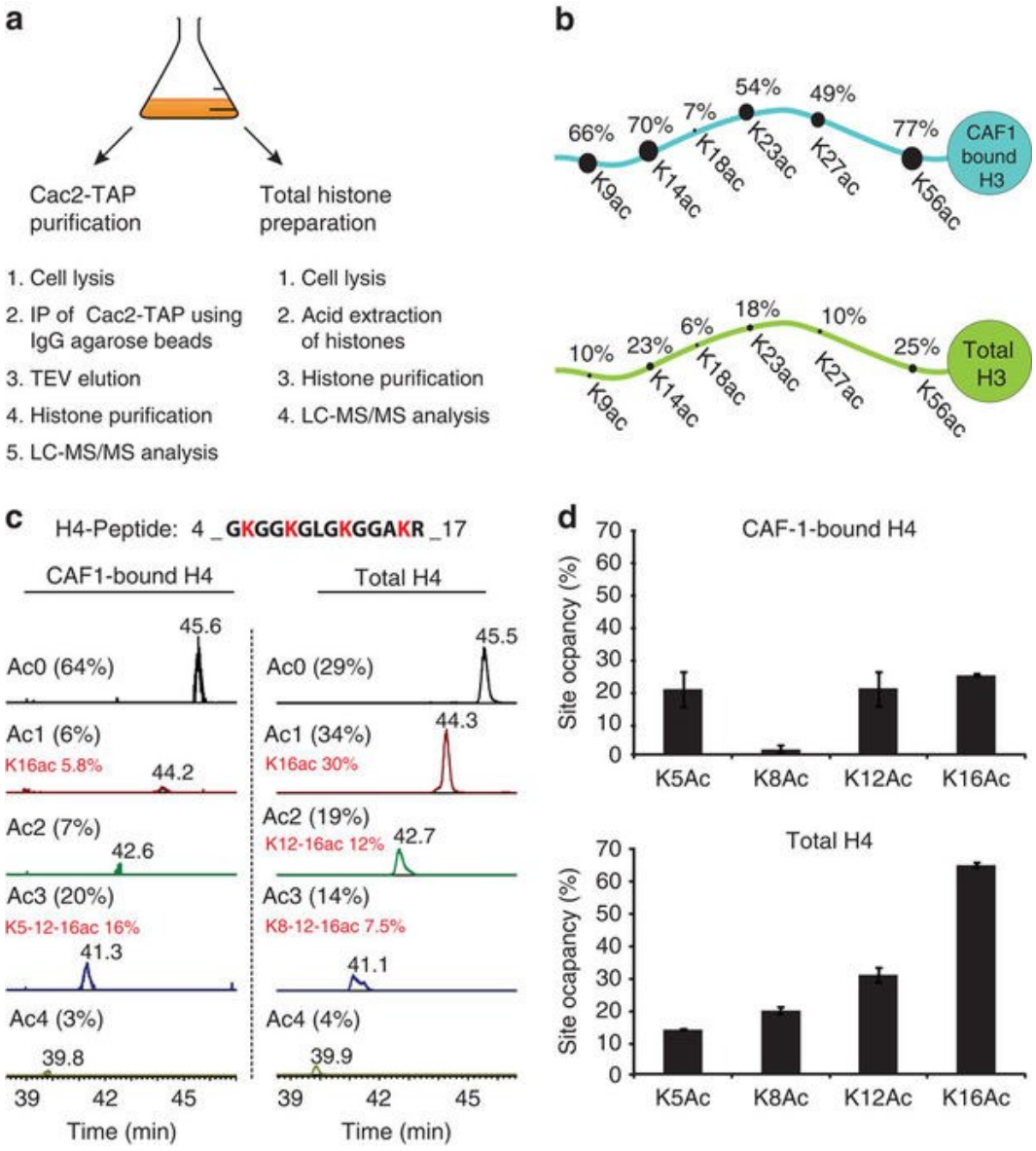

Fig 2.3. Analysis of acetylation site occupancies in CAF1 associated histones H3 and H4

(**a**) Schematic representation of the experimental workflow. Cac2-TAP was purified from 3.5 l of

yeast cell culture and the remainder (0.5 l) was processed for total histone preparation. Histones from both samples were fractionated by offline RP-HPLC and analyzed by LC-MS/MS. (**b**) Comparison of lysine acetylation site occupancies in total histone H3 (lower panel) and CAF1-bound H3 (upper panel). (**c**) Extracted ion chromatograms of histone H4 peptide 4-GKGGKGLGKGGAKR-17 acetylated at zero (Ac0), one (Ac1), two (Ac2), three (Ac3) or four (Ac4) lysine residues in CAF1-bound (left panel) or total histones (right panel). The predominant acetylation pattern in each group of isomers is highlighted in red. (**d**) Comparison of acetylation site occupancies at positions H4K5, H4K8, H4K12 and H4K16 in CAF1-bound H4 (upper panel) and total histone H4 (lower panel). Each bar graph represents the mean of two technical replicates with error bars showing the relative distance from the mean of the maximum and minimum values.

In contrast, a large fraction (64%, Fig. 2.3 c) of H4 molecules bound to CAF1 were not acetylated at any of the four lysine residues located in their N-terminal tail. Nonetheless, these results provide a potential explanation to a long-standing paradox. Hat1 is an enzyme that acetylates new H4 molecules at lysines 5 and 12, two sites of acetylation that are conserved from yeast to humans (Li et al., 2012). Given this, the paradox was that *S. cerevisiae* cells lacking Hat1 or cells where lysines 5 and 12 were mutated showed essentially no phenotype unless several lysines of H3 were also mutated to block their acetylation (Kelly et al., 2000; Qin and Parthun, 2002). The fact that, *in S. cerevisiae*, the acetylation of new H3 molecules is far more abundant than that of new H4 molecules provides a molecular basis for these genetic results. Our results also revealed an unexpected acetylation pattern in new H4 molecules where, in addition to lysines 5 and 12, lysine 16 was acetylated (Fig. 2.3 c, d). Until now, the dogma was that new H4 molecules were predominantly acetylated at lysines 5 and 12, but not at lysine 16. This

was based on pulse labeling of new histones with [^{3}H]-lysine and Edman sequencing to quantify phenylthiohydantoin derivatives of acetyl-lysine and lysine (Sobel et al., 1995). The sensitivity of this technique rapidly decreases as a function of distance from the N-terminus and this may account for the fact that lysine 16 acetylation in new H4 molecules was not previously reported. Based on MS data, the presence of K16 acetylation in H4 molecules bound to *S. cerevisiae* CAF1 was previously reported (Zhou et al., 2006) but its prevalence was unknown. For the first time, our experiments demonstrate that the most abundant form of H4 bound to *S. cerevisiae* CAF1 consists of molecules that are triacetylated at K5, K12 and K16, with significantly lower amounts of mono- and di-acetylated forms that also contain K16 acetylation (Fig. 2.3 c). Consistent with this, the acetylation site occupancies at K5, K12 and K16 were roughly 20% each in CAF1- bound H4, a pattern strikingly different from that observed in total histones (Fig. 2.3 d). In *S. cerevisiae*, the integrity of heterochromatin depends on removal of H4K16 acetylation by the deacetylase Sir2 (Rusche et al., 2003). Our results imply that Sir2-mediated deacetylation of H4K16 in new molecules deposited onto DNA during replication is likely important for the propagation of heterochromatin structure in proliferating cells.

2.5. Discussion

Iso-PeptidAce was initially created to solve a specific problem that had apparently been neglected, even though it was pointed out by Smith et al. more than 12 years ago (Smith et al., 2003). The problem of determining the relative abundance of multiple acetylated forms derived from the N-terminal tail of histone H4, which contains four acetylatable lysines, is compounded by the fact that several acetylated isomers co-elute during liquid chromatography and cannot be distinguished from each other based on the masses of MS2 fragments. The value of determining the relative abundance of acetylated isomers was illustrated by our studies of new histone molecules bound to CAF1. Unexpectedly, the predominant pattern of acetylation that we found consisted of H4 molecules tri-acetylated at K5, K12 and K16. Although further studies are necessary to assess its biological significance, the prevalence of this acetylation pattern has implications for both replication-coupled nucleosome assembly and the roles of histone deacetylases in the propagation of heterochromatin structures in proliferating cells. It is known that in addition to lysine acetylation and methylation, histones are also modified by numerous other types of PTMs. Among many others, these include mono- or dimethylation of arginine, and several acylated forms of lysine residues that contain formyl, butyryl, crotonyl, malonyl or succinyl moieties. In the current study, we did not determine the abundance of those types of PTMs because our method was developed with synthetic peptides carrying PTMs that were known to occur in yeast. Based on our data, we cannot rule out the possibility that other types of PTMs might also exist on the peptides that we studied. However, when coupled with recently developed multiplexed parallel reaction monitoring approaches (Gallien et al., 2012; Tang et al., 2014) we anticipate that our method will prove valuable

for deconvolution of a large number of isomeric/ isobaric peptides bearing numerous patterns of PTMs. We also expect that our method will prove an asset to investigate a broad range of biological problems related to protein lysine acetylation. For instance, our approach will be valuable to determine the in vivo substrate specificity of the multitude of bromodomain (BRD)-containing proteins that exist in model organisms and human cells (Filippakopoulos and Knapp, 2012). Previous in vitro studies have clearly shown that BRDs derived from chromatin-modifying enzymes bind with higher affinity to peptides that contain acetylated lysines located in close proximity (Filippakopoulos and Knapp, 2012). Moreover, because large protein complexes contain multiple BRDs located in different subunits of a given complex, deciphering their physiologically relevant acetylated substrates remains a formidable task. Proteomics studies performed in several species have identified a myriad of acetylation sites in proteins with a wide range of biological functions (Chen et al., 2012; Downey et al., 2015; Weinert et al., 2011). Supplementary Table 6 shows seven examples of known acetylated peptides where isomers could now be distinguished based on their fragmentation patterns. We, therefore, anticipate that, when combined with techniques to copurify protein complexes with their acetylated substrates, the method described here will help identify combinatorial patterns of lysine acetylation that are recognized by protein complexes involved in numerous biological processes.

2.6. Acknowledgments

We thank Dr. Sébastien Lemieux (UdeM) for his invaluable advice on the use of different bioinformatics tools and approaches. We also thank Éric Bonneil (UdeM) for his assistance with MS experiments. This work was carried out with financial support from the Canadian Institute for Health Research to A.V. (CIHR, FRN 125916) and the Natural Sciences and Engineering Research Council (NSERC 311598) to P.T. The Institute for Research in Immunology and Cancer receives infrastructure support from IRICoR, the Canadian Foundation for Innovation, and the Fonds de Recherche du Québec—Santé.

2.7. Author Contributions

N.A. designed and carried out the proteomics experiments. O.C-L. built and tested the Iso-PeptidAce deconvolution software. R.E.R. and C.P. produced HDAC inhibitor-treated cells and performed histone extraction. A.J. and R.E.R. isolated histones bound to yeast CAF1. N.A. analyzed data with help from O.C-L. P.T. and A.V. conceived and led the project. N.A., O.C.-L., P.T. and A.V. wrote the manuscript, with input from all the authors.

2.8. References

Abshiru, N., Ippersiel, K., Tang, Y., Yuan, H., Marmorstein, R., Verreault, A., and Thibault, P. (2013). Chaperone-mediated acetylation of histones by Rtt109 identified by quantitative proteomics. J. Proteomics *81*, 80–90.

Ahuja, R., Magnanti, T., and Orlin, J. (1993). Network Flows: Theory, algorithms, and applications. 846.

Albert, R. (2005). Scale-free networks in cell biology. J. Cell Sci. *118*, 4947–4957.

Arts, J., King, P., Mariën, A., Floren, W., Beliën, A., Janssen, L., Pilatte, I., Roux, B., Decrane, L., Gilissen, R., et al. (2009). JNJ-26481585, a novel “second-generation” oral histone deacetylase inhibitor, shows broad-spectrum preclinical antitumoral activity. Clin. Cancer Res. *15*, 6841–6851.

Bern, M., Finney, G., Hoopmann, M.R., Merrihew, G., Toth, M.J., and MacCoss, M.J. (2010). Deconvolution of mixture spectra from ion-trap data-independent-acquisition tandem mass spectrometry. Anal. Chem. *82*, 833–841.

Chen, Y., Zhao, W., Yang, J.S., Cheng, Z., Luo, H., Lu, Z., Tan, M., Gu, W., and Zhao, Y. (2012). Quantitative acetylome analysis reveals the roles of SIRT1 in regulating diverse substrates and cellular pathways. Mol. Cell. Proteomics *11*, 1048–1062.

Cho, D.-Y., Kim, Y.-A., and Przytycka, T.M. (2012). Chapter 5: Network biology approach to complex diseases. PLoS Comput. Biol. *8*, e1002820.

Courcelles, M., Bridon, G., Lemieux, S., and Thibault, P. (2012). Occurrence and detection of phosphopeptide isomers in large-scale phosphoproteomics experiments. J. Proteome Res. *11*, 3753–3765.

Deleu, S., Lemaire, M., Arts, J., Menu, E., Van Valckenborgh, E., King, P., Vande Broek, I., De Raeve, H., Van Camp, B., Croucher, P., et al. (2009). The effects of JNJ-26481585, a novel hydroxamate-based histone deacetylase inhibitor, on the development of multiple myeloma in the 5T2MM and 5T33MM murine models. Leukemia *23*, 1894–1903.

Downey, M., Johnson, J.R., Davey, N.E., Newton, B.W., Johnson, T.L., Galaang, S., Seller, C.A., Krogan, N., and Toczyski, D.P. (2015). Acetylome profiling reveals overlap in the regulation of diverse processes by Sirtuins, Gcn5, and Esa1. Mol. Cell. Proteomics *14*, 162–176.

Dutt, S., Dai, Y., Ren, H., and Fontanarosa, J. (2009). Selection of multiple SNPs in case-control association study using a discretized network flow approach. pp. 211–223.

Feller, C., Forné, I., Imhof, A., and Becker, P.B. (2015). Global and specific responses of the histone acetylome to systematic perturbation. Mol. Cell *57*, 559–572.

Filippakopoulos, P., and Knapp, S. (2012). The bromodomain interaction module. FEBS Lett. *586*, 2692–2704.

Filippakopoulos, P., Picaud, S., Mangos, M., Keates, T., Lambert, J.-P.P., Barsyte-Lovejoy, D., Felletar, I., Volkmer, R., Müller, S., Pawson, T., et al. (2012). Histone recognition and large-scale structural analysis of the human bromodomain family. Cell *149*, 214–231.

Gallien, S., Duriez, E., Crone, C., Kellmann, M., Moehring, T., and Domon, B. (2012). Targeted proteomic quantification on Quadrupole-Orbitrap mass spectrometer. Mol. Cell. Proteomics *11*, 1709–1723.

Hernan, C., Gorlick, R., Kolb, E.A., Morton, C.L., Manesh, D.M., Keir, S.T., Reynolds, P.C., Kang, M.H., Maris, J.M., Wozniak, A., et al. (2014). Initial testing (Stage 1) of the histone deacetylase inhibitor, Quisinostat (JNJ-26481585), by the pediatric preclinical testing program. J. Clin. Oncol. *61*, 245–252.

Huang, Y., Triscari, J.M., Tseng, G.C., Pasa-Tolic, L., Lipton, M.S., Smith, R.D., and Wysocki, V.H. (2005). Statistical characterization of the charge state and residue dependence of low-energy CID peptide dissociation patterns. Anal. Chem. *77*, 5800–5813.

Kapp, E.A., Schütz, F., Reid, G.E., Eddes, J.S., Moritz, R.L., O'Hair, R.A.J., Speed, T.P., and Simpson, R.J. (2003). Mining a tandem mass spectrometry database to determine the trends and global factors influencing peptide fragmentation. Anal. Chem. *75*, 6251–6264.

Kelly, T.J., Qin, S., Gottschling, D.E., and Parthun, M.R. (2000). Type B histone acetyltransferase Hat1p participates in telomeric silencing. Mol. Cell. Biol. *20*, 7051–7058.

Li, Q., Burgess, R., and Zhang Zhiguo (2012). All roads lead to chromatin: Multiple pathways for histone deposition. Biochim. Biophys. Acta *1819*, 238–246.

Qin, S., and Parthun, M.R. (2002). Histone H3 and the histone acetyltransferase Hat1p contribute to DNA double-strand break repair. Mol. Cell. Biol. *22*, 8353–8365.

Rusche, L.N., Kirchmaier, A.L., and Rine, J. (2003). The establishment, inheritance, and function of silenced chromatin in *Saccharomyces cerevisiae*. Annu. Rev. Biochem. *72*, 481–516.

Shechter, D., Dormann, H.L., Allis, C.D., and Hake, S.B. (2007). Extraction, purification and analysis of histones. Nat Protoc *2*, 1445–1457.

Sidoli, S., Schwämmle, V., Ruminowicz, C., Hansen, T.A., Wu, X., Helin, K., and Jensen, O.N. (2014). Middle-down hybrid chromatography/tandem mass spectrometry workflow for characterization of combinatorial post-translational modifications in histones.

Proteomics *14*, 2200–2211.

Smith, C.M., Gafken, P.R., Zhang, Z., Gottschling, D.E., Smith, J.B., and Smith, D.L. (2003). Mass spectrometric quantification of acetylation at specific lysines within the amino-terminal tail of histone H4. Anal. Biochem. *316*, 23–33.

Snyman, J.A. (2005). Practical mathematical optimization : an introduction to basic optimization theory and classical and new gradient-based algorithms (Springer).

Sobel, R.E., Cook, R.G., Perry, C.A., Annunziato, A.T., and Allis, C.D. (1995). Conservation of deposition-related acetylation sites in newly synthesized histones H3 and H4. Proc. Natl. Acad. Sci. U. S. A. *92*, 1237–1241.

Stühmer, T., Arts, J., Chatterjee, M., Borawski, J., Wolff, A., King, P., Einsele, H., Leo, E., and Bargou, R.C. (2010). Preclinical anti-myeloma activity of the novel HDAC-inhibitor JNJ-26481585: Research paper. Br. J. Haematol. *149*, 529–536.

Tang, H., Fang, H., Yin, E., Brasier, A.R., Sowers, L.C., and Zhang, K. (2014). Multiplexed parallel reaction monitoring (PRM) targets histone modifications on the Q-Exactive mass spectrometer. Anal. Chem. 140513170620003.

Tong, W.G., Wei, Y., Stevenson, W., Kuang, S.Q., Fang, Z., Zhang, M., Arts, J., and Garcia-Manero, G. (2010). Preclinical antileukemia activity of JNJ-26481585, a potent second-generation histone deacetylase inhibitor. Leuk. Res. *34*, 221–228.

Unnikrishnan, A., Gafken, P.R., and Tsukiyama, T. (2010). Dynamic changes in histone acetylation regulate origins of DNA replication. Nat. Struct. Mol. Biol. *17*, 430–437.

Venugopal, B., Baird, R., Kristeleit, R.S., Plummer, R., Cowan, R., Stewart, A., Fourneau, N., Hellemans, P., Elsayed, Y., Mcclue, S., et al. (2013). A phase I study of quisinostat (JNJ-26481585), an oral hydroxamate histone deacetylase inhibitor with evidence of target modulation and antitumor activity, in patients with advanced solid tumors. Clin. Cancer Res. *19*, 4262–4272.

Wang, J., Bourne, P.E., and Bandeira, N. (2014). MixGF: Spectral probabilities for mixture spectra from more than one peptide. Mol. Cell. Proteomics *13*, 3688–3697.

Weinert, B.T., Wagner, S.A., Horn, H., Henriksen, P., Liu, W.R., Olsen, J. V., Jensen, L.J., and Choudhary, C. (2011). Proteome-wide mapping of the Drosophila acetylome demonstrates a high degree of conservation of lysine acetylation. Sci. Signal. *4*, ra48.

Yuan, Z.-F., Lin, S., Molden, R.C., Cao, X.-J., Bhanu, N. V., Wang, X., Sidoli, S., Liu, S., and Garcia, B.A. (2015). EpiProfile quantifies histone peptides with modifications by extracting retention time and intensity in high-resolution mass spectra. Mol. Cell. Proteomics *14*, 1696–1707.

Zentner, G.E., and Henikoff, S. (2013). Regulation of nucleosome dynamics by histone modifications. Nat. Struct. Mol. Biol. *20*, 259–266.

Zhang, B., Pirmoradian, M., Chernobrovkin, A., and Zubarev, R.A. (2014). DeMix Workflow for efficient identification of cofragmented Peptides in high resolution data-dependent tandem mass spectrometry. Mol. Cell. Proteomics *13*, 3211–3223.

Zhou, H., Madden, B.J., Muddiman, D.C., Zhang, Z., Han, J., Liang, H., Zhang, Z., Liu, Y., Zhang, Z., Mer, G., et al. (2006). Chromatin Assembly Factor 1 interacts with histone H3 methylated at lysine 79 in the processes of epigenetic silencing and DNA repair †. Biochemistry *45*, 2852–2861.

2.9. Supplementary Data

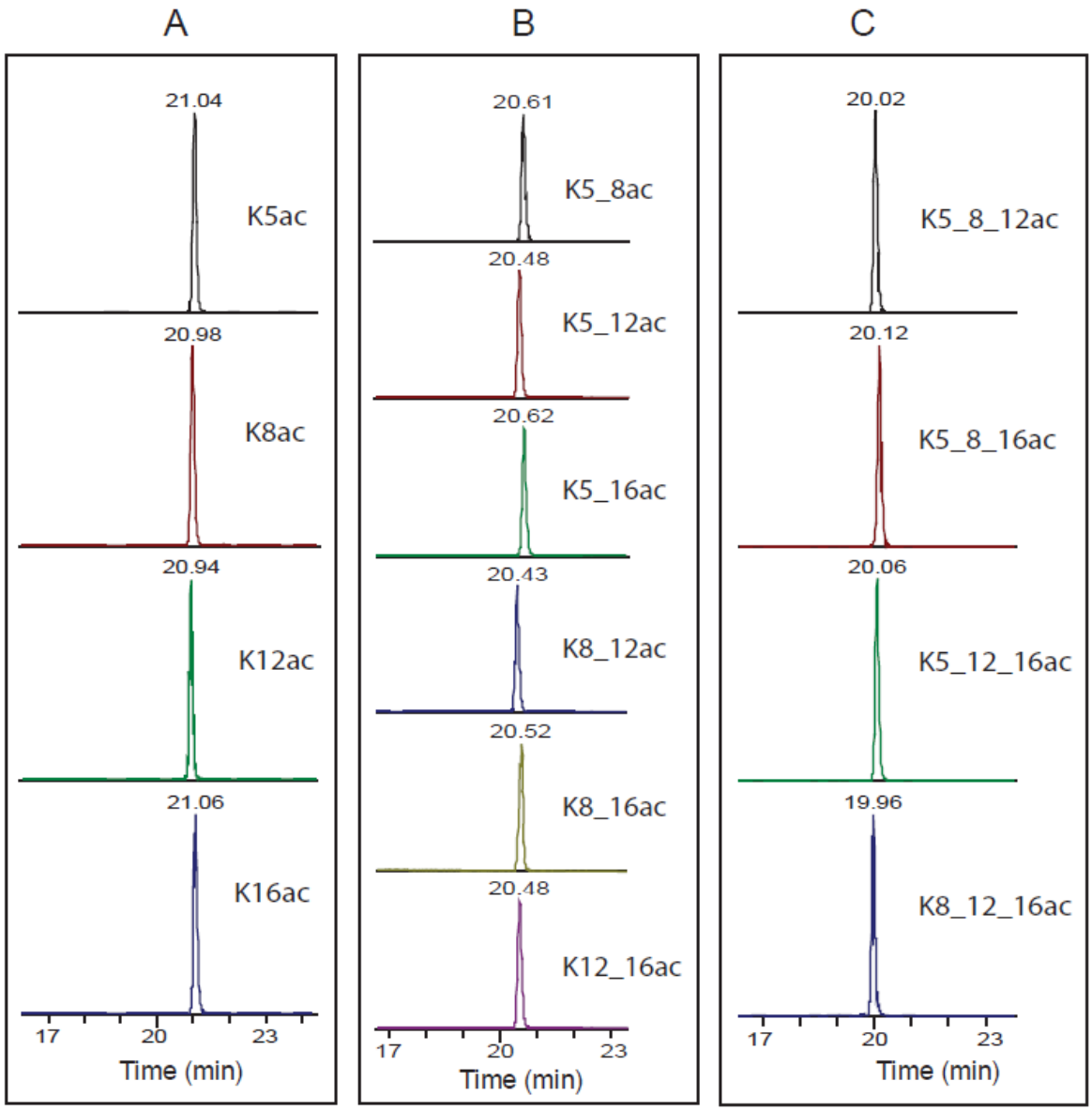

Supplementary Figure 2.1. Peptides within the same isomeric groups exhibit very narrow retention time differences. After in vitro propionylation and trypsin digestion of our synthetic peptides, we assessed their *m/z* ratio, charge state and retention time by LC-MS analysis. Shown in this figure are the extracted ion chromatograms of doubly charged isomers of (A) mono-acetylated and triply propionylated (*m/z* 740.93), (B) di-acetylated and di-propionylated (*m/z* 733.93), and (C) tri-acetylated and mono-propionylated (*m/z* 726.92) H4 peptide 4-GKGGKGLGKGGAKR-17.

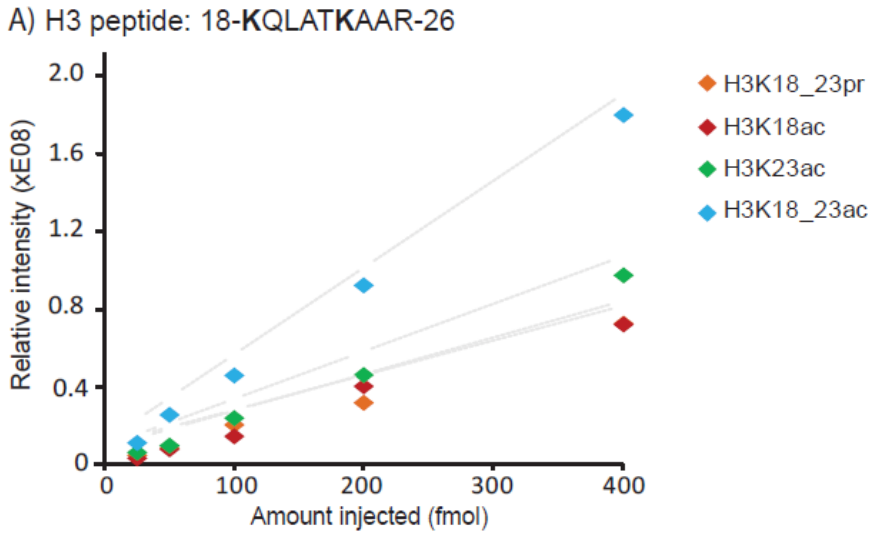

Signal response	Slope
K18_23pr	183967
K18ac	190984
K23ac	251676
K18_23ac	460783

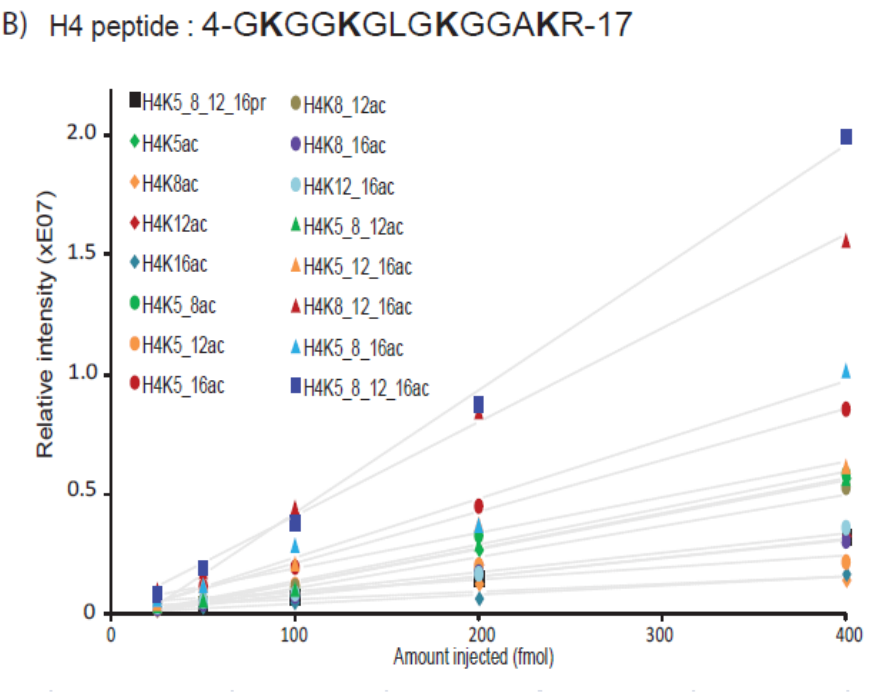

Signal response	Slope
K5/8/12/16pr	7898.8
K5Ac	14331
K8Ac	3181.5
K12Ac	8033.1
K16Ac	3818.7
K5/8Ac	15163
K5/12Ac	5051.5
K5/16Ac	21465
K8/12Ac	13017
K8/16Ac	7617.1
K12//16Ac	8762.5
K5/8/12Ac	14529
K5/8/16Ac	14799
K5/12/16Ac	39046
K8/12/16Ac	24572
K5/8/12/16Ac	51021

Supplementary Figure 2.2. MS signal responses of unmodified and acetylated H3 and H4 peptides. After *in vitro* propionylation and trypsin digestion of synthetic peptides, the relative MS response of each peptide was determined based on the curve of ion intensity versus amount injected for the nonacetylated and acetylated forms of (A) H3 peptide 18-KQLATKAAR-26 and (B) H4 peptide 4-GKGGKGLGKGGAKR-17. The tables on the right show the slopes of the lines determined from the linear equation that best-fit (as measured by R2 values) the signal responses.

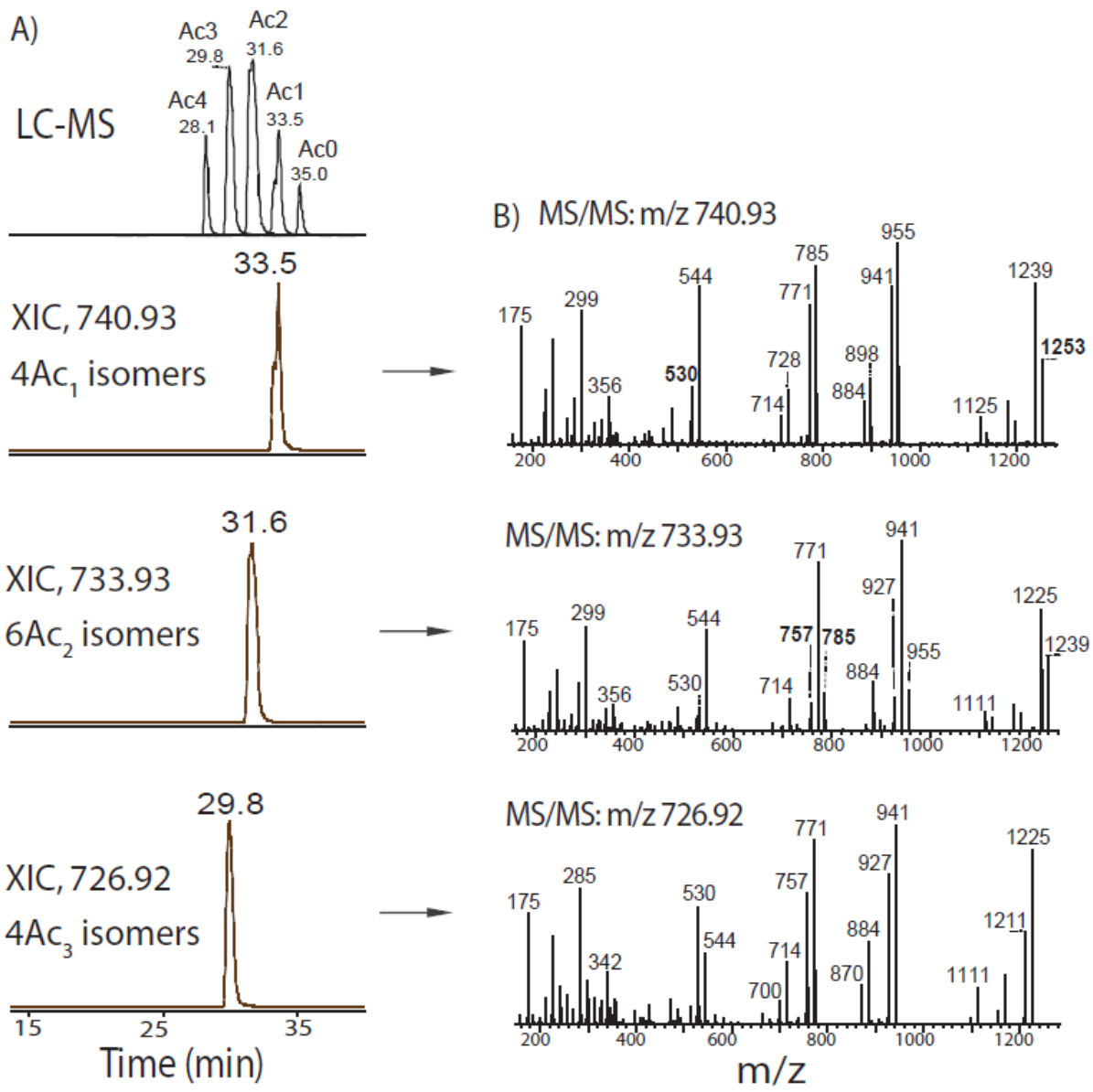

Supplementary Figure 2.3. Acetylated isomers co-elute from the reverse-phase column and produce composite MS/MS spectra upon fragmentation. A) LC-MS trace of a mixture of sixteen H4 peptides, and extracted ion chromatograms of co-eluting four mono-, six di- and four tri-acetylated isomers of peptide 4-GKGGKGLGKGGAKR-17 (top to bottom panels). B) Mixed MS/MS spectra of four mono-, six di- and four tri-acetylated isomers (from top to bottom panel).

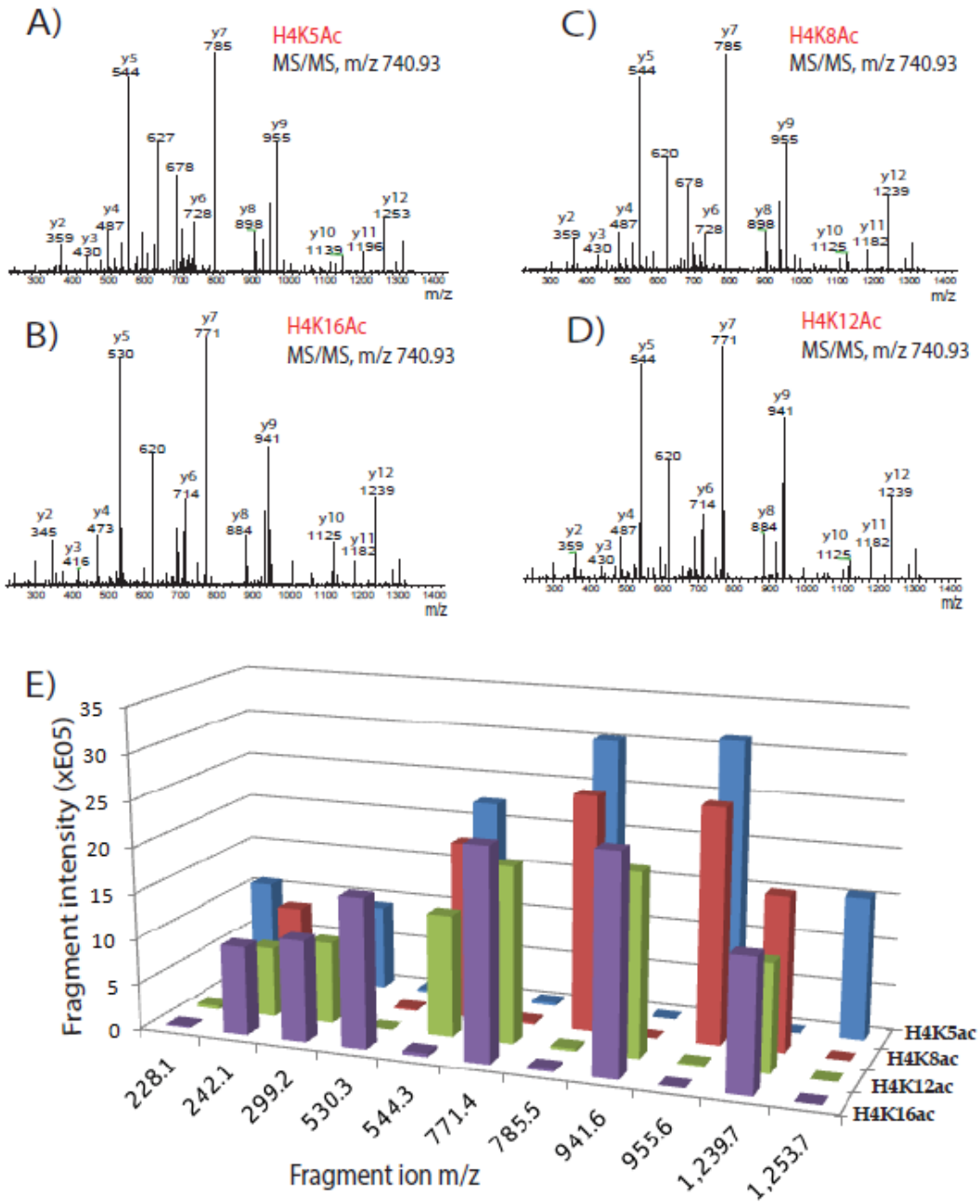

Supplementary Figure 2.4. Isomeric peptides produce distinct fragment ion patterns upon fragmentation in the MS. Representative fragment ion spectra of four mono-acetylated isomers of the peptide 4-GKGGKGLGKGGAKR-17: (A) H4K5ac, (B) H4K16ac, (C) H4K8ac, and (D) H4K12ac. The 'y' type fragment ions are indicated in each spectrum. E) A three-dimensional view of the distribution of selected 'b' and 'y' type fragment ions derived from the individual mono-acetylated isomers. The 'b' type fragment ions are shown at *m/z* 228.1 (b2, K5ac), 242.1 (b2, K5pr) and 299.2 (b3, K5pr). The 'y' type fragment ions are m/z 530.3, 544.30, 771.4, 785.5, 941.6, 955.6, 1239.7 and 1253.7.

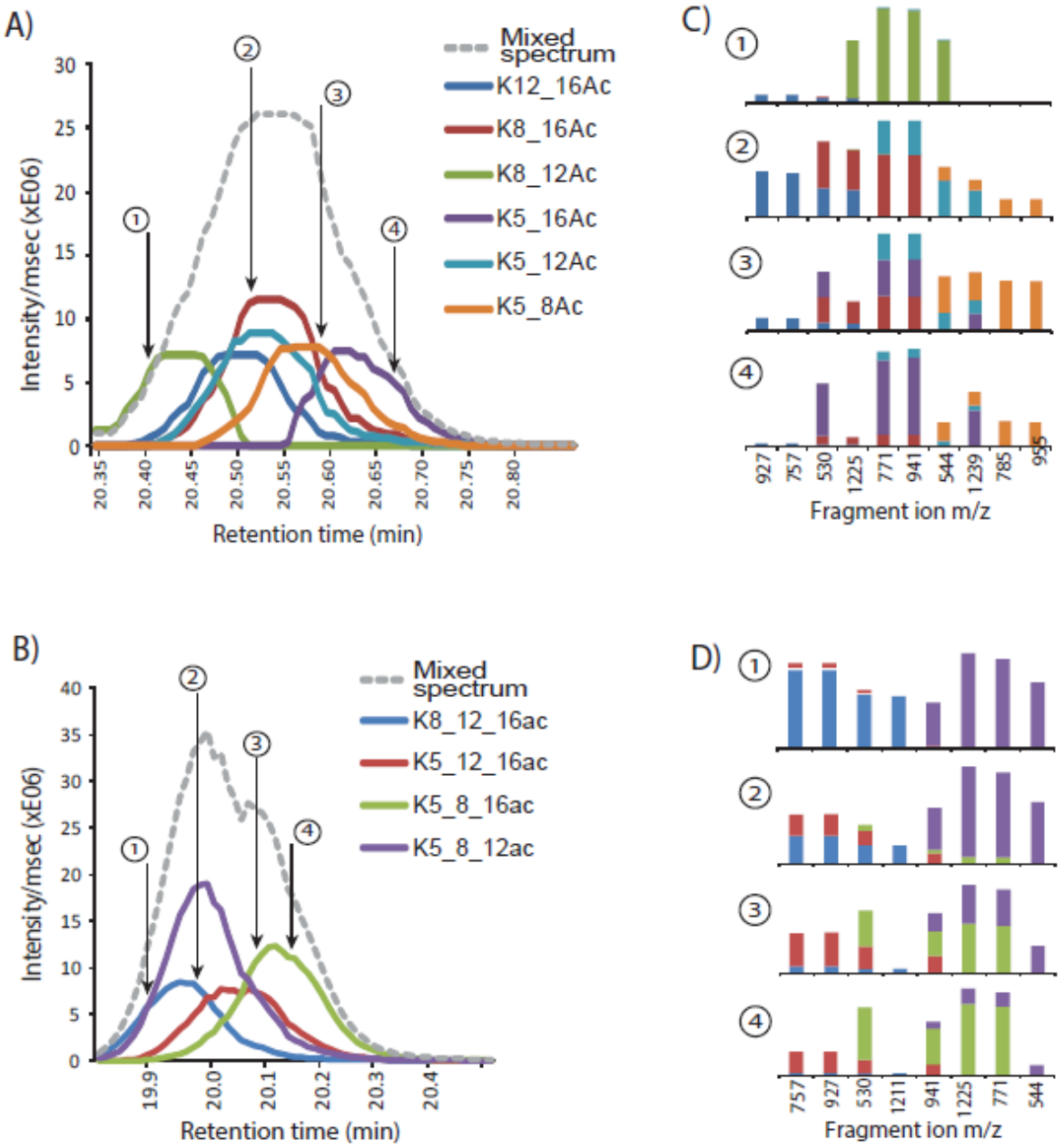

Supplementary Figure 2.5. Deconvolution of co-eluting di- and tri-acetylated isomers of histone H4 peptides by Iso-PeptidAce. Elution profiles before (dashed line) or after (colored lines) deconvolution of a mixture of (A) six di-acetylated, and (B) four tri-acetylated isomers of the peptide 4-GKGGKGLGKGGAKR-17. Distributions of fragment peaks of the deconvoluted di- (C) and tri-acetylated (D) isomers.

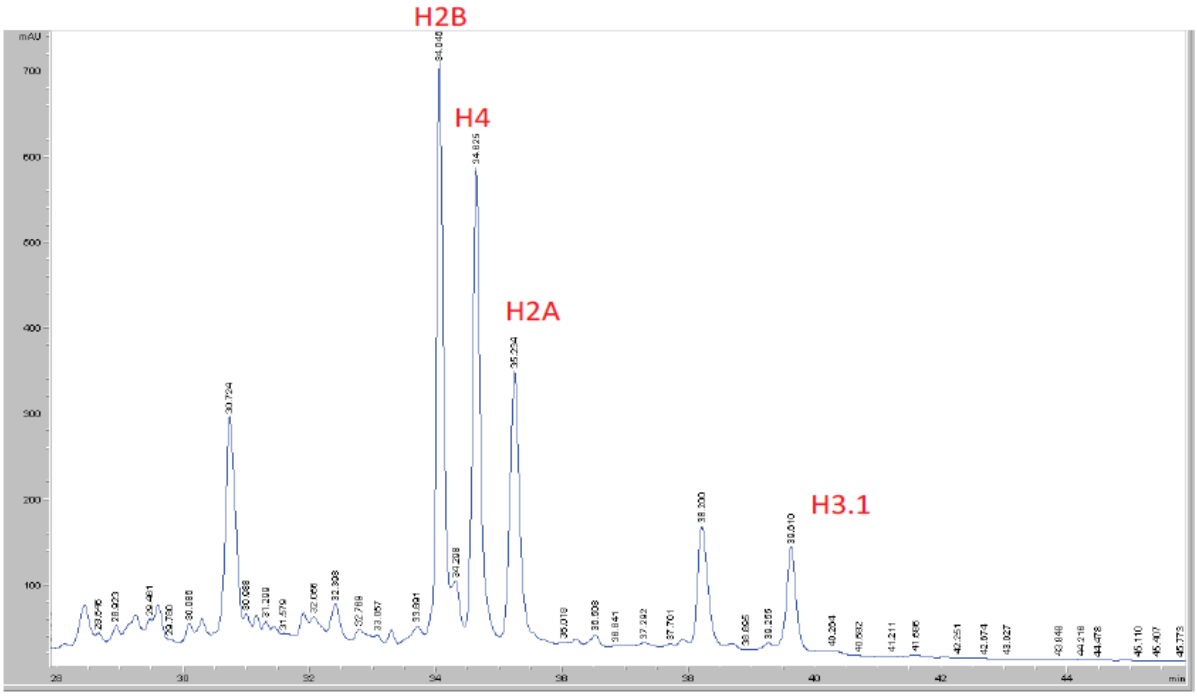

Supplementary Figure 2.6. Fractionation of total histones by RP-HPLC. Total histones were baseline separated as H2B, H4, H2A and H3.1 in increasing order of retention time. Histone H3.1 and H4 fractions were pooled and dried completely in a speed-vac concentrator. LC conditions: Pump A: 0.1% trifluoroacetic acid in 100% filtered water (v/v). Pump B: 0.1% trifluoroacetic acid in 100% acetonitrile (v/v)., flow rate:150□l/min, Absorbance wavelength: 214 nm, Column: Zorbax C8, 5□m, 2.1x150 mm

Supplementary Figure 2.7. MS/MS spectra of peptide isomers (Pg 113-132)

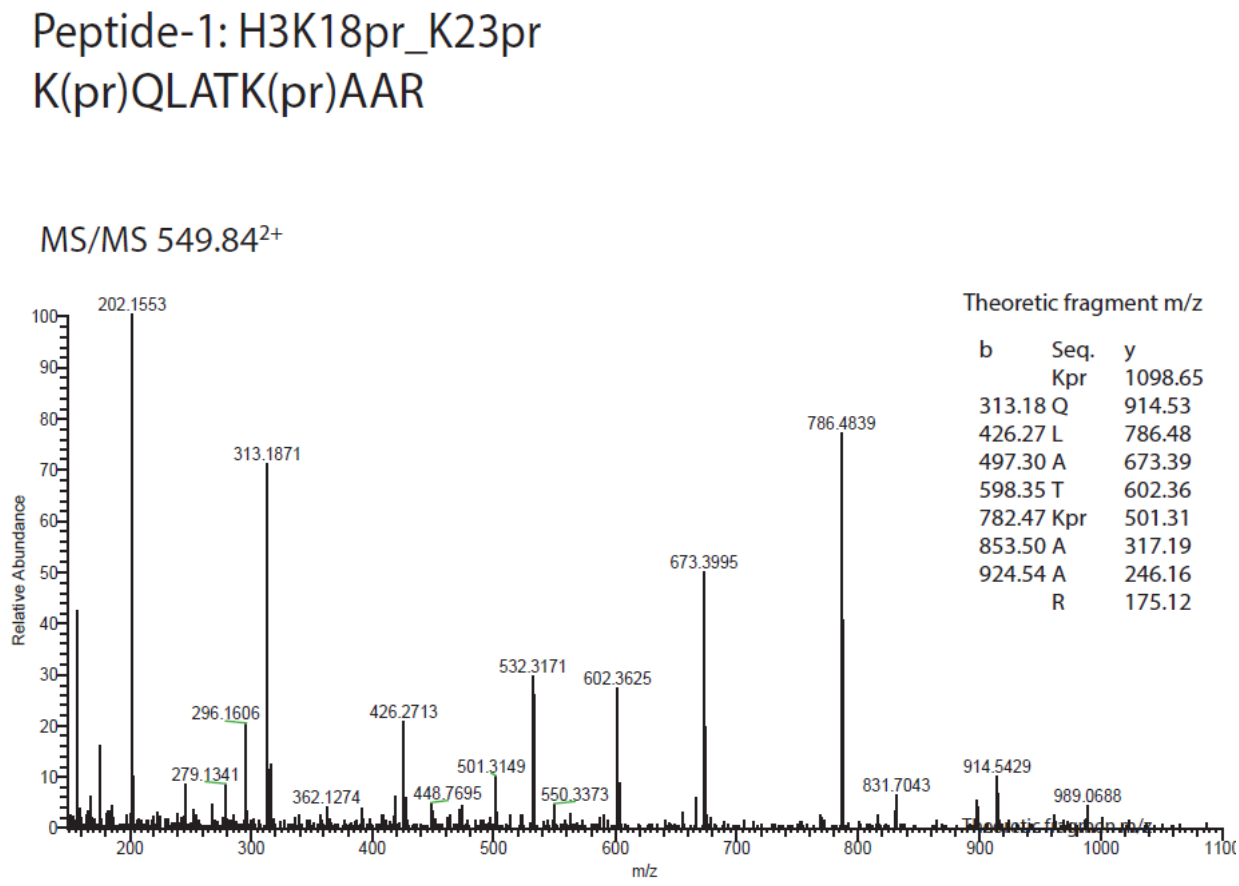

Peptide-2: H3K18ac_K23pr
K(ac)QLATK(pr)AAR

MS/MS 542.83^{2+}

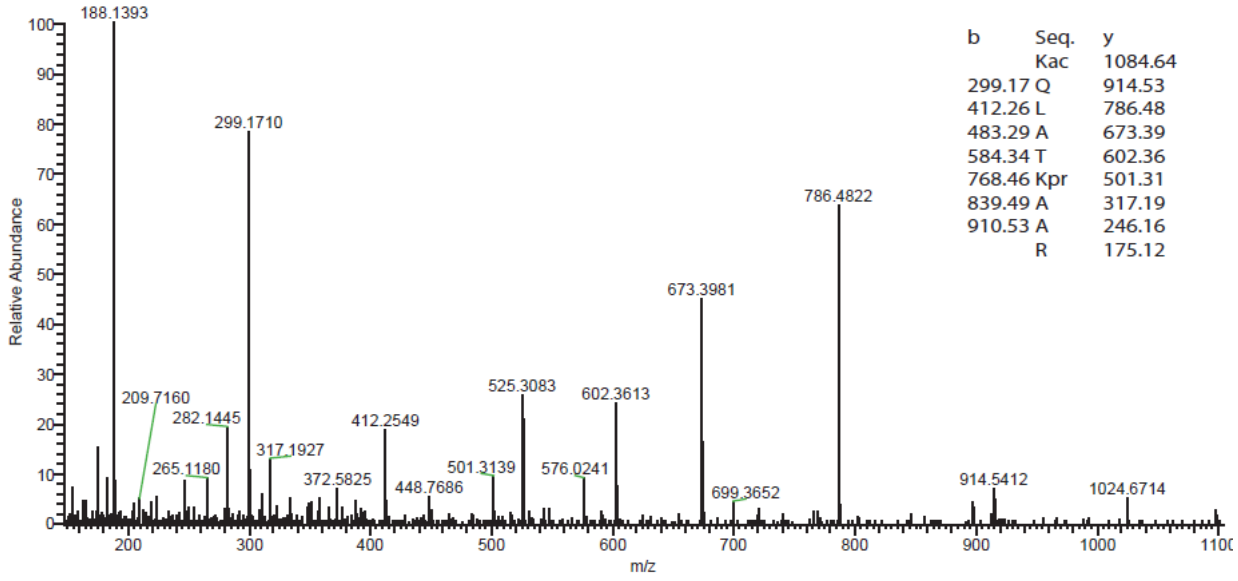

Peptide-3: H3K18pr_K23ac
K(pr)QLATK(ac)AAR

MS/MS 542.83^{2+}

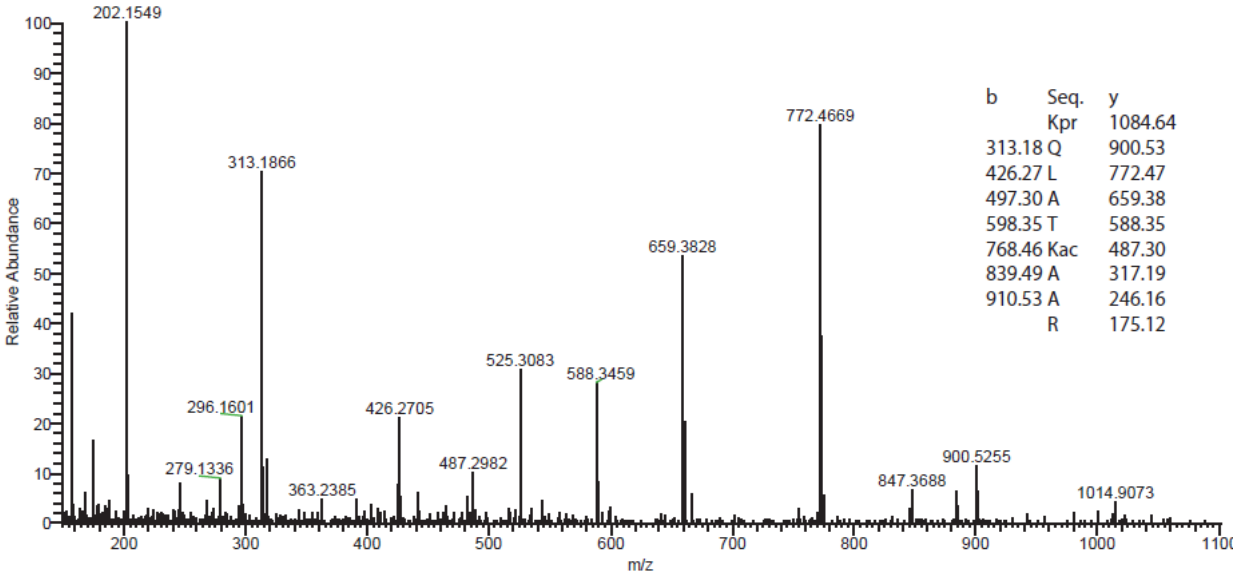

Peptide-4: H3K18ac_K23ac
K(ac)QLATK(ac)AAR

MS/MS 535.82^{2+}

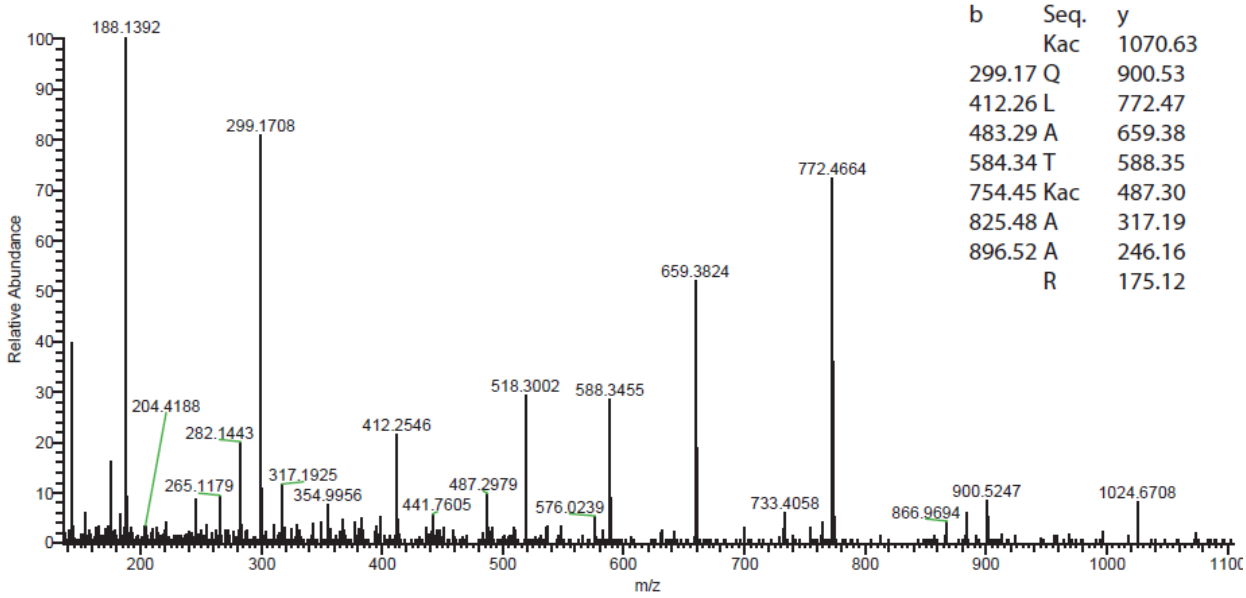

Peptide-5: H4K5_8_12_16pr
GK(pr)GGK(pr)GLGK(pr)GGAK(pr)R

MS/MS 747.94^{2+}

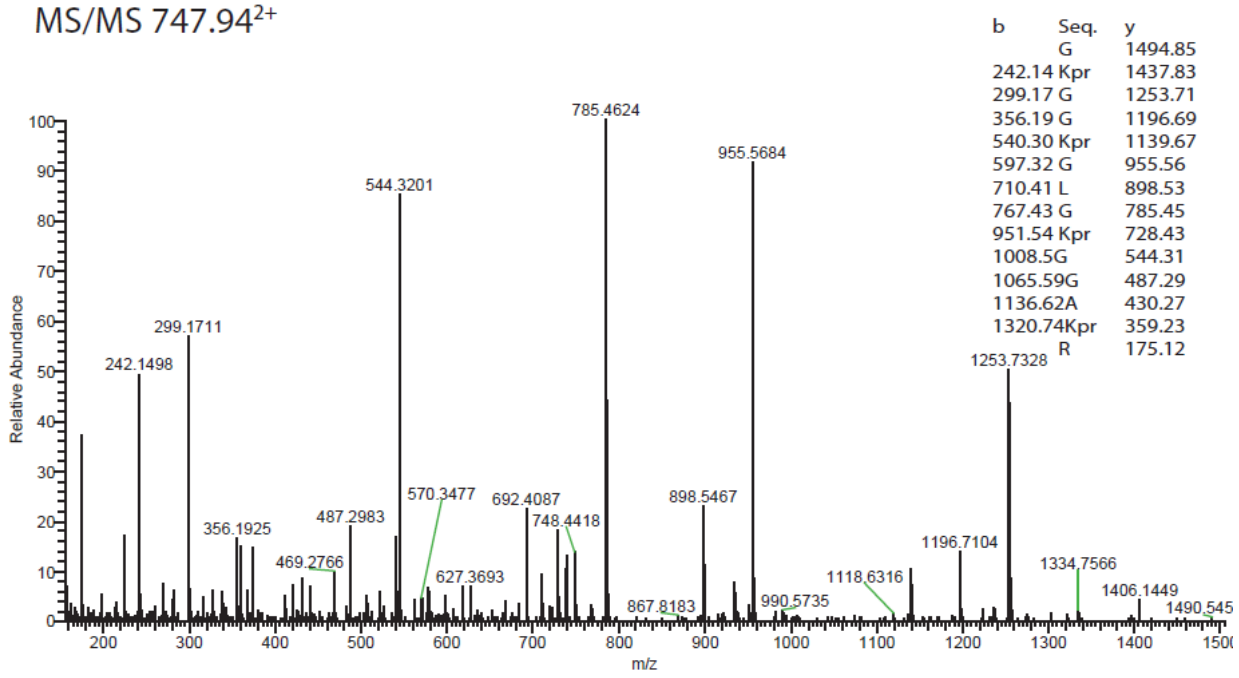

Peptide-6: H4K5ac/K8_12_16pr
GK(ac)GGK(pr)GLGK(pr)GGAK(pr)R

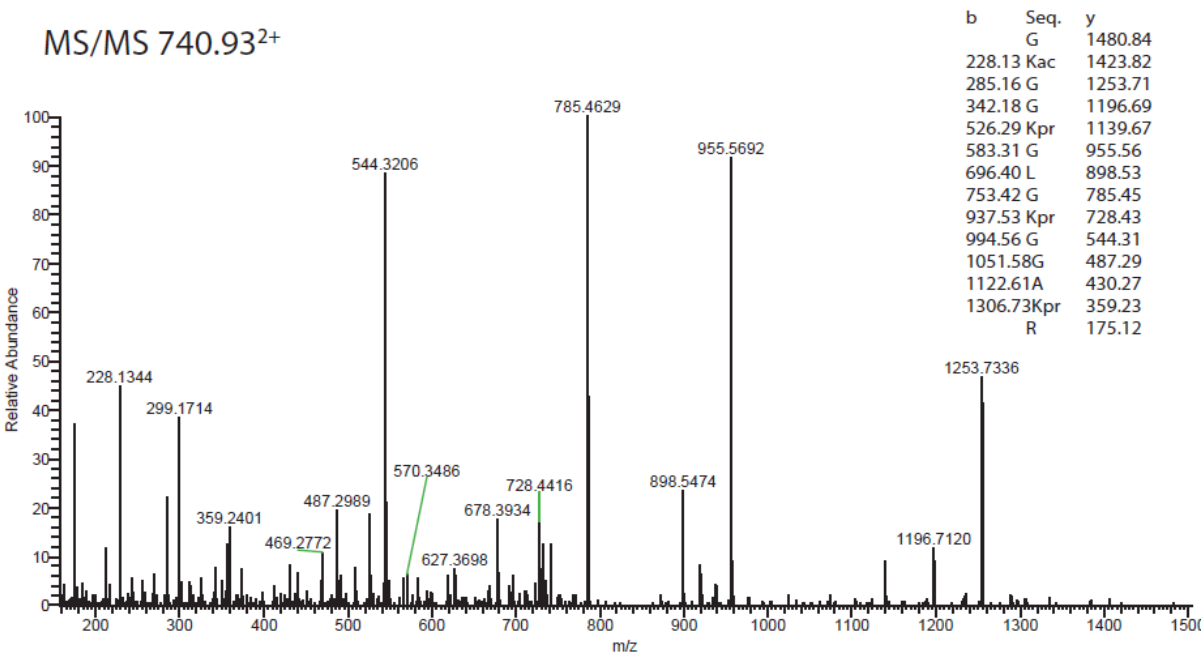

Peptide-7: H4K8ac/K5_12_16pr
GK(pr)GGK(ac)GLGK(pr)GGAK(pr)R

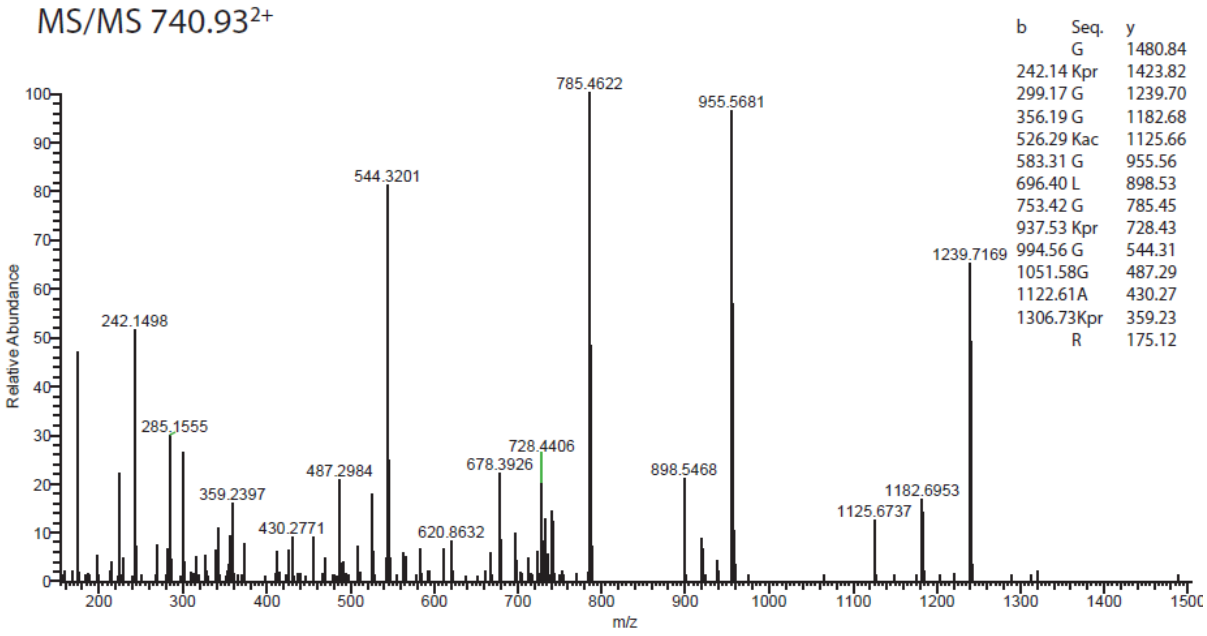

Peptide-8: H4K12ac/K5_8_16pr
GK(pr)GGK(pr)GLGK(ac)GGAK(pr)R

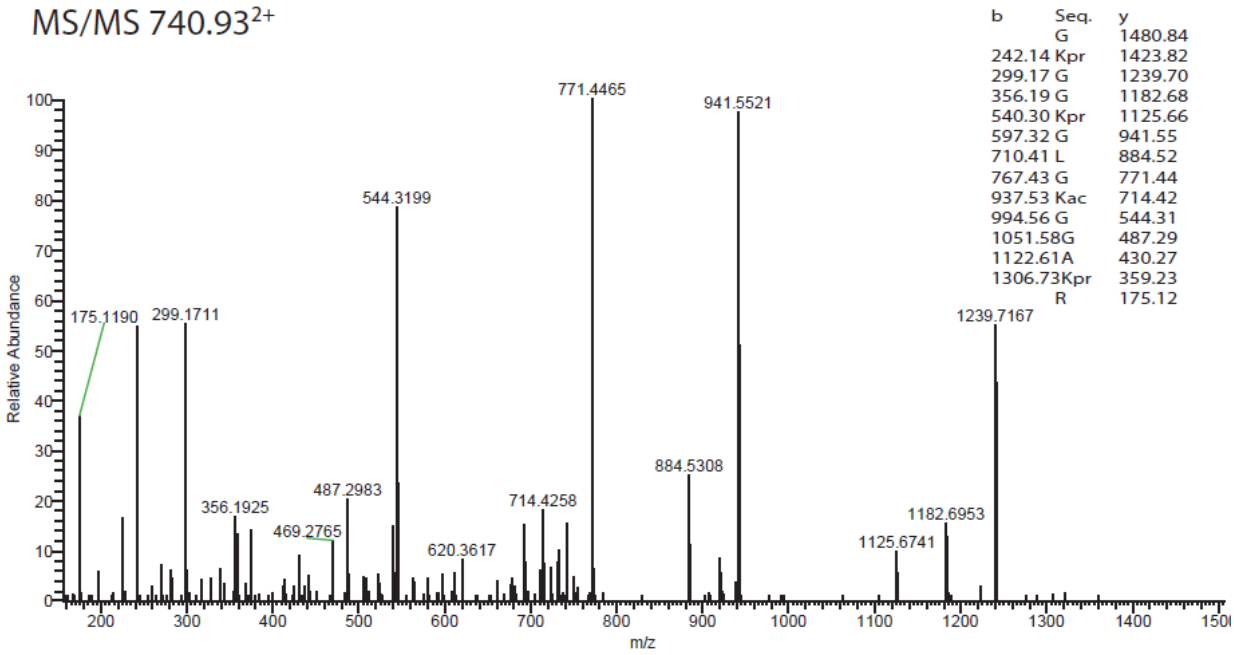

Peptide-9: H4K16ac/K5_8_12pr
GK(pr)GGK(pr)GLGK(pr)GGAK(ac)R

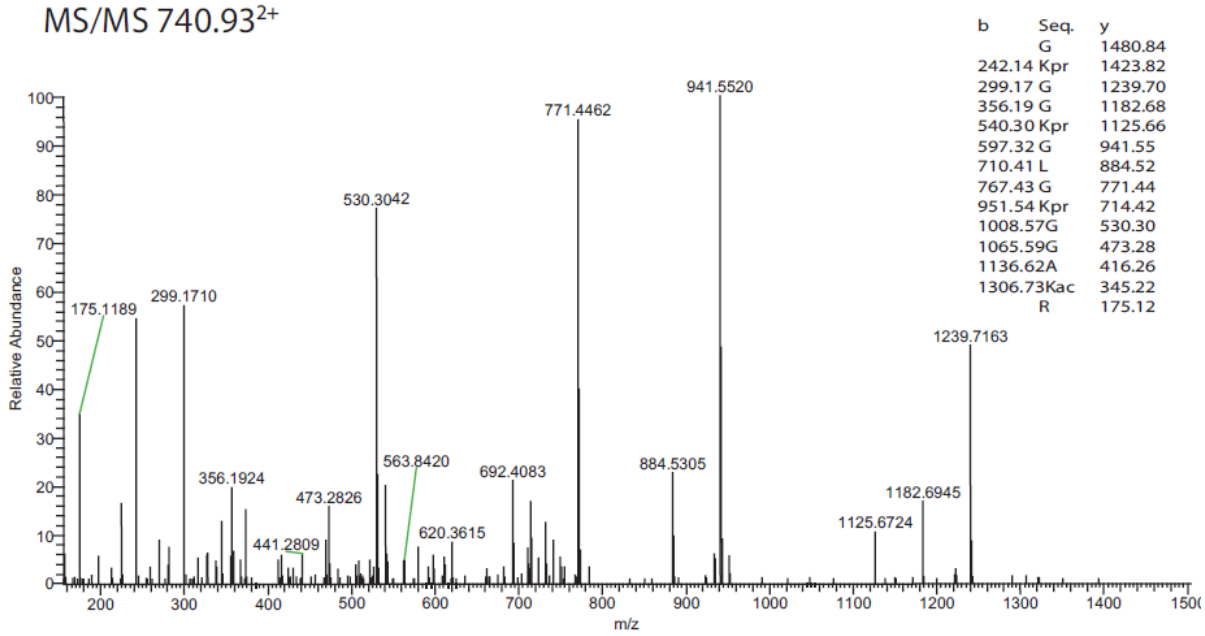

Peptide-10: H4K5_8ac/K12_16pr
GK(ac)GGK(ac)GLGK(pr)GGAK(pr)R

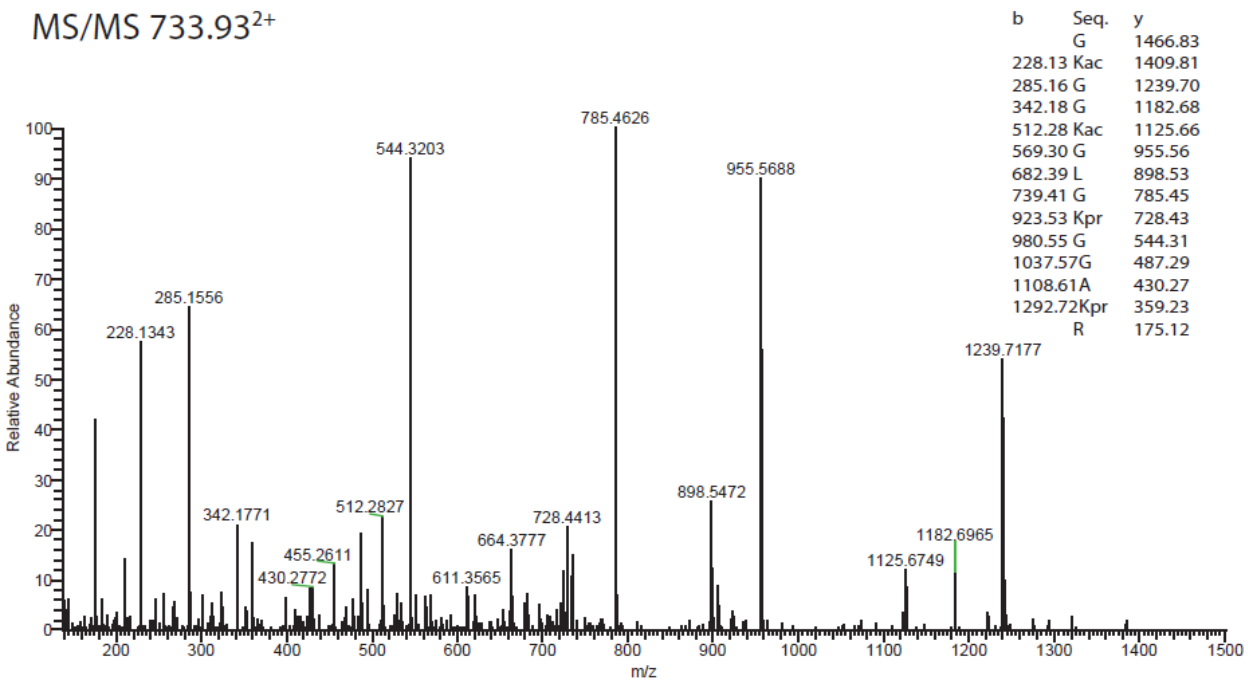

Peptide-11: H4K5_12ac/K8_16pr
GK(ac)GGK(pr)GLGK(ac)GGAK(pr)R

MS/MS 733.93^{2+}

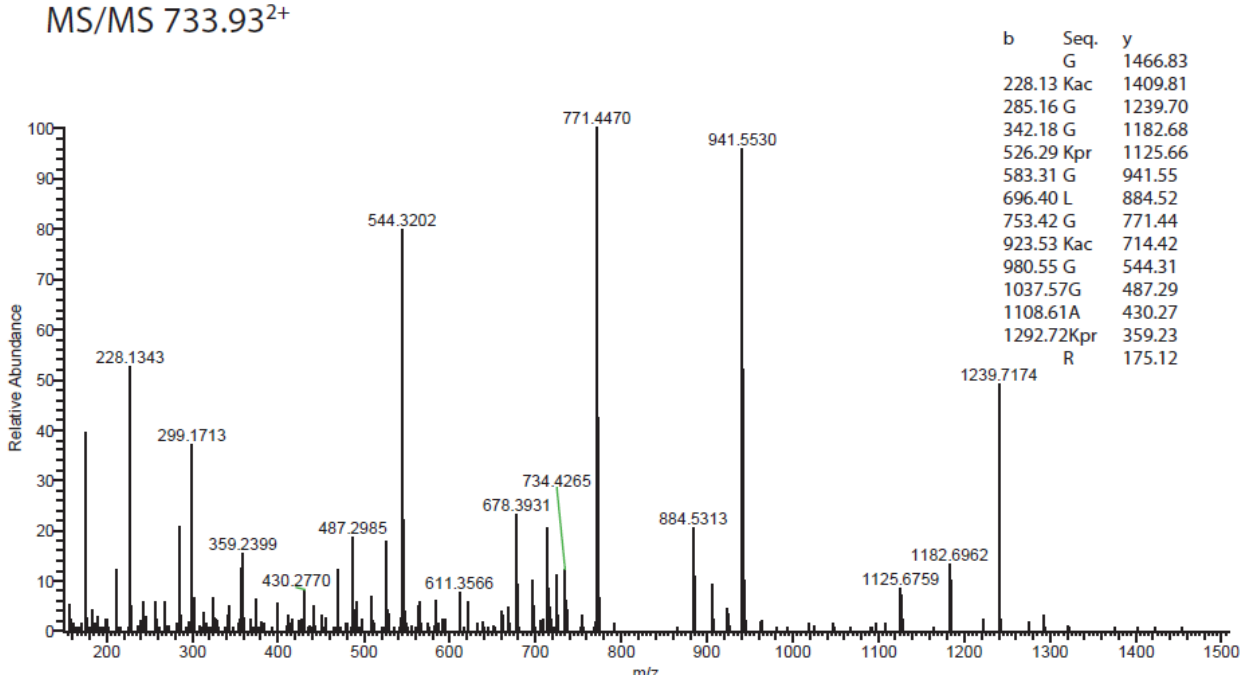

Peptide-12: H4K5_16ac/K8_12pr
GK(ac)GGK(pr)GLGK(pr)GGAK(ac)R

MS/MS 733.93^{2+}

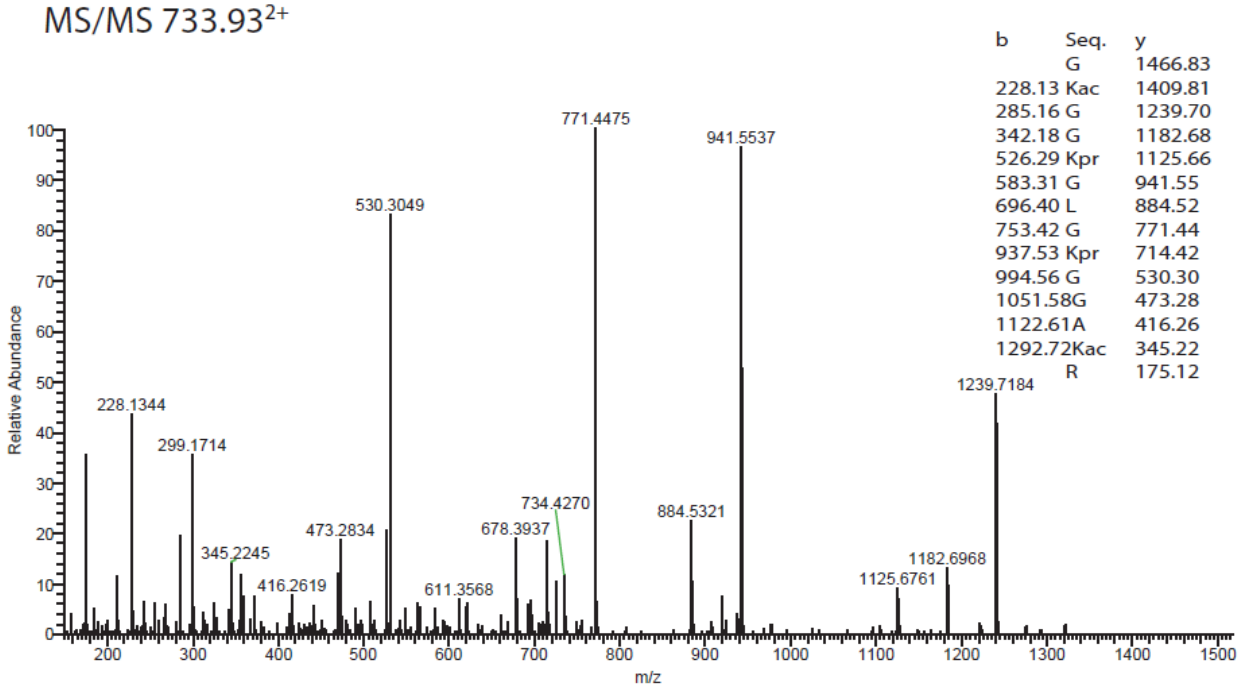

Peptide-13: H4K8_12ac/K5_16pr
GK(pr)GGK(ac)GLGK(ac)GGAK(pr)R

MS/MS 733.93^{2+}

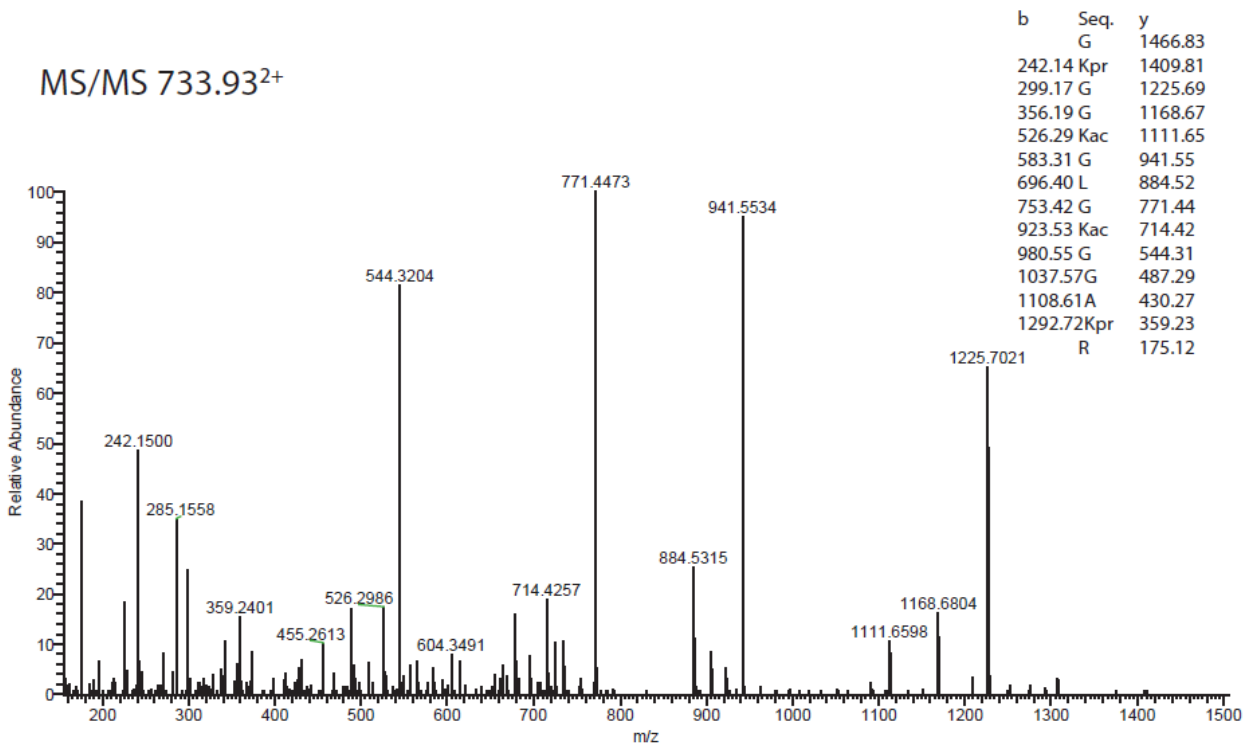

b	Seq.	y
	G	1466.83
242.14	Kpr	1409.81
299.17	G	1225.69
356.19	G	1168.67
526.29	Kac	1111.65
583.31	G	941.55
696.40	L	884.52
753.42	G	771.44
923.53	Kac	714.42
980.55	G	544.31
1037.57	G	487.29
1108.61	A	430.27
1292.72	Kpr	359.23
	R	175.12

Peptide-14: H4K8_16ac/K5_12pr
GK(pr)GGK(ac)GLGK(pr)GGAK(ac)R

MS/MS 733.93^{2+}

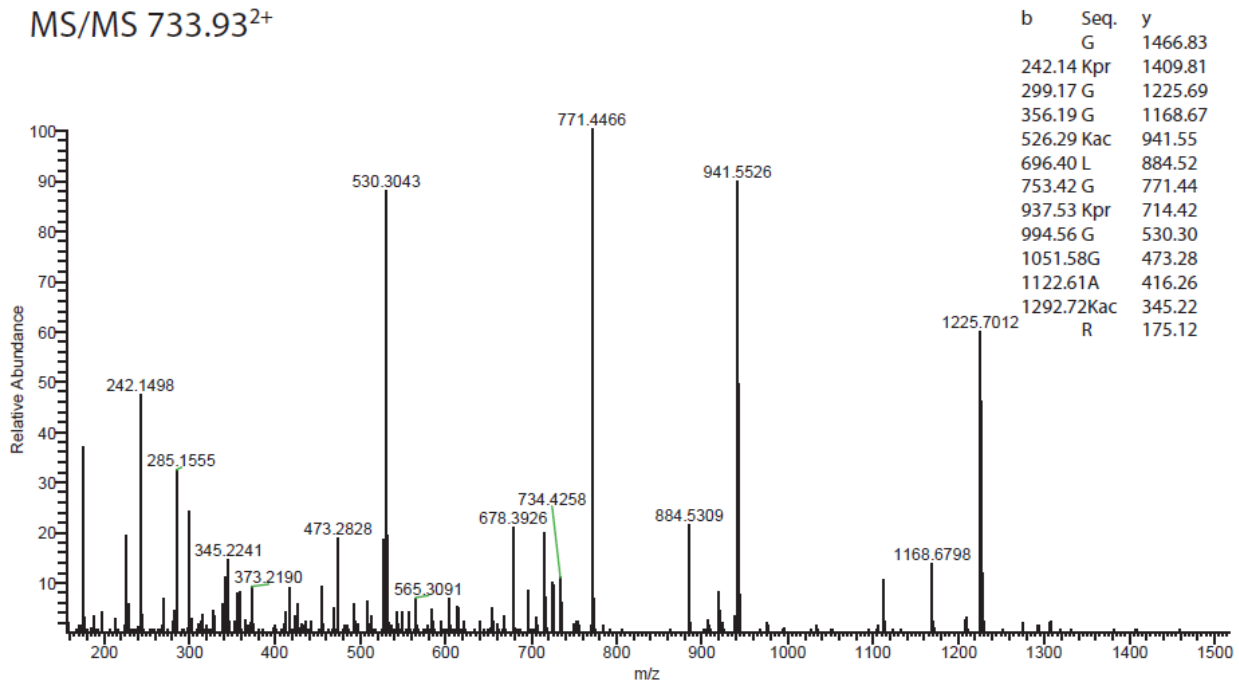

Peptide-15: H4K12_16ac/K5_8pr
GK(pr)GGK(pr)GLGK(ac)GGAK(ac)R

MS/MS 733.93^{2+}

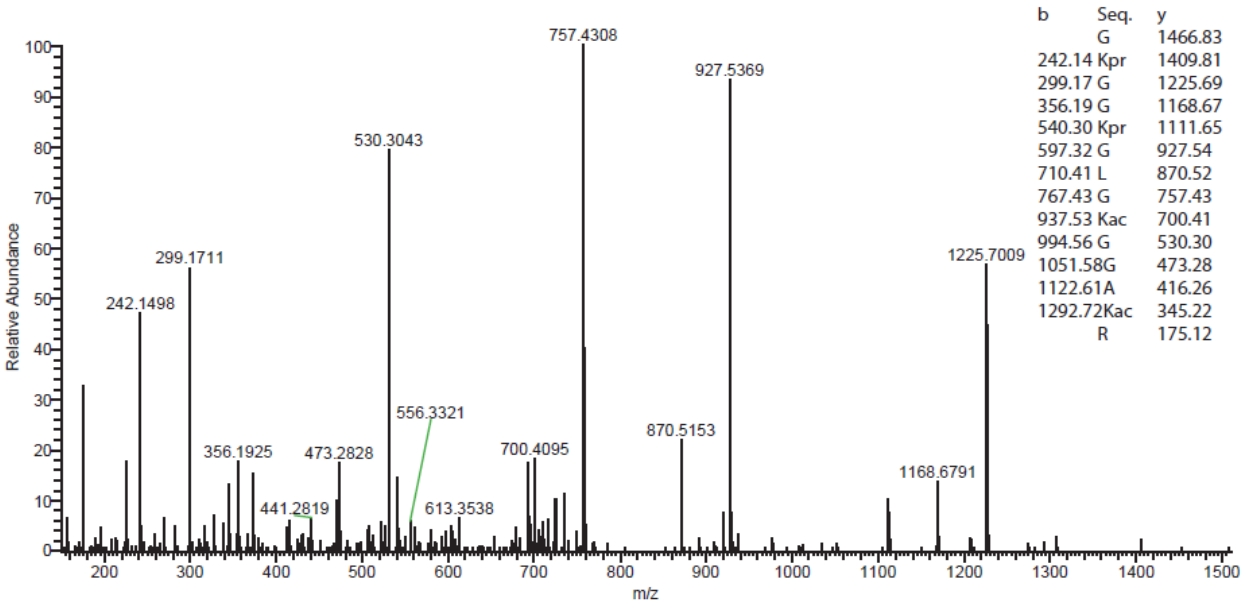

Peptide-16: H4K5_8_12ac/K16pr
GK(ac)GGK(ac)GLGK(ac)GGAK(pr)R

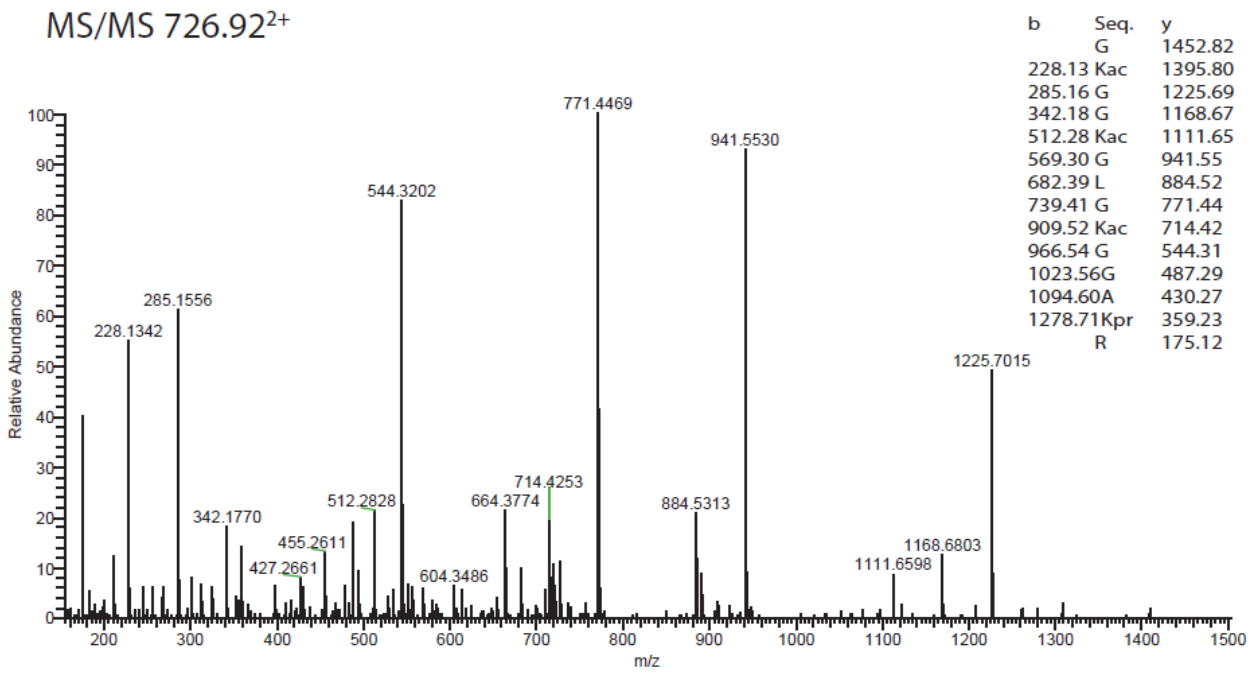

Peptide-17: H4K5_8_16ac/K12pr
GK(ac)GGK(ac)GLGK(pr)GGAK(ac)R

MS/MS 726.92^{2+}

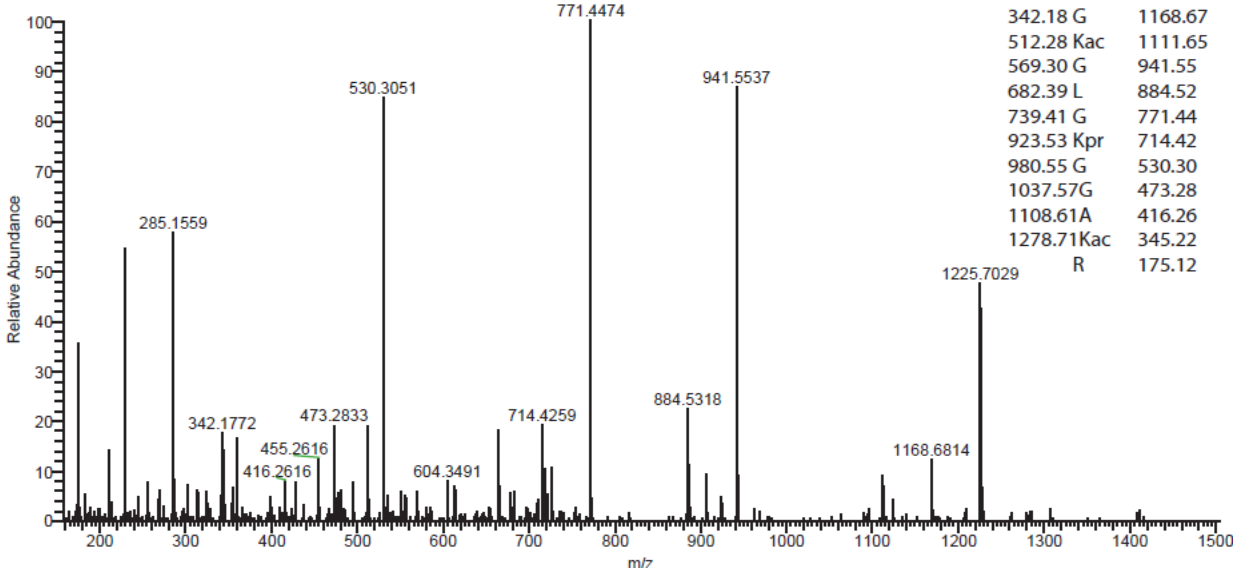

b	Seq.	y
	G	1452.82
228.13	Kac	1395.80
285.16	G	1225.69
342.18	G	1168.67
512.28	Kac	1111.65
569.30	G	941.55
682.39	L	884.52
739.41	G	771.44
923.53	Kpr	714.42
980.55	G	530.30
1037.57	G	473.28
1108.61	A	416.26
1278.71	Kac	345.22
	R	175.12

Peptide-18: H4K5_12_16ac/K8pr
GK(ac)GGK(pr)GLGK(ac)GGAK(ac)R

MS/MS 726.92^{2+}

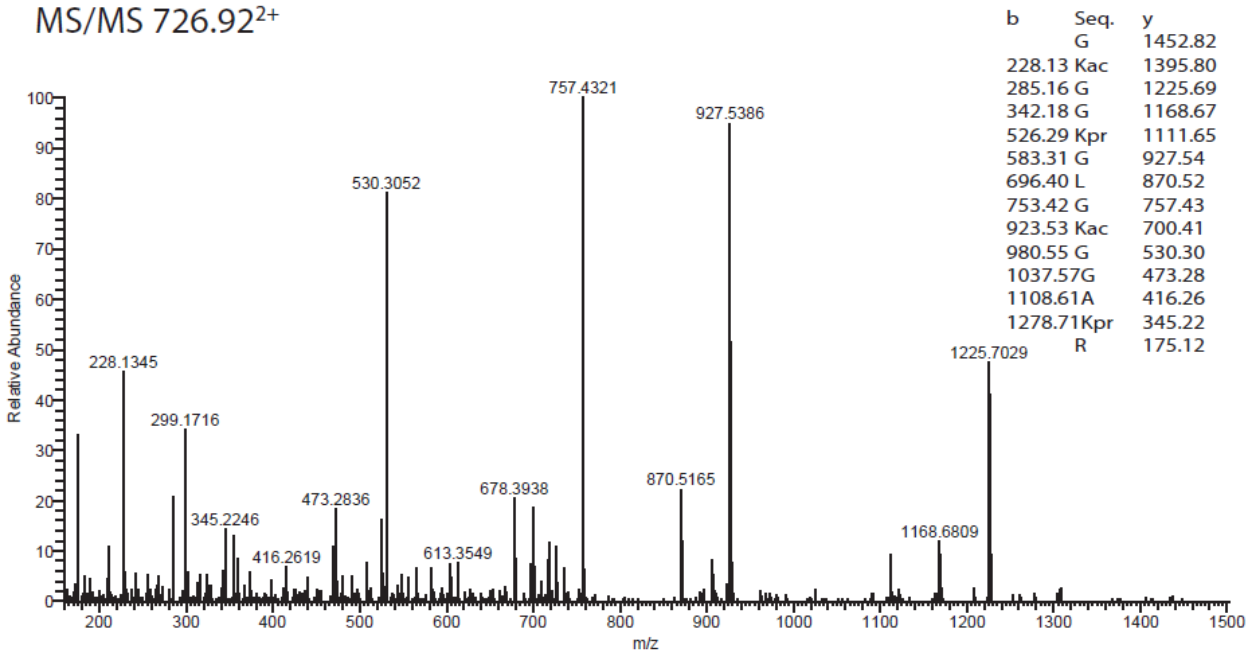

b	Seq.	y
	G	1452.82
228.13	Kac	1395.80
285.16	G	1225.69
342.18	G	1168.67
526.29	Kpr	1111.65
583.31	G	927.54
696.40	L	870.52
753.42	G	757.43
923.53	Kac	700.41
980.55	G	530.30
1037.57	G	473.28
1108.61	A	416.26
1278.71	Kpr	345.22
	R	175.12

Peptide-19: H4K8_12_16ac/K5pr
GK(pr)GGK(ac)GLGK(ac)GGAK(ac)R

MS/MS 726.92^{2+}

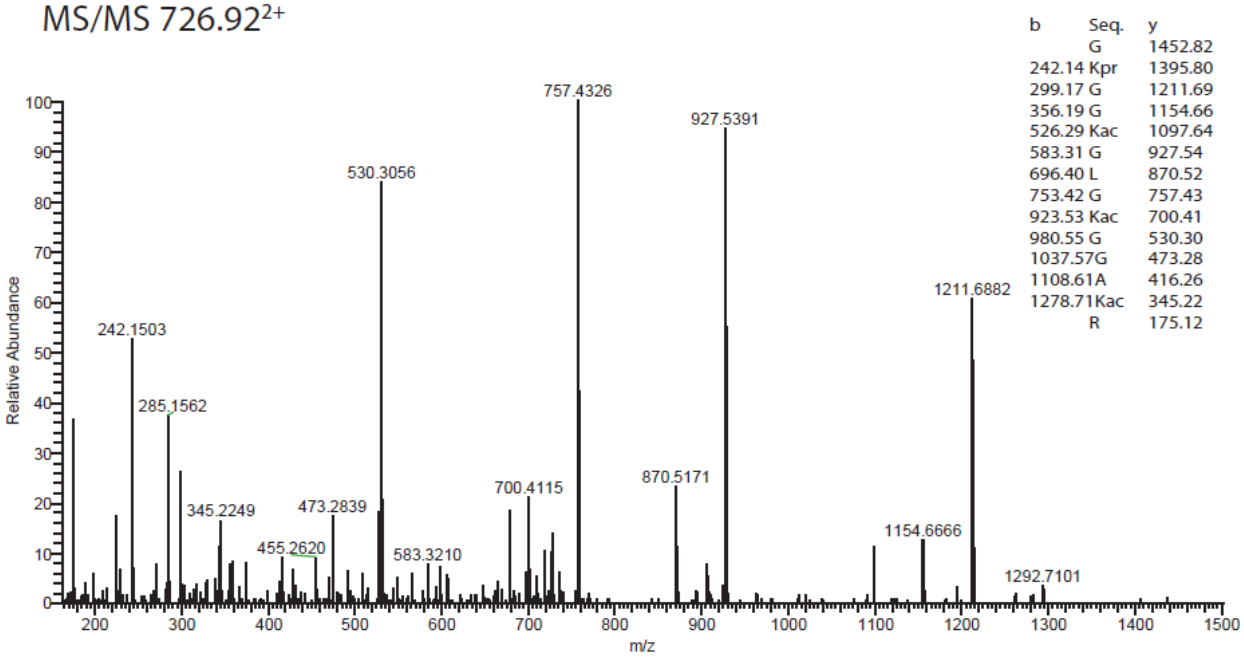

Peptide-20: H4K5_8_12_16ac
GK(ac)GGK(ac)GLGK(ac)GGAK(ac)R

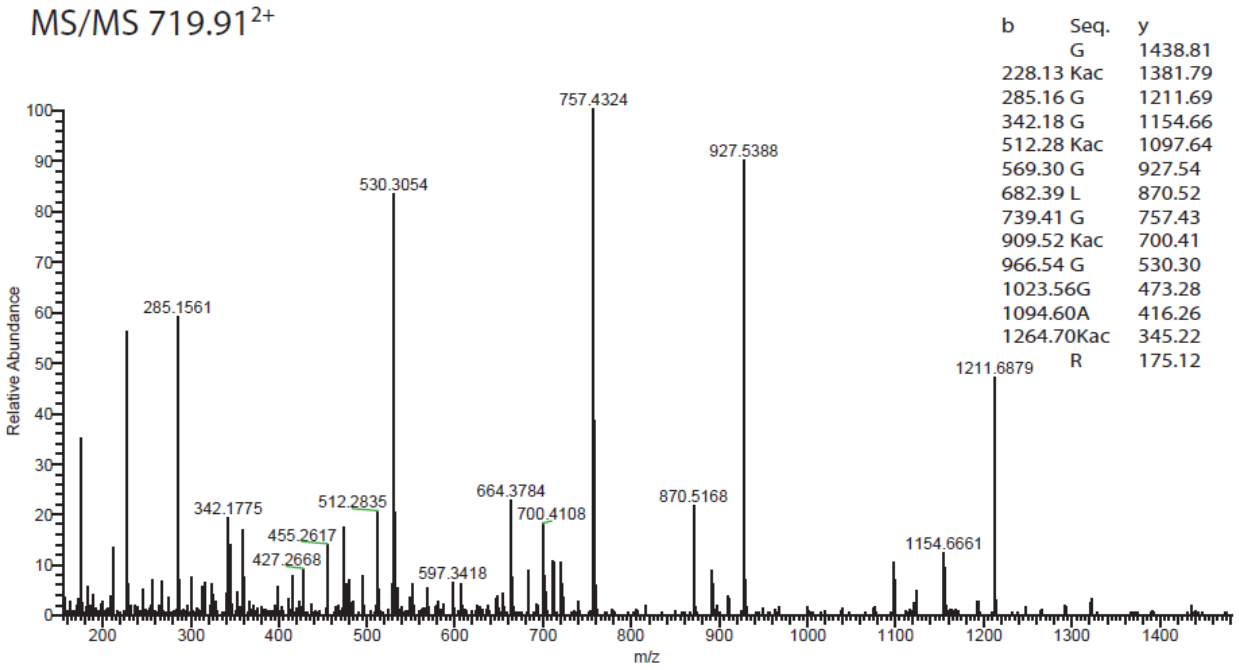

Supplementary Table 2.1. List of synthetic histones H3 (A) and H4 (B) peptides and their concentration in mM. The concentration of each peptide was determined based on triplicate UV absorbance measurements at 205 nm.

A)

H3 Peptides	Concentration (in mM)
Peptide 1: H3K18_K23NoAc	4.74
Peptide 2: H3K18Ac	5.58
Peptide 3: H3K23Ac	5.42
Peptide 4: H3K18_K23Ac	5.60

B)

H4 Peptides	Concentration (in mM)
Peptide 1: H4NoAc	0.60
Peptide 2: H4K5Ac	0.51
Peptide 3: H4K8Ac	0.57
Peptide 4: H4K12Ac	0.77
Peptide 5: H4K16Ac	0.79
Peptide 6: H4K5_8Ac	0.71
Peptide 7: H4K5_12Ac	0.68
Peptide 8: H4K5_16Ac	0.76
Peptide 9: H4K8_12Ac	0.70
Peptide 10: H4K8_16Ac	0.70
Peptide 11: H4K12_16Ac	0.71
Peptide 12: H4K5_8_12Ac	0.69
Peptide 13: H4K5_12_16Ac	0.75
Peptide 14: H4K8_12_16Ac	0.74
Peptide 15: H4K5_8_16Ac	0.82
Peptide 16: H4K5_8_12_16Ac	0.66

Supplementary Table 2.2. Synthetic H4 peptide standard dilutions. Standard curves for seven dilutions of mixtures of H4 (A) mono-, (B) di-, and (C) tri-acetylated peptides with peptide amounts ranging from 5 to 320 fmol were prepared. Two peptides from the mono- or tri-acetylated group and three peptides from the di-acetylated group were added to the mixture at a fixed amount of 80 fmol.

A) Mono-acetylated isomers

	Peptide amount (fmol)			
Sample #	H4K5Ac	H4K8Ac	H4K12Ac	H4K16Ac
1	5	80	5	80
2	10	80	10	80
3	20	80	20	80
4	40	80	40	80
5	80	80	80	80
6	160	80	160	80
7	320	80	320	80

B) Tri-acetylated isomers

	Peptide amount (fmol)			
Sample #	H4K5_8_12Ac	H4K5_8_16Ac	H4K5_12_16Ac	H4K8_12_16Ac
1	5	80	5	80
2	10	80	10	80
3	20	80	20	80
4	40	80	40	80
5	80	80	80	80
6	160	80	160	80
7	320	80	320	80

C) Di-acetylated isomers

	Peptide amount (fmol)					
Sample #	H4K5_8Ac	H4K5_12Ac	H4K5_16Ac	H4K8_12Ac	H4K8_16Ac	H4K12_16Ac
1	5	80	5	80	5	80
2	10	80	10	80	10	80
3	20	80	20	80	20	80
4	40	80	40	80	40	80
5	80	80	80	80	80	80
6	160	80	160	80	160	80
7	320	80	320	80	320	80

Supplementary Table 2.3. Amount of each peptide isomer determined by Iso-PeptidAce after deconvolution of mixtures of known amounts of (A) four mono- (B) four tri- and (C) six di-acetylated isomeric groups. Sample at 80 fmols was used for normalization of peptide intensities.

A) Mono-acetylated H4 peptides

Amount injected (fmol)	Amount determine by Iso-PeptidAce (fmol)			
	K5ac	K12ac	K8ac	K16ac
5	*1.33 ± 0.0	*5.05 ± 0.0	*74.28 ± 0.0	*74.52 ± 0.0
10	9.27 ± 4.4	12.36 ± 3.1	69.09 ± 7.51	66.59 ± 9.6
20	24.24 ± 8.2	25.17 ± 8.6	68.51 ± 8.9	67.18 ± 9.8
40	50.52 ± 12.3	49.49 ± 9.3	69.13 ± 8.7	68.23 ± 7.7
80	80	80	80	80
160	168.61 ± 4.4	181.21 ± 2.4	84.47 ± 7.6	86.99 ± 9.9
320	370.1 ± 58.4	401.15 ± 55.7	89.28 ± 0.3	89.21 ± 6.9

B) Tri-acetylated H4 peptides

Amount injected (fmol)	Amount determine by Iso-PeptidAce (fmol)			
	K5/8/12ac	K5/12/16ac	K5/8/16ac	K8/12/16ac
5	*1.92 ± 0.0	*2.44 ± 0.0	*65.4 ± 0.	*60.23 ± 0.0
10	7.47 ± 1.1	7.49 ± 0.3	93.9 ± 4.9	89.55 ± 10.1
20	15.38 ± 2.3	16.18 ± 1.2	99.13 ± 9.6	86.01 ± 7.6
40	35.1 ± 0.5	35.55 ± 1.0	95.25 ± 2.1	85.31 ± 9.7
80	80	80	80	80
160	155.82 ± 4.3	157.31 ± 8.7	76.56 ± 0.0	77.02 ± 1.5
320	295.55 ± 6.6	310.17 ± 20.9	78.86 ± 3.3	72.15 ± 3.4

C) Di-acetylated H4 peptides

Amount injected (fmol)	Amount determine by Iso-PeptidAce (fmol)					
	K5/8ac	K5/16ac	K8/16ac	K5/12ac	K8/12ac	K12/16ac
5	*3.7 ± 0.0	*1 ± 0.0	*6.92 ± 0	*70.98 ± 0.0	*286.89 ± 0	*114.68 ± 0.0
10	8.17 ± 1.0	4.31 ± 1.1	11.56 ± 2.0	85.64 ± 8.2	223.19 ± 8.7	110.13 ± 0.5
20	19.42 ± 4.8	17.03 ± 1.7	25.73 ± 1.8	96.52 ± 8.1	215.69 ± 5.2	114.52 ± 1.1
40	46.33 ± 2.9	52.58 ± 12.5	50.85 ± 4.1	101.69 ± 11.2	200.39 ± 26.2	115.94 ± 0.4
80	80	80	80	80	80	80
160	276.67 ± 21.2	459.33 ± 159.6	207.11 ± 3.9	104.26 ± 3.6	71.11 ± 3.6	98.01 ± 3.7
320	510.19 ± 63.7	1051.96 ± 500.8	372.77 ± 28.5	109.1 ± 0.6	65.78 ± 2.3	95.97 ± 1.37

Note: Each value represent the mean of two technical replicates + range error bar.
* This values were determined based on signal response of only one replicate

Supplementary Table 2.4 A-B. Calculated acetylation site occupancies of H3 and H4 peptides before or after HDACi treatment. Acetylation site occupancy of, for instance, H4K5ac, was determined by dividing the sum of normalized intensities of all peptides containing acetylated Lys-5 by the sum of normalized intensities of all forms of acetylated and un-acetylated H4 peptide 4-GKGGKGLGKGGAKR-17.

A) H3 acetylation site occupancy

Sample	H3K18ac	H3K23ac
DMSO-1h	4.23 ± 0.14	26.56 ± 0.66
DMSO-6h	6.03 ± 0.14	31.45 ± 0.93
DMSO-24h	5.89 ± 0.74	32.06 ± 0.98
MS275-1h	5.74 ± 0.15	32.03 ± 4.85
MS275-6h	10.64 ± 1.89	51.95 ± 6.32
MS275-24h	27.11 ± 1.67	63.35 ± 0.81
SAHA-1h	17.19 ± 2.46	55.89 ± 0.89
SAHA-6h	31.94 ± 0.28	71.92 ± 1.22
SAHA-24h	37.70 ± 6.36	79.73 ± 0.77
JNJ-1h	15.58 ± 1.17	59.95 ± 0.02
JNJ-6h	32.76 ± 2.66	76.55 ± 1.39
JNJ-24h	44.17 ± 1.53	82.77 ± 1.21

B) H4 acetylation site occupancy

Sample	H4K5ac	H4K8ac	H4K12ac	H4K16ac
DMSO-1h	2.68 ± 0.59	2.63 ± 0.46	5.14 ± 0.53	29.27 ± 1.27
DMSO-6h	3.05 ± 0.07	2.86 ± 0.02	5.88 ± 0.04	28.42 ± 1.00
DMSO-24h	3.43 ± 0.60	3.79 ± 0.51	7.52 ± 0.98	32.27 ± 0.08
MS275-1h	3.42 ± 0.16	3.66 ± 0.35	7.12 ± 0.58	31.79 ± 0.52
MS275-6h	13.54 ± 0.78	13.43 ± 1.25	22.77 ± 1.21	57.81 ± 0.45
MS275-24h	36.79 ± 2.90	35.66 ± 1.47	55.16 ± 0.05	80.28 ± 0.23
SAHA-1h	16.24 ± 1.89	17.98 ± 1.65	33.03 ± 3.86	57.19 ± 0.79
SAHA-6h	44.96 ± 1.19	38.59 ± 1.91	63.45 ± 0.81	80.77 ± 0.17
SAHA-24h	61.35 ± 0.21	51.05 ± 3.30	77.49 ± 0.40	89.77 ± 1.16
JNJ-1h	13.51 ± 1.96	14.83 ± 1.43	26.48 ± 3.10	51.90 ± 3.30
JNJ-6h	47.15 ± 1.38	39.41 ± 0.06	64.59 ± 0.85	80.96 ± 0.49
JNJ-24h	57.67 ± 0.39	47.59 ± 1.18	68.25 ± 2.07	89.00 ± 0.80

Note: Each value represent the mean of two technical replicates ± range error bars.

Supplementary Table 2.5. LC/MS intensity data for CAF-1-bound and total histones H3 and H4 peptides.

H3 Peptide sequence	m/z	Charge	PTM	LC/MS Intensity	
				CAF-1 bound	Total histone
9-KSTGGKAPR-17	507.2906	2	H3K9prK14pr	860033.68 ± 231000	390383113.88 ± 11300000
	493.2748	2	H3K9acK14pr	255287.72 ± 17000	35576306.85 ± 12000000
	500.2836	2	H3K9prK14ac	415406.09 ± 2060	109502233.83 ± 2840000
		2	H3K9acK14ac	2253016.49 ± 418000	19487793.22 ± 5660000
18-KQLASKAAR-23	542.827	2	K18prK23pr	493253.48 ± 265000	703000000 ± 137000000
	535.819	2	K18acK23pr	28786.03 ± 26500	40300000 ± 14600000
		2	K18prK23ac	608652.18 ± 46000	149875000 ± 59300000
	528.811	2	K18acK23ac	58024.76 ± 34300	17545000 ± 6020000
27-KSAPSTGGVKKPHR-40	809.4568	2	K27prK36prK37pr	47760.38 ± 3200	46475000 ± 12900000
	816.4646	2	K27prK36pr+me1K37pr	0.00E+00	13272500 ± 4710000
	795.4595	2	K27prK36me2K37pr	0.00E+00	8742500 ± 300000
	530.642	3	K27prK36me2K37pr	0.00E+00	50900000 ± 2100000
	802.4673	2	K27prK36me3K37pr	0.00E+00	15470000 ± 600000
	535.3139	3	K27prK36me3K37pr	0.00E+00	80525000 ± 3000000
	802.4491	2	K27acK36prK37pr	43890.86 ± 6660	9195000 ± 300000
	809.4569	2	K27acK36pr+me1K37pr	0.00E+00	2970000 ± 800000
	788.4518	2	K27acK36me2K37pr	0.00E+00	574750 ± 100000
	525.9702	3	K27acK36me2K37pr	0.00E+00	2940000 ± 100000
	795.4596	2	K27acK36me3K37pr	0.00E+00	609250 ± 130000
	530.6421	3	K27acK36me3K37pr	0.00E+00	3507500 ± 1330000
	539.9736	3	K27prK36prK37pr	182908.65 ± 11300	168275000 ± 6040000
	544.6455	3	K27prK36pr+me1K37pr	0.00E+00	41650000 ± 15600000
	398.2333	4	K27prK36me2K37pr	0.00E+00	58900000 ± 21800000
	401.7373	4	K27prK36me3K37pr	0.00E+00	105650000 ± 38700000
	535.3018	3	K27acK36prK37pr	163800.96 ± 61100	29250000 ± 1380000
	539.9737	3	K27acK36pr+me1K37pr	0.00E+00	8445000 ± 1800000
	394.7295	4	K27acK36me2K37pr	0.00E+00	3520000 ± 1240000
	398.23334	4	K27acK36me3K37pr	0.00E+00	4467500 ± 1590000
54-FQK$_{56}$STELLIR-63	645.8743	2	K56pr	80480.47 ± 9580	47700000 ± 5940000
	638.8666	2	K56ac	197734.94 ± 39500	15050000 ± 1630000
53-RFQK$_{56}$STELLIR-63	723.9248	2	K56pr	23625.85 ± 20000	13207500 ± 2960000
	482.9523	3	K56pr	11242.59	11172500 ± 2580000
	478.2805	3	K56ac	49589.66	3972500 ± 1440000
	716.9171	2	K56ac	167034.28 ± 107000	4497500 ± 1250000

H4 Peptide sequence	m/z	Charge	PTM	LC/MS Intensity	
				CAF-1 bound	Total histone
4-GKGGKGLGKGGAKR-17	747.9412	2	K5-8-12-16pr	438525.03 ± 2090	21069549.87 ± 178000
	740.9334	2	K5ac\K8-12-16pr	0.00E+00	21208.89 ± 3630
			K8ac\K5-12-16pr	0.00E+00	357774.80 ± 39300
			K12ac\K5-8-16pr	1744.11 ± 2470	2410070.69 ± 145000
			K16ac\K5-8-12pr	24985.21 ± 35300	21740122.97 ± 1810000
	733.9255	2	K5-8ac\K12-16pr	0.00E+00	31596.76 ± 2540
			K5-12ac\K8-16pr	0.00E+00	347870.13 ± 25700
			K5-16ac\K8-12pr	0.00E+00	1666742.07 ± 389000
			K8-12ac\K5-16pr	0.00E+00	815051.26 ± 64900
			K8-16ac\K5-12pr	0.00E+00	2629819.07 ± 255000
			K12-16ac\K5-8pr	0.00E+00	8159580.12 ± 323000
	726.9177	2	K5-8-12ac\K16pr	488.08 ± 690	254396.05 ± 58200
			K5-8-16ac\K12pr	976.16	2092262.66 ± 58900
			K5-12-16ac\K8pr	110061.69 ± 18200	1909117.03 ± 582000
			K8-12-16ac\K5pr	17472.77 ± 12400	4395165.79 ± 1010000
	719.9092	2	K5-8-12-16ac	0.00E+00	3553895.37 ± 593000

Note: Each intensity value represents the mean of two technical replicates ± range error bar

Supplementary Table 2.6. List of known acetylation sites in selected bromodomain substrates. Peptides containing multiple acetylated lysine residues generated from p53, GATA1, Cyclin T1, or MyoD are shown. List of publications for each of the previously identified acetylation sites is indicated.

Protein name	Interacting Bromodomain containing protein/s	Peptide segment containing multiple lysine residues	Known acetylation sites	Reference
p53	CREBBP, TAF1	290-RKKGEPHHELPPGSTKR-306	K292, K305	1-7
		306-RALPNNTSSSPQPKKKPLDGEYFTLQIR-333	K319, K320, K321	
		363- RAHSSHLKSKKGQSTSRHKKLMFKTEGP-390	K370, K372, K373, K381, K382, K386	
GATA1	BRD3	220- RTGHYLCNACGL YHKMNGQNRPLIRP KKR- 247	K233, K245, K246	8-10
		301- GIQTRNRKASGKGKKKRGSS -320	K308, K312, K314, K315, K316	
CyclinT1	BRD4	374-SQKQNSKSVPSAKVSLKEYR-393	K380, K386, K390	4, 11
MyoD	CREBBP or EP300	92- RCLLWACKACKRKTTNADR-110	K99, K102, K104	12, 13

1. Zeng, L., Zhang, Q., Gerona-Navarro, G., Moshkina, N. & Zhou, M.M (2008). Structural Basis of Site-Specific histone recognition by the bromodomains of human Coactivators PCAF and CBP/p300. *Structure* 16, 643-652.

2. Choudhary, C. et al. (2009) Lysine acetylation targets protein complexes and co-regulates major cellular functions. *Science* 325, 834-840.

3. Wu, S.Y. & Chiang, C.M (2009). Crosstalk between sumoylation and acetylation regulates p53-dependent chromatin transcription and DNA binding. *EMBO J* 28, 1246-1259.

4. Joubel, A., Chalkley, R.J., Medzihradszky, K.F., Hondermarck, H. & Burlingame, A.L. (2009) Identification of new p53 acetylation sites in COS-1 Cells. *Molecular & Cellular Proteomics* 8, 1167-1173.

5. Sen, N., Kumari, R., Singh, Manika I. & Das, S. HDAC5, a key component in temporal regulation of p53-mediated transactivation in response to genotoxic stress. *Molecular Cell* 52, 406-420 (2013).

6. Li, A.G. et al. An acetylation switch in p53 mediates Holo-TFIID recruitment. *Molecular Cell* 28, 408-421 (2007).

7. Tang, Y., Zhao, W., Chen, Y., Zhao, Y. & Gu, W. Acetylation is indispensable for p53 activation. *Cell* 133, 612-626 (2008).

8. Boyes, J., Byfield, P., Nakatani, Y. & Ogryzko, V. Regulation of activity of the transcription factor GATA-1 by acetylation. *Nature* 396, 594-598 (1998).

9. Lamonica, J.M., Vakoc, C.R. & Blobel, G.A. Acetylation of GATA-1 is required for chromatin occupancy, *Blood* 108, 3736-3738 (2006).

10. Lamonica, J.M. et al. Bromodomain protein Brd3 associates with acetylated GATA1 to promote its chromatin occupancy at erythroid target genes. *Proceedings of the National Academy of Sciences* 108, E159-E168 (2011).

11. Schröder, S. et al. Two-pronged binding with bromodomain-containing protein 4 liberates Positive Transcription Elongation Factor b from inactive ribonucleoprotein complexes. *Journal of Biological Chemistry* 287, 1090-1099 (2012).

12. Sartorelli, V. et al. Acetylation of MyoD directed by PCAF is necessary for the execution of the muscle program. *Molecular Cell* 4, 725-734 (1999).

13. Wei, L., Jamonnak, N., Choy, J., Wang, Z. & Zheng, W. Differential binding modes of the bromodomains of CREB-binding protein (CBP) and p300 with acetylated MyoD. *Biochemical and Biophysical Research Communications* 368, 279-284 (2008).

Supplementary Table 7. Representative raw intensity data obtained for deconvoluted H4 peptides for control and HDACi treated samples. For each sample Iso-PeptidAce reports five different groups of peptides: one un-acetylated (m/z 747.94), four mono-acetylated (m/z 740.93), six di-acetylated (m/z 733.93), four tri-acetylated (m/z 726.92) and one tetra-acetylated (m/z 719.91).

Sample	m/z	K5/8/12/16p	K5ac	K8ac	K12ac	K16ac	K5-8ac	K5-12ac	K5-16ac	K8-12ac	K8-16ac	K12-16ac	K5-8-12ac	K5-8-16ac	K5-12-16ac	K8-12-16ac	K5-8-12-16ac
DMSO-1h	747.9412	53193490	0	0	0	0	0	0	0	0	0	0	0	0	0	0	0
DMSO-1h	740.9334	0	1118565.8	600295.66	1524585	20640811	0	0	0	0	0	0	0	0	0	0	0
DMSO-1h	733.9255	0	0	0	0	0	30356.163	121454.66	448997.57	164131.9	650668.81	1614132.7	0	0	0	0	0
DMSO-1h	726.9177	0	0	0	0	0	0	0	0	0	0	0	68875.319	196951.05	304594.31	464535.07	0
DMSO-1h	719.9099	0	0	0	0	0	0	0	0	0	0	0	0	0	0	0	228420.77
DMSO-6h	747.9412	330345784	0	0	0	0	0	0	0	0	0	0	0	0	0	0	0
DMSO-6h	740.9334	0	7138759.9	4371375.1	11037086	113532233	0	0	0	0	0	0	0	0	0	0	0
DMSO-6h	733.9255	0	0	0	0	0	106905.51	922259.1	2882531.3	1186154.7	4190846.2	10690293	0	0	0	0	0
DMSO-6h	726.9177	0	0	0	0	0	0	0	0	0	0	0	570076.9	685540.63	1500377.3	1935327.3	0
DMSO-6h	719.9099	0	0	0	0	0	0	0	0	0	0	0	0	0	0	0	956313.59
DMSO-24h	747.9412	252369980	0	0	0	0	0	0	0	0	0	0	0	0	0	0	0
DMSO-24h	740.9334	0	6805232.5	3776014.2	11013798	103256179	0	0	0	0	0	0	0	0	0	0	0
DMSO-24h	733.9255	0	0	0	0	0	144381.42	839325.07	2953775	1086588.8	4991609.9	13363139	0	0	0	0	0
DMSO-24h	726.9177	0	0	0	0	0	0	0	0	0	0	0	699796.5	1059935.7	1333050.3	3321485.9	0
DMSO-24h	719.9099	0	0	0	0	0	0	0	0	0	0	0	0	0	0	0	1922397.9
JNJ-1h	747.9412	117991108	0	0	0	0	0	0	0	0	0	0	0	0	0	0	0
JNJ-1h	740.9334	0	3579092.5	2065993.4	8538676.4	69116557	0	0	0	0	0	0	0	0	0	0	0
JNJ-1h	733.9255	0	0	0	0	0	95794.614	1799725.9	3389114.9	1299683.9	6819343.7	22637785	0	0	0	0	0
JNJ-1h	726.9177	0	0	0	0	0	0	0	0	0	0	0	869015.04	1471884	5756752.7	8917221.3	0
JNJ-1h	719.9099	0	0	0	0	0	0	0	0	0	0	0	0	0	0	0	15793648
JNJ-6h	747.9412	21343259	0	0	0	0	0	0	0	0	0	0	0	0	0	0	0
JNJ-6h	740.9334	0	1552352.3	912976.7	3398663.7	21578614	0	0	0	0	0	0	0	0	0	0	0
JNJ-6h	733.9255	0	0	0	0	0	0	3107565.6	3384182.8	679579.3	4960207.4	23855621	0	0	0	0	0
JNJ-6h	726.9177	0	0	0	0	0	0	0	0	0	0	0	353824.87	2558696.8	19685251	10314397	0
JNJ-6h	719.9099	0	0	0	0	0	0	0	0	0	0	0	0	0	0	0	44014522
JNJ-24h	747.9412	14354938	0	0	0	0	0	0	0	0	0	0	0	0	0	0	0
JNJ-24h	740.9334	0	4932701.3	1559004.9	4235243.7	31651823	0	0	0	0	0	0	0	0	0	0	0
JNJ-24h	733.9255	0	0	0	0	0	0	4836787.2	14322620	1958944.9	13580479	43687024	0	0	0	0	0
JNJ-24h	726.9177	0	0	0	0	0	0	0	0	0	0	0	1078741.7	15278200	44872091	21809930	0
JNJ-24h	719.9099	0	0	0	0	0	0	0	0	0	0	0	0	0	0	0	97722934
MS275-1h	747.9412	114207314	0	0	0	0	0	0	0	0	0	0	0	0	0	0	0
MS275-1h	740.9334	0	2785652.3	1408977.1	4263409.8	46273838	0	0	0	0	0	0	0	0	0	0	0
MS275-1h	733.9255	0	0	0	0	0	94043.304	403426.92	1186584.9	383662.27	2126216	4650092	0	0	0	0	0
MS275-1h	726.9177	0	0	0	0	0	0	0	0	0	0	0	224730.36	283902.84	547496.26	1181549.5	0
MS275-1h	719.9099	0	0	0	0	0	0	0	0	0	0	0	0	0	0	0	448649.1
MS275-6h	747.9412	78903759	0	0	0	0	0	0	0	0	0	0	0	0	0	0	0
MS275-6h	740.9334	0	6452819.9	2135734.5	7275288.4	66565880	0	0	0	0	0	0	0	0	0	0	0
MS275-6h	733.9255	0	0	0	0	0	42800.07	1926339.3	8568523.6	1232820.1	13482835	24691483	0	0	0	0	0
MS275-6h	726.9177	0	0	0	0	0	0	0	0	0	0	0	414625.37	3299476.3	6943465	7553312.1	0
MS275-6h	719.9099	0	0	0	0	0	0	0	0	0	0	0	0	0	0	0	5474857.5
MS275-24h	747.9412	56100816	0	0	0	0	0	0	0	0	0	0	0	0	0	0	0
MS275-24h	740.9334	0	13371602	3754090.1	15879233	109492331	0	0	0	0	0	0	0	0	0	0	0
MS275-24h	733.9255	0	0	0	0	0	403928.19	14301966	26611451	10427031	35744391	82346857	0	0	0	0	0
MS275-24h	726.9177	0	0	0	0	0	0	0	0	0	0	0	2461500.5	17916056	53442510	45254099	0
MS275-24h	719.9099	0	0	0	0	0	0	0	0	0	0	0	0	0	0	0	99427878
SAHA-1h	747.9412	75994058	0	0	0	0	0	0	0	0	0	0	0	0	0	0	0
SAHA-1h	740.9334	0	2592751.3	2160809.1	7380152.7	59218084	0	0	0	0	0	0	0	0	0	0	0
SAHA-1h	733.9255	0	0	0	0	0	36591.862	1948206.7	2900381.4	1263431.6	4426044.6	20909804	0	0	0	0	0
SAHA-1h	726.9177	0	0	0	0	0	0	0	0	0	0	0	919790.2	1030266.6	6108924.6	9786072.5	0
SAHA-1h	719.9099	0	0	0	0	0	0	0	0	0	0	0	0	0	0	0	16180294
SAHA-6h	747.9412	57211740	0	0	0	0	0	0	0	0	0	0	0	0	0	0	0
SAHA-6h	740.9334	0	4828466.5	1942512.3	9214826.5	68102682	0	0	0	0	0	0	0	0	0	0	0
SAHA-6h	733.9255	0	0	0	0	0	127801.71	10024666	10964147	2429316.3	16225382	67054445	0	0	0	0	0
SAHA-6h	726.9177	0	0	0	0	0	0	0	0	0	0	0	986651.9	7060824.5	54073678	28417899	0
SAHA-6h	719.9099	0	0	0	0	0	0	0	0	0	0	0	0	0	0	0	109799946
SAHA-24h	747.9412	15965728	0	0	0	0	0	0	0	0	0	0	0	0	0	0	0
SAHA-24h	740.9334	0	4526983.4	1489077.1	5341307.5	28573177	0	0	0	0	0	0	0	0	0	0	0
SAHA-24h	733.9255	0	0	0	0	0	224305.2	6828544.3	11230370	5217006.4	11394546	47756468	0	0	0	0	0
SAHA-24h	726.9177	0	0	0	0	0	0	0	0	0	0	0	3000516	12272353	59453258	32648488	0
SAHA-24h	719.9099	0	0	0	0	0	0	0	0	0	0	0	0	0	0	0	139482620

Supplementary Methods

Iso-PeptidAce: In-silico separation of co-eluting peptides

Overview

Here we describe Iso-PeptidAce, a stand-alone software for the in-silico separation of co-eluting peptide isomers in high-resolution mass spectrometry data. Peptide isomers of interest need to be synthesized and processed individually in a high-resolution mass spectrometer, with dynamic exclusion turned off. Samples with unknown proportions of co-eluting peptide isomers processed in the same instrument, with a similar method will be separated by the software. Iso-PeptidAce can also quantify (relatively) co-eluting peptides from mixed samples. To our knowledge, this is the first software capable of such a feat.

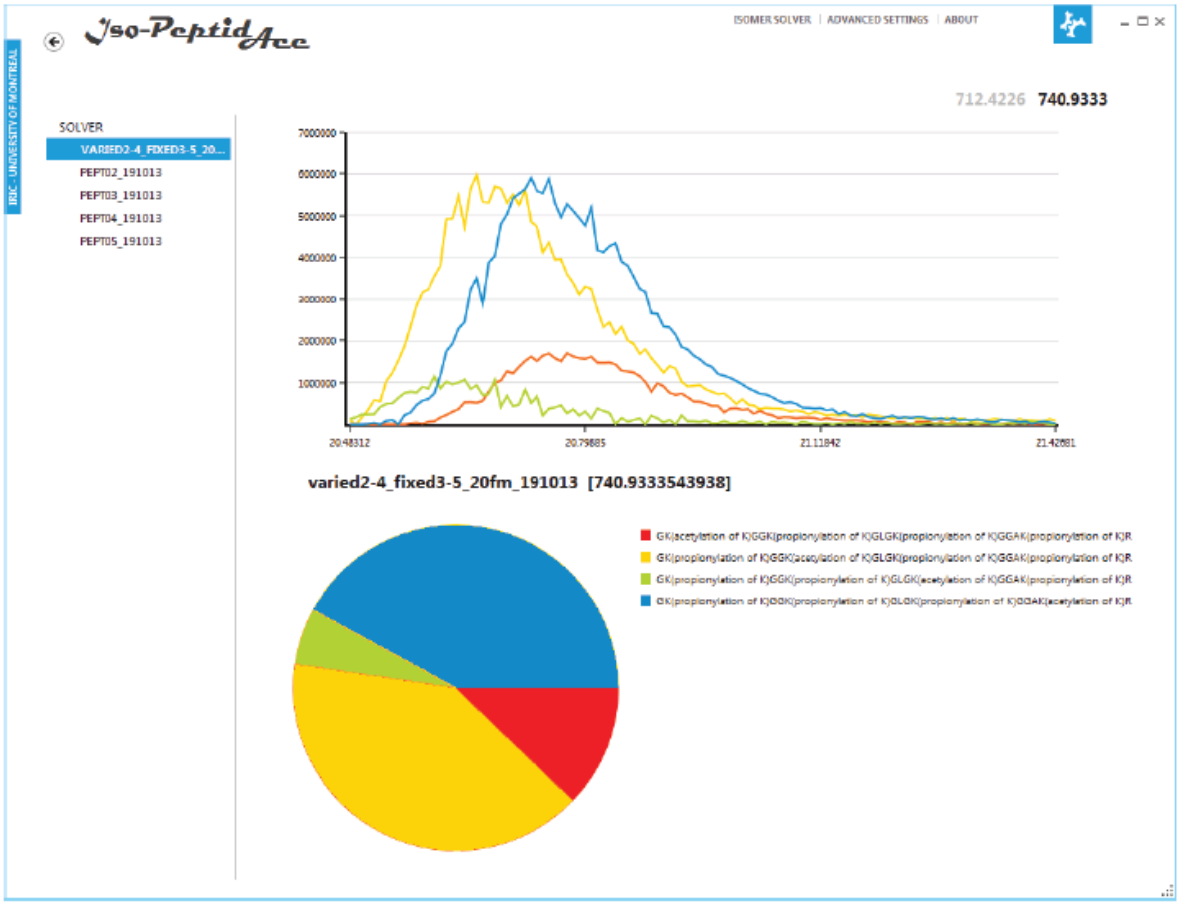

List of histone H4 peptides used for testing Iso-PeptidAce

Peptide 1	GK(propionylation of K)GGK(propionylation of K)GLGK(propionylation of K)GGAK(propionylation of K)R
Peptide 2	GK(acetylation of K)GGK(propionylation of K)GLGK(propionylation of K)GGAK(propionylation of K)R
Peptide 3	GK(propionylation of K)GGK(acetylation of K)GLGK(propionylation of K)GGAK(propionylation of K)R
Peptide 4	GK(propionylation of K)GGK(propionylation of K)GLGK(acetylation of K)GGAK(propionylation of K)R
Peptide 5	GK(propionylation of K)GGK(propionylation of K)GLGK(propionylation of K)GGAK(acetylation of K)R
Peptide 6	GK(acetylation of K)GGK(acetylation of K)GLGK(propionylation of K)GGAK(propionylation of K)R
Peptide 7	GK(acetylation of K)GGK(propionylation of K)GLGK(acetylation of K)GGAK(propionylation of K)R
Peptide 8	GK(acetylation of K)GGK(propionylation of K)GLGK(propionylation of K)GGAK(acetylation of K)R
Peptide 9	GK(propionylation of K)GGK(acetylation of K)GLGK(acetylation of K)GGAK(propionylation of K)R
Peptide 10	GK(propionylation of K)GGK(acetylation of K)GLGK(propionylation of K)GGAK(acetylation of K)R
Peptide 11	GK(propionylation of K)GGK(propionylation of K)GLGK(acetylation of K)GGAK(acetylation of K)R
Peptide 12	GK(acetylation of K)GGK(acetylation of K)GLGK(acetylation of K)GGAK(propionylation of K)R
Peptide 13	GK(acetylation of K)GGK(acetylation of K)GLGK(propionylation of K)GGAK(acetylation of K)R
Peptide 14	GK(acetylation of K)GGK(propionylation of K)GLGK(acetylation of K)GGAK(acetylation of K)R
Peptide 15	GK(propionylation of K)GGK(acetylation of K)GLGK(acetylation of K)GGAK(acetylation of K)R
Peptide 16	GK(acetylation of K)GGK(acetylation of K)GLGK(acetylation of K)GGAK(acetylation of K)R

Symbols used

- *MS1i, MS2i* = Injection Time for MS1 and MS2 Scans, in milliseconds
- *iMS* = ions per milliseconds
- *#ion* = Number of monoisotopic precursor ions fragmented in a scan
- *psm* = Peptide Spectrum Match
- *fi* = Fragment Intensity
- *nfi* = Normalized Fragment Intensity
- *n* = Number of fragments considered per characterized peptide
- *rt* = Scan Time
- *Δmz*= Precursor mass error, in ppm
- *mif* = Matching fragment ion divided by the number of theoretical ion tested
- c_j= Number of ions detected for peptide *j*
- *aMz* = List of selected fragment masses
- *ac* = Area Under the Curve
- *pc* = Peptide Count (Estimation of the number of a certain peptide in a sample)

Description of how spectral deconvolution is carried out by Iso-PeptidAce

Raw file extraction

Information is extracted from Raw files using ProteoWizard1 and MsFileReader. MS2 peak lists (masses and intensities) are stored per precursor mass and sorted by retention time. Spectrum precursor intensity, MS1 and MS2 injection times are also extracted.

Precursor intensity counts are converted to ions per millisecond (*iMS*):

$$iMS = Precursor\ Intensity\ Count / MS1\ injection\ time$$

For each different precursor mass in a file, a curve describing the number of ions flowing in the system at any given time is built using the computed *iMS* values. Linear interpolation is used to compute the area under the curve for a given time point. In particular, the number of ions that entered the CTrap and got fragmented (*#ion*) is estimated as the area under the curve between the beginning (*rt*) and the end of the scan (*rt* + *MS2i*).

$$\#ion = Area\ Under\ The\ Curve\ (from: rt,\ to: rt + MS2i)$$

These operations are made for each file (both mixed samples and synthetic peptide runs). For the synthetic peptide runs, spectrum fragment intensity counts (*fi*) are normalized (*nfi*) using the number of ions (*#ion*) that got fragmented.

$$nfi = fi / \#ion$$

Peptide Spectrum Matching

Iso-PeptidAce uses PeptidAce peptide spectrum matching abilities (which derives from Morpheus) to automatically identify peptide sequences and modifications across synthetic peptide runs. PeptidAce uses a no-enzyme in-silico protein digestion routine to parse the provided Fasta file for potential matches. All modifications (specified in the "Modifications.csv" user configurable Comma Separated Values file) are searched for. This automatic identification is useful to discover impurities in the peptide synthesis process.

PeptidAce matches peptides to spectrum by comparing theoretical ions (fragments *a*, *b*, *c*, *x*, *y* and *z*) within a specified ppm tolerance window. Peptide spectrum matches (*psm*) are scored by their cumulated normalized fragment intensities (*nfi*), number of matching ions versus unmatched theoretical ions (*mif*) and precursor accuracy (Δmz, normalized between [0,1]):

$$psm\ score = 0.33 \cdot \Delta mz + 0.33 \cdot mif + 0.33 \cdot nfi$$

In case of discrepancy (precursor with inconsistent *psm* across the elution curve), *psm* scores of similar peptides are summed together and the best peptide is associated with the precursor. Ambiguous spectra assigned to different peptides are discarded.

Describing the system as a Maximum Flow problem

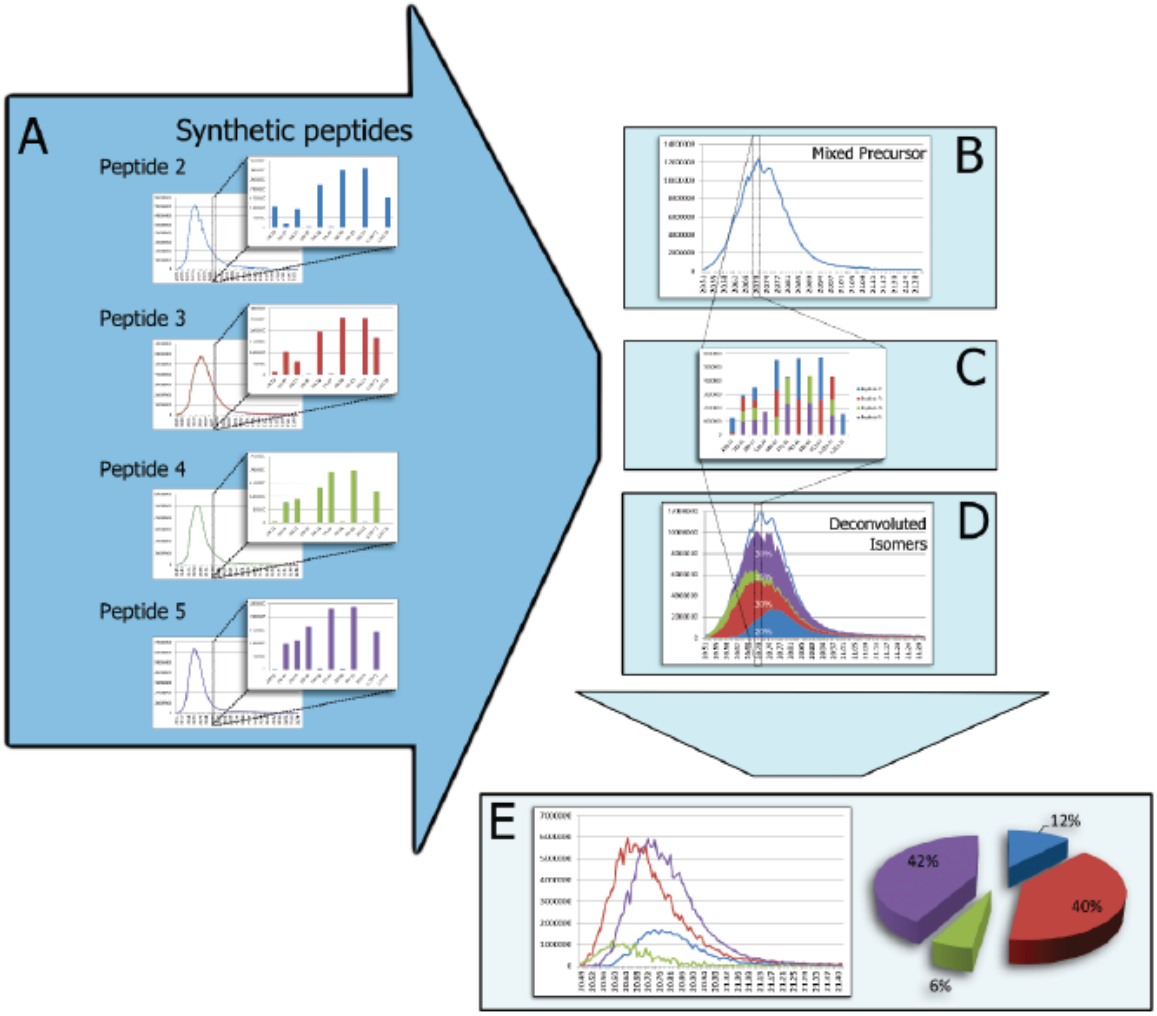

The network flow was built from mixed spectra and spectra acquired from peptide isomers. The objective, finding the maximum flow of the system, is stated as such:

How many ions of peptides isomer does it take to optimally fill the mixed spectrum fragment intensity counts

For each synthetic peptide found, normalized fragment intensities (*nfi*) of every spectrum were averaged. The *n* most intense fragments were chosen for each synthetic peptide. Only fragment masses with consistent normalized intensities (standard deviation above

50% of the mean) were considered reproducible enough. Unstable fragments were flagged and ignored in following analyses.

For synthetic peptides of similar masses, these *n* fragments were used to build a list of fragment masses (aMz), both with common and unique fragment masses. The *nfi* of their averaged spectrum was used to associate intensities to a list of fragment masses ($aMzj$, one aMz for each potential isomer *j*). A similar list of intensity count ($aMzm$) is built for the mixed spectrum *m* of matching precursor mass. For each mixed spectrum *m*, the Maximum Flow is defined by the sum of $aMzj$ that optimally fills the $aMzm$ fragment intensity counts (were cj is the number of ions for the *j* isomer, and $aMzt$ is the theoretical list being built):

$$aMz_t = \sum_{isomers}^{j}(c_j \cdot aMz_j) \text{ and } aMz_t \leq aMz_m$$

Thus, the network flow can be described as the source being connected to peptide isomers *j* (edges of unknown capacity) which are themselves connected to every selected fragments ***aMz*** (edge capacity determined by cj) linking to the sink (edge capacity determined by $aMzj$). When the maximum flow is reached, the first set of edges from the source represents the ratio of each peptide isomer found in the mixed spectrum.

Gradient Descent

Because of the dependencies between fragment intensities within a synthetic peptide spectrum, traditional approaches (such as PreFlow Push) could not be used. Instead, a Gradient Descent was implemented.

The Gradient Descent is an iterative approach with each step being closer to the Maximum Flow than the previous iteration. The initial state of the gradient descent (*c*

value for each *j* isomer) is computed as the number of times each *j* isomer can fit in the mixed spectrum.

$$c_j = aMzm/aMzj$$

This puts the system in an Overflow state (some fragment intensities within the theoretical aMz ($aMzt$) are over their capacity). There might also be Underflow (fragments of $aMzt$ lower than their capacity in $aMzm$).

Iteratively, until there is no Overflow in the network, the *j* isomer with the highest Overflow/Underflow score (objective function) has its c_j value reduced (ions are removed one unit at a time). Ambiguous states are resolved randomly.

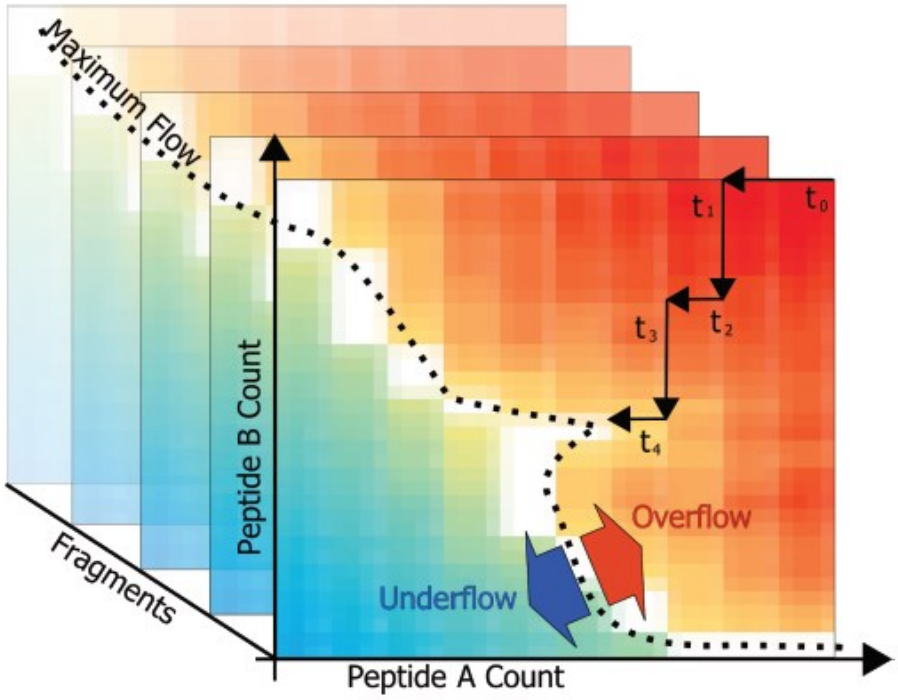

Deconvolution

In PeptidAce, the peak tops and areas under the curve of precursors are both reported for quantification purposes. Iso-PeptidAce also reports area under the curve of the individual isomers populating a mixed precursor elution profile. For each isomer *j*, the number of ions populating the spectrum (deduced by each Gradient Descent result) is

used to compute the number of ions per millisecond flowing in the system at different time points. The resulting, deconvoluted curve is traced through linear interpolation, which is in turn used to compute the area under the curve (ac_j) for that peptide.

Quantification

If peptide intensities are properly normalized based on the synthetic sample runs, it is possible to use this method for absolute quantification of peptides. When concentrations of spiked synthetic peptides are known, Iso-PeptidAce's area under the curve can be converted into absolute peptide counts. Assuming that synthetic peptide samples were processed exactly as the mixed spectrum samples, the number of peptides *j* in the sample *m* (pc_{mj}) is defined by the area under the curve (ac_{mj}) normalized by the synthetic peptide sample *s* information (peptide count in sample pc_{sj},
and area under the curve ac_{sj}).

$$pc_{mj} = ac_{mj} \cdot (pc_{sj}/ac_{sj})$$

Results

Experimental design

To assess the precision of the approach, we designed an experiment to test deconvolution across different peptide isomer concentration ratios. Because of its high level of complexity, characterization of acetylation sites in the Histone H4 peptide **[1]** was selected. The software method was tested for the mono, di and tri-acetylated versions of the peptides while all other lysine sites were propionylated. The next table depicts the concentrations normalized using the equimolar run (observed/expected):

	5fMol - 80fMol	10fMol - 80fMol	20fMol - 80fMol	40fMol - 80fMol	80fMol - 80fMol	160fMol - 80fMol	320fMol - 80fMol
Peptide 2	0.0 / 5	7.4 / 10	19.8 / 20	41.9 / 40	80.0 / 80	168.3 / 160	329.8 / 320
Peptide 3	72.7 / 80	74.0 / 80	72.9 / 80	73.6 / 80	80.0 / 80	74.8 / 80	83.7 / 80
Peptide 4	8.2 / 5	13.0 / 10	19.0 / 20	45.4 / 40	80.0 / 80	189.6 / 160	362.0 / 320
Peptide 5	75.7 / 80	75.9 / 80	78.1 / 80	74.8 / 80	80.0 / 80	72.9 / 80	81.9 / 80
Peptide 6	2.8 / 5	6.3 / 10	14.6 / 20	30.5 / 40	80.0 / 80	168.6 / 160	319.7 / 320
Peptide 7	53.0 / 80	60.6 / 80	67.8 / 80	69.6 / 80	80.0 / 80	74.1 / 80	82.2 / 80
Peptide 8	0.0 / 5	0.4 / 10	7.8 / 20	32.0 / 40	80.0 / 80	382.8 / 160	884.9 / 320
Peptide 9	215.8 / 80	177.4 / 80	150.4 / 80	165.4 / 80	80.0 / 80	44.4 / 80	27.1 / 80
Peptide 10	5.4 / 5	11.7 / 10	21.8 / 20	36.6 / 40	80.0 / 80	133.4 / 160	228.8 / 320
Peptide 11	78.5 / 80	81.9 / 80	82.8 / 80	84.6 / 80	80.0 / 80	66.6 / 80	66.4 / 80
Peptide 12	3.0 / 5	7.5 / 10	17.9 / 20	35.3 / 40	80.0 / 80	162.2 / 160	303.5 / 320
Peptide 13	93.8 / 80	92.4 / 80	90.4 / 80	95.1 / 80	80.0 / 80	67.8 / 80	71.6 / 80
Peptide 14	7.0 / 5	11.1 / 10	21.9 / 20	38.8 / 40	80.0 / 80	162.8 / 160	332.8 / 320
Peptide 15	79.5 / 80	81.8 / 80	81.0 / 80	78.8 / 80	80.0 / 80	73.7 / 80	65.2 / 80

Automatic identification of synthetic peptides

Automatic identification of peptide sequence and modification did not yield in any particular error. However, we did find impurities in the synthesized peptide samples. For instance, incomplete or non-acetylated forms of the peptides were seen in small quantities (less than 0.2% of total intensity). Cross-contamination of peptide forms was tested by running Iso-PeptidAce on a sample containing only one peptide form. The resulting contamination intensity detected were too low to be worth accounting for.

The consistency of the Gradient Descent approach

Despite the fact that each gradient descent is done independently of the others, the results are surprisingly consistent across the mixed elution profile. The deconvoluted elution profiles presented in this next figures are comparable to the profiles drawn from the synthetic peptide runs with conserved elution time order and consistent intensity ratios across the profile (no bulge).

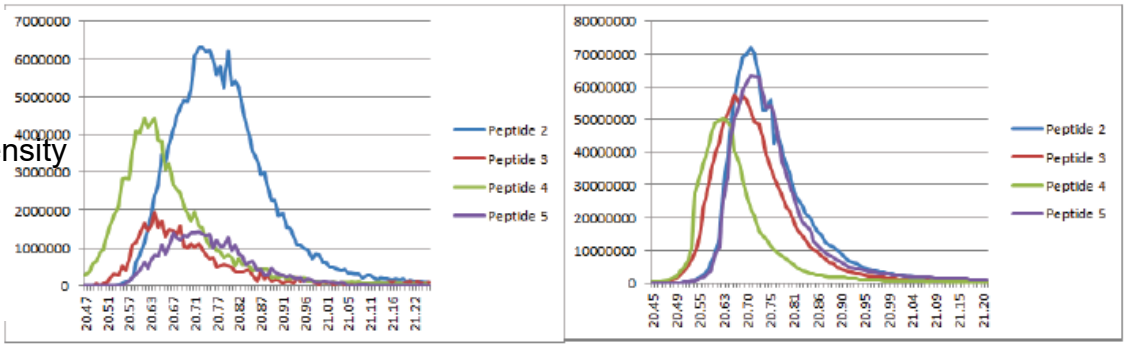

Elution profiles of mixed peptide spectra (left panel) and the individual synthetic peptide spectrum (right panel) after deconvolution by the gradient descent approach

Expected versus Observed Concentration

The precision of the method is shown in the next figure, where observed peptide concentration ratios are plotted against their expected values. The average difference between observed and expected concentration varies from 1.7% to 4.3% with a maximum recorded error of 35% (Di-Acetylation, 320fMol sample). These numbers are well within the error estimates of expected peptide count per sample (**80% purity** per synthetic peptide plus errors introduced during dilutions).

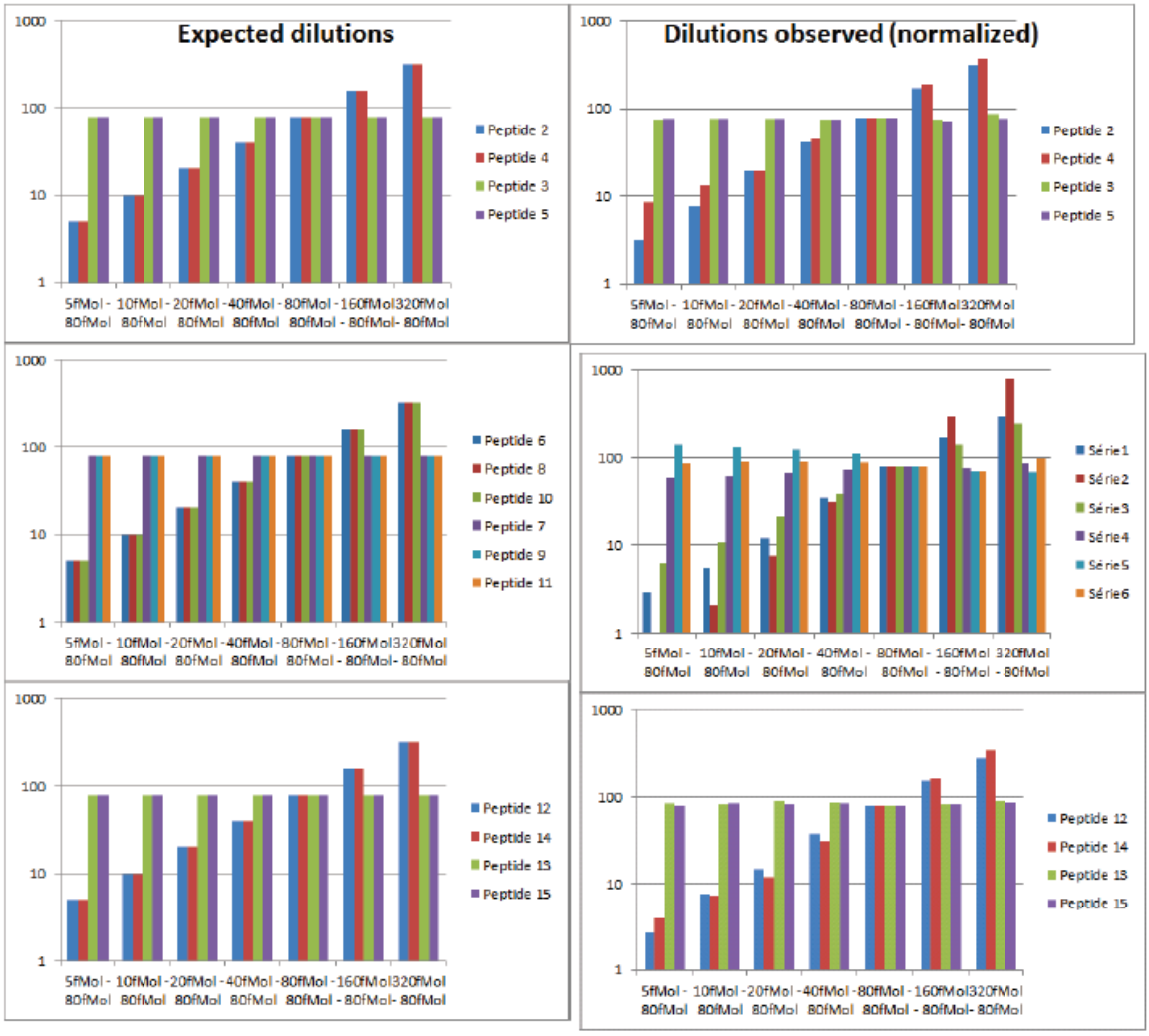

Concentration in fe

Concentration range

Concentration range

Expected (left panel) and observed (right panel) dilutions of peptide mixtures measured by Iso-PeptidAce

Conclusion

Iso-PeptidAce was successfully tested for three types of peptide positional isomers on a QExactive. Peptide fragmentation was done in HCD, but in theory, should work equally well with other fragmentation methods. All mixed spectra samples were resolved with accuracies below the errors that were expected from sample preparation and

manipulation. Furthermore, the included user interface makes the tool readily accessible to all scientists, not just bioinformaticians.

About PeptidAce

PeptidAce is an open source C# library that includes a lot of tools for peptide spectrum matching. It was based on the Morpheus open source project, with the ultimate aim of improving no-enzyme in-silico digestion of huge, unannotated transcriptome databases. It excels at identifying non-tryptic peptides and can identify peptides with non-standard fragmentation patterns. It can also be used for deep spectrum annotation, matching peaks to all types of fragments and modifications. The source code and the documentation of the library are accessible from the github page:

https://github.com/olivierlizotte/PeptidAce

About Iso-PeptidAce

The user interface for Iso-PeptidAce is built using .Net 4. It is compatible with 64-bit versions of Windows 7 (and up). To work with Thermo instruments, MsFileReader (64-bit version) must be installed first. Iso-PeptidAce installer can be downloaded for free from IRIC's Proteomic Platform website: http://proteomics.iric.ca/tools/Iso-PeptidAce

1. Kessner, D., Chambers, M., Burke, R., Agus, D. & Mallick, P. Bioinformatics 24, 2534-2536 (2008).

3. Unraveling site-specific and combinatorial histone modifications using high-resolution mass spectrometry in histone deacetylase mutants of fission yeast

Nebiyu Abshiru*, Roshan Elizabeth Rajan*, Alain Verreault & Pierre Thibault

This chapter corresponds to a published article
J. Proteome Res. 2016 **15**: 2132

*These authors contributed equally to this work

Nebiyu Abshiru designed and carried out the proteomics experiments and prepared the first draft of the manuscript. Roshan Elizabeth Rajan grew the fission yeast strains, isolated histones for MS analysis and contributed to the final draft of the manuscript.

3.1. Abstract

Histone deacetylases (HDACs) catalyze the removal of acetylation marks from lysine residues on histone and nonhistone substrates. Their activity is generally associated with essential cellular processes such as transcriptional repression and heterochromatin formation. Interestingly, abnormal activity of HDACs has been reported in various types of cancers, which makes them a promising therapeutic target for cancer treatment. In the current study, we aim to understand the mechanisms underlying the function of HDACs using an in-depth quantitative analysis of changes in histone acetylation levels in *Schizosaccharomyces pombe* (*S. pombe*) lacking major HDAC activities. We employed a targeted quantitative mass spectrometry approach to profile changes of acetylation and methylation at multiple lysine residues on the N-terminal tail of histones H3 and H4. Our analyses identified a number of histone acetylation sites that are significantly affected by *S. pombe* HDAC mutations. We discovered that mutation of the Class I HDAC known as Clr6 causes a major increase in the abundance of triacetylated H4 molecules at K5, K8, and K12. A *clr6−1* hypomorphic mutation also increased the abundance of multiple acetyl-lysines in histone H3. In addition, our study uncovered a few crosstalks between histone acetylation and methylation upon deletion of HDACs Hos2 and Clr3. We anticipate that the results from this study will greatly improve our current understanding of the mechanisms involved in HDAC-mediated gene regulation and heterochromatin assembly.

3.2. Introduction

Histone deacetylases (HDACs) are a class of enzymes that remove acetyl groups from modified lysines of histones and other proteins. Their activity is generally linked with transcriptional repression and heterochromatin formation (Hassig et al., 1998; Murakami, 2013). Many HDACs exist as components of multiprotein corepressor complexes. For example, the complex known as Sin3 comprises the HDAC Rpd3 in *Saccharomyces cerevisiae* and HDAC1/2 in humans (Kasten et al., 1997; Zhang et al., 1997). These complexes are recruited to specific genomic regions by interacting with DNA binding factors such as transcription factors and epigenetic modifiers such as DNA methyltransferases (DNMTs) and histone methyltransferases (HMTs). These interactions allow HDACs to easily access their target acetylated lysine residues for removal. For example, in *S. cerevisiae*, the Sin3/Rpd3 complex interacts with the DNA-binding protein Ume6 to target the deacetylation of histone H4 by Rpd3, which promotes transcriptional repression of adjacent genes (Kadosh and Struhl, 1997; Rundlett et al., 1998).

A number of previous studies have reported aberrant activities of HDACs in various types of cancers. Increased expression of HDAC2 was found in human gastric cancer (Song et al., 2005). HDAC1 was shown to be up-regulated in hormone refractory (HR) cancer and targets several transcription factors including the tumor suppressor protein p53 (Halkidou et al., 2004). Studies have also reported links between abnormal recruitment of HDACs and the pathogenesis of acute promyelocytic leukemia (Minucci et al., 2001). These findings have made HDACs one of the most promising targets for cancer therapy. A wide range of synthetic and natural small-molecule inhibitors (known as HDAC inhibitors,

HDACi) are currently being tested for treatment of different types of cancers. Several HDAC inhibitors have been developed and are known to increase acetylation of a small, specific subset of the acetylome including sites on histones and other chromatin-associated proteins (Schölz et al., 2015). To date, the Federal Drug Agency (FDA) has approved Vorinostat (Mann et al., 2007), Romidepsin (Bertino and Otterson, 2011) and Belinostat (Lee et al., 2015) for the treatment of peripheral/cutaneous T-cell lymphoma, and Panobinostat (Garnock-Jones, 2015) for multiple myeloma. However, most of these drugs indiscriminately target multiple HDACs, particularly class I and II HDACs, and are commonly referred to as pan-HDACi.

HDACs are best characterized by their activity toward histone substrates, though they are also known to deacetylate non-histone proteins. Their *in vivo* substrate specificity is commonly determined by measuring changes in the level of acetylation at given lysine residues in wild-type cells with the corresponding HDAC mutant. To this end, most studies rely on the capability of immunoassay techniques for site-specific detection of acetylation sites and for monitoring changes in the abundance of acetylated residues. However, this approach suffers from several limitations. Western blotting requires a specific antibody for each site under study and hence lacks the capability to map combinatorial modifications. Recent findings have shown that antibodies exhibit promiscuity when two or more protein modifications are placed in close proximity (Fuchs et al., 2011). For example, antibodies raised against the N-terminal tail histone H4 acetyl lysines were shown to preferentially detect polyacetylated epitopes rather than their specific target site (Rothbart et al., 2012). Antibodies are also limited in their abilities to provide

stoichiometries of acetylation, which has proven valuable in measuring and monitoring acetylation dynamics in various biological processes (Baeza et al., 2014; Weinert et al., 2014).

Recently, we developed Iso-PeptidAce, a quantitative method that combines high-resolution liquid chromatography-tandem mass spectrometry (LC-MS/MS) with bioinformatics tools to facilitate the quantification of histone peptides harboring multiple acetylation marks (Abshiru et al., 2015). This method allowed us to profile histone acetylation in human cells treated with different classes of HDAC inhibitors. In the current study, we employed this method to perform a quantitative and in-depth analysis of changes in histone modifications in fission yeast cells lacking specific HDACs, namely Hos2, Clr6, Clr3, and Sir2. Previous studies used traditional biochemical approaches such as immunoblotting and ChIP to assess the changes in acetylation of HDAC mutants (Bjerling et al., 2002; Nugent et al., 2010; Sinha et al., 2006; Wirén et al., 2005). Clr6, a Class I HDAC and an orthologue of *S. cerevisiae* Rpd3 and human HDAC1/2, is an essential gene required in genome-wide heterochromatin silencing (Grewal et al., 1998; Kim et al., 2004). Previous studies have reported the activity of Clr6 toward a few histone lysine residues (Bjerling et al., 2002). Hos2, another Class I HDAC, was previously shown to primarily target H4K16ac at genomic sites comprising highly active genes (Wirén et al., 2005). Its activity leads to increased gene expression at coding regions, a role contrary to the classical function of HDACs (Kurdistani and Grunstein, 2003). Clr3, the only Class II HDAC in fission yeast, has been shown to act cooperatively with the Class III HDAC Sir2 to promote gene silencing at mating-type loci, centromeres and telomeres (Bjerling

et al., 2002; Grewal et al., 1998). The primary targets for Clr3 and Sir2 were shown to be H3K14ac and H3K9ac, respectively.

In the present study, we determined the changes in abundance of multiple acetyl-lysine residues in histone H3 and H4 in wild-type and Hos2, Clr6, Clr3, and Sir2 mutant strains. In addition to the previously reported sites, we identified several novel acetyl-lysine residues affected by the HDAC mutations. The Clr6 mutant, for example, showed an increased abundance of peptides consisting of combinatorial acetylation motifs in histones H3 and H4.

3.3. Materials and Methods

3.3.1. Strains and Media

The *S. pombe* strains used in this study are listed in Table S3.1. Strains were grown at 25 °C in YE5S medium (yeast extract supplemented with 5 amino acids) (Forsburg and Rhind, 2006). We confirmed the phenotypic expression of antibiotic and auxotrophic markers of all strains by polymerase chain reaction (PCR) and growth on appropriate plates. The mating types of the strains were tested by PCR.

3.3.2. Histone Extraction

Histones were extracted by adapting a protocol used for acid extraction of histones from budding yeast (Guillemette et al., 2011). By starting from saturated overnight cultures, strains were grown at 25 °C in 400 mL of YE5S medium until they reached $O.D_{595}$ 1.0–1.5. Cells were harvested and washed sequentially with 100 mL of water, 25 mL of DTT

buffer (0.1 M Tris-HCl pH 9.5, 10 mM DTT), and 25 mL of Spheroplasting buffer (20 mM HEPES (NaOH) pH 7.4, 1.2 M Sorbitol). The wet cell pellets were weighed, resuspended in 12.5 mL of Spheroplasting buffer containing Zymolyase 100T (5 mg/g of cell pellet), and incubated at 30 °C until digestion was 90–95% complete. The extent of digestion was monitored by measuring absorbance at 600 nm using 1% w/v sodium dodecyl sulfate (SDS) solution. An aliquot of cells before addition of Zymolyase was used as a control. The pellets were gently resuspended in nuclear isolation buffer (NIB) (15 mM 2-(*N*-morpholino) ethanesulfonic acid (KOH) pH 6.6, 60 mM KCl, 15 mM NaCl, 5 mM $MgCl_2$, 1 mM $CaCl_2$, 0.25 M sucrose, 0.8% v/v Triton X-100, 1 mM PMSF). The NIB wash was repeated twice followed by Wash “A” (10 mM Tris-HCl pH 8.0, 75 mM NaCl, 0.5% v/v NP 40, 30 mM NaButyrate, 1 mM PMSF) and Wash “B” (10 mM Tris-HCl pH 8.0, 0.4 M NaCl, 30 mM NaButyrate,1 mM PMSF). The nuclear pellet was resuspended in 0.25 M HCl for 15 min, which extracts histones and other acid-soluble proteins. Trichloroacetic acid (TCA) was added to a final concentration of 20% v/v to the supernatant that contains histones. The histone pellet was washed with acetone, air-dried, and resuspended in water for offline purification of intact histones by reverse-phase high-performance liquid chromatography (RP-HPLC). Centrifugation for cell harvesting and steps until Wash B were done at 3000 rpm for 10 min at 4 °C. Histone extraction and final washes were done at 12 000 rpm for 10 min at 4 °C.

3.3.3. Histone Fractionation by RP-HPLC

Bulk histones from both wild-type and mutant strains were fractionated into individual core histones using an Agilent narrow-bore Zorbax C8 reverse-phase column (2.1 × 150 mm^2, 5 µm, 300 Å) on an Agilent 1200 HPLC system. Approximately 5 µg of bulk histones from each sample was loaded onto the C8 column at a flow rate of 150 µL/min. Histones were eluted from the column using a gradient of 5–80% aqueous acetonitrile (0.1% TFA) in 60 min. Fractions were collected in a 96-well plate every 30 s. Fractions containing histones H3 or H4 were pooled and dried in a SpeedVac concentrator.

3.3.4. Propionylation and Tryptic Digestion of Histone Proteins

In-solution tryptic digestion of core histones was performed as previously described (Abshiru et al., 2013). Briefly, a total of 2 µg of the HPLC-purified histones H3 and H4 was subjected to two rounds of propionylation by adding 200 µL of freshly prepared 2:1 (v/v) water/propionic anhydride (Sigma) mixture and vortexing the mixture for 30 min at room temperature. After each propionylation reaction, the samples were dried completely in a SpeedVac at 4 °C. To remove trace amounts of propionic anhydride left in the samples, a final round of evaporation was performed with the histones resuspended in 100 µL of 50 mM ammonium bicarbonate. The dried histone samples were redissolved in 100 µL of 50 mM ammonium bicarbonate and vortexed for 5 min. The digestion buffer was prepared by adding 200 µL of 50 mM ammonium bicarbonate in a vial containing 20 µg of lyophilized trypsin (Promega). About 0.5 µL of this solution was added to each histone sample and digested overnight at 37 °C. After digestion, samples were dried completely in a SpeedVac and then resuspended in 0.2% formic acid prior to LC-MS/MS analyses.

3.3.5. LC-MS/MS Analysis of Histone Peptides

Chromatographic separation of histone peptides was achieved on an EASY-nLC II system (Thermo scientific). A total of 2 µg of the histone digest was loaded and desalted on an in-house packed trap column (Jupiter C18 3 µm 300 Å particles from Phenomenex, 4 mm length, 360 µm i.d.) using water (0.2% formic acid) at a flow rate of 10 µL/min. After 5 min of desalting, the peptides were eluted onto an in-house packed analytical column (Jupiter C18 3 µm 300 Å particles from Phenomenex, 18 cm length, 150 µm i.d.) interfaced directly to the electrospray source (ESI) of a Q-Exactive Plus instrument (Thermo scientific). The peptides were eluted into the MS with a linear gradient of 5–60% aqueous acetonitrile (0.2% formic acid) at a flow rate of 600 nL/min over 60 min. MS data were acquired for two to three technical replicates per sample. The MS instrument was operated in positive ion mode and capillary voltage of 1.6 kV. MS scans were acquired in the Orbitrap analyzer over the range of 250–1500 m/z at a resolution of 70 000 and automatic gain control target value of 1.0×10^6. Parallel reaction monitoring (PRM) was performed using an inclusion list containing m/z, charge state, and collision energy (CE) values of H3 and H4 peptides to trigger MS/MS acquisition (Table S3.2). Every precursor ion found in the inclusion list was automatically selected for fragmentation in the HCD cell at a normalized CE setting of 27. The fragments were analyzed in the Orbitrap at a resolution of 35 000 and a target value of 5.5×10^5. The dynamic exclusion setting was disabled to acquire multiple MS/MS spectra per peptide.

3.3.6. Data Analysis

MS data were analyzed manually using Thermo Xcalibure Qual Browser software version 2.2 SP1.48 and an in-house built algorithm named Iso-PeptidAce. Raw LC-MS/MS files and FASTA sequences of histones H3 and H4 were submitted to Iso-PeptidAce for peptide-spectrum matching (PSM) and deconvolution of mixed MS/MS spectra of coeluting isomers. Deconvolution of mixed MS/MS spectra of isomeric peptides using Iso-PeptidAce was previously described (Abshiru et al., 2015). The following default parameters were used for the deconvolution. Precursor mass tolerance, 8 ppm; fragment mass tolerance, 0.05 Da; minimum number of fragment ions (per isomer) considered for deconvolution, 5; types of fragment ions considered, b and y; no missed cleavage. Iso-PeptidAce uses no-enzyme *in silico* protein digestion routine to parse the provided FASTA file for potential matches. Protein modifications included in PSM were oxidation of methionine residue (M, 15.9949); phosphorylation of serine, threonine, or tyrosine (S/T/Y, 79.9663); deamidation of asparagine and glutamine (N/Q 0.98400.9847); acetylation of lysine (K, 42.0106); propionylation of lysine (K, 56.0262); methylation of lysine (K, 14.0157); dimethylation of lysine (K, 28.0313); trimethylation of lysine (K, 42.0470); and acetylation of protein N-terminus (42.0106). All protein modifications were considered as variable modifications.

3.4. Results and Discussion

3.4.1. LC-MS/MS analysis of H3 and H4 peptides

The general experimental workflow is shown in Figure 3.1, panel A. Histone proteins were purified from a wild-type fission yeast strain or four mutant strains carrying HDAC mutations (*clr6–1*, *clr3*Δ, *sir2*Δ, and *hos2*Δ). Clr6 is essential for *S. pombe* viability (Grewal et al., 1998; Kunoh et al., 2008), and we could not use a strain with a complete deletion of the *clr6*$^{+}$ gene. Instead, we used a *clr6–1* hypomorphic mutant strain that was grown, along with all the other strains, at the semi-permissive temperature of 25 °C. Core histones were partially purified from exponentially growing cells and fractionated into individual core histones using offline RP-HPLC. Fractions containing histones H3 and H4 were pooled, dried in a SpeedVac, and subjected to *in vitro* propionylation to prevent trypsin cleavage at lysine residues that are not acetylated *in vivo*. Near complete propionylation efficiency was achieved for peptides comprising up to two free lysine residues. Peptides eluting from the analytical column were analyzed using a PRM mode whereby an inclusion list containing precursor *m*/*z*, charge state, and collision energy was used to trigger MS/MS acquisition. The values of the precursor *m*/*z* of the inclusion list were selected based on combinations of histone modifications previously reported for fission yeast (Sinha et al., 2010). The PRM approach allows the acquisition of high-resolution MS/MS spectra and accurate mass measurements in the Orbitrap mass analyzer. The capability of this approach to detect and quantify histone modifications of extremely low abundance (e.g., H3K18 methylation) was recently demonstrated (Abshiru et al., 2015; Tang et al., 2014).

3.4.2. Deconvolution of coeluting isomeric peptides and changes in acetylation at specific sites

In our study, some peptides with identical sequences but bearing different type of protein modifications were chromatographically resolved by LC-MS. For example, the two isobaric H3 peptides K27prK36me2K37pr (*m*/*z* 519.9788^{+3}) and K27acK36me3K37pr (*m*/*z* 519.9788^{+3}) were chromatographically separated (Figure S3.1). However, acetylated isomers of the H4 peptide 4-GKGGKGLGKGGAKR-17 eluted in the same retention time window and produced composite MS/MS spectra consisting of multiple common fragment ions. These MS/MS spectra did not contain diagnostic fragments that can unambiguously identify individual isomers. We have previously developed an algorithm called Iso-PeptidAce that can efficiently deconvolute such composite MS/MS spectra based on features associated with isomer-specific fragment ion patterns (Abshiru et al., 2015). In the current study, we employed this algorithm to deconvolute acetylated isomers in histone samples derived from wild-type and mutant fission yeast. The main steps in the deconvolution process are summarized in Figure 3.1, panel B. The output from Iso-PeptidAce is an Excel spreadsheet containing precursor intensity data for each isomer. The amounts of H3 or H4 peptides injected in the different samples were normalized based on the intensity of reference peptides that lack protein modification: H3:41-YRPGTVALR-49 (*m*/*z* 344.8698, 3+; *m*/*z* 516.8010, 2+) and H4:46-ISALVYEETR-55 (*m*/*z* 618.8270, 2+).

In each sample, the H4 peptide 4-GKGGKGLGKGGAKR-17 was present in five different isoforms (depending on the number of acetyl lysines): unacetylated (ac0), mono- (ac1),

di- (ac2), tri- (ac3), and tetra-acetylated (ac4). The mono-, di-, and tri-acetylated groups were, respectively, composed of four, six, and four isomeric peptides that eluted in the same retention time window (Figure 3.1 C, before deconvolution). Deconvolution by Iso-PeptidAce enabled the reconstruction of peak profiles for individual peptide isomer within each isomeric group (Figure 3.1 C, after deconvolution). The normalized intensity of the reconstructed peaks was used to determine acetylation levels at each site.

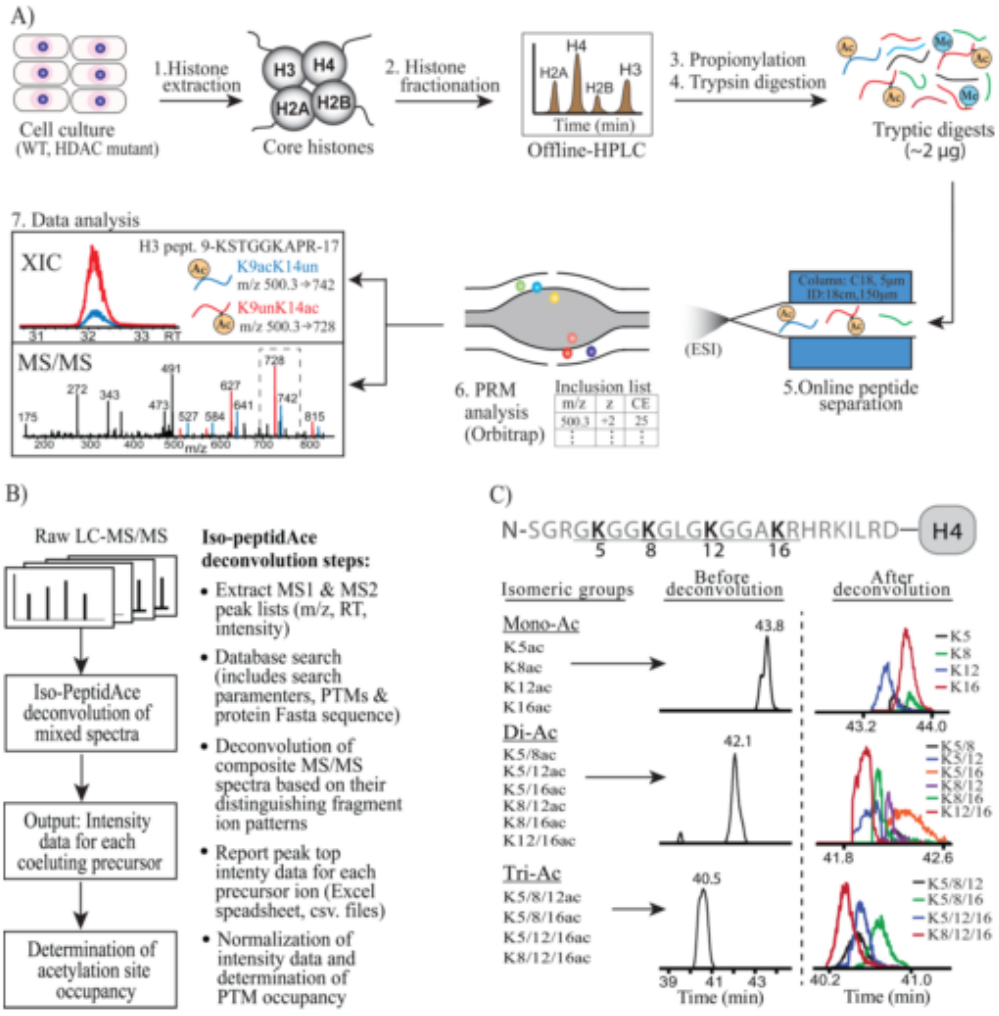

Figure 3.1. LC-MS/MS analysis of histone peptides

Figure 3.1. LC-MS/MS analysis of histone peptides

A) Overview of the experimental workflow. 1) Histones were isolated from the cultured wild-type and mutant *S.pombe* strains. 2) Bulk histones were fractionated into individual core histones (H2A, H2B, H3, and H4) using offline HPLC. 3,4) Fractions containing histones H3 and H4 were pooled and subjected to propionylation and tryptic digestion. 5) Approximately 2 µg of core histones H3 and H4 peptides were separated by reverse-phase C18 column directly interfaced to the ESI source of a Q-Exactive Plus MS. 6) Histone peptides were analyzed by PRM method whereby an inclusion list was used to trigger MS/MS acquisitions. 7) All MS data were analyzed based on peak intensities of ion chromatograms generated manually using the Xcalibur software (Thermo Scientific) or using in-house algorithm Iso-PeptidAce. Ion chromatogram panel shows the coelution of isomeric H3 peptides K9acK14pr (m/z 500.28^{+2}; ac, acetylated; pr, propionylated) and K9prK14ac (m/z 500.28^{+2}); MS/MS panel shows the cofragmentation of the isomers. Isomer-specific fragments are highlighted in blue (K9acK14pr) or red (K9prK14ac). B) Deconvolution of acetylated isomers of histones. Left panel: Raw LC-MS/MS were submitted to Iso-PeptidAce for deconvolution of mixed MS/MS spectra of coeluting isomers. The output from Iso-PeptidAce is a .csv file containing precursor intensities for each deconvoluted isomer. These intensity values were used to calculate changes in the abundance of acetyl-lysines. Right panel: Steps in the deconvolution of mixed MS/MS spectra using IsopeptidAce. C) Deconvolution of an acetylated isomer of fission yeast histone H4. The tryptic peptide 4-GKGGKGLGKGGAKR-17 exists in three different isomeric groups: mono-, di-, triacetylated isomers each comprising four, six, and four peptides. Before deconvolution, each isomeric group exists as a single chromatographic peak. However, after deconvolution by Iso-PeptidAce, distinct chromatographic peaks were obtained for each peptide in the isomeric groups.

3.4.3. Effects of HDAC mutations on global histone acetylation levels

The different types of protein modifications detected on H3 and H4 tails are illustrated in Figure 3.2, panel A. Those peptides comprising lysine residues that can be differentially modified by more than one type of modification (e.g., H3K9 and H3K27) gave rise to multiple combinatorial isoforms. To assess the effects of HDAC deletions on the global H3 or H4 acetylation levels, the normalized peak intensities of all the acetylated isoforms (including all charge states) were summed together. The global changes in acetylation are presented as the fold change (FC) in peptide abundance corresponding to the ratio of summed peptide intensities in the mutant relative to the wild-type samples. Among the HDAC mutants, the strain with a hypomorphic mutation in the Clr6 deacetylase showed the most significant increase in the global acetylation of both H3 and H4 even when the *clr6–1* mutant cells were grown at the permissive temperature of 25 °C (Figure 3.2 B and Table S3.3). We observed up to three-fold increase in total H3 acetylation and up to two-fold increase in H4 acetylation relative to the wild-type cells. Strains lacking the Hos2 deacetylase also exhibited up to 1.5-fold increase in the acetylation of both H3 and H4 (Figure 3.2 A). However, we did not see any significant change in global acetylation in Sir2 or Clr3 mutants. To further investigate the effects of Clr6 and Hos2 mutations on global histone H4 acetylation, we determined the FC values in the mutant relative to wild-type cells for each acetylated form of the peptide 4-GKGGKGLGKGGAKR-17. Our analysis showed that, in Clr6 mutants, nearly 19% of the H4 peptide is present in the tetra-acetylated form (H4 ac4), which is a six-fold increase compared to the abundance of H4 ac4 (3%) detected in wild-type cells (Figure 3.2 C and Table S3.4 A, B). The levels of the di- (H4 ac2) and triacetylated (H4 ac3) isoforms in the Clr6 mutant were also

elevated by up to two- and five-fold, respectively. The monoacetylated (H4 ac1) isoform did not change significantly, whereas the nonacetylated peptide (H4 ac0) decreased by about two-fold. These findings are clearly evidenced from the comparison of the extracted ion chromatograms of the different acetylated isoforms (Figure S3.2, top versus middle panel), which shows a progressive increase in abundance of ac1, ac2, ac3, and ac4 isoforms. Similarly, for the Hos2 mutant, the most significant change was observed for the tetra-acetylated isoform, which exhibited a four-fold increase in the abundance relative to the wild type (Figure 3.2 C). Moreover, the levels of the di- and triacetylated isoforms increased by up to two-fold. The increased abundance of the multiply acetylated isoforms in the Hos2 mutant is also apparent from the extracted ion chromatograms (Figure S3.2 D, bottom panel). Overall, these results suggest that Clr6 and Hos2 play a global role in the deacetylation of both histones H3 and H4.

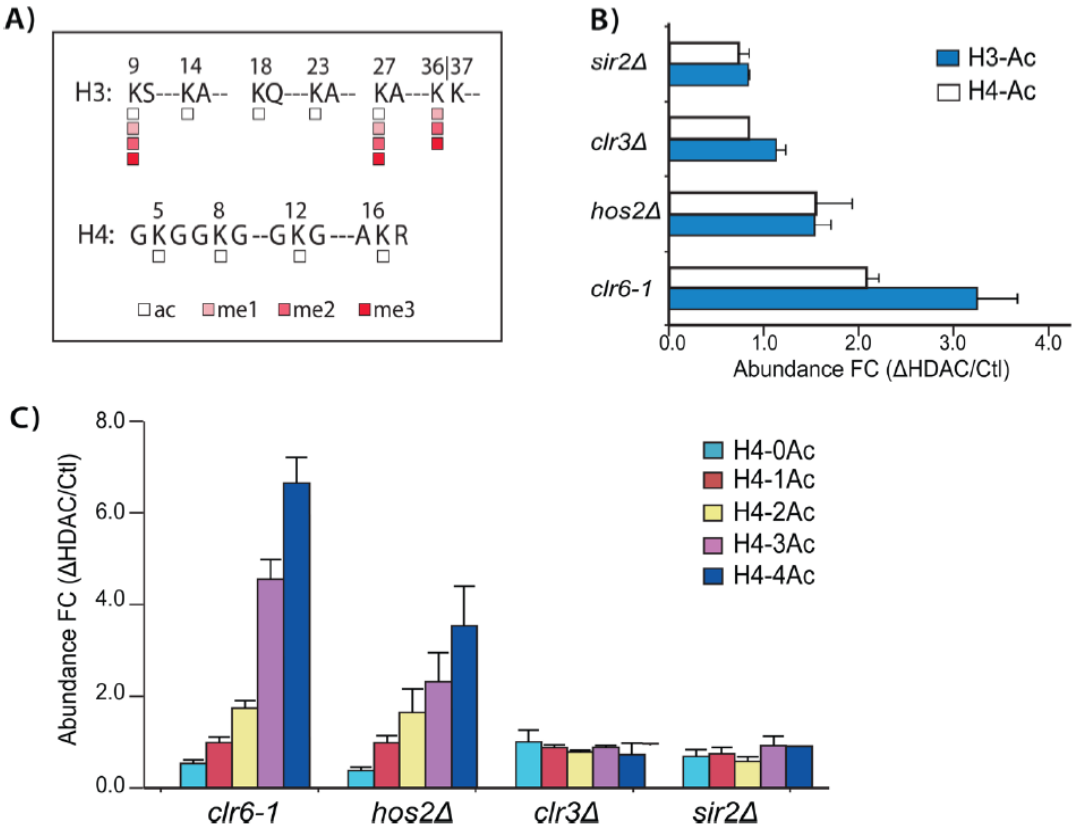

Figure 3.2. Analysis of global H3 and H4 acetylation in response to HDAC depletion

A) Illustration of the different types of modification detected on H3 and H4 tails (ac for acetylation; me1, me2, and me3 for mono-, di-, and trimethylation, respectively). B) Fold change (FC) ratios of abundances of global H3 and H4 acetylations in HDAC mutants: *clr6–1*, *hos2*Δ, *clr3*Δ, and *sir2*Δ relative to control samples. FC ratios were determined based on the summed intensities of all acetylated H3 or H4 peptides detected in the mutant relative to the wild-type. C) FC ratios of abundance for mono-, di-, tri-, and tetra-acetylated and a nonacetylated (propionylated) isoforms derived from the H4 peptide 4-GKGGKGLGKGGAKR-17 in the HDAC mutants. FC ratios were determined based on the calculated relative abundance of each isoform obtained after Iso-PeptidAce analysis.

3.4.4. Clr6 mutation affects the acetylation levels of multiple sites on the H3 tail

Thus far, very few studies have reported the activity of *S. pombe* HDACs toward histone H3. Bjerling et al. and Wiren et al. previously assessed the specificity of Clr6, Clr3, Sir2, and Hos2 toward H3K9ac and H3K14ac using antibodies raised against specific acetylated histone residues (e.g., H3K9ac, H3K14ac, H4K5ac, H4K8ac, H4K12ac, and H4K16ac) (Bjerling et al., 2002; Wirén et al., 2005). These studies monitored changes in acetylation at individual sites but could not directly determine the combinatorial changes in acetylation motifs. In the present study, we evaluated the impact of HDAC mutations on multiple sites on H3 N-terminal tail by determining the changes in acetylation between the mutant and wild-type samples. We also quantified changes in abundance of several acetylation motifs to determine the effect of the HDACs on combinatorial histone modifications. Our analysis confirmed the impact of the Clr6 mutation on the abundance of two previously characterized H3 sites (H3K9 and H3K14). We observed up to four-fold increase in the abundance of acetylation at both sites in the Clr6 mutant (Figure 3.3 A and Table S3.5 A, B). Surprisingly, the analysis of motif-specific changes revealed that loss of Clr6 activity has only a modest effect on the singly acetylated motifs K9acK14pr or K9prK14ac, which showed a two-fold increase in abundance (Figure 3.3 B and Table S3.5 C, D). In comparison, we observed a 13-fold increase in the abundance of the diacetylated motif K9acK14ac, which suggested a progressive accumulation of acetylation on each site in the Clr6 mutant. We also identified three sites whose acetylation was not previously reported to increase in *clr6* mutants: H3K18, K23 and K27. We observed a five-fold increase in the abundance of these acetylated residues upon Clr6 mutation (Figure 3.3 A and Table S3.5 A, B). Similar to the peptide containing K9

and K14, Clr6 mutation also caused accumulation of acetylation on K18 and K23, which is marked by a 15-fold increase in the abundance of the diacetylated motif K18acK23ac (Figure 3.3 B and Table S3.5 C, D). Moreover, loss of Clr6 activity caused a major increase in the acetylation of H3K27. Intriguingly, H3K27ac increased progressively with the number of methyl groups on K36, the largest increase being observed for the motif K27acK36me3 (Figure 3.3 C). However, we did not detect any modification on H3K37.

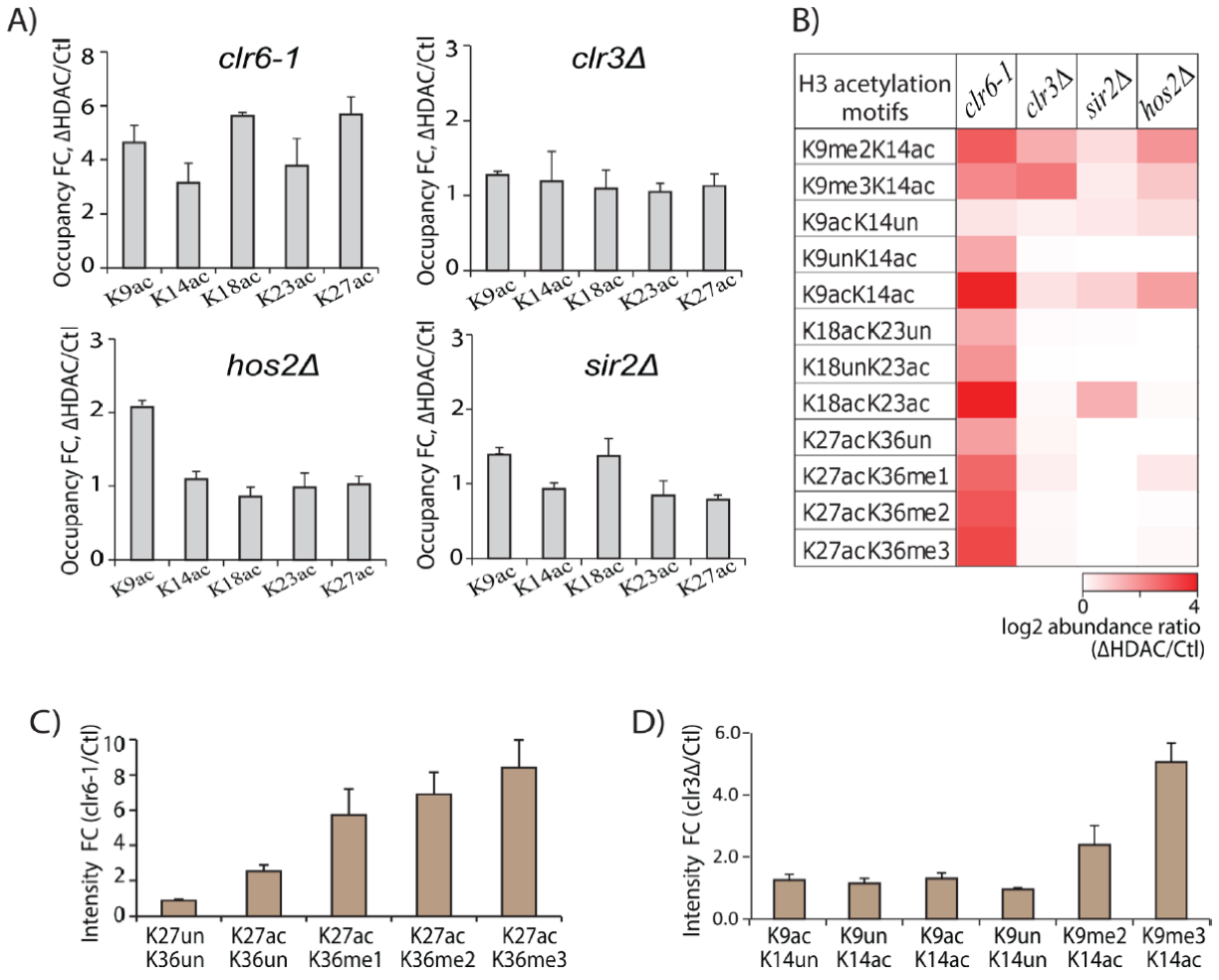

Figure 3.3. Analysis of changes in site-specific acetylation of H3 in response to HDAC depletion

Figure 3.3. Analysis of changes in site-specific acetylation of H3 in response to HDAC depletion

A) Fold changes in the abundance of H3K9ac, H3K14ac, H3K18ac, H3K23ac, and H3K27ac in HDAC mutants relative to the control. B) Heatmap of the mutant-to-control log2 fold changes of the normalized LC-MS signal responses of acetylated peptide motifs. C) Clr6 mutant to control intensity ratios of the nonacetylated (K27prK36pr) and K27ac-containing isoforms of the peptide 27-KAAPATGGVKKPHR-40. D) Clr3 mutant to control intensity ratios of acetylated and nonacetylated isoforms of H3 peptide 9-KSTGGKAPR-17. Error bars indicate standard deviations from two to three replicates.

3.4.5. Loss of Clr3 activity specifically affected the level of H3K14ac co-occurring with a di- or trimethylated H3K9

Previous studies have shown that Clr3 deacetylates K14 in H3 molecules localized in heterochromatin domains, namely the mating-type loci, pericentromeric regions, and telomeres (Bjerling et al., 2002; Hansen et al., 2005; Wirén et al., 2005). However, Clr3 was also shown to affect H3K14ac in bulk histones (Bjerling et al., 2002). In our study, LC-MS/MS analyses of H3 peptides from Clr3 mutant and wild-type *S. pombe* cells indicated that the abundance of H3K14ac or any of the other sites of acetylation that we monitored (H3–K9ac, K18ac, K23ac, and K27ac) was largely unaffected by the presence or absence of Clr3 (*clr3*Δ panel of Figure 3.3 A and Table S3. 5 A, B). Heterochromatin is generally devoid of acetylation at all these sites; the vast majority of H3 acetylation is confined to euchromatin. Therefore, the fact that the abundance of acetylation at all these sites (which is derived from histones present in euchromatin) is virtually the same in *clr3*Δ

and wild-type cells is consistent with the deacetylase activity of Clr3 being restricted to heterochromatic regions.

In wild-type cells, histone H3K9 methylation is a hallmark of heterochromatin regions. To directly assess whether the level of K14 acetylation in H3 molecules derived from heterochromatin was influenced by the absence of Clr3, we manually analyzed our raw LC-MS/MS data to determine if there were changes in signal intensities of the five different "acetylation motifs" that include H3K14 (i.e., K9me2K14ac, K9me3K14ac, K9acK14pr, K9prK14ac, and K9acK14ac). The motif K9me1K14ac was not well detected in our LC-MS/MS experiments. As shown in Figure 3, panel B and Table S3.5 C, D, the motifs K9me2K14ac and K9me3K14ac were, respectively, 2.5- and 4.5-fold more abundant in *clr3*Δ mutants than in wild-type cells. In contrast, we did not detect any significant change in the abundance of the singly or doubly acetylated peptide isoforms that contain H3K9 and K14 but lack K9 methylation. This suggests that the absence of the deacetylase Clr3 leads to an increase in H3K14ac in molecules that contain K9me2 or K9me3 but not in molecules that lack H3K9 methylation. This interpretation is strongly supported by the results presented in Figure 3, panel D and Figure S3.3, which show the fold change ratios in abundance of all the motifs that contain H3K9/K14 in *clr3*Δ mutants versus wild-type cells. The abundances of peptides K9acK14pr, K9prK14ac, K9acK14ac, and K9prK14pr are virtually the same in histones derived from *clr3*Δ mutant cells and wild-type cells (Figure 3D). In striking contrast, the K9me2K14ac and K9me3K14ac peptides are significantly more abundant in the mutant (Figure 3D). Overall, these results imply that

Clr3 removes H3K14ac present in heterochromatin that also contains H3K9 di- or trimethylation.

3.4.6. Sir2 and Hos2 mutation caused a moderate increase in acetylation of H3

The function of Sir2 has been widely implicated in the regulation of heterochromatin structure in fission yeast. In cooperation with Clr3, Sir2 promotes the recruitment of gene silencing complexes at the mating-type loci, telomeres and centromeres (Yamada et al., 2005). Previous *in vitro* and *in vivo* studies showed the activity of Sir2 toward H3K9 and H3K14 (Alper et al., 2013; Shankaranarayana et al., 2003). In the current study, we observed a modest increase in the abundance of H3K9ac and H3K18ac in Sir2 mutant compared to the wild type (Figure 3.3 A and Table S3.5 A, B). These changes are mostly attributed to the increased abundance of the diacetylated peptides comprising K9acK14ac and K18acK23ac, where we observed a 1.7- and 2.4-fold increase in acetylation in the Sir2 mutant (Figure 3.3 B and Table S3.5 C, D). Sir2 has been previously shown to have activity toward K9 and K14 but not K18 and K23.

We also assessed the impact of Hos2 deletion on histone H3 acetylation and observed a two-fold increase in K9ac, whereas K14ac, K18ac, K23ac, and K27ac remained unaffected (Figure 3.3 A and Table S3.5 A, B). The increased abundance of K9ac was largely attributed to the diacetylated motif K9acK14ac, which showed a three-fold increase in the Hos2 mutant. In contrast, the singly acetylated peptide K9acK14pr only showed a 1.5-fold increase in abundance in the Hos2 mutant.

3.4.7. Loss of Clr6 activity had a striking impact on the *in vivo* abundance of a triacetylated H4 tail

We first assessed the impact of the Clr6 mutation on the abundance of acetylation at individual lysines on H4 N-terminal tail. Our analysis showed that K5ac, K8ac, K12ac, and K16ac were elevated by 3.7-, 3.0-, 2.8-, and 1.6-fold, respectively (Figure 3.4 A and Table S3.6 A, B). These results suggest that the loss of Clr6 activity had minimal effect on K16ac. To confirm this observation, we examined the changes in the abundances of 15 different acetylated isoforms derived from the H4 peptide 4-GKGGKGLGKGGAKR-17.

As shown in Figure 3.4, panel B (and Table S3.6 C), the abundance of the monoacetylated motifs K5ac, K8ac, K12ac, and K16ac did not change noticeably with the Clr6 mutation. Only three of the six diacetylated isoforms, namely K5/8ac, K5/12ac, and K8/12ac, were significantly affected in the Clr6 mutant and showed an increase in acetylation by 7.5-, 3.5-, and 2.5-fold, respectively. Interestingly, upon loss of Clr6 activity, we noted a 13-fold increase in the abundance of the triacetylated motif K5/8/12ac, whereas other triacetylated motifs K5/8/16ac, K5/12/16ac, and K8/12/16ac displayed a three-fold increase in abundance on average. The tetra-acetylated isoform K5/8/12/16ac showed a six-fold change in abundance. These results highlight that Clr6 mutation largely affected the abundance of motifs comprising at least two of three lysines H4K5, H4K8, and H4K12, with the most affected combination being the triacetylated motif K5/K8/12ac. These results suggest that either Clr6 is mainly targeting the triacetylated motif

K5/K8/12ac or lack of Clr6 deacetylase is attracting a specific HAT that acetylates the three sites leading to accumulation of the triacetylated motif.

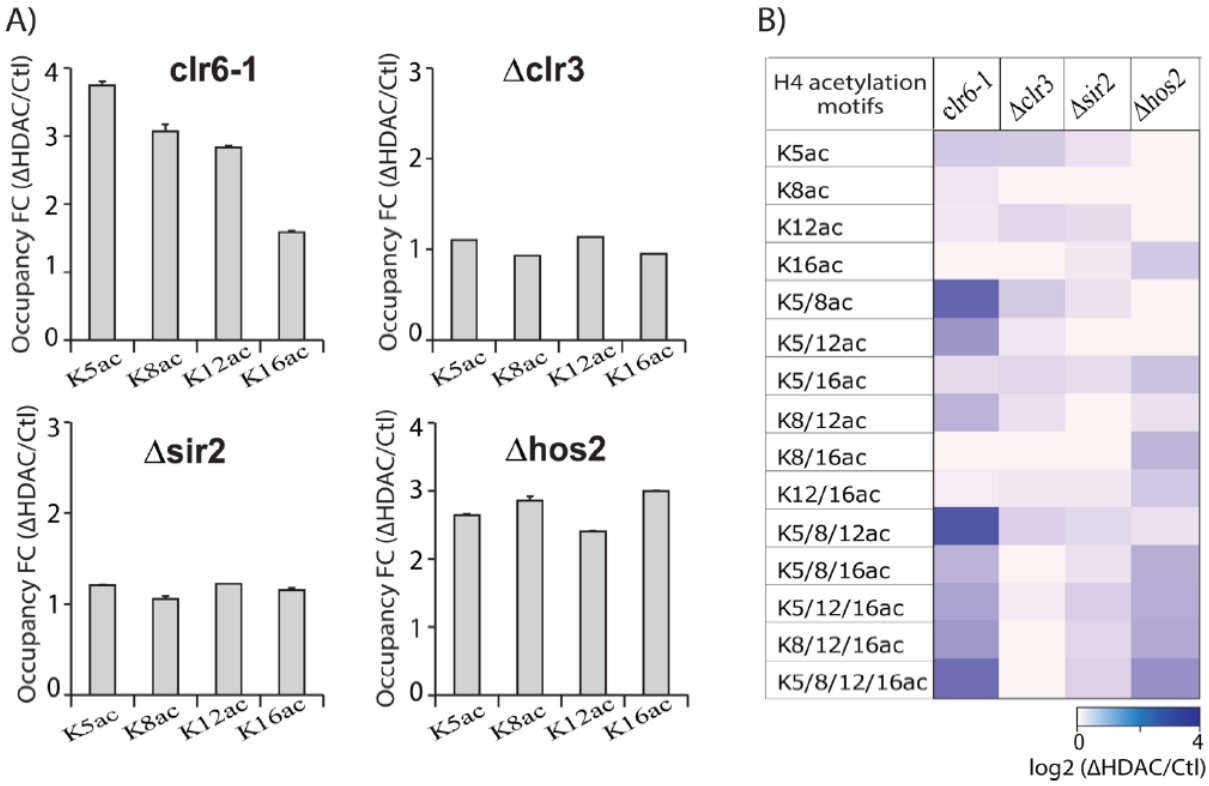

Figure 3.4. Analysis of changes in site-specific acetylation of H4 in response to HDAC depletion

A) Fold changes in the abundance of H4K5ac, H4K8ac, H4K12ac, and H4K16ac in the HDAC mutants relative to the control. B) Heatmap illustration of the log2 fold changes of the normalized LC-MS signal responses of 15 acetylated motifs in the mutant relative to the control sample. Error bars indicate standard deviations from three replicates.

3.4.8. Loss of Hos2 activity mainly affects H4 acetylation motifs that contain H4K16ac

The specificity of Hos2 for H4K16ac has been previously reported (Wirén et al., 2005). Interestingly, in contrast to other HDACs, Hos2-mediated deacetylation of H4K16 has been shown to promote transcriptional activation in both *S. pombe* and *S. cerevisiae* (Kurdistani and Grunstein, 2003). We first assessed the impact of Hos2 deletion on the acetylation of the four lysines in the H4 N-terminal tail. Loss of Hos2 resulted in 2–3-fold increase in acetylation at H4K5, H4K8, and H4K12 in addition to the previously known H4K16 (Figure 3.4 A, Table S3.6 A, B). To further confirm this unexpected result, we examined the changes in abundance of each of the 15 acetylated isoforms derived from the H4 peptide 4-GKGGKGLGKGGAKR-17. Our analysis indicated that the increase in acetylation observed for the first three lysines was largely attributable to the di-, tri, or tetra-acetylated isoforms that contained K16ac. As shown in Figure 3.4, panel B (and Table S3.6 D), the only monoacetylated motif that showed a significant increase in abundance was H4K16ac, where we observed a two-fold increase in acetylation in the *hos2*Δ mutant cells. Moreover, among the six diacetylated isoforms, only those containing K16ac (K5/16ac, K8/16ac, and K12/16ac) were increased in abundance in *hos2*Δ mutant cells. Similarly, the K16ac-containing triacetylated motifs (K5/8/16ac, K5/12/16ac, and K8/12/16ac) exhibited an average 2.8-fold increase in abundance, while the motif lacking the K16ac (K5/8/12ac) remained largely unaffected. The most pronounced change was observed for the tetra-acetylated motif K5/8/12/16ac, which increased by four-fold in the *hos2*Δ mutant cells. Overall, these results confirm the previously reported activity of Hos2 toward K16 acetylation. In addition, our approach demonstrated that the increase in

H4K16ac occurring in *hos2*Δ mutant cells is not only confined to the monoacetylated form, but also occurs in di-, tri-, and tetra-acetylated forms of H4, which was previously unknown.

3.4.9. Sir2 and Clr3 Affect the Methylation Status of the H3 Tail

Previous *in vitro* deacetylation assays have shown that Sir2 deacetylates H3K9 and H4K16 (Shankaranarayana et al., 2003). A more recent *in vitro* study has also reported that Sir2 preferentially deacetylates H3K4, H4K16, and, to a lesser extent, H3K9 and H3K14 (Alper et al., 2013). Although both studies reported the activity of Sir2 toward H4K16, *in vivo* ChIP analyses could not correlate these findings (Wirén et al., 2005). In the present study, we profiled the changes of H4 acetylation at sites K5, K8, K12, and K16 in *sir2*Δ and *clr3*Δ mutant strains and found no significant changes compared to wild-type cells, consistent with previous results obtained from ChIP analyses (Wirén et al., 2005) (Figure 3.4 A,B and Table S3.6 A,B).

Earlier reports have suggested the roles of Clr3 and Sir2 in modulating the levels of H3K9 methylation at silent mating-type loci and pericentric heterochromatin (Shankaranarayana et al., 2003; Yamada et al., 2005). In contrast, little is known about the impact of Clr6 or Hos2 activity on H3K9 methylation. We investigated how the loss of activity of Clr3, Clr6, Sir2, or Hos2 impacts the global methylation levels of H3K9 and H3K36. Figure 3.5, panel A shows the changes in methylation status of H3K9 and H3K36 and indicates that *clr3*Δ and *sir2*Δ exhibited an overall decrease in the levels of H3K9me2 and H3K9me3 (Figure 3.5 A, top panels and Table S3.7 A, B).

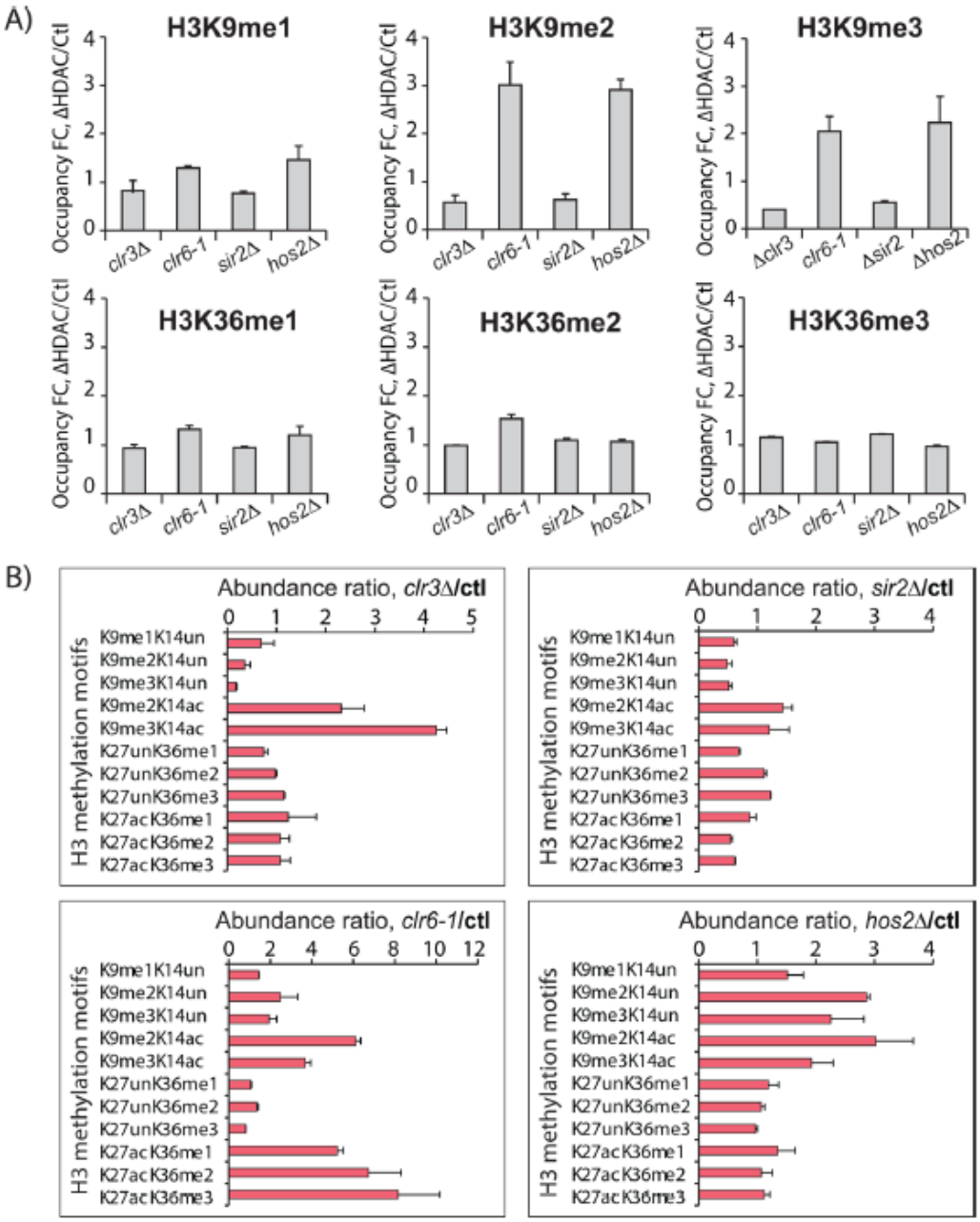

Figure 3.5. Analysis of the impacts of HDAC depletion on the methylation states of H3K9 and H3K36 A) Fold changes in the abundance of H3K9me1/me2/me3 (top panel) and H3K36me1/me2/me3 (bottom panel) in HDAC mutants relative to the control. B) Normalized abundance ratios of H3K9 and H3K36 methylation motifs in *clr3*Δ, *sir2*Δ, *clr6–1*, and *hos2*Δ mutants relative to the control. Error bars indicate standard deviations from two to three replicates.

Although this result might be surprising in view of those presented in Figure 3, panels B and D, this observation can be explained by the known fact that H3K9ac increases in *clr3*Δ and *sir2*Δ mutants (Bjerling et al., 2002; Shankaranarayana et al., 2003), which is likely paralleled by a corresponding decrease in H3K9 methylation as observed in Figure 5, panel A.

Histone peptides derived from heterochromatin that contain both H3K9 and H3K14 can exist in several forms. Therefore, we investigated which modification patterns were most significantly affected in each HDAC mutant. In the *clr3*Δ mutant, the modification patterns that were most significantly affected were K9me2/3K14pr and K9me2/3K14ac, which were affected in opposite fashion. While the patterns K9me2/3K14pr decreased five-fold in the *clr3*Δ mutant, in contrast, K9me2/3K14ac increased up to four-fold (Figure 3.5 B and Table S3.7 C, D). The increase in abundance of K9me2/3K14ac peptide strongly suggests that the persistence of H3K14ac in *clr3*Δ cells does not prevent H3K9 methylation, a proposal that is also supported by the decrease in abundance of the K9me2/3K14pr peptide. Collectively, these results imply that regardless of the presence or absence of H3K14ac, H3K9 remained methylated in heterochromatin.

For the *sir2*Δ mutant, we also observed a decrease in the abundance of K9me2/3K14pr and a corresponding increase in K9me2/3K14ac, but the magnitudes of those changes were smaller than those observed in *clr3*Δ mutants. A plausible explanation for the smaller effects noted for the *sir2*Δ mutant is that although Sir2 and Clr3 likely act on more than one type of heterochromatin (e.g., pericentric, sub-telomeric, rDNA or silent mating

type loci), overall Clr3 may deacetylate a larger number of nucleosomes than Sir2. Alternatively, Sir2 and Clr3 may both act at the same types of heterochromatin, but the deacetylase activity of Clr3 predominates in the heterochromatin region as previously reported (Alper et al., 2013). Consistent with their deacetylase activities being restricted to heterochromatin, the absence of Clr3 or Sir2 had almost no effect on the levels of K36 methylation (Figure 3.5 A), a known mark of actively transcribed chromatin.

In contrast to Clr3 and Sir2 mutants, the *clr6–1* and *hos2*Δ mutations resulted in up to three-fold increase in the abundance of K9 methylation (Figure 3.5 A, upper panel, and Table S3.7 A, B). We next attempted to uncover the modification patterns that were most significantly affected in *clr6–1* and *hos2*Δ mutants. In the *clr6–1* and *hos2*Δ mutants, the abundance of the K9me1/2/3K14ac increased by up to six-fold, while the propionylated forms of the same peptides also increased by up to three-fold (Figure 3.5 B and Table S3.7 C, D). Overall, our results revealed two distinct patterns of K9 methylation in the HDAC mutants. While Clr3 and Sir2 depletions correlated with a global reduction in the heterochromatin marks K9me2 and K9me3, the loss of Clr6 and Hos2 activities resulted in an opposite effect with an increase in abundance of the corresponding modifications. The fact that the *clr6–1* and *hos2*Δ mutations increased H3K9 methylation was unexpected because those enzymes are not known to act specifically on heterochromatin. One possible explanation for this surprising result may be that the *clr6-1* and *hos2*Δ mutations decrease the abundance or the activity of the enzyme that demethylates H3K9 (Epe1). Alternatively, these mutations may increase the abundance or activity of the H3K9 methyltransferase (Clr4). A third possibility that would not invoke

changes in the abundance of the enzymes that affect H3K9 methylation is the following. It is known in wild-type cells that spreading of heterochromatin containing H3K9 methylation is prevented by boundary elements. Interestingly, the H3K9 demethylase Epe1 has been located at those boundary elements by ChIP (Wang et al., 2013). In addition, those elements demarcate the boundaries between heterochromatin, which generally lacks histone acetylation, from euchromatin, which is enriched in acetylation. Among all sites, H4 molecules that contain K16ac show a strikingly different abundance on either side of the boundary elements, and the presence of this modification is crucial to restrict spreading of heterochromatin into euchromatin (Wang et al., 2013). Therefore, one hypothesis that might explain the unexpected increase in H3K9 methylation in *clr6–1* and *hos2*Δ cells is that due to a general increase in acetylation, the boundary elements may be defective in these mutants.

For convenience, Figure 6 summarizes the site-specific changes in acetylation associated with Clr6, Clr3, Sir2, and Hos2 deacetylase activities.

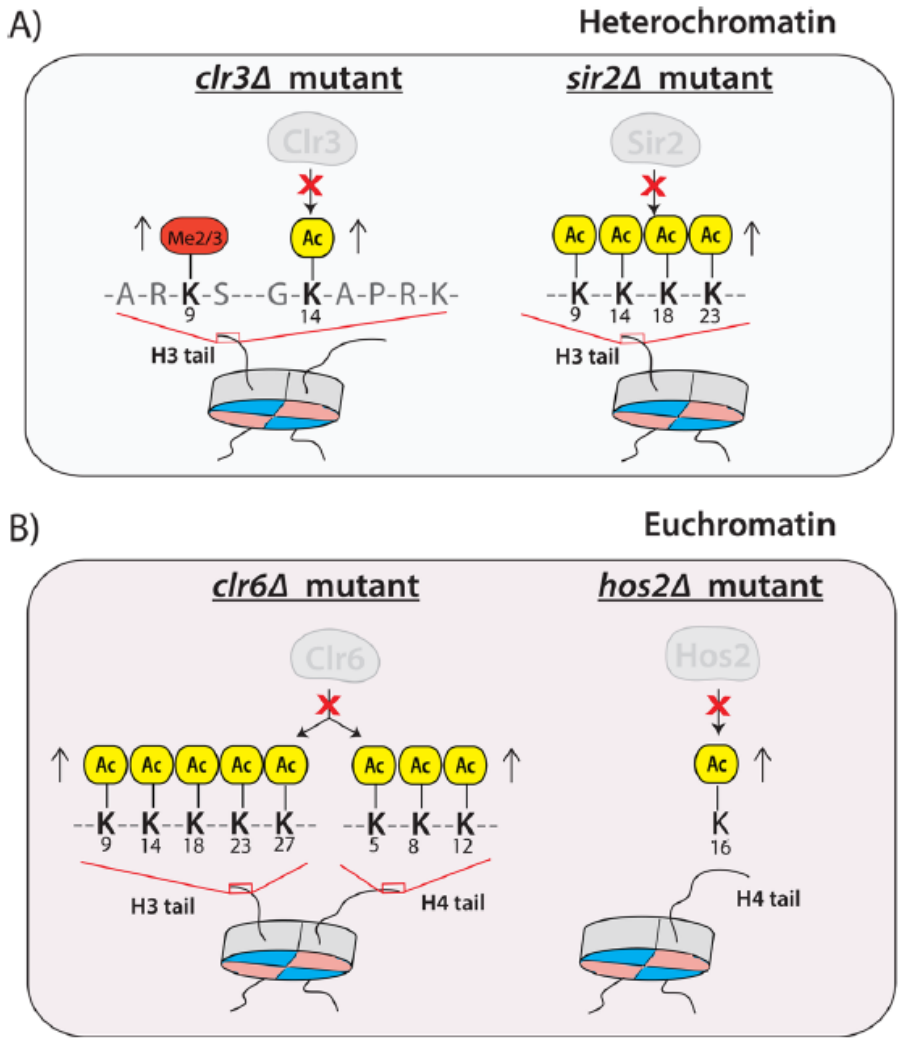

Figure 6. Summary of HDAC activities in fission yeast

A) Clr3 and Sir2 are both known to act in heterochromatin. The absence of the deacetylase Clr3 leads to an increase in H3K14ac in molecules that contain K9me2 or K9me3 but not in molecules that lack H3K9 methylation. In *sir2*Δ cells, we observed an increase in acetylation of residues K9, K14, K18, and K23 of histone H3. B) Clr6 and Hos2 are known to act in euchromatin. The absence of Clr6 has global effects on the acetylation levels of H3 K9, K14, K18, K23, and K27 and H4 K5, K8, and K12. The absence of Hos2 primarily resulted in an increase in acetylation of H4K16 that also contain di-, tri-, and tetra-acetylated forms of H4. Please read the *clr6Δ* mutant in panel B as *clr6-1*

3.5. Conclusion

High-resolution mass spectrometry was applied to deconvolute isomeric peptides from the N-terminal tails of histones H3 and H4. The use of parallel reaction monitoring in combination with bioinformatic tools such as Iso-PeptidAce enabled profiling of acetylation and methylation levels at specific sites of histones H3 and H4 in wild-type and mutant cells lacking the deacetylases Clr6, Clr3, Sir2, and Hos2. Among those four HDAC mutants, we found that *clr6-1* cells showed the most pronounced increases in acetylation of several lysine residues of H3 (K9, K14, K18, K23, K27) and H4 (K5, K8, K12). In contrast, the absence of Hos2, which like Clr6 predominantly acts in euchromatin, primarily increased the acetylation of H4K16. In the case of Clr3, our quantitative LC-MS/MS analyses revealed that this deacetylase targeted primarily H3K14ac in histones that also contained K9me2 or K9me3, a finding that is consistent with its activity being largely restricted to heterochromatin regions. Clr3 was previously reported to collaborate with Sir2 to promote the recruitment of gene silencing complexes at the mating-type loci, telomeres and centromeres. In our study, we identified that cells lacking Sir2 showed elevated acetylation levels at H3 K9, K14, K18, and K23. Although our analysis identified many sites where acetylation increases in *S. pombe* HDAC mutants, our approach cannot distinguish between indirect or direct targets. This would require *in vitro* deacetylase assays performed with purified fission yeast HDAC complexes and nucleosomes.

3.6. Acknowledgments

We thank Dr. Robin Allshire (University of Edinburgh) and Dr. Karl Ekwall (Karolinska Institute) for providing HDAC mutant strains of *S. pombe*. We also thank Éric Bonneil (UdeM) for the assistance with MS experiments. This work was carried out with financial support from the Canadian Institute for Health Research to A.V. (CIHR, FRN 125916) and the Natural Sciences and Engineering Research Council (NSERC 311598) to P.T. The Institute for Research in Immunology and Cancer (IRIC) receives infrastructure support from Genome Canada, IRICoR, the Canadian Foundation for Innovation, and the Fonds de Recherche du Québec-Santé (FRQS).

3.7. Author contributions:

P.T and A.V. conceived and led the project. N.A. designed and carried out the proteomics experiment. R.E.R. performed the biological experiments. N.A. analyzed data, wrote the first draft of the manuscript, and generated figures. N.A., R.E.R., P.T. and A.V. wrote the final draft of the manuscript.

3.8. References

Abshiru, N., Ippersiel, K., Tang, Y., Yuan, H., Marmorstein, R., Verreault, A., and Thibault, P. (2013). Chaperone-mediated acetylation of histones by Rtt109 identified by quantitative proteomics. J. Proteomics *81*, 80–90.

Abshiru, N., Caron-Lizotte, O., Rajan, R.E., Jamai, A., Pomies, C., Verreault, A., and Thibault, P. (2015). Discovery of protein acetylation patterns by deconvolution of peptide isomer mass spectra. Nat. Commun. *6*, 8648.

Alper, B.J., Job, G., Yadav, R.K., Shanker, S., Lowe, B.R., and Partridge, J.F. (2013). Sir2 is required for Clr4 to initiate centromeric heterochromatin assembly in fission yeast. EMBO J. *32*, 2321–2335.

Baeza, J., Dowell, J.A., Smallegan, M.J., Fan, J., Amador-Noguez, D., Khan, Z., and Denu, J.M. (2014). Stoichiometry of site-specific lysine acetylation in an entire proteome. J. Biol. Chem. *289*, 21326–21338.

Bertino, E.M., and Otterson, G. A. (2011). Romidepsin: a novel histone deacetylase inhibitor for cancer. Expert Opin. Investig. Drugs *20*, 1151–1158.

Bjerling, P., Silverstein, R.A., Thon, G., Caudy, A., Grewal, S., and Ekwall, K. (2002). Functional divergence between histone deacetylases in fission yeast by distinct cellular localization and in vivo specificity. Mol. Cell. Biol. *22*, 2170–2181.

Forsburg, S.L., and Rhind, N. (2006). Basic methods for fission yeast. Yeast *23*, 173–183.

Fuchs, S.M., Krajewski, K., Baker, R.W., Miller, V.L., and Strahl, B.D. (2011). Influence of combinatorial histone modifications on antibody and effector protein recognition. Curr. Biol. *21*, 53–58.

Garnock-Jones, K.P. (2015). Panobinostat: first global approval. Drugs *75*, 695–704.

Grewal, S.I.S., Bonaduce, M.J., and Klar, A.J.S. (1998). Histone deacetylase homologs regulate epigenetic inheritance of transcriptional silencing and chromosome segregation in fission yeast. Genetics *150*, 563–576.

Guillemette, B., Drogaris, P., Lin, H.-H.S., Armstrong, H., Hiragami-Hamada, K., Imhof, A., Bonneil, E., Thibault, P., Verreault, A., and Festenstein, R.J. (2011). H3 lysine 4 is acetylated at active gene promoters and is regulated by H3 lysine 4 methylation. PLoS Genet. *7*, e1001354.

Halkidou, K., Gaughan, L., Cook, S., Leung, H.Y., Neal, D.E., and Robson, C.N. (2004). Upregulation and nuclear recruitment of HDAC1 in hormone refractory prostate cancer. Prostate *59*, 177–189.

Hansen, K.R., Burns, G., Mata, J., Volpe, T. A., Martienssen, R. A., Bähler, J., and Thon, G. (2005). Global effects on gene expression in fission yeast by silencing and RNA interference machineries. Mol. Cell. Biol. *25*, 590–601.

Hassig, C.A., Tong, J.K., Fleischer, T.C., Owa, T., Grable, P.G., Ayer, D.E., and Schreiber, S.L. (1998). A role for histone deacetylase activity in HDAC1-mediated transcriptional repression. Proc. Natl. Acad. Sci. U. S. A. *95*, 3519–3524.

Kadosh, D., and Struhl, K. (1997). Repression by Ume6 involves recruitment of a complex containing Sin3 corepressor and Rpd3 histone deacetylase to target promoters. Cell *89*, 365–371.

Kasten, M.M., Dorland, S., and Stillman, D.J. (1997). A large protein complex containing the yeast Sin3p and Rpd3p transcriptional regulators. *17*, 4852–4858.

Kim, H.S., Choi, E.S., Shin, J.A., Jang, Y.K., and Park, S.D. (2004). Regulation of Swi6/HP1-dependent heterochromatin assembly by cooperation of components of the mitogen-activated protein kinase pathway and a histone deacetylase Clr6. J. Biol. Chem. *279*, 42850–42859.

Kunoh, T., Habu, T., and Matsumoto, T. (2008). Involvement of fission yeast Clr6-HDAC in regulation of the checkpoint kinase Cds1. Nucleic Acids Res. *36*, 3311–3319.

Kurdistani, S.K., and Grunstein, M. (2003). Histone acetylation and deacetylation in yeast. Nat. Rev. Mol. Cell Biol. *4*, 276–284.

Lee, H.-Z., Kwitkowski, V.E., Del Valle, P.L., Ricci, M.S., Saber, H., Habtemariam, B.A., Bullock, J., Bloomquist, E., Li Shen, Y., Chen, X.-H., et al. (2015). FDA Approval: Belinostat for the treatment of patients with relapsed or refractory peripheral T-cell lymphoma. Clin. Cancer Res. *21*, 2666–2670.

Mann, B.S., Johnson, J.R., Cohen, M.H., Justice, R., and Pazdur, R. (2007). FDA approval summary: vorinostat for treatment of advanced primary cutaneous T-cell lymphoma. Oncologist *12*, 1247–1252.

Minucci, S., Nervi, C., Coco, F. Lo, and Pelicci, P.G. (2001). Histone deacetylases: a common molecular target for differentiation treatment of acute myeloid leukemias ? Oncogene *20*, 3110–3115.

Murakami, Y. (2013). Histone deacetylases govern heterochromatin in every phase. EMBO J. *32*, 2301–2303.

Nugent, R.L., Johnsson, A., Fleharty, B., Gogol, M., Xue-Franzén, Y., Seidel, C., Wright, A.P., and Forsburg, S.L. (2010). Expression profiling of S. pombe acetyltransferase mutants identifies redundant pathways of gene regulation. BMC Genomics *11*, 59.

Rothbart, S.B., Lin, S., Britton, L.-M., Krajewski, K., Keogh, M.-C., Garcia, B. A. and Strahl, B.D. (2012). Poly-acetylated chromatin signatures are preferred epitopes for site-specific histone H4 acetyl antibodies. Sci. Rep. *2*, 489.

Rundlett, S.E., Carmen, A.A., Suka, N., Turner, B.M., and Grunstein, M. (1998). Transcriptional repression by UME6 involves deacetylation of lysine 5 of histone H4 by RPD3. Nature *392*, 831–835.

Schölz, C., Weinert, B.T., Wagner, S.A., Beli, P., Miyake, Y., Qi, J., Jensen, L.J., Streicher, W., Mccarthy, A.R., Westwood, N.J., et al. (2015). Acetylation site specificities of lysine deacetylase inhibitors in human cells. Nat. Biotechnol. *33*, 415–423.

Shankaranarayana, G.D., Motamedi, M.R., Moazed, D., and Grewal, S.I.S. (2003). Sir2 regulates histone H3 Lysine 9 methylation and heterochromatin assembly in fission yeast. Curr. Biol. *13*, 1240–1246.

Sinha, I., Wiren, M., and Ekwall, K. (2006). Genome-wide patterns of histone modifications in fission yeast. Chromosom. Res. *14*, 95–105.

Sinha, I., Buchanan, L., Rönnerblad, M., Bonilla, C., Durand-Dubief, M., Shevchenko, A., Grunstein, M., Stewart, A. F., and Ekwall, K. (2010). Genome-wide mapping of histone modifications and mass spectrometry reveal H4 acetylation bias and H3K36 methylation at gene promoters in fission yeast. Epigenomics *2*, 377–393.

Song, J., Noh, J.I.H., Lee, J.H., Eun, J.W.O.O., Ahn, Y.M.I.N., Kim, S.U.Y., Lee, S.U.G.H., Park, W.O.N.S., Yoo, N.A.M.J.I.N., and Lee, J.Y. (2005). Increased expression of histone deacetylase 2 is found in human gastric cancer. 264–268.

Tang, H., Fang, H., Yin, E., Brasier, A.R., Sowers, L.C., and Zhang, K. (2014). Multiplexed parallel reaction monitoring (PRM) targets histone modifications on the Q-Exactive mass spectrometer. Anal. Chem. 140513170620003.

Wang, J., Tadeo, X., Hou, H., Tu, P.G., Thompson, J., Yates, J.R., and Jia, S. (2013). Epe1 recruits BET family bromodomain protein Bdf2 to establish heterochromatin boundaries. Genes Dev. *27*, 1886–1902.

Weinert, B.T., Iesmantavicius, V., Moustafa, T., Schölz, C., Wagner, S.A., Magnes, C., Zechner, R., and Choudhary, C. (2014). Acetylation dynamics and stoichiometry in Saccharomyces cerevisiae. Mol. Syst. Biol. *10*, 716.

Wirén, M., Silverstein, R. a, Sinha, I., Walfridsson, J., Lee, H.-M., Laurenson, P., Pillus, L., Robyr, D., Grunstein, M., and Ekwall, K. (2005). Genome wide analysis of nucleosome density histone acetylation and HDAC function in fission yeast. EMBO J. *24*, 2906–2918.

Yamada, T., Fischle, W., Sugiyama, T., Allis, C.D., and Grewal, S.I.S. (2005). The nucleation and maintenance of heterochromatin by a histone deacetylase in fission yeast.

Mol. Cell *20*, 173–185.

Zhang, Y., Iratni, R., Erdjument-Bromage, H., Tempst, P., and Reinberg, D. (1997). Histone deacetylases and SAP18, a novel polypeptide, are components of a human Sin3 complex. Cell *89*, 357–364.

3.9. Supplementary Information

Table S3.1. Fission yeast strains used in this study

Strain name	Genotype	Source
1645	*h+ ade6-210 arg3-D4 his3-D1 leu1-32 ura4-D18*	Allshire Lab
1646	*h- ade6-210 arg3-D4 his3-D1 leu1-32 ura4-D18*	Allshire Lab
9351	*h+ sir2::NatR his3D arg3D leu1-32 ade6-210 ura4-D18*	Allshire Lab
5962	*h+ clr3::kanMX ade6-210 ura4-D18 leu1-32*	Allshire Lab
A3337	*h- clr6-1 ade6-210 leu1-32 ura4D-S/E his3-D1? arg3-D4?*	Allshire Lab
A3338	*h+ clr6-1 ade6-210 leu1-32 ura4D-S/E his3-D1? arg3-D4?*	Allshire Lab
Hu1026	*h- hos2::LEU2+ leu1- 32*	Ekwall lab

Table S3.2. Parallel Reaction Monitoring (PRM) inclusion list

Mass (m/z)	CS	CE	Modification	Sequence
319.8540	3+	27	H3-K9me1K14ac	Kme1STGGKacAPR
479.2774	2+	27	H3-K9me1K14ac	
514.2981	2+	27	H3-K9me1-prK14pr	Kme1-prSTGGK14APR
507.2904	2+	27	H3-K9me1-prK14ac	
324.5259	3+	27	H3-K9me1K14un	Kme1STGGKprAPR
486.2837	2+	27	H3-K9me1K14un	
324.5259	3+	27	H3-K9me2K14ac	Kme2STGGKacAPR
486.2837	2+	27	H3-K9me2K14ac	
329.1980	3+	27	H3-K9me3K14ac	Kme3STGGKacAPR
493.2936	2+	27	H3-K9me3K14ac	
329.1980	3+	27	H3-K9me2K14pr	Kme2STGGKprAPR
493.2936	2+	27	H3-K9me2K14pr	
333.8696	3+	27	H3-K9me3K14pr	Kme3STGGKprAPR
500.3002	2+	27	H3-K9me3K14pr	
507.2906	2+	27	H3-K9prK14pr	KprSTGGKprAPR
493.2748	2+	27	H3-K9acK14ac	KacSTGGKacAPR
500.2836	2+	27	H3-K9prK14ac	KprSTGGKacAPR
	2+	27	H3-K9acK14pr	KacSTGGKprAPR
542.8270	2+	27	H3-K18prK23pr	KprQLASKprAAR
535.8190	2+	27	H3-K18acK23pr	KacQLASKprAAR
	2+	27	H3-K18pK23ac	KprQLASKacAAR
528.8110	2+	27	H3-K18acK23ac	KacQLASKacAAR
793.4619	2+	27	H3-K27prK36prK37pr	KprAAPATGGVKprKprPHR
529.3103	3+	27	H3-K27prK36prK37pr	
786.4542	2+	27	H3-K27acK36prK37pr	KacAAPATGGVKprKprPHR
524.6385	3+	27	H3-K27acK36prK37pr	
772.4567	2+	27	H3-K27acK36me2K37pr	KacAAPATGGVKme2KprPHR
515.3069	3+	27	H3-K27acK36me2K37pr	
386.7320	4+	27	H3-K27acK36me2K37pr	
779.4645	2+	27	H3-K27acK36me3K37pr	KacAAPATGGVKme3KprPHR
519.9788	3+	27	H3-K27acK36me3K37pr	
390.2359	4+	27	H3-K27acK36me3K37pr	
793.4620	2+	27	H3-K27acK36me1-prK37pr	KacAAPATGGVKme1-prKprPHR
529.3104	3+	27	H3-K27acK36me1-prK37pr	
779.4645	2+	27	H3-K27prK36me2K37pr	KprAAPATGGVKme2KprPHR
519.9788	3+	27	H3-K27prK36me2K37pr	
390.2359	4+	27	H3-K27prK36me2K37pr	
786.4724	2+	27	H3-K27prK36me3K37pr	KprAAPATGGVKme3KprPHR
524.6507	3+	27	H3-K27prK36me3K37pr	
393.7398	4+	27	H3-K27prK36me3K37pr	
800.4697	2+	27	H3-K27prK36me1-prK37pr	KprAAPATGGVKme1-prKprPHR
533.9822	3+	27	H3-K27prK36me1-prK37pr	
344.8698	3+	27	-	YRPGTVALR
516.8010	2+	27	-	

Continued, Table S3.2.

747.9412	2+	27	H4-K5prK8prK12prK16pr	GKprGGKprGLGKprGGAKprR
740.9334	2+	27	H4-K5acK8prK12prK16pr	GKacGGKprGLGKprGGAKprR
			H4-K5prK8acK12prK16pr	GKprGGKacGLGKprGGAKprR
			H4-K5prK8prK12acK16pr	GKprGGKprGLGKacGGAKprR
			H4-K5prK8prK12prK16ac	GKprGGKprGLGKprGGAKacR
733.9255	2+	27	H4-K5acK8acK12prK16pr	GKacGGKacGLGKprGGAKprR
			H4-K5acK8prK12acK16pr	GKacGGKprGLGKacGGAKprR
			H4-K5acK8prK12prK16ac	GKacGGKprGLGKprGGAKacR
			H4-K5prK8acK12acK16pr	GKprGGKacGLGKacGGAKprR
			H4-K5prK8acK12prK16ac	GKprGGKacGLGKprGGAKacR
			H4-K5prK8prK12acK16ac	GKprGGKprGLGKacGGAKacR
726.9177	2+	27	H4-K5acK8acK12acK16pr	GKacGGKacGLGKacGGAKprR
			H4-K5acK8acK12prK16ac	GKacGGKacGLGKprGGAKacR
			H4-K5acK8prK12acK16ac	GKacGGKprGLGKacGGAKacrR
			H4-K5prK8acK12acK16ac	GKprGGKacGLGKacGGAKacR
719.9099	2+	27	H4-K5acK8acK12acK16ac	GKacGGKacGLGKacGGAKacR
618.8270	2+	27	-	ISALVYEETR

CS - Charge State
CE - Collision Energy
Highlighted in yellow - Peptides used for normalization of total histone abundances

Table S3.3. Analysis of global H3 and H4 acetylation in HDAC mutants

Sample	Relative Abundance FC (ΔHDAC/Ctl) ±SD	
	H3-ac	H4-ac
clr6-1	3.25 ± 0.43	2.08 ± 0.13
hos2Δ	1.54 ± 0.17	1.55 ± 0.39
clr3Δ	1.13 ± 0.10	0.84 ± 0.02
sir2Δ	0.83 ± 0.02	0.73 ± 0.12

FC- Fold change
SD - Standard deviation SD - Standard deviation (determined based on 2-3 replicates)

Fold change ratios of global H3 and H4 acetylation in HDAC mutants relative to the control.

Table S3.4. Analysis of changes in the level of acetylated isoforms of H4 in response to HDAC deletion

A)

Sample	Relative intensity (%) ± SD				
	H4_ac0	H4_ac1	H4_ac2	H4_ac3	H4_ac4
WT	52.91 ± 5.3	22.98 ± 0.1	14.79 ± 0.3	5.79 ± 0.4	3.53 ± 0.3
clr6-1	22.23 ± 1.1	18.04 ± 2.2	20.40 ± 1.5	20.81 ± 0.4	18.52 ± 0.2
hos2Δ	21.43 ± 2.2	24.44 ± 4.0	26.14 ± 7.7	14.36 ± 2.8	13.63 ± 4.5
clr3Δ	57.08 ± 8.7	21.98 ± 1.5	12.63 ± 0.3	5.57 ± 0.2	2.74 ± 0.7
sir2Δ	51.10 ± 6.0	24.57 ± 4.5	12.18 ± 1.9	7.59 ± 1.0	4.56 ± 0.2

B)

Sample	Relative Abundance FC ratio (ΔHDAC/Ctl) ± SD				
	H4_ac0	H4_ac1	H4_ac2	H4_ac3	H4_ac4
clr6-1	0.53 ± 0.1	0.99 ± 0.1	1.74 ± 0.2	4.55 ± 0.4	6.65 ± 0.6
hos2Δ	0.38 ± 0.1	0.98 ± 0.2	1.64 ± 0.5	2.32 ± 0.6	3.54 ± 0.9
clr3Δ	1.01 ± 0.3	0.88 ± 0.1	0.79 ± 0.0	0.89 ± 0.0	0.73 ± 0.2
sir2Δ	0.69 ± 0.1	0.75 ± 0.1	0.58 ± 0.1	0.93 ± 0.2	0.91 ± 0.0

FC- Fold change
SD - Standard deviation (determined based on 3 replicates)

A) Relative abundances of a non-acetylated (H4_Ac0), mono-(H4_Ac1), di- (H4_Ac2), tri-(H4_Ac3) and tetra- (H4_Ac4) acetylated isoforms of the H4 peptide 4-GKGGKGLGKGGAKR-17.

B) Fold change of relative abundance of the non-acetylated and acetylated isoforms of the H4 peptide in the HDAC mutant relative to the control.

Table S3.5. Analysis of site-specific acetylation of H3 in HDAC mutants

A)

Modification	Stoichiometry (%) ± SD				
	WT	*clr6-1*	*clr3Δ*	*sir2Δ*	*hos2Δ*
H3K9ac	2.34 ± 0.17	10.30 ± 1.47	2.98 ± 0.09	3.26 ± 0.25	9.48 ± 1.04
H3K14ac	14.46 ± 2.18	44.92 ± 3.50	16.84 ± 3.09	13.34 ± 0.89	23.72 ± 1.53
H3K9me1	0.20 ± 0.01	0.29 ± 0.02	0.14 ± 0.05	0.12 ± 0.01	0.37 ± 0.04
H3K9me2	1.02 ± 0.06	3.04 ± 0.60	0.65 ± 0.18	0.63 ± 0.08	2.73 ± 0.62
H3K9me3	2.80 ± 0.30	5.77 ± 1.49	1.12 ± 0.13	1.53 ± 0.06	5.16 ± 0.04
H3K18ac	0.28 ± 0.04	1.61 ± 0.26	0.30 ± 0.03	0.39 ± 0.01	0.91 ± 0.18
H3K23ac	6.12 ± 0.81	20.84 ± 5.78	6.34 ± 0.10	5.06 ± 0.52	9.29 ± 1.21
H3K27ac	2.67 ± 0.10	14.14 ± 2.55	3.02 ± 0.55	1.82 ± 0.19	3.99 ± 0.37
H3K27me1	7.34 ± 0.38	9.64 ± 0.14	5.60 ± 0.12	5.08 ± 0.11	9.17 ± 0.51
H3K27me2	9.86 ± 0.48	15.07 ± 0.14	9.76 ± 0.37	10.80 ± 0.12	9.57 ± 0.18
H3K27me3	57.67 ± 0.11	52.90 ± 1.09	66.40 ± 0.55	70.19 ± 0.40	62.06 ± 1.00

B)

Modification	FC (ΔHDAC/Ctl) ± SD			
	clr6-1	*clr3Δ*	*sir2Δ*	*hos2Δ*
H3K9ac	4.43 ± 0.94	1.27 ± 0.05	1.39 ± 0.01	2.11 ± 0.38
H3K14ac	3.16 ± 0.72	1.19 ± 0.39	0.93 ± 0.08	1.09 ± 0.11
H3K9me1	1.43 ± 0.02	0.69 ± 0.26	0.60 ± 0.04	1.90 ± 0.29
H3K9me2	3.01 ± 0.76	0.65 ± 0.21	0.63 ± 0.11	2.90 ± 0.22
H3K9me3	2.04 ± 0.32	0.40 ± 0.01	0.55 ± 0.04	2.23 ± 0.54
H3K18ac	5.64 ± 0.12	1.09 ± 0.25	1.38 ± 0.23	0.86 ± 0.13
H3K23ac	3.50 ± 1.41	1.04 ± 0.12	0.84 ± 0.20	0.98 ± 0.20
H3K27ac	5.33 ± 1.16	1.13 ± 0.16	0.68 ± 0.05	1.02 ± 0.11
H3K27me1	1.32 ± 0.09	0.76 ± 0.06	0.69 ± 0.02	1.20 ± 0.19
H3K27me2	1.53 ± 0.09	0.99 ± 0.01	1.10 ± 0.04	1.07 ± 0.05
H3K27me3	0.92 ± 0.02	1.15 ± 0.01	1.22 ± 0.01	0.97 ± 0.03

A) Acetylation and methylation site stoichiometry of H3 lysine residues in WT and HDAC mutants. B) Fold change ratios of acetylation and methylation sites in the HDAC mutants relative to the control.

Continued, Table S5.3.

C)

PTM motfis	Stoichiometry (%) ± SD				
	WT	clr6-1	Δclr3	Δsir2	Δhos2
H3K9me2K14ac	0.15 ± 0.01	0.93 ± 0.05	0.37 ± 0.03	0.23 ± 0.01	0.90 ± 0.25
H3K9me3K14ac	0.65 ± 0.04	0.18 ± 0.05	0.56 ± 0.03	0.00 ± 0.00	0.38 ± 0.01
H3K9acK14pr	1.75 ± 0.16	2.44 ± 0.25	2.20 ± 0.02	2.30 ± 0.17	4.12 ± 0.02
H3K9prK14ac	13.50 ± 2.14	35.70 ± 2.34	15.06 ± 3.33	12.00 ± 0.73	17.23 ± 0.06
H3K9acK14ac	0.58 ± 0.00	7.90 ± 1.23	0.78 ± 0.11	0.96 ± 0.08	4.12 ± 1.73
H3K18acK23pr	0.22 ± 0.05	0.52 ± 0.08	0.23 ± 0.01	0.22 ± 0.01	0.53 ± 0.16
H3K18prK23ac	6.05 ± 0.80	19.75 ± 5.60	6.27 ± 0.08	4.90 ± 0.51	9.69 ± 1.12
H3K18acK23ac	0.07 ± 0.01	1.09 ± 0.17	0.08 ± 0.02	0.16 ± 0.00	0.46 ± 0.08
K27acK36pr	1.07 ± 0.06	3.06 ± 0.51	1.23 ± 0.05	0.74 ± 0.15	0.96 ± 0.06
K27acK36me1	0.46 ± 0.11	2.37 ± 0.44	0.54 ± 0.12	0.39 ± 0.04	0.73 ± 0.07
K27acK36me2	0.31 ± 0.03	2.05 ± 0.35	0.34 ± 0.09	0.17 ± 0.01	0.55 ± 0.08
K27acK36me3	0.83 ± 0.11	6.66 ± 1.25	0.92 ± 0.28	0.52 ± 0.07	1.49 ± 0.16

D)

H3 acetylation motifs	Log2 abundance FC (ΔHDAC/Ctl)			
	clr6-1	*clr3*Δ	sir2Δ	*hos2*Δ
K9me2K14ac	2.60	1.27	0.55	1.65
K9me3K14ac	1.87	2.10	0.33	0.88
K9acK14pr	0.42	0.30	0.38	0.54
K9prK14ac	1.34	0.07	-0.20	-0.11
K9acK14ac	3.71	0.44	0.73	1.48
K18acK23pr	1.27	0.10	0.07	-0.80
K18prK23ac	1.68	0.04	-0.32	-0.03
K18acK23ac	3.96	0.15	1.23	0.12
K27acK36un	1.49	0.20	-0.50	-0.38
K27acK36me1	2.39	0.30	-0.21	0.39
K27acK36me2	2.69	0.15	-0.90	0.07
K27acK36me3	2.95	0.16	-0.69	0.15

C) The stoichiometry of the individual acetylation and methylation PTM motifs

D) Log2 fold change of the normalized intensities of H3 acetylation motifs in the mutant compared to the control.

Table S3.6. Analysis of acetylation stoichiometry of H4 lysine residues in HDAC mutants

A)

Sample	Acetylation stoichiometry (%) ± SD			
	H4K5ac	H4K8ac	H4K12ac	H4K16ac
WT	13.13 ± 0.00	14.96 ± 0.00	19.00 ± 0.00	29.49 ± 0.00
clr3Δ	15.54 ± 1.75	12.94 ± 2.57	21.57 ± 1.76	25.26 ± 2.36
clr6-1	49.13 ± 0.83	45.85 ± 1.56	53.88 ± 0.37	46.59 ± 0.77
sir2Δ	16.91 ± 0.08	15.79 ± 0.47	23.19 ± 0.05	34.04 ± 0.58
hos2Δ	30.75 ± 1.74	35.34 ± 2.37	39.58 ± 2.27	67.67 ± 2.84

B)

Sample	FC (ΔHDAC/Ctl) ± SD			
	H4K5ac	H4K8ac	H4K12ac	H4K16ac
clr3Δ	1.10 ± 0.13	0.94 ± 0.17	1.14 ± 0.09	0.96 ± 0.08
clr6-1	3.74 ± 0.06	3.07 ± 0.10	2.84 ± 0.02	1.58 ± 0.03
sir2Δ	1.21 ± 0.01	1.06 ± 0.03	1.22 ± 0.00	1.15 ± 0.02
hos2Δ	1.98 ± 0.01	2.14 ± 0.04	1.80 ± 0.01	2.24 ± 0.00

A) The stoichiometry of acetylation for H4K5ac, H4K8ac, H4K12ac and H4K16ac in the wild-type and HDAC mutants.

B) Fold change of abundance for H4K5ac, H4K8ac, H4K12ac and H4K16ac in the mutant relative to the control.

Continued, Table S3.6.

C)

PTM motifs	Acetylation stoichiometry (%) ± SD				
	WT	clr6-1	Δclr3	Δsir2	Δhos2
H4K5_8_12_16pr	56.65 ± 0.15	22.23 ± 0.07	56.92 ± 3.24	51.17 ± 0.99	21.68 ± 2.40
H4K5ac	2.17 ± 0.25	3.63 ± 0.34	3.51 ± 0.36	2.57 ± 0.40	0.80 ± 0.25
H4K8ac	3.29 ± 0.16	3.77 ± 0.10	3.04 ± 0.13	2.99 ± 0.36	1.63 ± 0.17
H4K12ac	4.38 ± 0.13	4.85 ± 0.58	6.10 ± 0.48	5.64 ± 0.56	3.21 ± 0.39
H4K16ac	12.13 ± 0.81	5.75 ± 0.45	9.36 ± 0.65	13.29 ± 0.19	18.94 ± 0.81
H4K5_8ac	0.43 ± 0.14	3.07 ± 0.05	0.70 ± 0.06	0.50 ± 0.07	0.43 ± 0.04
H4K5_12ac	1.53 ± 0.14	5.11 ± 0.16	1.74 ± 0.17	1.40 ± 0.01	1.56 ± 0.12
H4K5_16ac	1.70 ± 0.27	2.36 ± 0.13	2.37 ± 0.45	2.14 ± 0.06	4.73 ± 0.27
H4K8_12ac	1.46 ± 0.00	3.36 ± 0.36	1.78 ± 0.60	0.86 ± 0.32	2.12 ± 0.14
H4K8_16ac	3.12 ± 0.24	1.75 ± 0.44	1.12 ± 0.41	2.31 ± 0.10	7.91 ± 0.70
H4K12_16ac	4.52 ± 0.09	4.74 ± 0.09	4.94 ± 0.13	4.96 ± 0.15	9.16 ± 1.22
H4K5_8_12ac	0.62 ± 0.1	7.39 ± 0.55	0.93 ± 0.04	0.84 ± 0.00	0.90 ± 0.01
H4K5_8_16ac	1.56 ± 0.08	3.56 ± 0.01	1.40 ± 0.32	1.84 ± 0.28	4.30 ± 0.00
H4K5_12_16ac	1.97 ± 0.02	5.48 ± 0.14	2.10 ± 0.29	3.05 ± 0.16	4.57 ± 0.13
H4K8_12_16ac	1.34 ± 0.14	4.41 ± 0.04	1.18 ± 0.05	1.86 ± 0.11	4.61 ± 0.09
H4K5_8_12_16ac	3.15 ± 0	18.54 ± 0.84	2.79 ± 0.97	4.59 ± 0.41	13.45 ± 1.67

D)

H4 acetylation motifs	Log2 abundance FC (ΔHDAC/Ctl)			
	clr6-1	*clr3Δ*	*sir2Δ*	*hos2Δ*
H4K5_8_12_16un	-1.26	0.09	-0.06	-1.28
H4K5ac	0.83	0.79	0.33	-1.82
H4K8ac	0.28	-0.03	-0.06	-1.02
H4K12ac	0.23	0.56	0.45	-0.93
H4K16ac	-0.99	-0.29	0.22	0.82
H4K5_8ac	2.93	0.81	0.31	-0.99
H4K5_12ac	1.83	0.28	-0.05	-0.12
H4K5_16ac	0.45	0.56	0.41	0.95
H4K8_12ac	1.28	0.39	-0.69	0.38
H4K8_16ac	-0.74	-1.37	-0.35	1.24
H4K12_16ac	0.15	0.22	0.22	0.86
H4K5_8_12ac	3.65	0.66	0.51	0.31
H4K5_8_16ac	1.28	-0.06	0.32	1.37
H4K5_12_16ac	1.56	0.18	0.72	1.39
H4K8_12_16ac	1.81	-0.09	0.57	1.47
H4K5_8_12_16ac	2.65	-0.08	0.63	1.93

C)Acetylation stoichiometry of the individual PTM motifs.

D) Log2 fold change ratios of the normalized intensities of acetylated isoforms of the H4 peptide 4-GKGGKGLGKGGAKR-17 in the mutant compared to the control.

Table S3.7. Analysis of the methylation levels of H3K9 and H3K36 in the HDAC mutants

A)

Modification	Methylation stoichiometry (%) ± SD				
	WT	*clr3Δ*	*clr6-1*	*sir2Δ*	*hos2Δ*
K9me1	0.20 ± 0.01	0.14 ± 0.03	0.29 ± 0.01	0.12 ± 0.00	0.34 ± 0.04
K9me2	1.02 ± 0.04	0.65 ± 0.13	3.05 ± 0.43	0.64 ± 0.06	3.18 ± 0.63
K9me3	2.80 ± 0.21	1.12 ± 0.09	5.77 ± 1.05	1.53 ± 0.04	5.15 ± 0.04
K36me1	7.34 ± 0.27	5.60 ± 0.08	9.64 ± 0.10	5.08 ± 0.08	8.81 ± 0.51
K36me2	9.86 ± 0.34	9.76 ± 0.26	15.07 ± 0.10	10.80 ± 0.09	9.70 ± 0.18
K36me3	57.67 ± 0.08	66.40 ± 0.39	52.90 ± 0.77	70.19 ± 0.28	62.77 ± 1.00

B)

Modification	Stoichiometry FC (ΔHDAC/Ctl) ± SD			
	clr3Δ	*clr6-1*	*sir2Δ*	*hos2Δ*
K9me1	0.69 ± 0.26	1.43 ± 0.02	0.60 ± 0.04	1.91 ± 0.29
K9me2	0.65 ± 0.21	3.01 ± 0.76	0.63 ± 0.11	2.91 ± 0.22
K9me3	0.40 ± 0.00	2.04 ± 0.32	0.55 ± 0.04	2.23 ± 0.54
K36me1	0.76 ± 0.06	1.32 ± 0.09	0.69 ± 0.02	1.20 ± 0.19
K36me2	0.99 ± 0.01	1.53 ± 0.09	1.10 ± 0.04	1.07 ± 0.05
K36me3	1.15 ± 0.01	0.92 ± 0.02	1.22 ± 0.01	0.97 ± 0.03

A) The stoichiometry of methylation for H3K9me1/me2/me3 and H3K36me1/me2/me3 in the wild-type and mutant samples.

B) Fold change ratios of abundance for H3K9me1/me2/me3 and H3K36 me1/me2/me3 in the mutant relative to the control.

Continued, Table S3.7.

C)

Motif Stochiometry	Stoichiometry (%) ± SD				
	WT	Δclr3	clr6-1	Δsir2	Δhos2
K9me1K14pr	0.20 ± 0.01	0.14 ± 0.05	0.29 ± 0.02	0.12 ± 0.00	0.34 ± 0.04
K9me2K14pr	0.86 ± 0.07	0.30 ± 0.08	2.13 ± 0.55	0.42 ± 0.04	2.27 ± 0.37
K9me3K14pr	2.63 ± 0.29	0.47 ± 0.09	5.22 ± 1.52	1.35 ± 0.00	4.75 ± 0.04
K9me2K14ac	0.15 ± 0.01	0.36 ± 0.10	0.93 ± 0.05	0.22 ± 0.05	0.90 ± 0.25
K9me3K14ac	0.15 ± 0.00	0.65 ± 0.04	0.56 ± 0.03	0.18 ± 0.05	0.38 ± 0.01
K27prK36me1	6.88 ± 0.48	5.06 ± 0.24	7.27 ± 0.29	4.69 ± 0.15	8.09 ± 0.44
K27prK36me2	9.55 ± 0.44	9.43 ± 0.27	13.03 ± 0.21	10.63 ± 0.11	9.15 ± 0.25
K27prK36me3	56.86 ± 0.03	65.51 ± 0.86	46.25 ± 0.14	69.70 ± 0.50	61.30 ± 1.13
K27acK36me1	0.46 ± 0.11	0.54 ± 0.12	2.38 ± 0.44	0.39 ± 0.04	0.73 ± 0.07
K27acK36me2	0.31 ± 0.03	0.34 ± 0.09	2.05 ± 0.36	0.17 ± 0.01	0.55 ± 0.08
K27acK36me3	0.83 ± 0.11	0.92 ± 0.28	6.66 ± 1.25	0.52 ± 0.07	1.49 ± 0.16

D)

H3 methylation motifs	Abundance FC (HDAC/Ctl)			
	clr3Δ	*clr6-1*	*sir2Δ*	*hos2Δ*
K9me1K14pr	0.69	1.43	0.60	1.58
K9me2K14pr	0.35	2.48	0.48	2.86
K9me3K14pr	0.18	1.95	0.51	2.26
K9me2K14ac	2.33	6.11	1.43	3.02
K9me3K14ac	4.26	3.69	1.20	1.93
K27prK36me1	0.74	1.06	0.68	1.19
K27prK36me2	0.99	1.36	1.11	1.07
K27prK36me3	1.15	0.81	1.23	0.97
K27acK36me1	1.24	5.24	0.87	1.35
K27acK36me2	1.08	6.73	0.54	1.07
K27acK36me3	1.08	8.17	0.62	1.12

C) Methylation stoichiometry of the individual PTM motifs

D) Log2 fold change of abundance for the normalized intensities of various H3 methylation motifs in the mutant compared to the control.

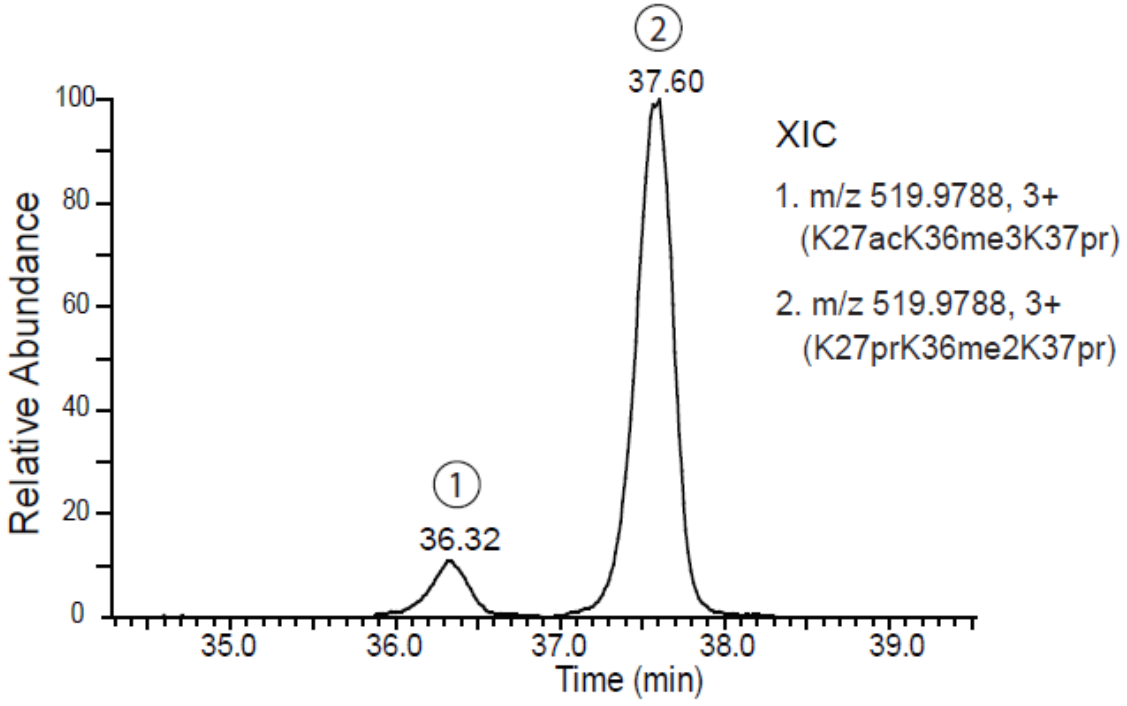

Figure S3.1. Representative ion chromatogram of separated isobaric peptides

Differentially modified isoforms of the peptide 27-KAAPATGGVKKPHR-40 (K27acK36meK37pr) and (K27prK36meK37pr) were chromatographically separated by the RP analytical column.

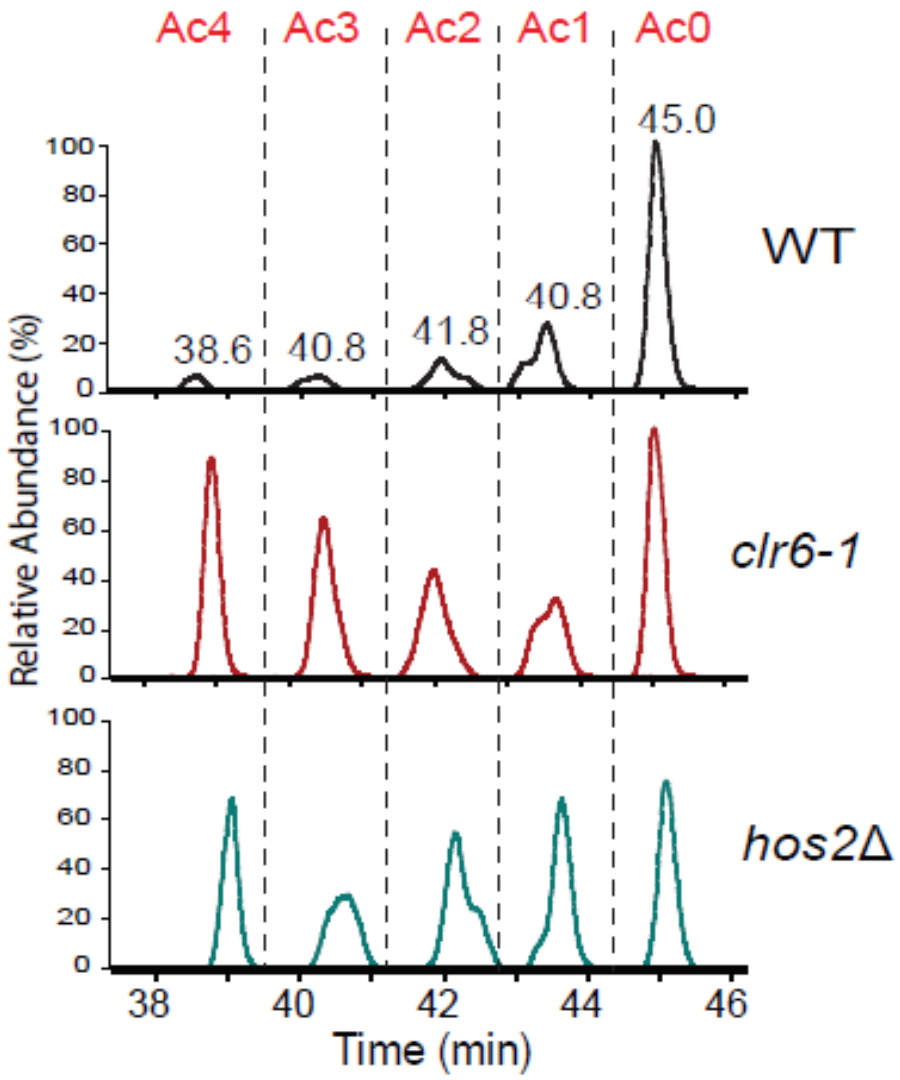

Figure S3.2. Analysis of global H4 acetylation in response to HDAC depletion

Representative extracted ion chromatograms illustrating the relative intensities of the five acetylated and non-acetylated isoforms of the H4 peptide in wild-type (top panel), *clr6-1* (middle panel) and *hos2Δ* (bottom panel) strains. The intensities of the chromatograms in each panel are normalized to the most abundant peak.

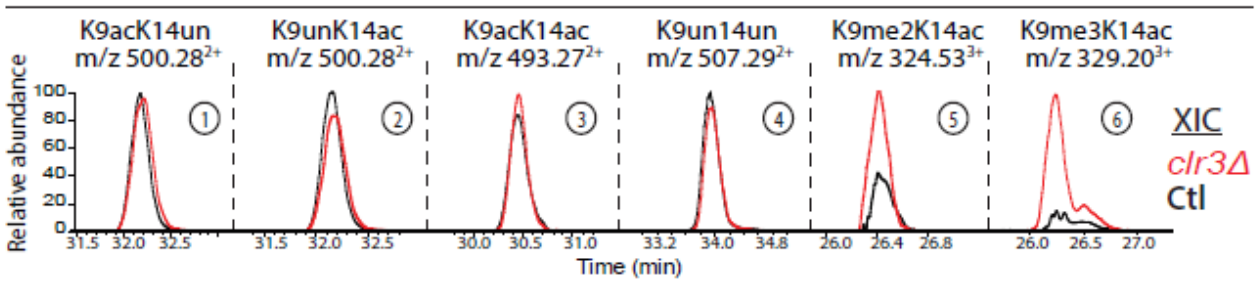

Figure S3.3. Analysis of the impact of the Clr3 mutation on the PTM isoforms of H3 peptide 9-KSTGGKAPR-17

Representative overlayed ion chromatograms (XIC) illustrating changes in the relative abundance of a non-modified (panel 4) and K14ac containing (panels 1-3 and 5-6) isoforms of the peptide 9-KSTGGKAPR-17 in *clr3Δ* mutant relative to the control. The y-axis in each XIC panel was scaled to the signal response of the most abundant peptide.

4. A novel evolutionarily conserved pattern of histone acetylation

Roshan Elizabeth Rajan*, Nebiyu Abshiru*, Charles Homsi,

Amogh Gopinathan Nair, Eric Bonneil, Pierre Thibault, Alain Verreault

*These authors contributed equally to this work

Nebiyu Abshiru carried out the proteomics analyses in Figure 1 and 3. Roshan Elizabeth Rajan prepared histone samples for Fig 1, constructed histone mutants, performed genetic analyses described in Figure 2 and 4, and prepared the first draft of the manuscript. Charles Homsi and Eric Bonneil performed MS analysis. Amogh Gopinathan Nair repeated the genetic analyses in Figure 4.

4.1. Abstract

Acetylation occurs both on the N-terminal tail domains and the core domains of histones. Here, we report the discovery of a novel pattern of histone acetylation that occurs on the N-terminal tail of H3. Using a novel quantitative mass spectrometry approach that we developed, we uncovered a strikingly abundant pattern of histone acetylation that is evolutionarily conserved. In fission yeast, fruit flies and humans, we discovered that H3 molecules at highly acetylated at lysines 14 and 23 with significantly lower levels of acetylation at lysines 18 and 23. We show that *Schizosaccharomyces pombe* mutant cells that cannot acetylate H3-K14 (*H3-K14R*) exhibit much more severe phenotypes than those that cannot acetylate H3-K23 (*H3-K23R*). Although this result suggests that H3-K14ac and K23ac may not participate in the same biological functions, this is not necessarily the case because we provide genetic evidence suggesting that the numerous severe phenotypes of the *H3-K14R* strain (sensitivity to a diverse group of chemicals that perturb either chromosome segregation or the DNA damage) are caused by mutation of the lysine, rather than a loss of H3-K14 acetylation. Our results highlight the difficulty of unambiguously assigning functions to modifications of specific histone lysine residues and provide a foundation to further studies aimed at determining the true functions of the abundant acetylation of H3-K14 and H3-K23.

4.2. Introduction

The genetic material of eukaryotes is organized into chromatin, the fundamental unit of which is the nucleosome core particle (NCP). Each NCP consists of 147 bp of DNA wrapped around an octameric protein core. The protein core is composed of two molecules each of four core histone proteins, H2A, H2B, H3 and H4 (Luger et al., 1997). Core histones have two structurally and functionally distinct domains, a globular domain, known as the histone-fold, and a conformationally flexible and highly charged amino-terminal domain, commonly known as the histone tail (Luger and Richmond, 1998). Even though chromatin efficiently packages the genetic material, it poses a significant obstacle to cellular processes that use a DNA template, such as DNA replication, transcription and DNA repair (Groth et al., 2007). Cells have evolved a number of mechanisms to regulate access to DNA. These include covalent modifications of histones, chromatin remodeling complexes that disrupt histone-DNA interactions, and replacement of canonical histones with specialized histone variants. Post-translational modifications (PTMs) of histones dynamically regulate chromatin structure and function.

Histone acetylation is, by far, the most extensively studied PTM. This reversible modification occurs on lysine residues and is catalyzed by two families of enzymes: histone acetyltransferases (HATs) and histone deacetylases (HDACs), which respectively catalyze the addition and removal of acetyl groups from lysine side chains (Marmorstein and Zhou, 2014). Acetylation neutralizes the positive charge of lysines and eliminates electrostatic interactions between those histone residues and DNA. In addition, acetylated lysines form docking platforms for bromodomain-

containing proteins that bind to acetylated lysine residues within specific structural contexts. Histone acetylation plays regulatory roles in diverse biological processes such as chromatin assembly, gene transcription and the DNA damage response (Shahbazian and Grunstein, 2007). However, assigning functions to site-specific histone acetylation has remained a daunting task for two reasons. First, many sites of acetylation in core histones have redundant functions. Second, histone acetyltransferases (HATs) and histone deacetylases (HDACs) modify a broad range of targets that include both histone and non-histone proteins (Glozak et al., 2005), thus complicating the inference of function from mutational studies.

Here we describe the identification of a pattern of acetylation that is evolutionarily conserved from yeast to humans. We found that two lysine residues of histone H3, K14 and K23, are highly acetylated in organisms that range from fission yeast to humans. We identified enzymes required for this acetylation *in vivo*. Mst2 for H3-K23 and both Mst2 and, to a lesser extent, Gcn5, for H3-K14 acetylation. We conducted genetic experiments to determine the function of H3K14 and H3K23 acetylation in the fission yeast *Schizosaccharomyces pombe*.

In the fission yeast *Schizosaccharomyces pombe*, we show that an *H3-K14R* strain mutant strain exhibits much more severe phenotypes than an *H3-K23R* mutant. Although this result suggests that H3-K14ac and K23ac may not participate in the same biological functions, this is not necessarily the case because we provide genetic evidence suggesting that the severe phenotypes of the *H3-K14R* strain (sensitivity to a diverse group of chemicals that perturb cells via different mechanisms) are caused by mutation of the lysine, rather than a loss of H3-K14 acetylation. Our results

highlight the difficulty of unambiguously assigning functions to modifications of specific histone lysine residues and provide a foundation to further studies aimed at determining the true functions of H3-K14ac and H3-K23ac.

4.3. Results

4.3.1. High stoichiometry of acetylation on histone H3-K14 and H3-K23

During DNA replication, duplication of DNA is accompanied by a transient genome-wide disruption of chromatin structure and concomitant histone synthesis. During replication, chromatin structure is rapidly re-established (within 100-200 base pairs behind the replication machinery (Smith and Whitehouse, 2012); onto nascent DNA duplexes. This is achieved through two distinct processes. Pre-existing histones, also known as parental histones, located ahead of replication forks are transferred onto the two nascent chromatids. This occurs concomitantly with the deposition of newly synthesized histones onto DNA, a process called replication-coupled nucleosome assembly (Verreault, 2000). Newly synthesized H3 and H4 are acetylated at multiple lysine residues prior to their genome-wide deposition onto nascent DNA. As a result, nucleosome assembly during DNA replication provides a very abundant source of acetylation. The most striking pattern of acetylation of new histones is the diacetylation of histone H4 at K5 and K12, which is evolutionarily conserved from yeast to humans. New H3 molecules are also acetylated, but early studies conducted by metabolic labeling with [^{3}H] acetate and Edman sequencing suggested that the pattern and sites of H3 acetylation are less conserved than those of new H4 molecules (Benson et al., 2006; Sobel et al., 1995). It is, therefore, possible that the

heterogeneity observed in different species may reflect the very low sensitivity of [^{3}H] acetate labeling Edman sequencing. For these reasons, we focused our study on the acetylation of H3 molecules.

There is evidence that new histones have to be deacetylated to promote the formation of mature chromatin onto newly replicated DNA, as measured by the acquisition of resistance to deoxyribonuclease (DNase) I that is typical of mature chromatin (Annunziato and Seale, 1983; Perry and Annunziato, 1989). Because of this, we were interested to determine whether clinically relevant HDAC inhibitors might exert some of their biological effects (Falkenberg and Johnstone, 2014; Marks and Xu, 2009) by interfering with chromatin maturation. Towards this goal, we sought to determine whether HDAC inhibitors enhance the acetylation of newly synthesized histones.

In an earlier study from our laboratory (Drogaris et al., 2012), we demonstrated that HDAC inhibitors cause a global increase in the acetylation of the N-terminal tails of H3 and H4, but we could not assess whether this increase in acetylation occurred in newly synthesized and/or pre-existing histones. To differentiate new histones from pre-existing histones, we used metabolic labeling with arginine containing heavy isotopes of carbon and nitrogen: [$^{13}C_6$,$^{15}N_4$] arginine (hArg). Metabolic labeling was combined with a quantitative mass spectrometry approach to determine the stoichiometries of acetylation on lysine residues in the N-terminal tail of H3. Following a pulse with hArg, two types of histones can be distinguished. The parental histones generate tryptic peptides that end in light arginine, whereas new histones produce tryptic peptides that end in hArg, giving a rise to mass difference of 10 Da that can be readily identified by mass spectrometry. Asynchronously growing HeLa cells were

exposed to short pulses (1 to 20 min) of hArg, washed, transferred to media containing light arginine and incubated for times for up to 24 hrs in the absence of hArg (Fig. 1A, schematic). Pulses as short of 3 min produced insufficient amounts of new histones labeled with hArg. Although some tryptic peptides in hArg were detected, this prevented us from accurately determining acetylation stoichiometries of new histones by mass spectrometry. Because of this, we chose a pulse of 20 min for our analyses. In adherent HEK293T cells, new H3 molecules containing hArg showed a remarkably high stoichiometry of lysine 14 and 23 acetylation (hereafter H3-K14ac and H3-K23ac). Even in the absence of chase with light Arg or HDAC inhibitor, 20-30% of H3 molecules were acetylated at K14 and K23 (time 0 in Fig. 4.1.A, bottom left and right-hand side panels). Those stoichiometries of acetylation increased as a function of time (Fig. 4.1.A, bottom left graph, 1h to 12h time points). Because the shortest pulse with hArg that we employed lasted 20min, and the delay from histone synthesis in the cytoplasm to their deposition onto nascent DNA has been estimated to be very short (Annunziato et al., 1982), we cannot distinguish between two non-mutually exclusive possibilities. First, it seems likely that a portion of the new H3 molecules that we detected by labeling cells with hArg were acetylated prior to their deposition into nascent chromatin. Alternatively, a fraction of the acetylation that we detected in hArg-labeled histones may have occurred after deposition of the new H3 molecules onto nascent DNA. Those two possibilities are obviously not mutually exclusive.

In addition to the acetylation of new H3 molecules, we observed high stoichiometries of H3-K14ac and K23ac (between 20 and 30%) in parental histones that contain light

Arg (Fig. 4.1.A bottom right panel). In contrast, H3-K9ac and K18ac were far less abundant than H3-K14ac and K23ac in both new histones and parental histones (Fig. 1A, left and right graphs). In adherent HeLa cells treated with SAHA (suberoyl anilide hydroxamic acid, also known as vorinostat), a potent inhibitor of class I, II and IV HDACs, there was a time-dependent increase in H3-K14ac and K23ac in both new and parental histones (supplementary Fig. 4.1.A). Continuous exposure to SAHA for up to 24h led to an increase in the stoichiometries of H3-K14ac and K23ac up to 60 to 80%, but this occurred to similar extents in both parental histones and new histones.

To determine whether the unexpectedly high stoichiometry of H3-K14ac and K23ac could be detected in cell lines other than HEK293T, we omitted the pulse-labeling step with hArg, and simply harvested asynchronously proliferating adherent HeLa cells. Interestingly, even in the absence of SAHA, 20-40% of all H3 molecules (a mixture of both parental and new histones) contained H3-K14ac and K23ac in HeLa cells (Fig. 4.1.B). This was also true for two cell lines grown in suspension: HuT78 and H9 (Supplementary Fig. 4.1.B). To determine whether high levels of H3-K14ac and H3-K23ac were also present in non-transformed cells, we first used the diploid cell line IMR90 (Fig. 4.1.C). In IMR90 cells, we observed a stoichiometry of H3-K14ac and H3-K23ac of roughly 15-20%, and considerably lower levels of H3-K9ac and H3-K18ac (Fig. 4.1.C). In addition, we isolated circulating peripheral blood mononuclear cells (PBMCs) from four healthy donors. These cells are quiescent when initially isolated, but they can be induced to proliferate *in vitro* using the mitogen phytohemagglutinin P (PHA-P) (Supplementary Fig. 4.1.C). On day 0 prior to the

addition of PHA-P, flow cytometry analysis for DNA content showed a single sharp peak corresponding to cells in the G0/G1 phase of the cell cycle (Supplementary Fig. 4.1.D, left-hand side panel). Following stimulation with PHA-P, a subset of PBMCs progressed through S-phase, but a significant portion of cells failed to re-enter the cell cycle as indicated by the persistence of the sharp peak of cells with DNA contents typical of G0/G1 cells (Supplementary Fig. 4.1.D, right-hand side panel). Populations of PBMCs before and after treatment with PHA-P showed similarly high stoichiometries of H3-K14ac and K23ac (20-40%) with considerably lower levels of H3-K9ac and K18ac (Fig. 4.1.D). This result clearly indicates that high stoichiometries of H3-K14ac and K23ac are detectable in PBMCs arrested in G0/G1. However, this does not rule out the possibility that a significant portion of H3-K14ac and K23ac in these G0/G1 cells may have initially arisen in new histones deposited throughout the genome during the round of DNA replication that preceded cell cycle arrest of PBMCs in G0 phase of the subsequent cell cycle. In order to assess the potential evolutionary conservation of the H3 acetylation pattern that we uncovered, we isolated histones from asynchronously proliferating *Drosophila* S2 cells and *Schizosaccharomyces pombe* cells. Interestingly, high stoichiometries of H3-K14ac and H3-K23ac (20-40%) and, consistent with earlier results, much lower levels of H3-K9ac and K18ac, were observed in both *Drosophila* S2 and *S. pombe* cells (Fig. 4.1.E).

4.3.2. Phenotypes of fission yeast cells that cannot acetylate H3-K14 or H3-K23

We sought to determine the functions of high levels H3-K14ac and K23ac using a genetically tractable model organism in which cells that express only mutant histones

can be generated. Since the pattern of acetylation that we identified was not obvious in budding yeast, we pursued our studies with the fission yeast *Schizosaccharomyces pombe*. Prior studies of H3-K14 mutant cells in fission yeast (Mellone et al., 2003; Wang et al., 2012) were helpful at the onset of our studies (see below). Using the elegant strategy described by Mellone and colleagues (Mellone et al., 2003), we generated isogenic *S. pombe* strains where the only source of histone H3 carries mutations of lysines into arginines at residues 14 and/or 23. We selected lysine-to-arginine mutations to preserve the positive charge of the lysines but prevent their acetylation. Mutants were backcrossed twice to a wild-type strain in order to minimize the probability that undesirable mutations influence the results of our phenotypic analyses. Despite the high abundance of H3-K23ac, *H3-K23R* mutant cells proliferated as rapidly as wild-type cells (Fig. 4.2.A, green and black curves). In striking contrast, the *H3-K14R* mutant proliferated considerably slower than wild-type cells (Fig. 4.2.A, pink and black curves) and the double mutant *H3-K14R K23R* proliferated even more slowly than the *H3-K14R* single mutant (Fig. 4.2.A, red and pink curves).

In *S. pombe*, and all the cell types in which we addressed this question, we found that histone H3-K9 is acetylated at a significantly lower level than H3-K14 (Fig. 4.1.). Nonetheless, we decided to compare the phenotypes of *H3-K9R* and *H3-K14R* mutants because a previous study had indicated that cells carrying mutations of either H3-K9 of H3-K14 shared a number of phenotypes related to pericentric heterochromatin (Mellone et al., 2003). Among others, these phenotypes included

sensitivity to thiabendazole, silencing defects of reporter genes integrated into pericentric heterochromatin and, consistent with this, dissociation of Swi6 from pericentric heterochromatin (Mellone et al., 2003). *S. pombe* Swi6 is a functional and structural homolog of heterochromatin binding protein 1 (HP1). All these phenotypes of *H3-K9R* mutant cells have been attributed to a lack of H3-K9 methylation. This modification is needed to anchor Swi6/HP1 to pericentric heterochromatin which, in turn, is important to maintain the integrity of pericentric heterochromatin and, as result, faithful mitotic chromosome segregation (Mellone et al., 2003). Consistent with the above, we found that *H3-K9R* and *H3-K14R* mutants were both very sensitive to the microtubule-depolymerizing agent thiabendazole (TBZ) (Fig. 4.2.D). There is currently no evidence that H3-K14 is methylated. Structures of Swi6/HP1 bound to peptides spanning methylated H3-K9 indicate that the chromodomain of HP1 makes contacts mainly with the four amino acids preceding H3-K9 (Nielsen et al., 2002). Therefore, the reason why *H3-K14R* and *H3-K9R* mutant cells share a number of pericentric heterochromatin defects is far from obvious. One possibility that would account for these observations may be that the *H3-K14R* mutation somehow results in a loss of H3-K9 methylation, but we do not have any evidence that this is the case. Given the high abundance of both H3-K14ac and H3-K23ac, it seemed possible that acetylation of both residues may create a doubly acetylated surface (DAS) whose recognition by effector proteins was abolished by mutation of either H3-K14 or H3-K23. However, the fact that *H3-K23R* mutant cells do not exhibit any proliferation defect (Fig. 4.2.A) or TBZ sensitivity argues against an H3-K14ac and K23ac DAS being necessary to achieve wild-type rates of proliferation or resistance to TBZ.

A previous study showed that cells lacking H3-K14 acetylation due to lysine 14 to arginine mutation (H3K14R), are sensitive to many DNA damage-inducing agents (Wang et al 2012). We assayed the sensitivities of our histone mutants to a number of genotoxic agents that cause different types of DNA lesions: hydroxyurea (HU), an inhibitor of ribonucleotide reductase that depletes deoxyribonucleotides and results in replication fork stalling, methyl methane sulfonate (MMS), an agent that alkylates adenine to produce 3-methyladenine, a lesion that block replicative DNA polymerases, and camptothecin (CPT), a DNA topoisomerase 1 inhibitor that causes DNA single- and double-strand breaks. Our *H3-K23R* mutant strain was not sensitive to MMS or hydroxyurea and showed only modest sensitivity to camptothecin. In striking contrast, *H3-K14R* mutant cells were sensitive to all the drugs tested (Fig. 4.2.C). The plate assays with histone mutants showed that the sensitivity of *H3-K14R K23R* mutant to DNA damaging agents was comparable to that of the *H3-K14R* mutant. However, real-time monitoring of mutants grown in liquid media containing the appropriate drugs revealed that the double mutant has increased sensitivity compared to *H3-K14R*. (Supplementary Fig. 4.2.).

We tested whether any of the histone mutants were sensitive to salt stress conditions. *H3-K23R* was not sensitive to salt stress. *H3-K14R* and *H3-K14R K23R* showed comparable salt sensitivity suggesting that H3-K23 does not contribute to the salt stress response (Fig. 4.2.E). We also tested the histone mutants for their sensitivity to inhibitors of several cellular processes. *H3-K23R* was not sensitive to thiabendazole (TBZ, microtubule poison), mycophenolic acid (MPA, inhibitor of transcriptional elongation), brefeldin A (inhibits protein transport from the

endoplasmic reticulum to the Golgi), caffeine (DNA damage response kinase inhibitor) and formamide (a protein denaturing agent) (Figures 4.2.D and 4.2.F). The *H3-K14R* single mutant and the double mutant were highly sensitive to MPA, TBZ, caffeine and formamide, suggesting that H3 lysine 14 has diverse functions, unlike H3 lysine 23.

4.3.3. Mst2 and Gcn5 contribute to H3-K14 and H3-K23 acetylation

We sought to identify the enzymes that acetylate H3-K14 and H3-K23. Mst2, an MYST family acetyltransferase has been shown to be an H3-K14 specific HAT in *S. pombe* (Wang et al JBC 2012). Mst2 has been assigned as the fission yeast orthologue of *S. cerevisiae* Sas2 though it is phylogenetically related also to *Sc*Sas3, the catalytic subunit of NuA3, which acetylates H3-K14 and H3-K23. In addition to Mst2, Gcn5 has also been shown to contribute to H3-K14 acetylation in *S. pombe* (Nugent et al. 2010., Wang et al 2012). In addition, there is some evidence that Mst2 also acetylate H3-K23 (Wang et al., 2012, Fig. 2C). However, the authors failed to notice the contribution of Mst2 to H3-K23 acetylation. We took these two candidate HATs to test whether they contribute to acetylation of H3-K14 and K23. Unlike previous studies that relied on acetylation site-specific antibodies, we employed a quantitative mass spectrometry method (Abshiru et al. 2015) to profile changes in acetylation in cells that lack Mst2 and/or Gcn5. For each lysine on the N-terminal tails of H3 and H4, we determined the fold-change ratios of acetylation abundance in mutants compared to the wild-type. We discovered that Mst2 is the major acetyltransferase that contributes to both H3-K14 and H3-K23 acetylation. In cells lacking Mst2, the relative abundance of H3-K23 acetylation was reduced by four-fold

(Fig. 4.3.A, 4.3.B). We also found that Gcn5 acetylates H3-K23. To the best of our knowledge, this is the first report of an H3-K23 acetyltransferase in *S. pombe*.

H3-K14 acetylation was also significantly reduced in cells lacking Mst2. The most dramatic change was observed when this mark co-exists with a tri-methylated K9 in the motif K9me3K14ac, which decreased 4-fold in the Mst2 mutant (Supplementary Fig 4.3.A). Trimethylated H3K9 is a hallmark of heterochromatin, which includes pericentromeric, sub-telomeric regions and mating-type loci in *S. pombe* (Grewal and Jia, 2007). Previous studies have shown that loss of Mst2 bypasses the requirement of RNAi pathway for the assembly pericentric heterochromatin (Reddy et al., 2011). Moreover, loss of Mst2 strengthens telomeric silencing (Gomez et al., 2005). Our results strengthen the understanding that Mst2 complex antagonizes heterochromatic silencing.

In cells lacking Gcn5, acetylation of H3-K9 and H3-K18 were greatly affected (Fig. 4.3.A). Loss of Gcn5 also caused a decrease in H3-K27 acetylation (Fig. 4.3.A). Loss of Gcn5 has been shown to affect H3 acetylation on lysines 9, 18, 23 and 27 in budding yeast (Suka et al., 2001). In *S. cerevisiae*, Rtt109 and Gcn5 contribute to H3-K27 acetylation and this is shown to be important for replication-dependent nucleosome assembly (Burgess et al., 2010). However, contrary to previous reports, we did not see a decrease in H3-K14ac in the Gcn5 mutant (Fig. 4.3.A, 4.3.B and Supplementary Fig. 4.3.A). To examine this observation in more detail, we extracted ion chromatograms (XICs) representing the acetylated and non-acetylated forms of the H3 peptide $_{9}$-KSTGGKAPR-$_{17}$. Raw LC-MS data of samples from Gcn5-deficient and wild-type cells were used. The overlayed XIC peaks (Δ*gcn5*/control) for four

peptides that are acetylated at K9, K14, or both, and a non-acetylated form of the same peptide, are illustrated in Fig. 4.3.C. The y-axis in each XIC panel was scaled to the signal corresponding to the most abundant peptide. Based on this analysis, we saw a reduction in H3-K14ac in cells lacking Gcn5, but only when this mark occurs with H3-K9ac. This motif (H3K9acK14ac), however, represents only 1% of the total population of H3 peptides detected with the same sequence. Interestingly, the mono-acetylated motif K9un K14ac (Fig. 4.3.B), which corresponds to 30% of the peptides with the above sequence, did not show any significant change in abundance in cells lacking Gcn5. It is known that both H3-K9 acetylation and H3-K14 acetylation co-occur at some promoters and facilitate transcriptional activation in budding yeast and human cells (Karmodiya et al., 2012; Pokholok et al., 2005; Wang et al., 2008). However, in fission yeast, levels of H3-K14ac do not show any correlation with gene expression (Sinha et al., 2006, 2010).

In cells lacking both Gcn5 and Mst2, the degrees of acetylation at all the five H3 sites were significantly reduced (Fig. 4.3.A, 4.3.B). The changes were more dramatic for the di-acetylated motifs H3-K9ac K14ac and H3-K18ac K23ac (Supplementary Fig. 4.3.A), which were barely detected in the MS data.

We then assessed the importance of Mst2 and Gcn5 for acetylation of four histone H4 sites, K5, K8, K12 and K16. The absence of Gcn5 and/or Mst2 did not affect the degree of acetylation of these H4 lysine residues. An earlier report by Wang and colleagues showed using fluorography of tritiated acetyl-CoA that purified Mst2 has no acetyltransferase activity towards nucleosomal H4 (Wang et al., 2012). We only observed a modest change in the abundance of PTM motifs for example, up to a 2-

fold decrease in H4-K5ac in the Δ*gcn5* or Δ*mst2* single mutants and about 2-fold decrease in K8ac K16ac in the double mutant (Fig. 4.3.C, 4.3.D and Supplementary Fig. 4.3.B).

We previously reported that Clr6, and to a lesser extent Hos2, were required *in vivo* for deacetylation of H3-K14 and H3-K23 associated with euchromatin (Abshiru et al 2016). Cells lacking Clr3 and Sir2, on the other hand, showed an increase in H3-K14ac only when it is present with a dimethylated or trimethylated H3-K9, suggesting that these two enzymes selectively remove K14 acetylation from H3 molecules present in heterochromatin (a hallmark of which is the presence of H3-K9 methylation).

4.3.4. The phenotypes of Δ*mst2* and H3-K14R mutant cells are not equivalent

The phenotypes of the *H3-K14R* and *H3-K23R* mutants did not show much overlap suggesting that they act in distinct cellular processes. In striking contrast to the H3-K23R mutants, *H3-K14R* mutant cells exhibited many severe phenotypes. To establish that the phenotypes that we observe for *H3-K14R* and *H3-K23R* strains are, at least in part, due to a lack of acetylation, rather than a change in the identity of the amino acid, we deleted *mst2*$^{+}$, the major acetyltransferase for H3-K14 and H3-K23. We did not delete *gcn5*$^{+}$ for two reasons: first, the contribution of Gcn5 to H3-K14 acetylation was minimal (Fig. 4.3.A) and that to H3-K23 acetylation was about twenty percent. Second, Gcn5 has both histone and non-histone substrates. We reasoned that deleting Gcn5 would generate phenotypes which need not necessarily be due to the lack of acetylation on H3-K14 and K23. Moreover, loss of Mst2, rather than that

of Gcn5, rescued heterochromatin formation in mutants where the RNA interference machinery was disabled. This rescue of heterochromatin function is thought to arise from reduced histone H3-K14 acetylation in ∆*mst2* cells (Reddy et al., 2011). Gcn5 is also the catalytic subunit of the SAGA complex, an evolutionarily conserved multi-subunit complex that acts as a transcriptional coactivator. Loss of Gcn5 thus can probably alter the expression of many genes which could indirectly contribute to the phenotypes that we are studying. Our results showed that deleting *mst2*$^{+}$ in wild-type cells results in very low levels of acetylation on H3-K14 and H3-K23 (Fig. 4.3.A). We made three acetyltransferase mutants: *H3-WT* ∆*mst2, H3-K14R* ∆*mst2 and H3-K23R* ∆*mst2*. These mutant strains retained only one copy of histone genes as described previously. In *H3-K14R* ∆*mst2* and *H3-K23R* ∆*mst2* mutants, in addition to the identity of the lysine being altered, the acetylation of K23 and K14 would be reduced four-fold, respectively.

We assayed the proliferation of HAT mutants (Figures 4.4.A and 4.4.B), the sensitivity of mutants to DNA damaging agents such as hydroxyurea, MMS and CPT (Fig. 4C). We also compared the growth of mutants in the presence of microtubule poison thiabendazole (TBZ) (Fig. 4.4.D). The mutants were also tested for their sensitivity to formamide, mycophenolic acid, caffeine and brefeldin A (Fig. 4.4.E). We also assessed the sensitivity of cells lacking Mst2 to salt stress (Supplementary Fig. 4.4.A). We did not find the *H3-WT Δmst2* and *H3-K23R Δmst2* cells to be more sensitive compared to *H3-WT* and *H3-K23R* in any of the conditions tested. The *H3-K14R* and *H3-K14RΔmst2* strains, however, showed comparable phenotypes which we reckon is due to the lysine to arginine mutation at position 14. There were subtle

differences in sensitivities of *H3-WT Δmst2* and *H3-K23R Δmst2.* These were evident only when strains were grown in liquid media containing the drugs were monitored real-time. To summarize, our results show that it is the loss of lysine rather than the loss of acetylation that is resulted in severe phenotypes of the *H3-K14R* mutant.

4.4. Discussion

Lysine acetylation of histones is a well-studied post-translational modification which plays important cellular roles. However, the redundancy of modifying enzymes and plethora of non-histone substrates make it difficult to ascribe specific functions to site-specific acetylation. Here we describe the identification of an unprecedented pattern of histone H3 N-terminal tail acetylation that is evolutionarily conserved from yeast to humans. We observe high stoichiometry of acetylation at H3-K14 and H3-K23 and much less abundant acetylation at H3-K9 and H3-K18. The stoichiometry of acetylation on H3-14 and H3-K23 (20-40%) that we found suggests that, at least in some genomic regions, on average, roughly one in every two nucleosomes contains an H3 molecule with K14 and/or K23 acetylation. Despite high levels of acetylation, the *H3-K23R* mutant had only a few modest phenotypes (Fig. 4.2. and Supplementary Fig. 4.2.). The *H3-K14R* mutant, on the other hand, exhibited very strong phenotypes. Previously, histone mutants have been shown to phenocopy the loss of a modifying enzyme (Moazed, 2013; Pengelly et al., 2013). Strikingly, this was not the case with the histone mutants that we studied. The lysine 14 to arginine mutation has more severe phenotypes than the loss of *mst2*, the major acetyltransferase for H3-K14 and K23 (Fig. 4.4. and Supplementary Fig. 4.4.). This could probably be because the

residual level of acetylation contributed by Gcn5, in cells lacking Mst2, might be sufficient to drive cellular functions. However, figure 4.3.B shows that loss of Gcn5 decreased the abundance of a small fraction of H3-K14 acetylated peptides (about 1%), which were also acetylated on K9.

We surmise that the numerous strong phenotypes of the *H3-K14R* mutant are primarily due to the fact that a non-modified lysine was changed into an arginine. It is well established that readers recognize and bind to modified residues. By altering the identity of the amino acid, the binding surface for modifying enzymes and/or readers may have been changed for the amino acid or for any of its neighboring residues. For example, H3 lysine 14 to arginine mutation abolished Swi6 recruitment and silencing at pericentric heterochromatin regions (Mellone et al., 2003) but this effect could not be reproduced by abrogating H3K14ac through inactivation of both Gcn5 and Mst2 (Reddy et al., 2011). Even though structural studies have shown that the Swi6 counterpart HP1 does not make any direct contacts with H3-K14 (Jacobs et al., 2001; Nielsen et al., 2002), mutating this residue causes of delocalization of Swi6. Consistent with this, we find that at least some of the strong phenotypes (sensitivity to MMS, CPT, HU, TBZ, mycophenolic acid, caffeine and formamide) of *H3-K14R* mutants are also observed in *H3-K9R* mutants (Fig. 4.2. and Supplementary Fig. 4.2.). In addition, the H3K14R mutation could, in principle, affect the acetylation of H3-K9 because the residues flanking the target lysine are important for determining the substrate selectivity and substrate affinity of Gcn5 N-acetyltransferases (Poux and Marmorstein, 2003).

In addition to acetylation, lysine residues can also be modified by methylation, sumoylation, ubiquitination and short-chain acylation. High-sensitivity mass spectrometry methods have successfully generated an immense and growing catalog of histone modifications, particularly short chain lysine acylations, which are different from acetylation in hydrocarbon chain length, or charge (Nature Reviews Molecular Cell Biology 18, 90–101 2017). These include propionylation (Kpr), butyrylation (Kbu), 2-hydroxyisobutyrylation (Khib), succinylation (Ksucc), malonylation (Kma), glutarylation (Kglu), crotonylation (Kcr) and β-hydroxybutyrylation (Kbhb). We did not look for these modifications in our analysis for the following reasons. A dedicated assay is required to identify them and calculate their abundance. Acyls of coenzyme A (Acyl-CoA) other than acetyl-coA have been implicated in a number of cellular functions such as fatty acid biosynthesis and in the citric acid cycle. They are very abundant in the cell and are highly reactive like acetyl-coenzyme A. One could argue that it is the loss of one of these modifications, rather than the loss of acetylation, that gave rise to the strong phenotypes of the *H3-K14R* mutant. However, there has not been any reports of an enzyme (writer) for acylations in *S. pombe*. It is not yet known if any of the *S. pombe* effector (reader) proteins would preferentially read an acylation as opposed to an acetylation.

We identified a pattern of acetylation, high abundance of acetylation at H3-K14 and H3-K23 and low acetylation at H3-K19 and H3-K18. However, it was not possible to study the role of H3-K14ac with an H3-K14R mutation (or a *Δmst2* single mutation because of the residual H3-K14ac catalyzed by Gcn5). So, mutating histone residues and the major acetyltransferase responsible for the pattern of acetylation that we

identified did not help us to discover the function(s) of H3-K14 and H3-K23 acetylation. We believe that an indirect approach would help us come closer to defining the functions of H3-K14 acetylation and H3-K23 acetylation. This approach requires finding answers to three questions about the pattern of acetylation that we discovered: 1) 'Where' in the genome are very high levels H3-K14 and H3-23 acetylation occur? 2) It would also be informative to determine 'when' high stoichiometries of H3-K14 and H3-K23 acetylation are found in the cell. We have preliminary results which point to that new histones prior to deposition on chromatin have a very high stoichiometry of acetylation (Abshiru et al., 2015). Recent structural studies of karyopherin Kap123, the most abundant karyopherin in budding yeast, which transports histones H3 and H4 by recognizing their nuclear localization signal (NLS), identified that there are two lysine binding pockets in Kap123. These lysine binding regions bind to H3-K14 and H3-K23 respectively and are important for the affinity of histones to karyopherin. Mutation of lysines 14 and 23 to alanine or glutamine reduced the affinity of histones to karyopherin *in vitro*, by four-fold (An et al., 2017; Blackwell et al., 2007). It is plausible that one of the functions of an evolutionarily-conserved pattern of H3-K14 acetylation and H3-K23 acetylation is to release H3-H4 from the import factors. This might explain the high stoichiometry of acetylation on histones bound to CAF-1 (Abshiru et al., 2015). 3) Another important question is 'how' this pattern of acetylation occurs in cells. We have been able to partially address this question by identifying the histone acetyltransferases that are responsible for H3-K14 and H3-K23 acetylation *in vivo*. Our previous results allude to Clr6 being the HDAC responsible for deacetylating H3-K14ac and H3-K23ac in the

euchromatic regions (Abshiru et al., 2016). We believe systematically addressing ‘where’, ‘when’ and ‘how’ these modifications occur in the genome, will be helpful in deducing the function(s) of H3-K14ac and H3-K23ac.

4.5. Materials and Methods

4.5.1. Cell culture and SILAC labeling

HeLa, HEK 293T and IMR90 cells were grown in DMEM (Gibco) supplemented with 10% FBS (Wisent) and 1% penicillin/streptomycin. Hut78, H9 and human PBMCs were grown in RPMI-1640 supplemented with 10% FBS (Wisent) and 1% penicillin/streptomycin. All cells were maintained in a 37°C incubator with a humidified atmosphere of 5% CO_2. For SILAC labeling, cells grown in DMEM to 70-80% confluency were transferred to SILAC-DMEM, supplemented with 10% dialyzed FBS and 1% penicillin/streptomycin. The SILAC-DMEM was supplemented with light lysine and light or heavy arginine. SILAC amino acids were prepared as 1000X stock solutions, lysine 146 mg ml^{-1} and arginine 84 mg ml^{-1}, in phosphate buffered saline (PBS), filtered and stored at 4°C for up to 6 months. For pulse-chase experiments, cells were grown in SILAC-DMEM without lysine or arginine for 24h, washed twice with PBS and SILAC DMEM containing light lysine and heavy arginine were added for 20 minutes. After 20 minutes, the cells were washed with PBS, cells were fed with SILAC-DMEM supplemented with light lysine and light arginine for up to 24 h. For treatment with SAHA, asynchronously growing cells were treated with 1 μM of SAHA for up to 24 h. After treatment, the cells were collected, centrifuged at 1,000 r.p.m. at room temperature, washed with PBS, and flash frozen in liquid nitrogen. Control cells

were treated with DMSO. Two biological replicates were prepared for each condition and each experiment was repeated a minimum of two times.

4.5.2. Isolation and in-vitro proliferation of peripheral blood mononuclear cells (PBMCs)

Human PBMCs for *in-vitro* proliferation were isolated from venous blood samples by density gradient centrifugation method using Ficoll-Histopaque as previously described (Panda et al., 2012). About 10 ml of blood from four donors were collected in EDTA-coated vacutainers (BD). Ficoll was layered (1:3 v/v ficoll to blood) on blood samples diluted with an equal volume of PBS in a 50 ml falcon tube and the tubes were centrifuged at 1500 r.p.m for 30 min at room temperature with the brake 'OFF'. The whitish layer, 'buffy coat', containing PBMCs was gently aspirated and transferred aseptically into sterile centrifuge tubes. The suspension of cells was washed twice with PBS and resuspended in RPMI-1640. The cells were counted using a hemocytometer and $5x10^6$ cells were cultured in RPMI-1640 supplemented with 20% FBS, 1% Penicillin/Streptomycin and 5 µg/ml phytohemagglutinin-P (PHA-P) for 72 hrs at 37°C in a humidified CO_2 incubator. $2x10^6$ cells from 'day 0' and 'day 3' were used for isolation of histones and $1x10^6$ cells were used for cell cycle analysis.

4.5.3. Cell cycle analysis by flow cytometry

$1x10^6$ cells were collected, washed in PBS, fixed in ice-cold 70% ethanol diluted in PBS and stored at -20°C until the day of analysis. To detect DNA, cells were stained with propidium iodide (200 µl from a 50 µg/ml stock in PBS supplemented with 50 µl

of 250 µg/ml RNase A) for 1 h at 37°C. Stained cells were analyzed by flow cytometry on a BD FACSCanto. Data were analyzed and processed by ModFit.

4.5.4. Yeast strains and media

The *S. pombe* strains used in this study are listed in Table S-1. Strains were grown and maintained in YE5S medium (yeast extract supplemented with 5 amino acids) at 30°C using standard techniques (Forsburg and Rhind, 2006). Matings were performed on malt extract agar plates for 2–3 days at 25°C. Transformations were carried out by electroporation and lithium acetate/dimethyl sulfoxide(DMSO) methods (Murray et al., 2016).

4.5.5. Construction of histone and HAT mutants

The histone mutants (*H3-WT*, *H3-K14R*, *H3-K23R* and *H3-K14R K23R*) were made as described previously (Mellone et al., 2003). Briefly, two overlapping PCR products encompassing the 5' and 3' ends of the histone gene, with overlap in the region bearing the mutation were generated using genomic DNA from a wild-type strain (AVP01). The PCR products were gel purified, mixed together in equal amount, and used as template in a third PCR in which the two external primers were used to amplify the entire *h3.2* locus and generate a mutated *h3.2* gene. The PCR fragments were introduced into a strain containing *h3.2Δ::ura4*$^{+}$ by electroporation. Cells were grown overnight at 25°C in liquid medium and plated on YES Agar containing 5-FOA, which is toxic to *ura4*$^{+}$ cells. Transformants were checked by PCR to ensure proper integration and loss of the *ura4*$^{+}$ gene. Mutated histone *h3.2* was sequenced to

confirm the incorporation of the mutation. The *h3.2* mutants were crossed with a strain bearing the *ura4*$^{+}$ gene inserted immediately downstream of the *h4.2* gene to mark a wild-type h3.2/h4.2 gene pair and lacking the two remaining histone gene pairs (*h3.2/h4.2Δ:: ura4*$^{+}$ *h3.1/ h4.1Δ::his3*$^{+}$ *h3.3/h4.4Δ::arg3*$^{+}$, FY4640). Progeny were plated on medium containing 5-FOA and lacking arginine and histidine to select for mutated histone *h3.2* as the only source of histones H3. Yeast strains containing deletions of Mst2 were constructed using a PCR-based module method as described previously (Chen et al., 2015).

4.5.6. Drug sensitivity assays

S. pombe strains were grown to mid-logarithmic phase, serially diluted 10-fold and 5 µl aliquots were spotted onto YES plates containing 0.005% methyl methane sulphonate (MMS), 2-16 µM camptothecin (CPT), 2.5-10 mM hydroxyurea (HU), 10 µg/ml thiabendazole (TBZ), benomyl, 25 µM mycophenolic acid, 2% v/v formamide, 10 mM caffeine, 10 µg ml^{-1} brefeldin A, 0.2 M sodium chloride, 0.1 M calcium chloride and 1.0 M potassium chloride. Plates were incubated at 30 °C for 3–5 days and photographed. All assays were repeated a minimum of two times.

4.5.7. Histone isolation

Histones from cultured mammalian and *Drosophila* cells were isolated using acid extraction as previously described (Shechter et al., 2007). Briefly, nuclei from 10^7 cells were isolated with a hypotonic lysis buffer, followed by histone extraction using 0.2M H_2SO_4 and TCA precipitation. The concentration of histone samples was

determined by Micro-BCA assay (Pierce). Histones from *S. pombe* were extracted by adapting a protocol used for acid extraction of histones from budding yeast (Guillemette et al., 2011). By starting from saturated overnight cultures, strains were grown at 25 °C in 400 mL of YE5S medium until they reached $O.D_{595}$ 1.0−1.5. Cells were harvested and washed sequentially with 100 mL of water, 25 mL of DTT buffer (0.1 M Tris-HCl pH 9.5, 10 mM DTT), and 25 mL of Spheroplasting buffer (20 mM HEPES (NaOH) pH 7.4, 1.2 M Sorbitol). The wet cell pellets were weighed, resuspended in 12.5 mL of Spheroplasting buffer containing Zymolyase 100T (5 mg/g of cell pellet), and incubated at 30 °C until digestion was 90−95% complete. The extent of digestion was monitored by measuring absorbance at 600 nm using 1% w/v sodium dodecyl sulfate (SDS) solution. An aliquot of cells before addition of Zymolyase was used as a control. The pellets were gently resuspended in nuclear isolation buffer (NIB) (15 mM 2-(N-morpholino) ethanesulfonic acid (KOH) pH 6.6, 60 mM KCl, 15 mM NaCl, 5 mM MgCl2, 1 mM CaCl2, 0.25 M sucrose, 0.8% v/v Triton X-100, 1 mM PMSF). The NIB wash was repeated twice followed by Wash “A” (10 mM Tris-HCl pH 8.0, 75 mM NaCl, 0.5% v/v NP 40, 30 mM NaButyrate, 1 mM PMSF) and Wash “B” (10 mM Tris-HCl pH 8.0, 0.4 M NaCl, 30 mM NaButyrate,1 mM PMSF). The nuclear pellet was resuspended in 0.25 M HCl for 15 min, which extracts histones and other acid-soluble proteins. Trichloroacetic acid (TCA) was added to a final concentration of 20% v/v to the supernatant that contains histones. The histone pellet was washed with acetone, air-dried, and resuspended in water for offline purification of intact histones by reverse-phase high-performance liquid chromatography (RP-HPLC). Centrifugation for cell harvesting and steps until Wash B were done at 3000

rpm for 10 min at 4 °C. Histone extraction and final washes were done at 12 000 rpm for 10 min at 4 °C. Further purification of core histones was performed by reverse-phase HPLC.

4.5.8. Histone Fractionation by RP-HPLC

Bulk histones from both wild-type and mutant strains were fractionated into individual core histones using an Agilent narrow-bore Zorbax C8 reverse-phase column (2.1 × 150 mm2, 5 μm, 300 Å) on an Agilent 1200 HPLC system. Approximately 5 μg of bulk histones from each sample was loaded onto the C8 column at a flow rate of 150 μL/min. Histones were eluted from the column using a gradient of 5−80% aqueous acetonitrile (0.1% TFA) in 60 min. Fractions were collected in a 96-well plate every 30 s. Fractions containing histones H3 or H4 were pooled and dried in a SpeedVac concentrator.

4.5.9. Propionylation and Tryptic Digestion of Histone Proteins

In solution tryptic digestion of core histones was performed as previously described (Abshiru et al., 2013). Briefly, a total of 2 μg of the HPLC- purified histones H3 and H4 were subjected to two rounds of propionylation by adding 200 μL of freshly prepared 2:1 (v/v) water/propionic anhydride (Sigma) mixture and vortexing the mixture for 30 min at room temperature. After each propionylation reaction, the samples were dried completely in a SpeedVac at 4 °C. To remove trace amounts of propionic anhydride left in the samples, a final round of evaporation was performed with the histones resuspended in 100 μL of 50mM ammonium bicarbonate. The dried

histone samples were redissolved in 100 µL of 50 mM ammonium bicarbonate and vortexed for 5 min. The digestion buffer was prepared by adding 200 µL of 50 mM ammonium bicarbonate in a vial containing 20 µg of lyophilized trypsin (Promega). About 0.5 µL of this solution was added to each histone sample and digested overnight at 37 °C. After digestion, samples were dried completely in a SpeedVac and then resuspended in 0.2% formic acid prior to LC−MS/MS analyses.

4.5.10. LC−MS/MS Analysis of Histone Peptides

Chromatographic separation of histone peptides was achieved on an Eksigent nano-LC system. A total of 2 µg of the histone digest was loaded and desalted on an in-house packed trap column (Jupiter C18 3 µm 300 Å particles from Phenomenex, 4 mm length, 360 µm i.d.) using water (0.2% formic acid) at a flow rate of 10 µL/min. After 5 min of desalting, the peptides were eluted onto an in-house packed analytical column (Jupiter C18 3 µm 300 Å particles from Phenomenex, 18 cm length, 150 µm i.d.) interfaced directly to the electrospray source (ESI) of Orbitrap Elite instrument (Thermo scientific). The mass spectrometer was operated in a data-dependent acquisition mode with full scan (m/z 300 – 2000) resolution set to 60 000, with a target value of 1.0×10^6. The six most abundant precursor ions were selected for fragmentation in the LTQ by CID at a normalized CE setting of 35. Fragment ions were analyzed in the LTQ ion trap over the mass range of m/z 200 – 2000 with a target value of 1.0×10^4.

4.5.11. Data Analysis

MS data were analyzed using the Xcalibur software (version 2.0.7). Peak lists were generated using the Mascot distiller software (version 2.3.2.0, Matrix science) where MS processing was achieved using the LCQ_plus_zoom script. Database searches were performed using the search engine Mascot (version 2.2.0, Matrix Science, London, UK) against custom UniProt human histone database. The tolerance window for precursor mass values and fragment ion mass values were set to ±15 ppm and 0.5 Da, respectively. The number of allowed missed cleavage sites for trypsin was set to 5 and acetylation (K), propionylation (K), oxidation (M), and deamidation (NQ) were all selected as variable modifications. No fixed modification was included in the search. All peptide identifications were transferred to ProteoConnections (Abshiru et al., 2013), an in-house developed bioinformatics tool, to generate a .csv (comma separated value) file that can be opened and modified in Excel. The .csv output file contained only distinct peptides (peptide with maximum score is kept) with assigned Mascot score of greater than or equal to 20. Manual MS/MS spectra verification was performed on each modified peptide to confirm the sequence assignment. The clustering of peptide abundances across different experimental conditions was performed using in-house tools as described previously (Abshiru et al., 2013).

4.6. Figure Legends

Figure 4.1. High stoichiometry of acetylation of H3K14 and H3K23 is evolutionarily conserved

A) High stoichiometry of H3-K14 and H3-K23 in old and new histones. HEK 293T cells were exposed to heavy isotope-labeled [$^{13}C_6$,$^{15}N_4$]-arginine for 20 min, washed in PBS and transferred to media containing light arginine for up to 24 hrs. Cells were harvested at the indicated time points, histones isolated and analyzed by mass spectrometry.

B) High levels of acetylation at H3-K14 and H3-K23 in HeLa cells. Histones were isolated from asynchronously growing HeLa cells, treated with DMSO or HDAC inhibitor SAHA (dissolved in DMSO for 24 hrs and analyzed by MS.

C) Non-transformed cell lines also show high levels of H3-K14 and H3-K23 acetylation. Asynchronously proliferating human lung fibroblasts, IMR90, grown to about 75% confluence were used to isolate histones and analyze them by MS.

D) Quiescent cells also show high stoichiometries of H3-K14 and H3-K23 acetylation. Peripheral Blood Mononuclear Cells (PBMCs) were isolated using Ficoll gradient separation. One-half of the cells ($2.5x10^6$) were grown in the presence of phytohemagglutinin-P (PHA-P) for 72 hrs. Histones were isolated from cells before and after *in vitro* stimulation with PHA-P and analyzed by MS.

E) High stoichiometry of acetylation on H3-K14 and H3-K23 is evolutionarily conserved. *Drosophila* S2 cells and wild-type fission yeast show strikingly abundant acetylation at H3-K14 and H3-K23. The data presented come from one representative experiment performed with three independent cultures of *S. pombe*. For mass spectrometry analysis of histone acetylation, purified intact histone proteins were propionylated *in vitro* before trypsin digestion.

Figure 4.2. H3-K14 has diverse functions compared to H3-K23

A) *H3-K14R* and *H3-K14R K23R* mutants have a growth lag. Representative growth curves for WT and histone H3 mutant cells in rich media (YES) at 30°C.

B) Comparative growth assay of histone mutants on rich media. Ten-fold serial dilutions of cells were grown on YES Agar at 30°C and 36°C for 3 days.

C) *H3-K14R* and *H3-K14R K23R* mutants are sensitive to DNA damage. Ten-fold serial dilutions of exponentially growing WT and histone mutants were plated on YES Agar with MMS (0.005% and 0.01%), camptothecin (8 μM and 16 μM) and hydroxyurea (2.5 mM and 5 mM) and grown 2-3 days at 30°C.

D) *H3-K14R* and *H3-K14R K23R* mutants are sensitive to microtubule poison thiabendazole.

E) *H3-K14R K23R* is sensitive to salt stress. Serial dilutions of the histone mutants were grown in YES Agar containing 0.1M $CaCl_2$, 1.0 M KCl and 0.2 M NaCl for 2-3 days at 30°C.

F) *H3-K14R* mutant cells show numerous strong phenotypes. WT and histone mutants were grown to exponential phase in liquid YES medium, serially diluted ten-fold and spotted onto YES Agar containing brefeldin A (10 μg/ml), mycophenolic acid (25 μg/ml), caffeine (10 mM) and formamide (2% v/v) and were grown for 2-3 days at 30°C.

Figure 4.3. Gcn5 and Mst2 contribute to H3-K14 and H3-K23 acetylation in *Schizosaccharomyces* pombe

A) Relative abundance in H3 N-terminal tail acetylation in wild-type fission yeast and cells lacking *gcn5*$^+$ and/or *mst2*$^+$. Crude histones were isolated from asynchronously growing cells, fractionated to individual core histones using offline HPLC and analyzed by MS.

B) Fold changes in the abundance of H3 acetylation in Δ*HAT* strains relative to the WT.

C) Loss of *gcn5*$^{+}$ specifically decreases H3 peptides doubly acetylated at K9 and K14. Overlayed extracted ion chromatograms (XICs) illustrating differences in abundances of K14ac containing peptides (panel 1-3) and a non-acetylated peptide (panel 4) in ∆*gcn5* cells relative to WT. The indicated percentages represent the relative abundances in the percentage of the corresponding isoforms among the total H3 peptides detected with the same sequence. The y-axis in each XIC panel category was scaled to the signal response of the most abundant peptide.

D) Relative abundance of H4 N-terminal tail acetylation in fission yeast cells lacking *gcn5*$^{+}$ and/or *mst2*$^{+}$. Histones were isolated from indicated strains and analyzed by MS.

E) Fold changes in the abundance of H4 acetylation in ∆*HAT* strains relative to the WT.

Figure 4.4. Loss of *mst2*+ does not phenocopy H3K14R

A) Representative growth curves for WT and histone H3 mutant cells lacking *mst2*+ in rich media (YES) at 30°C.

B) Comparative growth assay of histone and Mst2 mutants on rich media. Ten-fold serial dilutions of cells were grown on YES Agar at 30°C and 36°C.

C) *H3-K14R* and *H3-K14R K23R* mutants are more sensitive to DNA damage than *Δmst2* cells. WT and mutant strains were grown to exponential phase in liquid YES medium, serially diluted ten-fold, spotted onto YES Agar containing MMS (0.005%), camptothecin (8 µM and 16 µM) and hydroxyurea (2.5 mM and 5 mM) and grown 2-3 days at 30°C.

D) *Δmst2* cells are not sensitive to microtubule drug thiabendazole.

E) *Δmst2* cells do not phenocopy the severe phenotypes of *H3-K14R* and *H3-K14R K23R*.

4.7. Figures

Figure 4.1.

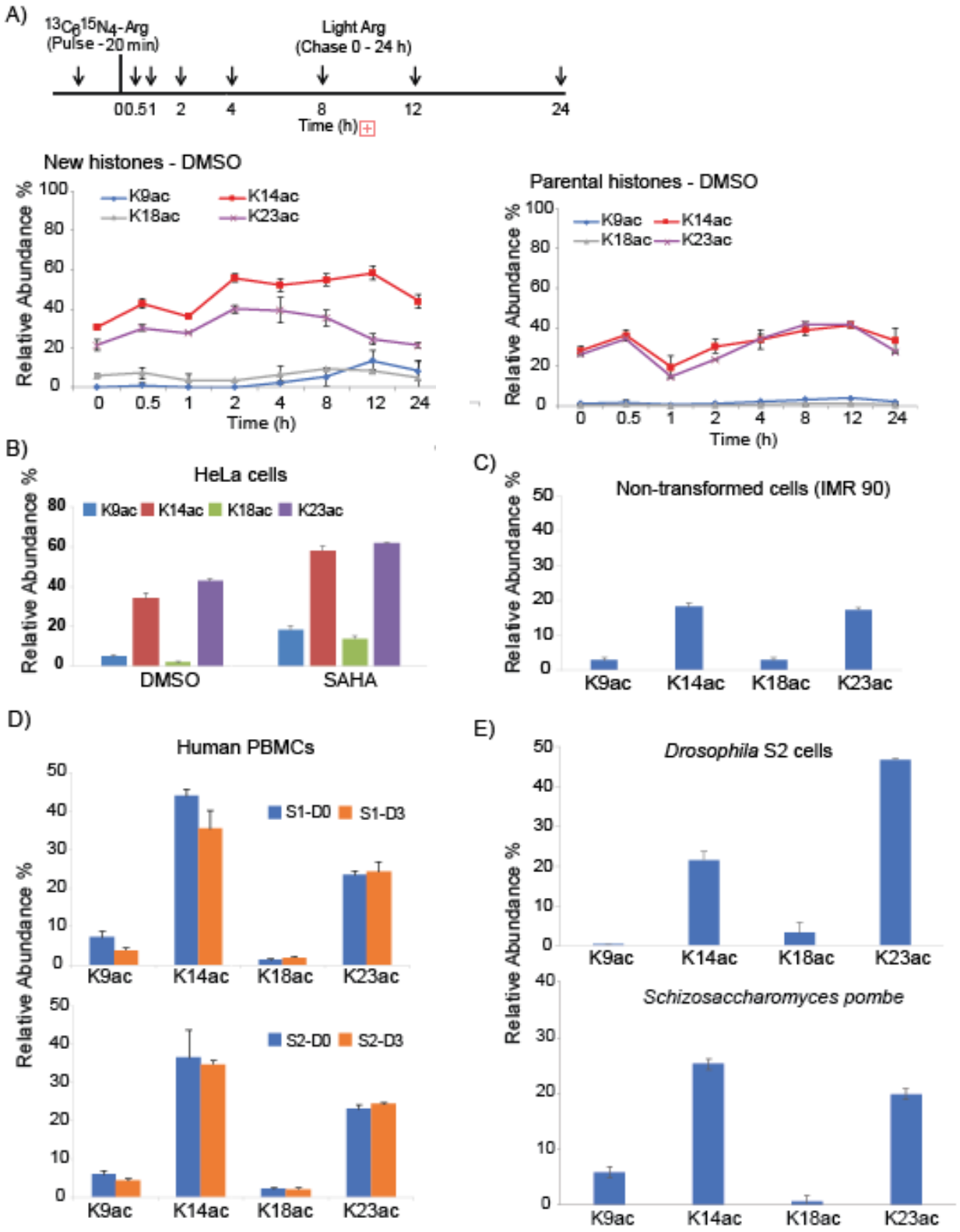

Figure 4.2.

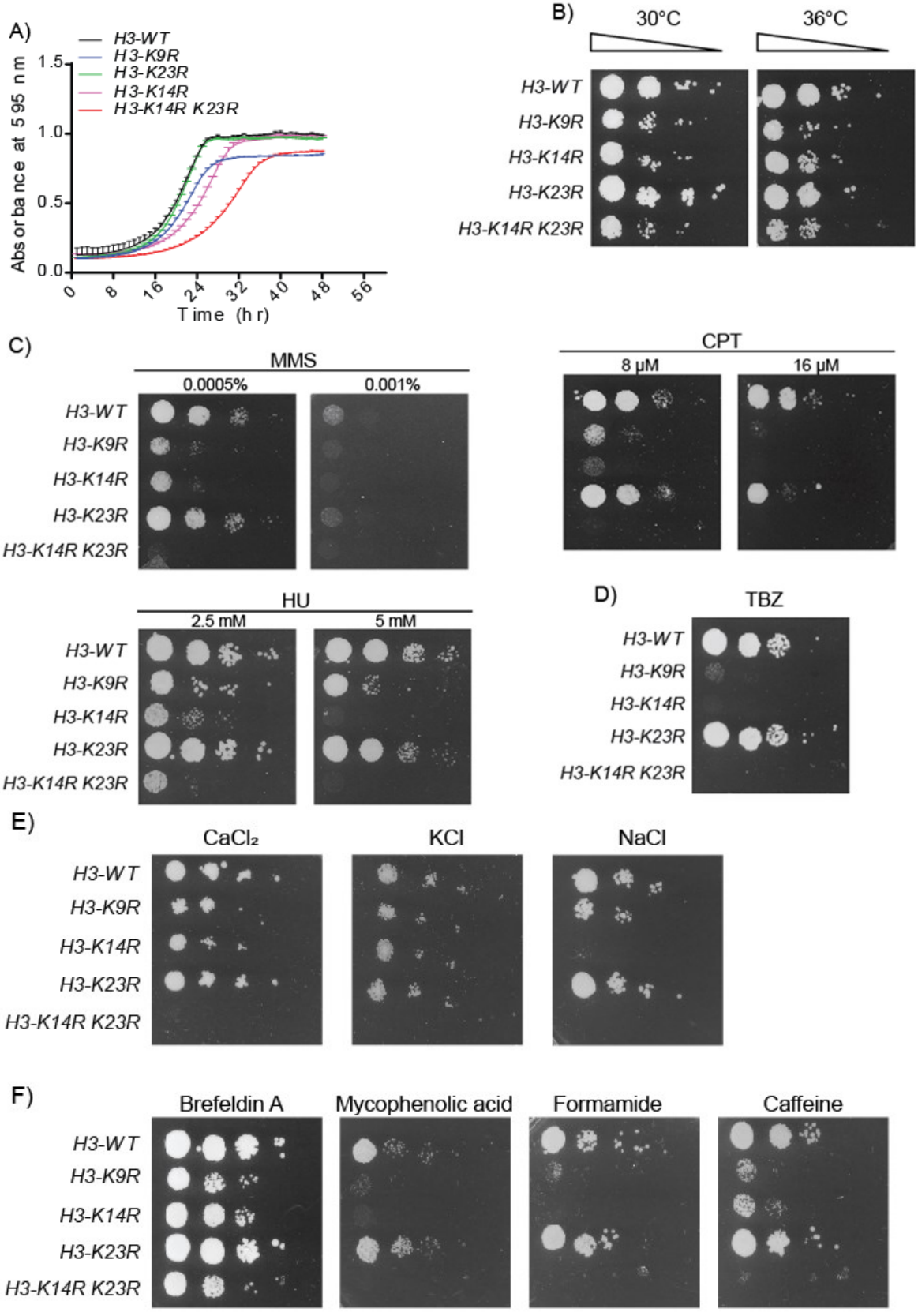
A)
H3-WT
H3-K9R
H3-K23R
H3-K14R
H3-K14R K23R
Absorbance at 595 nm
1.5
1.0
0.5
0.0
0
8
16
24
32
40
48
56
Time (hr)
B)
30°C
36°C
H3-WT
H3-K9R
H3-K14R
H3-K23R
H3-K14R K23R
C)
MMS
0.0005%
0.001%
H3-WT
H3-K9R
H3-K14R
H3-K23R
H3-K14R K23R
CPT
8 µM
16 µM
HU
2.5 mM
5 mM
H3-WT
H3-K9R
H3-K14R
H3-K23R
H3-K14R K23R
D)
TBZ
H3-WT
H3-K9R
H3-K14R
H3-K23R
H3-K14R K23R
E)
CaCl₂
KCl
NaCl
H3-WT
H3-K9R
H3-K14R
H3-K23R
H3-K14R K23R
F)
Brefeldin A
Mycophenolic acid
Formamide
Caffeine
H3-WT
H3-K9R
H3-K14R
H3-K23R
H3-K14R K23R

Figure 4.3.

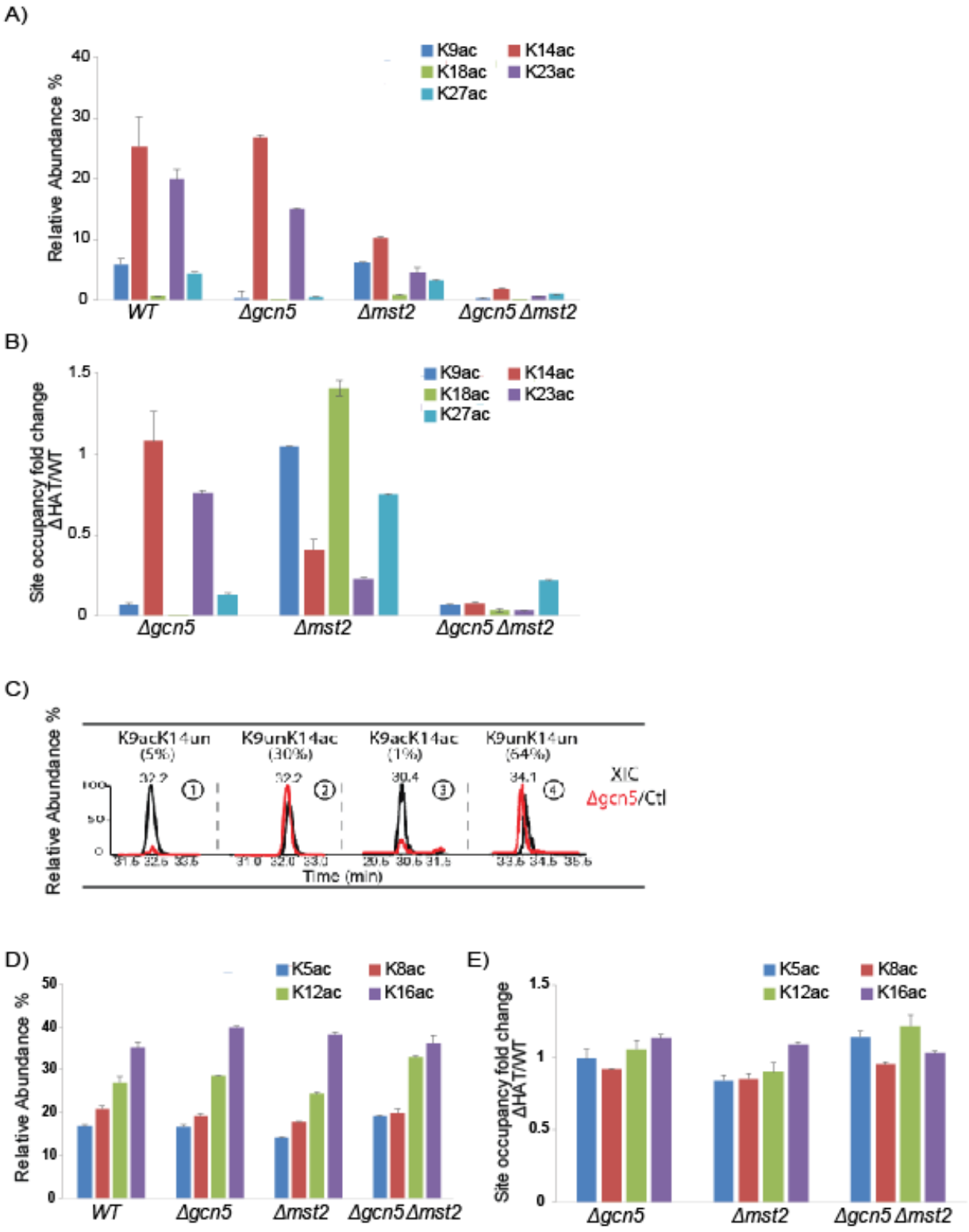
A)
K9ac
K14ac
K18ac
K23ac
K27ac
Relative Abundance %
40
30
20
10
0
WT
Δgcn5
Δmst2
Δgcn5 Δmst2
B)
K9ac
K14ac
K18ac
K23ac
K27ac
Site occupancy fold change ΔHAT/WT
1.5
1
0.5
0
Δgcn5
Δmst2
Δgcn5 Δmst2
C)
Relative Abundance %
K9acK14un (5%)
K9unK14ac (30%)
K9acK14ac (1%)
K9unK14un (64%)
XIC
Δgcn5/Ctl
Time (min)
D)
K5ac
K8ac
K12ac
K16ac
Relative Abundance %
50
40
30
20
10
0
WT
Δgcn5
Δmst2
Δgcn5Δmst2
E)
K5ac
K8ac
K12ac
K16ac
Site occupancy fold change ΔHAT/WT
1.5
1
0.5
0
Δgcn5
Δmst2
Δgcn5 Δmst2

Figure 4.4.

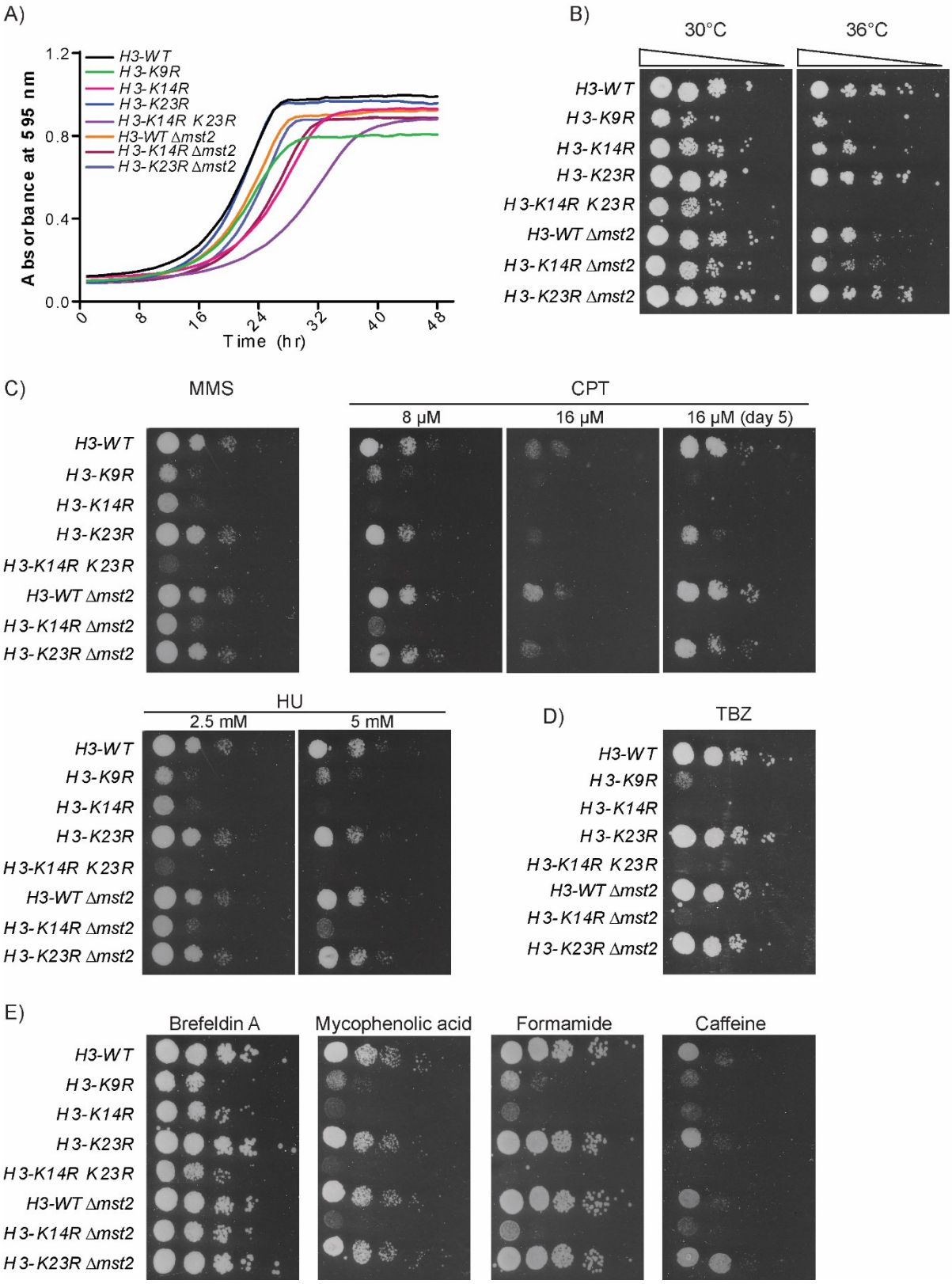
A)
H3-WT
H3-K9R
H3-K14R
H3-K23R
H3-K14R K23R
H3-WT Δmst2
H3-K14R Δmst2
H3-K23R Δmst2
Absorbance at 595 nm
Time (hr)
B)
30°C
36°C
C)
MMS
CPT
8 μM
16 μM
16 μM (day 5)
HU
2.5 mM
5 mM
D)
TBZ
E)
Brefeldin A
Mycophenolic acid
Formamide
Caffeine

4.8. References

Abshiru, N., Ippersiel, K., Tang, Y., Yuan, H., Marmorstein, R., Verreault, A., and Thibault, P. (2013). Chaperone-mediated acetylation of histones by Rtt109 identified by quantitative proteomics. J. Proteomics *81*, 80–90.

Abshiru, N., Caron-Lizotte, O., Rajan, R.E., Jamai, A., Pomies, C., Verreault, A., and Thibault, P. (2015). Discovery of protein acetylation patterns by deconvolution of peptide isomer mass spectra. Nat. Commun. *6*, 8648.

Abshiru, N., Rajan, R.E., Verreault, A., and Thibault, P. (2016). Unraveling site-specific and combinatorial histone modifications using high-resolution mass spectrometry in histone deacetylase mutants of fission yeast. J. Proteome Res. *15*, 2132–2142.

An, S., Yoon, J., Kim, H., Song, J., Cho, U., and Arbor, A. (2017). Structure-based nuclear import mechanism of histones H3 and H4 mediated by Kap123. Elife. 6: e30244

Annunziato, A.T., and Seale, R.L. (1983). Histone deacetylation is required for the maturation of newly replicated chromatin. J. Biol. Chem. *258*, 12675–12684.

Annunziato, A.T., Schindler, R.K., Riggs, M.G., and Seale, R.L. (1982). Association of newly synthesized histones with replicating and nonreplicating regions of chromatin. J. Biol. Chem. *257*, 8507–8515.

Benson, L.J., Gu, Y., Yakovleva, T., Tong, K., Barrows, C., Strack, C.L., Cook, R.G., Mizzen, C.A., and Annunziato, A.T. (2006). Modifications of H3 and H4 during chromatin replication, nucleosome assembly, and histone exchange. J. Biol. Chem. *281*, 9287–9296.

Blackwell, J.S., Wilkinson, S.T., Mosammaparast, N., and Pemberton, L.F. (2007). Mutational analysis of H3 and H4 N termini reveals distinct roles in nuclear import. J. Biol. Chem. *282*, 20142–20150.

Burgess, R.J., Zhou, H., Han, J., and Zhang, Z. (2010). A role for Gcn5 in replication-coupled nucleosome assembly. Mol. Cell *37*, 469–480.

Chen, J.-S., Beckley, J.R., McDonald, N. a., Ren, L., Mangione, M., Jang, S.J., Elmore, Z.C., Rachfall, N., Feoktistova, A., Jones, C.M., et al. (2015). Identification of new players in cell division, DNA damage response, and morphogenesis through construction of Schizosaccharomyces pombe deletion strains. G3 (Bethesda). *5*, 361–370.

Drogaris, P., Villeneuve, V., Pomiès, C., Lee, E.-H., Bourdeau, V., Bonneil, É., Ferbeyre, G., Verreault, A., and Thibault, P. (2012). Histone deacetylase inhibitors globally enhance H3/H4 tail acetylation without affecting H3 lysine 56 acetylation. Sci. Rep. *2*, 1–12.

Falkenberg, K.J., and Johnstone, R.W. (2014). Histone deacetylases and their inhibitors in cancer, neurological diseases and immune disorders. Nat. Rev. Drug Discov. *13*, 673–691.

Forsburg, S.L., and Rhind, N. (2006). Basic methods for fission yeast. Yeast *23*, 173–183.

Glozak, M.A., Sengupta, N., Zhang, X., and Seto, E. (2005). Acetylation and deacetylation of non-histone proteins. Gene *363*, 15–23.

Grewal, S.I.S., and Jia, S. (2007). Heterochromatin revisited. Nat. Rev. Genet. *8*, 35–46.

Groth, A., Rocha, W., Verreault, A., and Almouzni, G. (2007). Chromatin challenges during DNA replication and repair. Cell *128*, 721–733.

Guillemette, B., Drogaris, P., Lin, H.-H.S., Armstrong, H., Hiragami-Hamada, K., Imhof, A., Bonneil, E., Thibault, P., Verreault, A., and Festenstein, R.J. (2011). H3 lysine 4 is acetylated at active gene promoters and is regulated by H3 lysine 4 methylation. PLoS Genet. *7*, e1001354.

Jacobs, S.A., Taverna, S.D., Zhang, Y., Briggs, S.D., Li, J., Eissenberg, J.C., Allis, C.D., and Khorasanizadeh, S. (2001). Specificity of the HP1 chromo domain for the methylated N-terminus of histone H3. EMBO J. *20*, 5232–5241.

Karmodiya, K., Krebs, A.R., Oulad-Abdelghani, M., Kimura, H., and Tora, L. (2012). H3K9 and H3K14 acetylation co-occur at many gene regulatory elements, while H3K14ac marks a subset of inactive inducible promoters in mouse embryonic stem cells. BMC Genomics *13*, 424.

Luger, K., and Richmond, T.J. (1998). The histone tails of the nucleosome. Curr. Opin. Genet. Dev. *8*, 140–146.

Luger, K., Mäder, A.W., Richmond, R.K., Sargent, D.F., Richmond, T.J., and Mä, A.W. (1997). Crystal structure of the nucleosome core particle at 2.8 A resolution. Nature *389*, 251–260.

Marks, P.A., and Xu, W.-S. (2009). Histone deacetylase inhibitors: Potential in cancer therapy. Expert Opin. Investig. Drugs *107*, 600–608.

Marmorstein, R., and Zhou, M.-M. (2014). Writers and readers of histone acetylation: structure, mechanism, and inhibition. Cold Spring Harb. Perspect. Biol. *6*, a0187762.

Mellone, B.G., Ball, L., Suka, N., Grunstein, M.R., Partridge, J.F., and Allshire, R.C. (2003). Centromere silencing and function in fission yeast is governed by the amino terminus of histone H3. Curr. Biol. *13*, 1748–1757.

Moazed, D. (2013). Chromatin: A tail of repression. Curr. Biol. *23*, R456–R459.

Murray, J.M., Watson, A.T., and Carr, A.M. (2016). Transformation of Schizosaccharomyces pombe: Lithium acetate/dimethyl sulfoxide procedure. Cold Spring Harb. Protoc. *2016*, 394–396.

Nielsen, P.R., Nietlispach, D., Mott, H.R., Callaghan, J., Bannister, A., Kouzarides, T., Murzin, A.G., Murzina, N. V, and Laue, E.D. (2002). Structure of the HP1 chromodomain bound to histone H3 methylated at lysine 9. Nature *416*, 103–107.

Panda, S.K., Kumar, S., Tupperwar, N.C., Vaidya, T., George, A., Rath, S., Bal, V., and Ravindran, B. (2012). Chitohexaose activates macrophages by alternate pathway through TLR4 and blocks endotoxemia. PLoS Pathog. *8*. e1002717

Pengelly, A.R., Copur, O., Jackle, H., Herzig, A., and Muller, J. (2013). A histone mutant reproduces the phenotype caused by loss of histone-modifying factor Polycomb. Science *339*, 698–700.

Perry, C.A., and Annunziato, A.T. (1989). Influence of histone acetylation on the solubility, H1 content and DNase I sensitivity of newly assembled chromatin. Nucleic Acids Res. *17*, 4275–4291.

Pokholok, D.K., Harbison, C.T., Levine, S., Cole, M., Hannett, N.M., Lee, T.I., Bell, G.W., Walker, K., Rolfe, P.A., Herbolsheimer, E., et al. (2005). Genome-wide map of nucleosome acetylation and methylation in yeast. Cell *122*, 517–527.

Poux, A.N., and Marmorstein, R. (2003). Molecular Basis for Gcn5 / PCAF histone acetyltransferase selectivity for histone. Biochemistry *42*, 14366–14374.

Reddy, B.D., Wang, Y., Niu, L., Higuchi, E.C., Marguerat, S.B., Bähler, J., Smith, G.R., and Jia, S. (2011). Elimination of a specific histone H3K14 acetyltransferase complex bypasses the RNAi pathway to regulate pericentric heterochromatin functions. Genes Dev. *25*, 214–219.

Shahbazian, M.D., and Grunstein, M. (2007). Functions of site-specific histone acetylation and deacetylation. Annu. Rev. Biochem. *76*, 75–100.

Shechter, D., Dormann, H.L., Allis, C.D., and Hake, S.B. (2007). Extraction, purification and analysis of histones. Nat Protoc *2*, 1445–1457.

Sinha, I., Wiren, M., and Ekwall, K. (2006). Genome-wide patterns of histone modifications in fission yeast. Chromosom. Res. *14*, 95–105.

Sinha, I., Buchanan, L., Rönnerblad, M., Bonilla, C., Durand-Dubief, M., Shevchenko, A., Grunstein, M., Stewart, A. F., and Ekwall, K. (2010). Genome-wide mapping of histone modifications and mass spectrometry reveal H4 acetylation bias and H3K36 methylation at gene promoters in fission yeast. Epigenomics *2*, 377–393.

Smith, D.J., and Whitehouse, I. (2012). Intrinsic coupling of lagging-strand synthesis to chromatin assembly. Nature *483*, 434–438.

Sobel, R.E., Cook, R.G., Perry, C.A., Annunziato, A.T., and Allis, C.D. (1995). Conservation of deposition-related acetylation sites in newly synthesized histones H3 and H4. Proc. Natl. Acad. Sci. U. S. A. *92*, 1237–1241.

Suka, N., Suka, Y., Carmen, A.A., Wu, J., and Grunstein, M. (2001). Highly specific antibodies determine histone acetylation site usage in yeast heterochromatin and euchromatin. Mol. Cell *8*, 473–479.

Verreault, A. (2000). De novo nucleosome assembly: new pieces in an old puzzle. Genes Dev. *14*, 1430–1438.

Wang, Y., Kallgren, S.P., Reddy, B.D., Kuntz, K., López-Maury, L., Thompson, J., Watt, S., Chun, M., Hou, H., Shi, Y., et al. (2012). Histone H3 lysine 14 acetylation is required for activation of a DNA damage checkpoint in fission yeast. J. Biol. Chem. *287*, 4386–4393.

Wang, Z., Zang, C., Rosenfeld, J.A., Schones, D.E., Barski, A., Cuddapah, S., Cui, K., Roh, T.-Y., Peng, W., Zhang, M.Q., et al. (2008). Combinatorial patterns of histone acetylations and methylations in the human genome. Nat. Genet. *40*, 897–903.

4.9. Supplementary Information

Supplementary Figure legends

Supplementary Figure 4.1.

A) SAHA affects the stoichiometry of H3 N-terminal tail histone acetylation in new and old histones.

B) High levels of acetylation at H3-K14 and H3-K23 in Hut78 and H9 T-cell lymphoma cell lines.

C) Workflow for in-vitro proliferation and histone analysis of human peripheral blood mononuclear cells (PBMCs)

D) Representative cell-cycle profiles of PBMCs before and after in-vitro proliferation with the mitogen phytohemagglutinin-P (PHA-P)

Supplementary Figure 4.2.

A) Representative growth curves of histone mutants in YES liquid media containing hydroxyurea.

B) Growth curves of histone mutants in YES liquid media containing camptothecin.

C) Growth curves of histone mutants in YES liquid media containing thiabendazole.

Supplementary Figure 4.3.

A) Heatmap representation of the log2 fold changes of normalized LC−MS signals of histone H3 acetylated peptides.

B) Heatmap representation of the log2 fold changes of normalized LC−MS signals of H4 acetylated peptides in mutants relative to the control sample.

Supplementary Figure 4.4.

A) Comparison of salt stress sensitivity of histone mutants lacking Mst2. Serial dilutions of the indicated strains were grown in YES Agar containing 0.1M $CaCl_2$ or 1.0 M KCl for 2-3 days at 30°C.

B) Representative growth curves of Mst2 mutants in YES liquid media containing camptothecin.

C) Representative growth curves of Mst2 mutants in YES liquid media containing hydroxyurea.

D) Representative growth curves of Mst2 mutants in YES liquid media containing thiabendazole.

Supplementary Table 4.1.

Fission yeast strains used in this study

Strain name	Genotype	Source
AVP033	*h+ h3.2 h3.1/h4.1::his3+ h3.3/h4.3::arg+ leu1-32 ura4D18, his3D1 arg3D3 otr(Sph1):ade6*	This study
AVP034	*h+ h3.2K23R h3.1/h4.1::his3+ h3.3/h4.3::arg+ leu1-32 ura4D18, his3D1 arg3D3 otr(Sph1):ade6*	This study
AVP035	*h- h3.2K14R-1 h3.1/h4.1::his3+ h3.3/h4.3::arg+ leu1-32 ura4D18, his3D1 arg3D3 otr(Sph1):ade6*	This study
AVP036	*h+ h3.2K14R-2 h3.1/h4.1::his3+ h3.3/h4.3::arg+ leu1-32 ura4D18, his3D1 arg3D3 otr(Sph1):ade6*	This study
AVP037	*h+ h3.2K14R K23R-1 h3.1/h4.1::his3+ h3.3/h4.3::arg+ leu1-32 ura4D18, his3D1 arg3D3 otr(Sph1):ade6*	This study
AVP038	*h- h3.2K14R K23R-2 h3.1/h4.1::his3+ h3.3/h4.3::arg+ leu1-32 ura4D18, his3D1 arg3D3 otr(Sph1):ade6*	This study
AVP049	*h+ h3.2 h3.1/h4.1::his3+ h3.3/h4.3::arg+ leu1-32 mst2::hphNT1 ura4D18, his3D1 arg3D3 otr(Sph1):ade6*	This study
AVP050	*h+ h3.2K23R h3.1/h4.1::his3+ h3.3/h4.3::arg+ mst2::hphNT1 leu1-32 ura4D18, his3D1 arg3D3 otr(Sph1):ade6*	This study
AVP051	*h- h3.2K14R-1 h3.1/h4.1::his3+ h3.3/h4.3::arg+ mst2::hphNT1 leu1-32 ura4D18, his3D1 arg3D3 otr(Sph1):ade6*	This study
6072	*h3.2K9R h3.1/h4.1::his3+ h3.3/h4.3::arg+ leu1-32 ura4D18, his3D1 arg3D3 otr(Sph1):ade6*	Allshire Lab
FY4754	*h3.2::ura4+; leu1-32 ura4D18 his3D1 arg3D ade6-210*	Allshire Lab
FY4640	*h4.2::ura4 h3.1/h4.1::his3+ h3.3/h4.3::arg3+ leu1-32 ura4D18 his3D1 arg3D4 ade6-210 otr1R(SphI):ade6*	Allshire Lab
FY2943	*h- gcn5::kanMX ura4D18 leu1-32 ade6-M21? his3D1*	Forsburg Lab
FY1890	*h+ mst2::ura4+ ura4D18 ade6-M210 leu1-32*	Forsburg Lab
FY3361	*h+ gcn5d::kanMX6 mst2d::ura4+ ura4D18 ade6-M21? leu1-32 his3D1*	Forsburg Lab

Supplementary Figure 4.1.

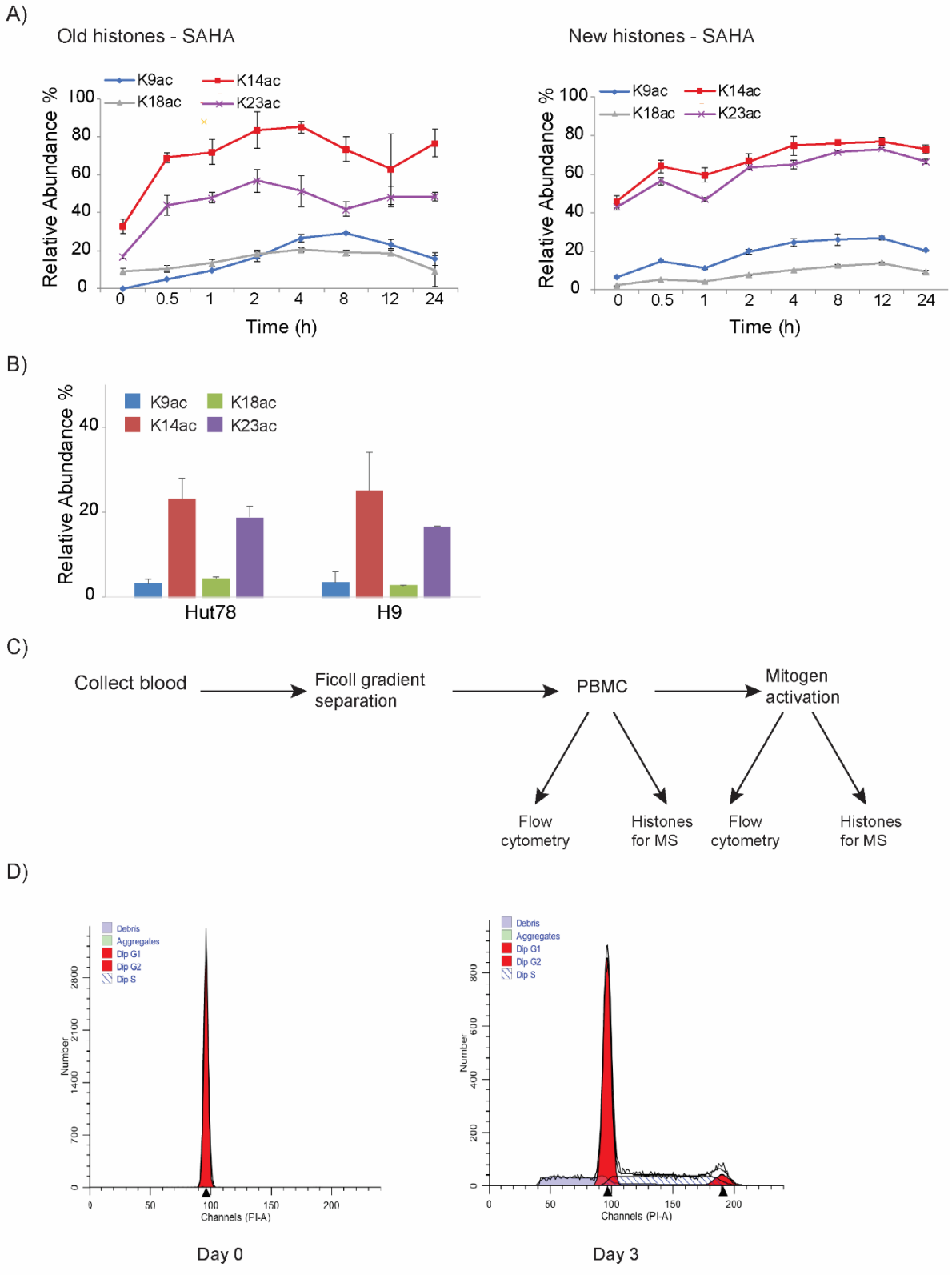

Supplementary Figure 4.2.

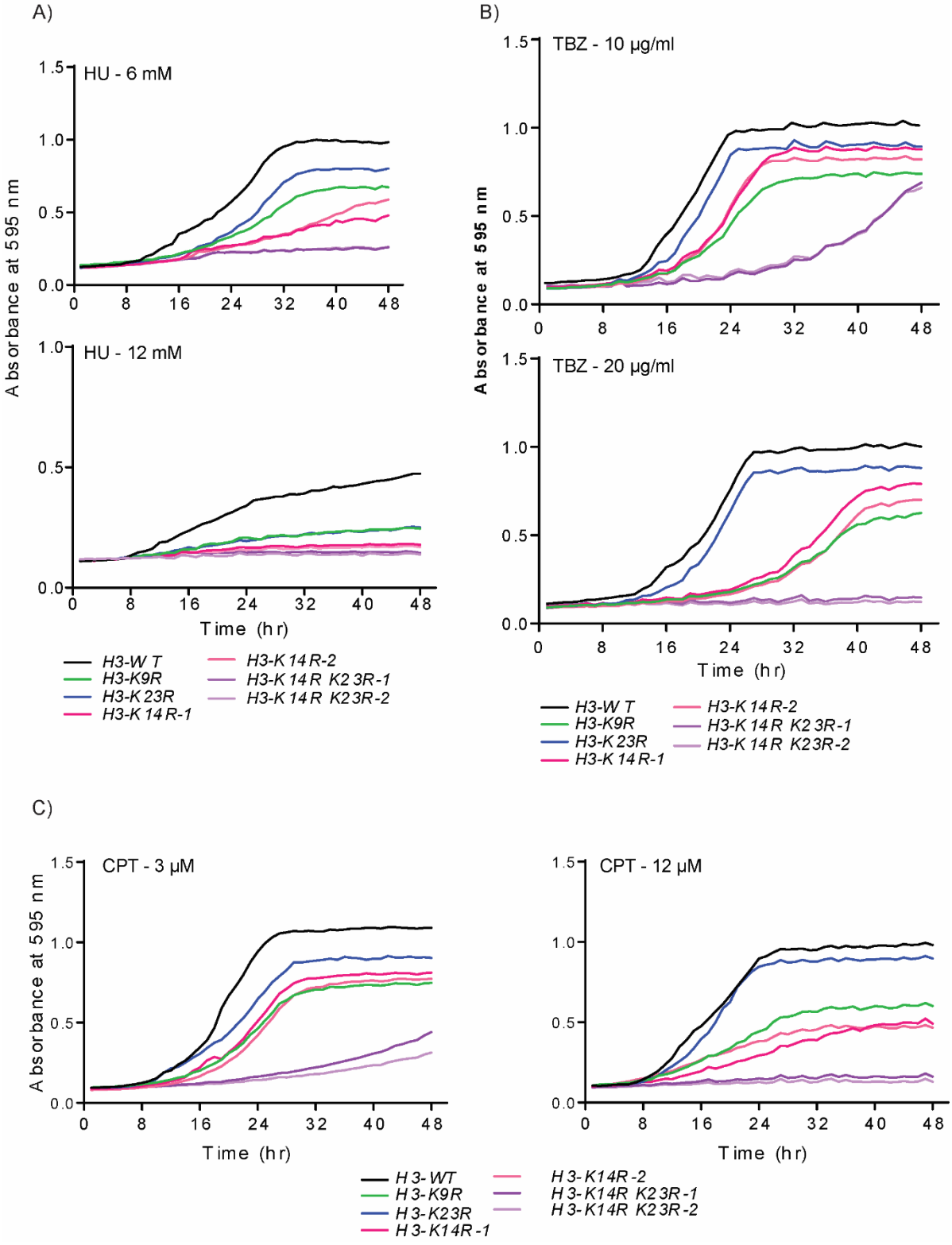

Supplementary Figure 4.3.

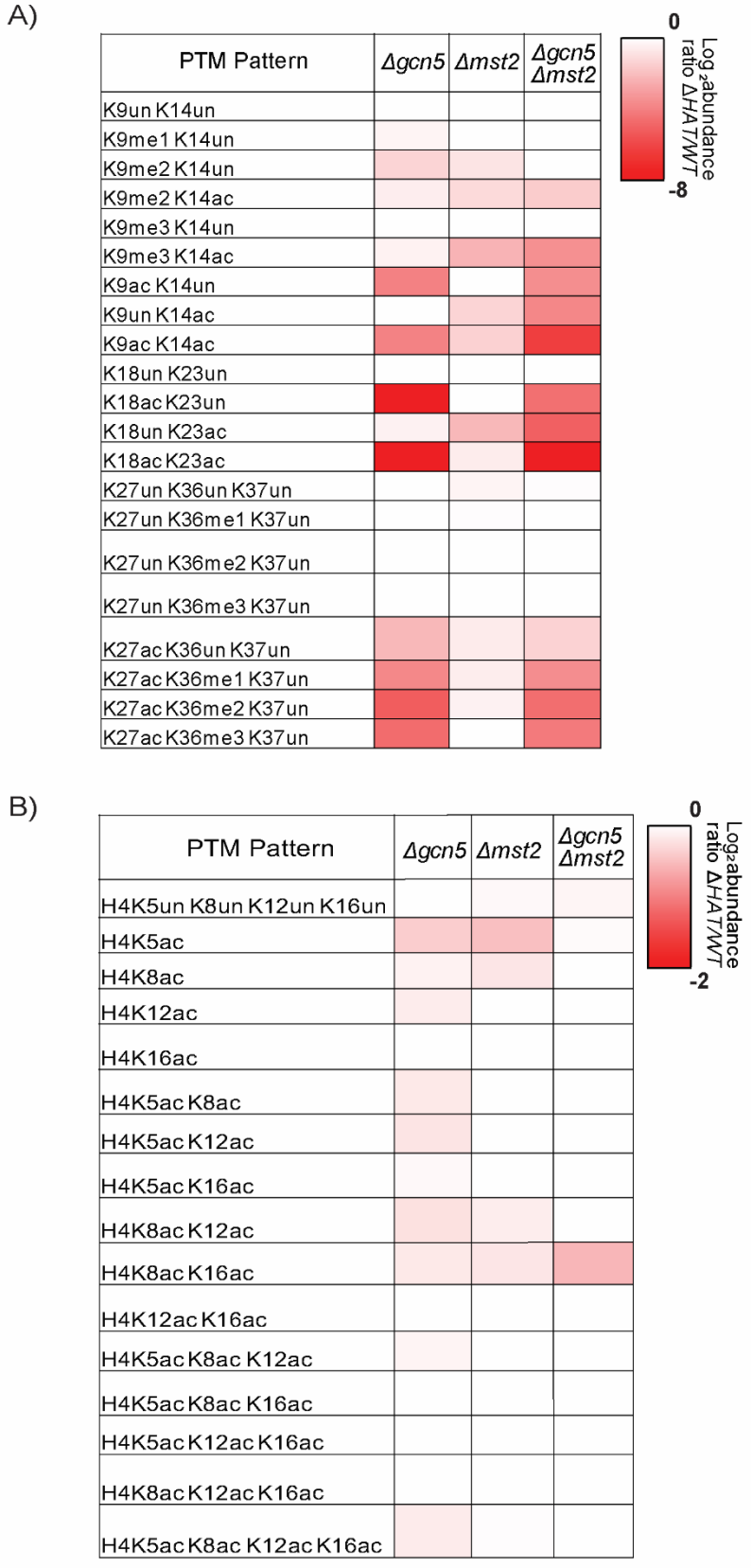

Supplementary Figure 4.4.

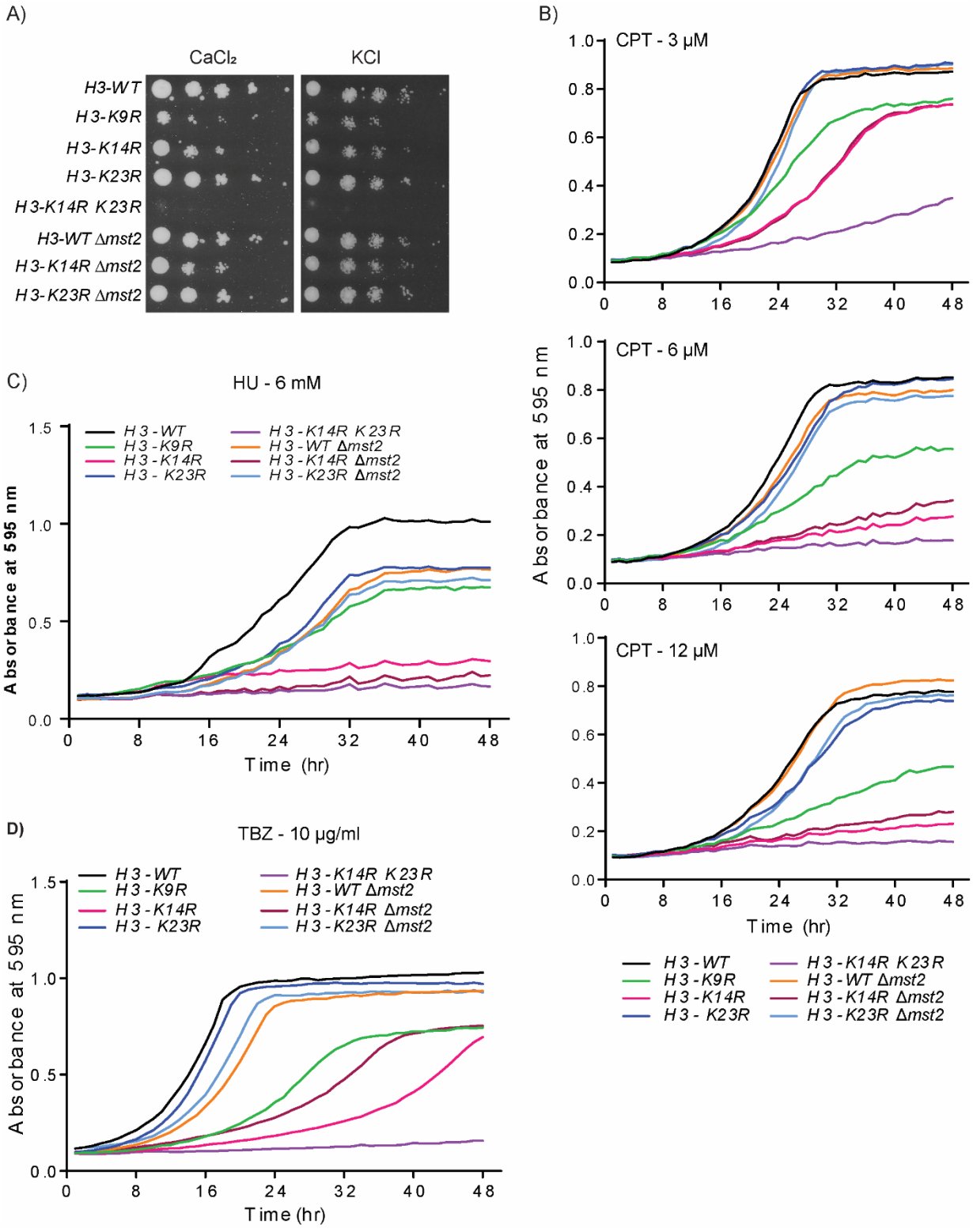

5. Conclusions and Perspectives

Histone post-translational modifications have been at the heart of academic and biomedical research since their discovery five decades ago. Researchers have focused on identifying, mapping and understanding the functions of various PTMs. Recent years have seen an increasing number of studies correlating PTMs to various cancers, metabolic and immune disorders (Bhaumik et al., 2007; Di Cerbo and Schneider, 2013; Morgan and Shilatifard, 2015). Technological advancements in mass spectrometry have been key to the rapid identification of many previously unknown sites and modifications. However, there are several challenges that limit the full scope of histone PTM studies. In this thesis, we have employed complementary approaches: bioinformatics tools, mass spectrometry methods, biochemical and genetic tools to determine the stoichiometry of acetylation on the N-terminal tail of histones and their functional significance.

5.1 Iso-PeptidAce as a valuable tool to analyze isomeric peptides

In Chapter 2, we report the development of a novel Mass Spectrometry method to determine the stoichiometries of isomeric peptides. The Bottom Up mode of analysis is the most commonly employed MS method for studying histone modifications. This conventional method involves the use of a protease such as trypsin to generate peptides that can be resolved by liquid chromatography. Trypsin cleaves at the C-terminal side of arginine and unmodified or mono-methylated lysine residues. Due to a large number of lysine and arginine residues in histones, many peptides flanked by arginines that are produced using this approach bear more than one internal lysine

residue. These peptides can be modified at a single site or multiple sites. Oftentimes, a single modification such as acetylation can occur on different lysine residues of the same peptide, generating positional isomers. In addition to having exactly the same mass, such isomeric peptides co-elute and cannot be effectively resolved using conventional RP-LC/MS. We combined bioinformatic tools with high-resolution MS to develop an algorithm to deconvolute the co-eluting isomeric peptides. Although it could in principle be exploited to study isomeric peptides containing other types of modification, we mainly used Iso-PeptidAce to determine changes in abundance of lysine acetylation in the N-terminal tail of histone H4, in which a single tryptic peptide contains four internal lysines all of which can be acetylated. Two of these sites, H4-K5 and H4-K12, are considered important for DNA-replication coupled nucleosome assembly. In addition, this method can also be applied to histone H3 peptides that have more than one internal lysine. Some examples of such biologically significant multi-lysine containing peptides are the K9, K14 containing tryptic peptide, the peptide that has both K18 and K23 and the K27, K36 and K37 containing peptide.

We successfully validated this method using complex biological samples. In Chapter 2, we describe the applicability of this method to analyze histones isolated from cells treated with three histone deacetylase inhibitors. Histone deacetylase inhibitors have been in the limelight as potential therapeutic agents in the treatment of cancers, neurological disorders and immune diseases (Falkenberg and Johnstone, 2014; Marks and Xu, 2009; West and Johnstone, 2014). Our study focused on the changes in the acetylation of histone H3 and H4 following treatment with three clinically-relevant broad spectrum HDACi: vorinostat also known as SAHA which is FDA-

approved for treatment of Cutaneous T-Cell Lymphoma (CTCL), entinostat or MS-275 which is in Phase III clinical trial for breast cancer and quisinostat (JNJ-26481585) which is also in Phase II clinical trials for CTCL and ovarian cancer (www.clinicaltrials.gov). DMSO-treated cells had lysines that were mostly non-acetylated or mono-acetylated. However, SAHA and JNJ treatment generated di, tri and tetra-acetylated H4 peptides as early as 6 hours, unlike MS-275 which gave rise to tri and tetra-acetylated peptides only by the end of 24 hours. Our method thus has the potential to be used to monitor temporal changes in site-specific histone acetylation in clinical trials of HDAC inhibitors. Further, our method can also be optimized to monitor changes in the acetylation of non-histone proteins. To our knowledge, this is the first study demonstrating the effects of the quisinostat on site-specific acetylation of histones. It is interesting to note that none of the HDACs that we used increased the site occupancy to a hundred percent. One reason could be that even high concentrations of HDAC inhibitors would not lead to acetylation of all the residues of histones and/or non-histone proteins as this would be detrimental to the cell. Another plausible reason could be that there is a pool of histones that are not ‘continuously’ acetylated or deacetylated.

Using Iso-PeptidAce we also demonstrate that it is useful when biological samples are limited as in the case of histones associated with Chromatin Assembly Factor 1, a protein complex known to deposit newly synthesized H3/H4 molecules onto nascent DNA during replication (Kaufman et al., 1995). H4 molecules associated with CAF-1 have been shown to be di-acetylated at H4-K5 and H4-K12 in human cells

(Verreault et al., 1996). However, we observed that CAF-1-bound H4 is acetylated on K16 with roughly 20% stoichiometry, in addition to K5 and K12. In stark contrast to H4 molecules bound to CAF1, total histone H4 molecules were differentially acetylated at all the four N-terminal lysine residues - K5, K8, K12 and K16 in increasing order of acetylation occupancy (15 to 65%). Our data challenge the existing dogma of the acetylation pattern of H4 molecules bound to CAF-1. It would be worth studying the role of H4-K16 acetylation in DNA replication-dependent histone deposition. H4-K16 acetylation is one of the few modifications that has been shown to have a direct role in chromatin structure. In an elegant study, the use of chromatin containing H4 molecules homogeneously acetylated at K16 was shown to destabilize the formation of 30-nm fibers and inhibit inter-fiber interactions (Shogren-Knaak M et al. 2006). On the contrary, using fluorescence in situ hybridization (FISH) probes on genomic areas where H4K16 acetylation is present it has been demonstrated that loss of H4-K16ac does not alter chromatin compaction in embryonic stem cells (Taylor et al., 2013). H4K16 is important for the DNA damage response (Sharma et al., 2010) and loss of H4K16 acetylation has been shown to be a hallmark of many human cancers (Fraga et al., 2005). In budding yeast, H4K16 acetylation is found throughout the genome except at silent loci and heterochromatin (Smith et al., 2003; Suka et al., 2001). Another interesting question that follows our result is what are the enzymes that acetylate H3 and H4 in new histones. In *S. cerevisiae,* H4K16 is acetylated primarily by the histone acetyltransferase Sas2 (Kimura et al., 2002; Suka et al., 2002). It was also shown that Sas2 shows epistatic interactions with Cac1, the largest subunit of CAF-1 complex, and Asf1, a chromatin

assembly factor (Meijsing and Ehrenhofer-Murray, 2001). It is thus possible that Sas2 acetylates new H4 molecules at lysine 16 during its association with Cac1.

One important question that arises when we study CAF1-associated histones is whether the CAF1-bound histones reflect chromatin assembly processes other than replication such as replication-independent nucleosome assembly at sites of histone dissociation during transcription. This is not very likely because CAF-1-mediated nucleosome assembly requires PCNA-dependent DNA synthesis (either DNA replication *per se* or DNA synthesis linked to repair processes (e.g. nucleotide excision repair). Even though we cannot completely rule out the possibility of nucleosomal histones (histone H3-H4 derived from nucleosomes in which DNA is wrapped around the histones) associating with CAF-1 during purification, we are confident that a major fraction of histones co-purified with CAF-1 is involved in nucleosome assembly coupled with DNA synthesis. This is because, histone peptides bound to CAF-1 lack modifications characteristic of transcription, such as H3-K36 methylation (Supplementary Table 2.5). To ensure that there is absolutely no mixing of nucleosomal histones with CAF-1 during cell lysis or CAF-1 purification, an internal control should be added during the purification. For example, cell extracts from a SILAC strain of *S. pombe* grown in a stable heavy isotope of arginine and/or lysine can be added to the cell extracts of the CAF1- tagged strain during purification. The presence of heavy histones associated with CAF-1 is a good indicator of whether nucleosomal histones associate non-specifically with CAF-1 during the purification.

H3-K18 and H4-K8 are two sites on CAF1-associated histones that have very low levels of acetylation. This tends to suggest that the acetylation on these sites may not be necessary for chromatin assembly when the other sites are intact. In *Saccharomyces cerevisiae* cells lacking the N-terminal tail of H3 (residues 4-30, removing H3-K9, -14, -K18, -K23 and -K27), three residues on the N-terminal tail of H4, H4-K5, -8, and-12 are required in a highly redundant manner. Nucleosome assembly is strongly impaired only when these three lysines are mutated simultaneously (Ma et al., 1998). H4-K8 acetylation has been shown to recruit human SWI/SNF at the interferon beta (IFN-β) locus (Agalioti et al., 2002) and thus may have locus-specific functions in chromatin remodeling and/or transcription. In *S pombe,* acetylation of H3-K18 at gene promoters has been correlated with gene expression (Sinha et al., 2010). Thus, although H3-K18 and H4-K8 acetylation are relatively rare in total histones, it is highly likely that the acetylation of these residues is regulated at specific loci for functions other than chromatin assembly.

In chapter 3, we extended the use of Iso-PeptidAce to look at *in vivo* changes in acetylation of histone H3 and H4 in fission yeast mutants lacking histone deacetylases: Clr3, Clr6, Sir3 and Hos2. These HDACs have been extensively characterized using immunoblots and ChIPs particularly with respect to their role in heterochromatin (Millar and Grunstein, 2006; Wirén et al., 2005). Iso-PeptidAce overcomes some of the challenges that antibody-based methods suffer from such as antibody cross-reactivity and epitope occlusion. Also, antibody-based methods cannot provide information on stoichiometries of modifications or give insights into

combinatorial modifications. On the other hand, given that rigorously-tested modification-specific antibodies are available, chromatin immunoprecipitation (ChIP) assays can help determine where a specific modification is located in the genome which, in turn, can provide valuable information regarding the function of that modification.

The ability of Iso-PeptidAce to deconvolute multiple co-eluting isomers was most valuable while studying *in vivo* HDAC activity. We could distinguish the effect of various HDACs on different chromatin regions. For example, conditional inactivation of *clr6*$^{+}$ resulted in an increase in H3-K14ac, but only when H3-K14ac and H3-K9ac were present in the same H3 molecules, suggesting a role for Clr6 in deacetylating K14 in H3 molecules associated with euchromatin. Strikingly, the increase in H3-K14ac in cells lacking *clr3*$^{+}$ or s*ir2*$^{+}$ corresponded to the fraction of peptides where K14 acetylation occurs in the same H3 molecules with di- or trimethylated H3-K9, marks that are mainly or perhaps exclusively present in heterochromatin.

Another remarkable finding is the role of Clr6 in globally affecting the acetylation of many lysine residues on both H3 and H4. The *S. cerevisiae* ortholog of Clr6, known as Rpd3, is not an essential gene, but perhaps the global increases in acetylation of a broad spectrum of lysine residues that occur upon inactivation of Clr6 might account for the fact that the *clr6*$^{+}$ is essential for viability in *S. pombe*. Even the hypomorphic mutant *clr6-1*, which has reduced deacetylase activity at the permissive temperature grows slowly at low temperature. However, further studies are required to conclude

whether the increase in acetylation of multiple residues of H3 and H4 that arises upon depletion of Clr6 is direct or indirect. It is likely that inactivation of Clr6 reduces the abundance or activity of an HDAC or an HDAC coactivator, thus leading to the increase in acetylation stoichiometries that we observed.

It is interesting to note that H3K27 acetylation is low on peptides harboring H3K36me (Supplementary Table 3.7 C, D). This reciprocal relationship between H3-K27 acetylation and H3-K36 methylation has been previously reported and has been functionally characterized (Fiedler et al., 2013). Phosphorylation of the C-terminal domain of the elongating RNA polymerase II (RNAPII) recruits both the H3-K36 methyltransferase, Set2, and the small complex containing the deacetylase Rpd3, known as Rpd3S, to regions of active transcription. Set2 methylates H3-K36, which is in turn recognized by the chromodomain of Eaf3, a subunit of Rpd3S, that preferentially binds di- or trimethylated H3-K36. This results in Rpd3S-mediated deacetylation of H3-K27. Thus, in the body (ORF) of a transcribed gene, histone H3 is methylated at K36 and deacetylated at K27. (Lee and Shilatifard, 2007).

Another striking result from our study of histone deacetylase mutants in fission yeast is the increase in H3-K9 methylation in *clr6-1* and Δ*hos2* mutants. It is counterintuitive that the loss of HDACs should increase methylation. In euchromatic regions, histones are hyperacetylated while heterochromatic regions are marked by hypoacetylation of histones. Often, the heterochromatin-euchromatin border is loosely defined and exhibits an extended transition zone. In certain cases, these transition zones include

specific DNA sequences, known as boundary elements, which are characterized by sharp transitions in histone modification profiles It seems possible that *clr6-1* and Δ*hos2* mutants allow the *de novo* formation of heterochromatin at ectopic sites. Chromatin immunoprecipitation combined with DNA sequencing (ChIP-Seq) with antibodies specific for dimethylated or trimethylated H3-K9 (H3-K9me2 or H3-K9me3) in *clr6-1* or ∆*hos2* mutants will be useful to monitor the formation of ectopic heterochromatin in the whole genome.

Our results do not imply that the sites where *in vivo* changes in acetylation were observed in HDAC mutants are directly deacetylated by the corresponding HDACs. It is likely that the changes in acetylation observed *in vivo* may be an indirect consequence of changes in physiology brought about by the absence of that HDAC. The substrate specificity of a given HDAC can be tested by *in vitro* deacetylase assays. For example, in order to test whether Clr6 can "*directly*" deacetylate multiple residues of H3 and H4, it would be necessary to purify the protein complex containing Clr6 from wild-type cells and assay its deacetylase activity by mass spectrometry using nucleosomes acetylated at multiple lysine residues as substrate.

5.2 A novel evolutionarily conserved pattern of histone acetylation

In Chapter 4, we present the identification of a pattern of H3 acetylation. It needs to be emphasized that we would have missed this pattern of acetylation had we not looked for stoichiometry. We discovered that two lysine residues in the N-terminal tail

of histone H3, K14 and K23 had strikingly high levels of acetylation, between 20-40% in many different types of mammalian cells, *Drosophila* S2 cells and fission yeast. In contrast, the levels of acetylation for H3-K9 and H3-K18 acetylation were less than 10%. Even though we found a similar pattern in *S. cerevisiae*, there also existed high levels of H3-K9 acetylation in addition to H3-K14 and K23 acetylation. The high levels of H3-K9 acetylation observed in *S. cerevisiae* may be due, at least in part, to the absence of H3-K9 methylation. There have been previous studies reporting high levels of H3-K14 acetylation and H3-K23 acetylation in human cells and in *S. pombe* (Sinha et al., 2010; Sridharan et al., 2013; Thomas et al., 2006a; Young et al., 2009). However, the authors did not identify the presence of a pattern. The stoichiometries of H3 acetylation reported in *S. pombe* is a massive over-estimation, which is most likely because of incomplete propionylation (discussed in detail in Chapter 1). An early report from the laboratory of Morton Bradbury studied sites and levels of acetylation on the five N-terminal tail lysines of histone H3, from sodium butyrate-treated HeLa S3 cells, by Edman sequencing (Marvin et al., 1990). The abundance of acetylation was calculated at each site by measuring the ratio of phenylthiohydantoin-derivatives of acetylated lysine to total lysine at a given site for the various acetylated forms (mono, di, tri, tetra and penta-acetyl). In the mono-acetylated forms of H3, acetylation of H3-K14 and H3-K23 showed an abundance of about 50% whereas, in the diacetylated H3, abundance at H3-K14 and H3-K23 reached a soaring 90%. These results suggest that H3-K14 and -K23 are likely the most preferred sites of acetylation.

To elucidate the functions of this high stoichiometry of acetylation, we chose a genetically tractable organism, where this pattern was evident, and which is amenable to genetic disruptions. Fission yeast fitted all the criteria and offered reliable tools to study histone modifications. *S. pombe* genome contains three copies of histone H3 and H4 which occur as gene pairs at three distinct chromosomal loci. We took advantage of an elegant study where strains were constructed such that only one pair of histone H3 and H4 genes were retained. The other two pairs of H3 and H4 genes were replaced with auxotrophic markers (Mellone et al., 2003). The use of this system allows us to study mutations that come from the only source of histones.

In *S. pombe*, we created two single mutants, *H3-K14R* and *H3-K23R*, and a double mutant *H3-K14R K23R* and studied their phenotypes. Interestingly, the *H3-K23R* mutant proliferated at the same rate as wild-type cells and exhibited no sensitivity to a variety of chemicals that we tested. It showed at best a modest sensitivity to HU and CPT. The *H3-K14R* showed a pronounced delay in cell proliferation and exhibited sensitivity to a broad range of chemicals. The double mutant had even more severe phenotypes than either of the two single mutants. This was not very evident from spot assays on plates but became apparent from real-time monitoring of growth in liquid media (Supplementary Figure 2).

H3-K14 acetylation has been widely studied in model organisms ranging from budding yeast to mammalian cells and numerous unrelated functions are ascribed to it. First, based on genome-wide ChIP assays H3-K14 and H3-K9 acetylation were

found enriched at promoters and showed a strong positive correlation with transcriptional activity (Karmodiya et al., 2012; Pokholok et al., 2005; Wang et al., 2008). In fission yeast, four H3 acetylation sites at gene promoters correlated with gene expression: K18ac > K27ac > K9ac > K23ac, in descending order. K18ac, K27ac, K9ac and K23ac levels were higher at gene promoters of highly expressed genes in fission yeast. However, levels of H3-K14ac did not show any correlation with gene expression (Sinha et al., 2006, 2010).

Second, the second bromodomain (BD2) of the tandem bromodomain (TBD) of Rsc4, a subunit of the chromatin remodeling complex known as "Remodels the Structure of Chromatin (RSC), has been shown to bind H3 molecules acetylated at K14 (Kasten et al., 2004; VanDemark et al., 2007). Acetylation of lysine 25 in the first bromodomain (BD1) of Rsc4 antagonizes its binding to H3-K14ac and releases Rsc4 thus forming an important regulatory mechanism of RSC binding (VanDemark et al., 2007).

Third, H3-K14 acetylation has also been shown to be a mark of newly synthesized histones in *Tetrahymena*, *Drosophila* and mammalian cells (Benson et al., 2006; Sobel et al., 1995). Using mutagenesis and a telomeric reporter gene, H3-K14 was found to act redundantly with Hat1 for the formation of silent chromatin in the vicinity of telomeres (Kelly et al., 2000). Interestingly, Hat1 is an enzyme that cannot acetylate nucleosomal histones and specifically acetylates new H4 molecules at H4-K5 and H4-K12 prior to their deposition onto nascent DNA behind replication forks (Parthun et al., 1996; Verreault et al., 1997). Acetylations of new H3 and H4

molecules are functionally redundant to promote rapid nucleosome assembly at DNA replication forks (Burgess and Zhang, 2010; Li et al., 2008). Therefore, the aforementioned synergy between the H3-K14 and Hat1 mutations suggests that rapid nucleosome assembly is important to establish sub-telomeric heterochromatin in proliferating cells.

Fourth, the Yng1 subunit of the NuA3 histone acetyltransferase (HAT) complex that modifies H3-K14, was found to bind H3-K4me3 and promote transcription of a subset of *S. cerevisiae* genes (Taverna et al., 2006).

Fifth, mutations of H3-K14 affect the integrity of pericentric heterochromatin and the fidelity of mitotic chromosome segregation in fission yeast (Mellone et al., 2003). Intriguingly, these phenotypes of *H3-K14R* mutant cells appear to be related, through an unknown mechanism, to dissociation of Swi6 (known as HP1 in other eukaryotes) from pericentric heterochromatin (Mellone et al., 2003). This suggests the existence of an unexpected link between H3-K14 and H3-K9 methylation since the latter is crucial to bind to and retain Swi6/HP1 within pericentric heterochromatin where it plays an important role in mitotic chromosome segregation.

Sixth, in the absence of a wild-type allele, point mutation of H3-K14 was lethal in *Neurospora crassa* (Adhvaryu et al., 2011). In a heterozygous state, the H3-K14 mutation caused a semi-dominant loss of heterochromatin silencing and DNA methylation. The H3-K23 mutant, however, was viable.

H3-K23 acetylation has received a lot less attention compared to H3-K14 acetylation. In *Drosophila* and HeLa cells, it is found as a mark of newly synthesized histones along with H3-K14 (Benson et al., 2006; Sobel et al., 1995). The H3-K23 residue has been shown to stabilize the interaction between H3-K27me3 and the chromodomain of Polycomb (Fischle et al., 2003). Another study showed that TRIM24, a coactivator for estrogen receptor-induced transcription in humans, associated with unmodified H3-K4 and -K23ac of the same H3 tail through its plant homeodomain (PHD) finger and bromodomain, respectively (Tsai et al., 2010). In addition, in *Drosophila* the levels of H3-K23 acetylation at two genes, *Eip74EF* and *Eip75B,* inducible by ecdysone, the master hormonal regulator, have been shown to correlate with the transcriptional activity of these two genes at the pupal stage. This suggests an involvement of H3K23ac in ecdysone-induced transcriptional activation, which is important for triggering metamorphosis from larval to the pupal stage (Bodai et al., 2012).

Work from Mark Parthun's group has established that lysines 14 and 23 function together in the DNA damage response. For example, of all the permutations of lysine-to-arginine double mutants in the N-terminal tail of histone H3 (*e.g. H3-K9R K18R* and many others), the only one that conferred sensitivity to the alkylating agent MMS was the *H3-K14R K23R* double mutant (Qin and Parthun, 2002). *H3-K14R K23R* mutant cells also exhibited a defect in recombination-mediated repair of DNA double-strand breaks (DSBs) and a less prominent defect in the repair of DSBs by Non-Homologous End Joining (NHEJ) (Qin and Parthun, 2002). In *S. cerevisiae*, the Q308K hypomorphic allele of *POB3*, a subunit of the Facilitates Chromatin

Transcription (FACT) complex was synthetic lethal with mutations of H3 lysine residues 14 and 23 (Nair et al., 2011). In addition, work in fission yeast has suggested but did not provide a compelling proof, that H3-K14 acetylation functions in the activation of the DNA damage checkpoint through the recruitment of RSC (Wang et al., 2012). In our opinion, however, the authors did not formally prove that H3-K14ac is needed for DNA damage checkpoint activation. The authors base their argument on a modest decrease in sensitivity to DNA damage in an *H3-K14A* mutant compared to the *H3-K14R* mutant.

Both H3-K14 and H3-K23 thus seem to have diverse functions and, at least in some cases, act in a redundant manner. One important question is whether the phenotypes that result from H3-K14 or H3-K23 mutation are truly due to a loss of acetylation, rather than a loss of identity of a non-modified lysine or a lysine bearing modifications other than acetylation. The functions of H3-K14 and H3-K23 could be divided into two categories. The first category is dependent upon the identity of the lysine, which might be important for a) binding of a modifying enzyme: the residues flanking the target lysine are important for determining the substrate selectivity and substrate affinity of Gcn5 N-acetyltransferases (GNATs) (Poux and Marmorstein, 2003) b) binding of a reader directly to the lysine or a nearby residue. A good example is the dissociation of Swi6 localization from pericentric heterochromatin when lysine 14 of histone H3 is mutated (Mellone et al., 2003).

The second group of functions is dependent upon post-translational modifications of H3-K14 and H3-K23. These acetylation-dependent functions of H3-K14 and H3-K23 may be mediated through the binding of reader molecules (*e.g.* bromodomain-containing protein complexes). Alternately, the abundant presence of acetylation at the sites that we identified might hinder the binding of proteins that should not inappropriately localize to specific loci. In this scenario, high stoichiometries of H3-K14 and H3-K23 acetylation would serve to protect specific loci from adventitious functional interference that would arise in the absence of acetylation. In order to determine whether certain phenotypes are truly due to a lack of histone acetylation, epistasis studies between specific histone lysine mutations, and mutations that abolish acetylation without perturbing the corresponding lysine can be very informative. To perform this type of epistasis analysis, we first had to find the enzymes responsible for the majority of H3-K14 and H3-K23 acetylation.

The MYST and GNAT families of HATs have been implicated in H3-K14 and H3-K23 acetylation. In *S. cerevisiae*, Sas3 and Gcn5 have been shown to acetylate a significant portion of the total H3-K14 and H3-K23 acetylation. The combined loss of these two HATs is synthetically lethal in *S. cerevisiae* (Howe et al., 2001). However, the lethality of *sas3*Δ *gcn5*Δ cells cannot solely be attributed to the absence of H3-K14 and H3-K23 acetylation because *S. cerevisiae* H3-K14R H3-K23R double mutants are viable. In *S. pombe*, Mst2, the ortholog of *S. cerevisiae* Sas2 and Sas3, is responsible for a substantial portion of H3-K14 acetylation. In addition, Gcn5 has

also been shown to contribute to H3-K14 acetylation in fission yeast (Nugent et al., 2010; Wang et al., 2012).

In *Drosophila*, Enok, an MYST family HAT, functions as the major HAT that mediates H3-K23 acetylation *in vivo* and this modification regulates oocyte polarization (Huang et al., 2014).

In human cells, KAT6B also known as MORF has been reported to possess H3-K23 acetyltransferase activity (Simo-Riudalbas et al., 2015). Another human MYST family HAT, HBO1, has also been shown to acetylate H3-K14 in K562 leukemic cells (Mishima et al., 2011). In mouse embryos, knockout of HBO1 resulted in a global loss of H3-K14 acetylation in primary embryonic fibroblasts (Kueh et al., 2011).

For our work in *S. pombe*, we created strains that lack Gcn5, Mst2 or both and looked at their histone acetylation profile by mass spectrometry. Loss of both Mst2 and Gcn5 led to a massive reduction in the acetylation of five lysine residues, K9, K14, K18, K23 and K27 on the N-terminal tail of H3 but had little effect on the N-terminal tail of H4. Interestingly, we saw a four-fold reduction in the acetylation of both H3-K14 and H3-K23 acetylation in cells lacking Mst2. This result challenges the previous report that Mst2 was an H3-K14 specific lysine acetyltransferase (Wang et al., 2012). In fact, results of the *in vitro* Edman sequencing presented in the paper suggest some degree of acetylation at H3-K23 by the purified Mst2 complex. However, the authors did not seem to notice this (Figure 1 Wang et al., 2012). In addition to Mst2, we saw that

Gcn5 is also responsible for H3-K23 acetylation contributing to about 20% of all H3-K23 acetylation.

We then attempted to uncover the roles of H3-K14 and H3-K23 acetylation by epistasis analysis by combining histone and HAT mutants. However, there exists a caveat in interpreting the results of such genetic studies. Though it is extremely valuable to understand if the different components work in a given genetic pathway, it is oftentimes difficult to differentiate whether the observed hypersensitivity or loss of function is due to direct effects or indirect effects. For example, histone mutants that we made may have direct roles by making chromatin alterations that are giving rise to the phenotypes we observe. Alternatively, the histone mutants, particularly *the H3-K14R* mutant, may cause repression of genes involved in DNA damage response or prevent the binding of an effector protein involved in DNA damage response, implying indirect roles. Wang and colleagues analyzed by microarray the differences in gene expression in strains that caused a loss of H3-K14 acetylation: *Δgcn5, Δmst2*, *Δgcn5 Δmst2* and *H3-K14R* (Wang et al., 2012). The gene expression profiles of *Δgcn5 Δmst2* and *H3-K14R* were very different and those of *Δgcn5 Δmst2* were similar to *Δgcn5*, consistent with another study of fission yeast HATs (Nugent et al., 2010).

In our epistasis analysis, we used strains where we could distinguish the contributions of H3-K14 acetylation and H3-K23 acetylation toward sensitivity to a variety of inhibitors. We made single mutants, H3-K14R, H3-K23R and H3-WT- *Δmst2* and

double mutants, *H3K23R Δmst2* and *H3K14R Δmst2.* Surprisingly, the absence of Mst2, the HAT that contributes to about 80% percent of the acetylation of H3-K14 and H3-K23, did not phenocopy the severe phenotypes of *H3-K14R* mutant cells. It is possible that the remaining H3-K14 acetylation in cells lacking Mst2 is sufficient to alleviate the severe phenotypes observed in *H3-K14R* mutant cells. However, we cannot exclude the possibility that the severe phenotypes observed with the *H3K14R* mutant may not be the result of a loss of acetylation, but instead, reflect the structural alteration of a lysine caused by its mutation into an arginine.

In vitro, acetylation of H3-K14 within the context of H3 peptides did not affect binding of Swi6, the *S. pombe* HP1 homolog (Yamada et al., 2005). This is consistent with structures of Swi6/HP1 homologs bound to K9-methylated peptides. These structures show that the chromodomain of Swi6/HP1 homologs, which anchors the proteins to methylated H3-K9, does not make contacts with the H3 tail beyond serine 10 (Jacobs and Khorasanizadeh, 2002; Nielsen et al., 2002). Given this, it is not clear how mutation of H3-K14 causes mislocalization of Swi6 from pericentric heterochromatin that contains K9-methylated histone H3 (Mellone et al., 2003). *In vitro*, the presence or absence of H3-K14 acetylation does not affect the activity of the H3-K9 methyltransferase Clr4 (Nakayama et al., 2001). However, it remains possible that the state of acetylation of H3-K14 may interfere with the methylation of H3-K9 *in vivo*. However, the absence of both Gcn5 and Mst2, which essentially abolishes acetylation of H3-K14, does not affect Swi6 localization *in vivo*, but the *H3-K14R* mutation does (Reddy et al., 2011). This suggests the possibility that it is not the lack

of H3-K14 acetylation that leads to delocalization of Swi6 from pericentric heterochromatin. Instead, it seems possible that, *in vivo*, an acetylated or a non-acetylated H3-K14 is necessary to guide proteins that catalyze H3-K9 methylation or recognize this modification, but that the presence of a lysine cannot be substituted by an arginine at the position.

Importantly, I found that at least some of the strong phenotypes (sensitivity to MMS, CPT, HU, TBZ, mycophenolic acid, caffeine and formamide) of *H3-K14R* mutants are also observed in *H3-K9R* mutants, which cannot be methylated and consequently cannot bind to Swi6. Since both strains exhibit delocalization of Swi6, these genetic results suggest that the strong phenotypes of both strains may result from defects in pericentric heterochromatin, possibly leading to mitotic chromosome segregation defects.

Interesting work from Jacques Cote's laboratory has shown that associated factors or subunits rather than the HATs determine the specificity of histone substrates. The human MYST family of acetyltransferases have five members: HIV Tat-interacting 60 kDa protein (TIP60), monocytic leukemia zinc finger protein (MOZ), MOZ-related factor (MORF), HAT bound to ORC1 (HBO1) and human males-absent on the first (hMOF). MOZ, MORF and HBO1 exist as tetrameric complexes. The noncatalytic subunits of these complexes are Inhibitor of growth 4/5 (ING4/5), a homolog of yeast Esa1-associated factor 6 (EAF6) and bromodomain-PHD finger protein (BRPF) 1, 2 or 3 (Ullah et al., 2008; Yang, 2015). JADE (protein encoded by gene (J) for apoptosis

and differentiation in epithelial proteins) proteins take the place of ING proteins in some complexes. For example, HBO1 occur as two complexes depending on their scaffold proteins. The HBO1-JADE complex acetylates histone H4 on lysines 5, 8 and 12 while the HBO1 complexes containing BRPF1 target histone H3 lysines 14 and 23 (Lalonde et al., 2013). Moreover, an exhaustive study of human bromodomain containing proteins revealed that the flanking residues are critical in the binding of bromodomains (Filippakopoulos et al., 2012). Even though not directly related to our work, these studies underscore the importance of the identity of the amino acid.

5.3 Future Perspectives

Histones and their post-translational modifications continue to challenge researchers. Many questions remain to be answered about these relatively small architectural proteins: their regulation, their roles in various cellular processes and their deregulation in diseases. Cutting-edge mass spectrometry and continuous improvements in analytical methodologies have enhanced our ability to identify PTMs. Due to their high sensitivity, these techniques have generated long lists of histone post-translational modifications which bring along the formidable task of finding their physiological functions, identifying the enzymes responsible for the modifications and the effector proteins that bind to specific modifications, as well as the crosstalk between the ever-increasing repertoire of modifications.

We discovered an evolutionarily conserved pattern of histone acetylation. However, we were unable to unambiguously define the roles of H3-K14 and H3-K23 acetylation in *S. pombe*, one of few model organisms in which histones residues can be mutated to assess the functions of post-translational modifications. Partly because of the phenotypes of the H3-K14R mutation that could not be attributed to a loss of acetylation, our genetic analyses were inconclusive. Because this powerful genetic approach cannot be exploited in our case, we hope that an indirect approach will take us closer to defining the functions of H3-K14 and H3-K23 acetylation. This approach will involve finding answers to the three questions depicted in Figure 5.1.

First, it is imperative to know where in the genome high levels of acetylation of H3-K14 and H3-K23 occur and, the genomic regions where high stoichiometries of H3-K14 and H3-K23 acetylation are not tolerated. Studies in budding yeast and fission yeast have shown that the pericentromeric and sub-telomeric heterochromatin regions contain very low levels of H3 and H4 acetylation (Braunstein et al., 1993; Ekwall et al., 1997; Suka et al., 2001). In *S. cerevisiae*, very high levels of acetylation, about 50-80%, are found on five lysines (H3-K9, K14, K23, K27 and K56) on histone H3 associated with Cac2, a subunit of the CAF-1 complex that deposits new H3-H4 molecules on to nascent DNA "*throughout the genome*" during DNA replication. This result is consistent with other data showing that newly synthesized histones are acetylated at multiple sites (Benson et al., 2006; Masumoto et al., 2005; Sobel et al., 1995). The total histones isolated from the same cultures as the histones bound to

CAF-1 showed relatively low levels of acetylation, except on H3-K14, H3-K23 and H3-K56 which were 20-25% acetylated (Abshiru et al., 2015).

In order to uncover at least one moment when new H3 molecules acquire high stoichiometries of H3-K14 and H3-K23 acetylation, it would be important to investigate whether newly synthesized H3 molecules associated with Pcf2, the fission yeast ortholog of *S. cerevisiae* Cac2, are also marked by high levels of acetylation at multiple lysine residues. Recent structural studies of karyopherin Kap123, the most abundant karyopherin in budding yeast, which transports histones H3 and H4 by recognizing their nuclear localization signal (NLS), identified that there are two lysine binding pockets in Kap123.

These lysine binding regions bind to H3-K14 and H3-K23 respectively and are important for the affinity of histones to karyopherin. Mutation of lysines 14 and 23 to alanine or glutamine reduced the affinity of histones to karyopherin *in vitro*, by four-fold (An et al., 2017; Blackwell et al., 2007). It is plausible that one of the functions of an evolutionarily-conserved pattern of H3-K14 acetylation and H3-K23 acetylation is to release H3-H4 from the import factors. This might explain the high stoichiometry of acetylation on histones bound to CAF-1 (Abshiru et al., 2015).

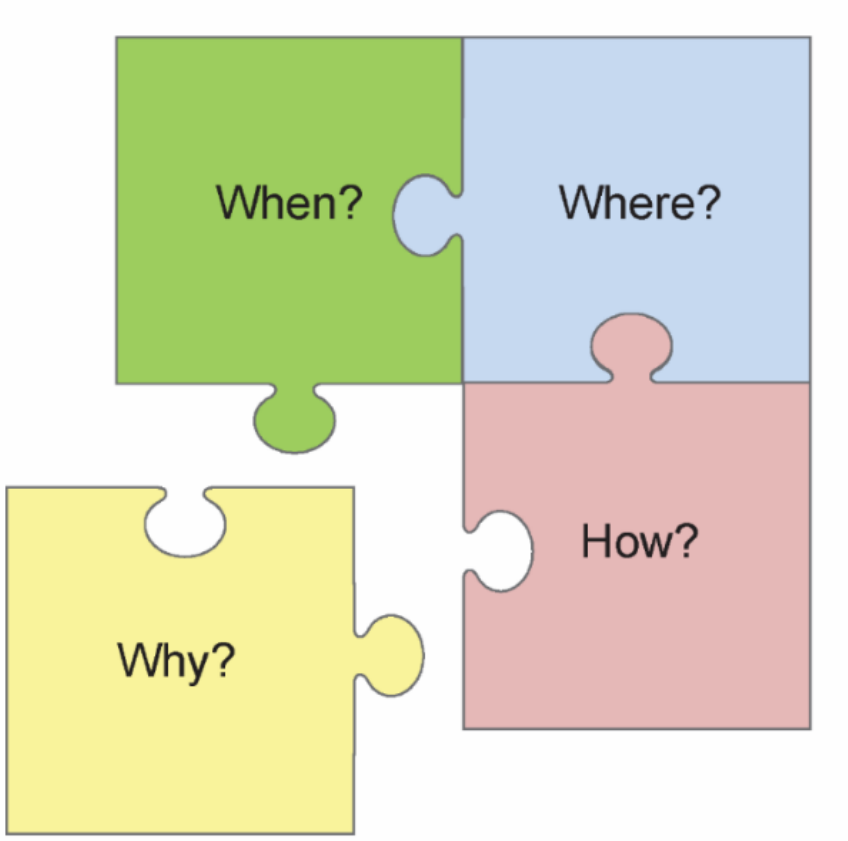

Fig 5.1 Indirect approach to defining the function(s) of H3-K14 and H3-K23 acetylation in *S. pombe*

It would also be informative to determine during which phase of the cell cycle high stoichiometries of H3-K14 and H3-K23 acetylation are found. Is this limited to a specific cell cycle phase or do high levels of acetylation at K14 and K23 persist throughout the cell cycle at a large number of loci? Given that we observed high stoichiometries of H3-K14 and H3-K23 acetylation in quiescent PBMCs, it would be surprising if any cell cycle phase would be completely devoid of H3-K14ac and H3-K23ac.The third question would be to address how this acetylation occurs in cells.

We have partially uncovered this by identifying the HATs responsible for H3-K14 and H3-K23 acetylation in *S. pombe*, but the identification of the deacetylase(s) and putative reader molecules will provide valuable insights into the physiological function(s) and regulation of this evolutionarily conserved pattern of histone acetylation. However, it is plausible that this pattern of histone acetylation does not necessarily have the same function(s) in fission yeast and higher eukaryotes.

In addition, though technically challenging to investigate, it would be interesting to know if both H3-K14 acetylation and H3-K23 acetylation co-occur on the same histone tail or even on the same nucleosome. Based on the stoichiometry of about 20-40%, it appears that one in every two or three nucleosomes have an H3 molecule that is acetylated at lysine 14 and/or lysine 23. Given that the heterochromatin regions are hypoacetylated, this estimate would indicate that there are some loci in the genome where almost all the nucleosome have H3 acetylated at K14 and/or K23. Further, the discovery of the reader molecules that recognize H3-K14 or H3-K23 acetylation independently of each other or as a pattern of acetylation (assuming that H3-K14 and H3-K23 acetylation occasionally function together), will help uncover how cells interpret this acetylation. Bromodomains bind to acetylated lysine residues within specific structural contexts. In many cases, polypeptide subunits that contain bromodomains are subunits of multi-protein complexes involved in chromatin modification and/or chromatin remodeling. In most bromodomain proteins, there exists other protein-protein interaction domains [plant homeodomain (PHD) fingers, Pro-Trp-Trp-Pro (PWWP) domains, Bromo-adjacent homology (BAH) domains], and

multiple bromodomains. For example, the Polybromo1 (PB1) protein, one of the subunits of the human SWI/SNF chromatin remodeling complex contains six bromodomains (Fujisawa and Filippakopoulos, 2017). Given this, it seems plausible that various subunits of a multi-subunit HAT complex or chromatin remodeling complex independently recognize both H3-K14 and H3-K23 acetylation to regulate various cellular processes.

The high stoichiometry of H3-K14 and H3-K23 acetylation that we discovered and the enzymes responsible for it are evolutionarily conserved. The human orthologs of the *S. pombe* HATs responsible for H3-K14 and H3-K23 acetylation are hGcn5, MORF, (HBO1), Tip60 and hMOF. They have been implicated in vertebrate development and are frequently mutated in cancers. The *MOZ* gene was first identified as a fusion partner in the recurrent chromosome translocation t(8;16) (p11;p13) associated with acute myeloid leukemia, where the zinc finger and acetyltransferase domain of *MOZ* is fused to another HAT known as CBP, thus producing an aberrant transcript encoding the fusion protein MOZ-CBP (Borrow et al., 1996; Yang, 2004). In the leukemia-associated chromosome translocation t(8;22) (p11;q13), the zinc finger and acetyltransferase domain of the *MOZ* gene is fused to the gene encoding p300, thus producing the fusion protein MOZ-p300 (Chaffanet et al., 2000). The *MOZ* gene is also rearranged in hematologic malignancies with the inversion inv(8)(p11q13), thus generating fusion proteins with TIF2 (transcription intermediary factor 2, a known partner of p300/CBP) that promote self-renewal of leukemic stem cells (Aikawa et al., 2010; Carapeti et al., 1998; Deguchi et al., 2003; Huntly et al., 2004; Liang et al.,

1998). The *MOZ* gene is also fused to a novel partner, *LEUTX* (leucine twenty homeobox), in therapy-related acute myeloid leukemia with the translocation t(8;19) (p11;q13) (Chinen et al., 2014).

The *MORF* gene is fused to the *CBP* gene in patients carrying the translocation t(10;16) (q22;p13) associated with acute myeloid leukemia (Kojima et al., 2003; Panagopoulos et al., 2001). The mouse *moz* gene is required for maintaining fetal hematopoietic stem cells (Katsumoto et al., 2006; Thomas et al., 2006b). Mice homozygous for a catalytic mutation of *moz* have a shortened lifespan, low body weight, small thymus and spleen, and proliferation defects in various hematopoietic progenitors (Deguchi et al., 2003; Perez-Campo et al., 2009). Mice heterozygous for *MORF* mutations are normal even though they only have about 10% of the *MORF* mRNA found in wild-type animals. In contrast, mice homozygous for loss-of-function mutations in *MORF* die at about 3 weeks of age and display dwarfism, craniofacial abnormalities and cerebral defects (Thomas et al., 2000). The Morf protein is also important for regulating adult neurogenesis in mice (Merson et al., 2006). Neural stem cells isolated from mice that have a hypomorphic MORF allele (*Qkf^{gt})* exhibited reduced self-renewal capacity and a reduced ability to produce differentiated neurons (Sheikh et al., 2012). Direct links to diseases have not yet been uncovered for human HBO1, but mouse Hbo1 is essential for embryo development (Kueh et al., 2011). In human cells, but not in mice, HBO1 is important for DNA replication (Kueh et al., 2011; Miotto and Struhl, 2008, 2010). MOZ and MORF are also altered in solid tumors. The *MORF* gene is mutated in four different developmental disorders:

Noonan syndrome-like disorder, Ohdo syndrome, genitopatellar syndrome and blepharophimosis–ptosis–epicanthus inversus syndrome. In addition to craniofacial abnormalities, patients suffering from these disorders suffer from cognitive defects and intellectual disabilities (reviewed in Yang, 2015). Even though there is a divergence in the number of HATs, some of the cellular processes regulated by H3-K14 and H3-K23 acetylation are likely conserved from yeast to humans.

We identified a pattern of abundant acetylation at H3-K14 and H3-K23 and much less abundant acetylation at H3-K9 and H3-K18. It was not possible to study the role of H3-K14ac with an H3-K14R mutation (or a *Δmst2* single mutation because of the residual H3-K14ac catalyzed by Gcn5). It is not currently possible to conclude that H3-K14ac and H3-K23ac function "together" (in the sense that both modifications need to be recognized simultaneously to perform a specific function). This model would predict that abolishing either H3-K14ac alone or H3-K23ac alone would result in the same phenotype. But our results do not lead us in that direction. Even so, the high levels of H3-K14ac and H3-K23ac in cells and the prominent role of Mst2 in their acetylation led to an exciting hypothesis which we call the *'histone shielding'* hypothesis. This idea was inspired by work from Songtao Jia laboratory (Wang et al., 2015). Wang and colleagues discovered that Mst2 controls heterochromatin spreading and prevents ectopic heterochromatin assembly. The combined loss of Mst2 and a putative H3-K9 demethylase, Epe1, resulted in heterochromatin spreading and massive ectopic heterochromatin, presumably by setting the stage ready for H3-K9 to be methylated. Consequently, there were severe growth defects

due to inactivation of essential genes. Surprisingly, the authors found that the cells quickly adapt to this by accumulating heterochromatin at genes required for heterochromatin assembly such as Clr4, the histone H3-K9 methyltransferase. As mentioned earlier, during DNA-replication coupled nucleosome assembly, CAF-1 complex deposits new H3-H4 molecules on to nascent DNA throughout the genome. We have previously shown that in budding yeast, histone H3 associated with CAF-1 is acetylated at many sites with high levels (between 50-80%) of stoichiometry (Abshiru et al., 2015). Even though it needs to be tested whether this holds true in fission yeast, studies have shown H3-K14 and H3-K23 to be marks of newly synthesized histones in Drosophila and human cells. (Benson et al., 2006; Marvin et al., 1990; Sobel et al., 1995). We hypothesize that high stoichiometries of acetylation in newly synthesized histones bound to CAF-1 are necessary to protect or shield new histones from being ‘polluted’ with inappropriate H3-K9 methylation and subsequent gene inactivation at loci where it is undesirable. We believe that the co-ordinated effort of HATs, Gcn5 and Mst2, and the lysine demethylase Epe1, ensures that the histone pool is ‘shielded’.

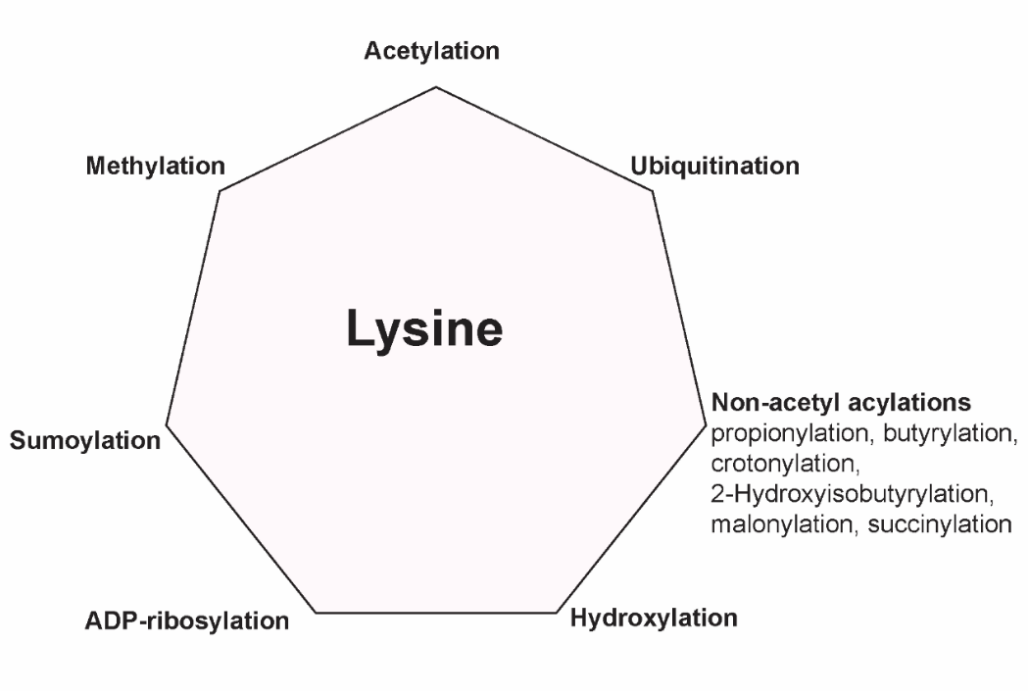

Fig 5.2 Known modifications occurring on histone lysine residues

In summary, this thesis integrates complementary approaches to understand the functions of an abundant and evolutionarily conserved pattern of histone acetylation. Despite our efforts, we were not successful in delineating the functions of acetylation on H3-K14 and H3-K23. Our study demonstrates the difficulty in conclusively attributing functions to histone modifications, a feat complicated by the different modifications possible on lysine residues, particularly in evolutionarily complex organisms (Figure 5.2).

This study also emphasizes the benefits of using a genetically tractable model organism where histones can be mutated to decipher the functions of histone

modifications. In higher eukaryotes, it would be impossible to perform the genetic studies that we conducted. The advent of CRISPR technology might facilitate such studies in mammalian cells in the future, although the existence of numerous copies of each core histone gene (Marzluff et al., 2002) will remain a challenge to generating cells carrying specific histone point mutations. There is still much to understand about the roles of the evolutionarily conserved pattern of histone acetylation that we observed. However, a sound understanding of the cellular processes that are dependent upon H3-K14 and H3-K23 acetylation will provide valuable insights into the molecular mechanisms that underlie cancers and developmental disorders.

5.4 References

Abshiru, N., Caron-Lizotte, O., Rajan, R.E., Jamai, A., Pomies, C., Verreault, A., and Thibault, P. (2015). Discovery of protein acetylation patterns by deconvolution of peptide isomer mass spectra. Nat. Commun. *6*, 8648.

Adhvaryu, K.K., Berge, E., Tamaru, H., Freitag, M., and Selker, E.U. (2011). Substitutions in the amino-terminal tail of Neurospora histone H3 have varied effects on DNA methylation. PLoS Genet. *7*.

Agalioti, T., Chen, G., and Thanos, D. (2002). Deciphering the transcriptional histone acetylation code for a human gene. Cell *111*, 381–392.

Aikawa, Y., Katsumoto, T., Zhang, P., Shima, H., Shino, M., Terui, K., Ito, E., Ohno, H., Stanley, E.R., Singh, H., et al. (2010). PU.1-mediated upregulation of CSF1R is crucial for leukemia stem cell potential induced by MOZ-TIF2. Nat. Med. *16*, 580–585, 1p following 585.

An, S., Yoon, J., Kim, H., Song, J., Cho, U., and Arbor, A. (2017). Structure-based nuclear import mechanism of histones H3 and H4 mediated by Kap123. Elife.

Benson, L.J., Gu, Y., Yakovleva, T., Tong, K., Barrows, C., Strack, C.L., Cook, R.G., Mizzen, C.A., and Annunziato, A.T. (2006). Modifications of H3 and H4 during chromatin replication, nucleosome assembly, and histone exchange. J. Biol. Chem. *281*, 9287–9296.

Bhaumik, S.R., Smith, E., and Shilatifard, A. (2007). Covalent modifications of histones during development and disease pathogenesis. Nat Struct Mol Biol *14*, 1008–1016.

Blackwell, J.S., Wilkinson, S.T., Mosammaparast, N., and Pemberton, L.F. (2007). Mutational analysis of H3 and H4 N termini reveals distinct roles in nuclear import. J. Biol. Chem. *282*, 20142–20150.

Bodai, L., Zsindely, N., Gáspár, R., Kristó, I., Komonyi, O., and Boros, I.M. (2012). Ecdysone induced gene expression is associated with acetylation of histone H3 lysine 23 in Drosophila melanogaster. PLoS One *7*, e40565.

Borrow, J., Stanton, V.P., Anderson, J.M., Becher, R., Behm, F.G., Chaganti, R.S.K., Civin, C.I., Disteche, C., Dube, I., Frischauf, A.M., et al. (1996). The translocation t(8;16)(p11;p13) of acute myeloid leukaemia fuses a putative acetyltransferase to the CREB-binding protein. Nat Genet. *14*, 353–356.

Braunstein, M., Rose, A.B., Holmes, S.G., Allis, C.D., and Broach, J.R. (1993). Transcriptional silencing in yeast is associated with reduced nucleosome acetylation. Genes Dev. *7*, 592–604.

Burgess, R., and Zhang, Z. (2010). Roles for Gcn5 in promoting nucleosome assembly and maintaining genome integrity. Cell Cycle *9*, 3051–3057.

Carapeti, M., Aguiar, R.C., Goldman, J.M., and Cross, N.C. (1998). A novel fusion between MOZ and the nuclear receptor coactivator TIF2 in acute myeloid leukemia. Blood *91*, 3127–3133.

Di Cerbo, V., and Schneider, R. (2013). Cancers with wrong HATs: The impact of acetylation. Brief. Funct. Genomics *12*, 231–243.

Chaffanet, M., Gressin, L., Preudhomme, C., Soenen-Cornu, V., Birnbaum, D., and Pébusque, M.J. (2000). MOZ is fused to p300 in an acute monocytic leukemia with t(8;22). Genes Chromosom. Cancer *28*, 138–144.

Chinen, Y., Taki, T., Tsutsumi, Y., Kobayashi, S., Matsumoto, Y., Sakamoto, N., Kuroda, J., Horiike, S., Nishida, K., Ohno, H., et al. (2014). The Leucine Twenty Homeobox (LEUTX) Gene, which lacks a histone acetyltransferase domain, is fused to KAT6A in therapy-related Acute Myeloid Leukemia with t(8;19)(p11;q13). Genes. Chromosomes Cancer *53*, 299–308.

Deguchi, K., Ayton, P.M., Carapeti, M., Kutok, J.L., Snyder, C.S., Williams, I.R., Cross, N.C.P., Glass, C.K., Cleary, M.L., and Gilliland, D.G. (2003). MOZ-TIF2-induced acute myeloid leukemia requires the MOZ nucleosome binding motif and TIF2-mediated recruitment of CBP. Cancer Cell *3*, 259–271.

Ekwall, K., Olsson, T., Turner, B.M., Cranston, G., and Allshire, R.C. (1997). Transient inhibition of histone deacetylation alters the structural and functional imprint at fission yeast centromeres. Cell *91*, 1021–1032.

Falkenberg, K.J., and Johnstone, R.W. (2014). Histone deacetylases and their inhibitors in cancer, neurological diseases and immune disorders. Nat. Rev. Drug Discov. *13*, 673–691.

Fiedler, K.L., Bheda, P., Dai, J., Boeke, J.D., Wolberger, C., and Cotter, R.J. (2013). A quantitative analysis of histone methylation and acetylation isoforms from their deuteroacetylated derivatives: application to a series of knockout mutants. J. Mass Spectrom. *48*, 608–615.

Filippakopoulos, P., Picaud, S., Mangos, M., Keates, T., Lambert, J.-P.P., Barsyte-Lovejoy, D., Felletar, I., Volkmer, R., Müller, S., Pawson, T., et al. (2012). Histone recognition and large-scale structural analysis of the human bromodomain family. Cell *149*, 214–231.

Fischle, W., Wang, Y., Jacobs, S.A., Kim, Y., Allis, C.D., and Khorasanizadeh, S. (2003). Molecular basis for the discrimination of repressive methyl-lysine marks in histone H3 by Polycomb and HP1 chromodomains. Genes Dev. *17*, 1870–1881.

Fraga, M.F., Ballestar, E., Villar-garea, A., Boix-chornet, M., Espada, J., Schotta, G., Bonaldi, T., Haydon, C., Ropero, S., Petrie, K., et al. (2005). Loss of acetylation at Lys16 and trimethylation at Lys20 of histone H4 is a common hallmark of human cancer. *37*, 391–400.

Fujisawa, T., and Filippakopoulos, P. (2017). Functions of bromodomain-containing proteins and their roles in homeostasis and cancer. Nat. Rev. Mol. Cell Biol. *18*, 246–262.

Howe, L.L., Auston, D., Grant, P., John, S., Cook, R.G., Workman, J.L., and Pillus, L. (2001). Histone H3 specific acetyltransferases are essential for cell cycle progression. Genes Dev. *15*, 3144–3154.

Huang, F., Paulson, A., Dutta, A., Venkatesh, S., Smolle, M., Susan, M., and Workman, J.L. (2014). Histone acetyltransferase enok regulates oocyte polarization by promoting expression of the actin nucleation factor spire. Genes Dev. *28*, 2750–2763.

Huntly, B.J.P., Shigematsu, H., Deguchi, K., Lee, B.H., Mizuno, S., Duclos, N., Rowan, R., Amaral, S., Curley, D., Williams, I.R., et al. (2004). MOZ-TIF2, but not BCR-ABL, confers properties of leukemic stem cells to committed murine

hematopoietic progenitors. Cancer Cell *6*, 587–596.
Jacobs, S.A., and Khorasanizadeh, S. (2002). Structure of HP1 chromodomain bound to a lysine 9 – methylated histone H3 tail. Science (80-.). *295*, 2080–2084.

Karmodiya, K., Krebs, A.R., Oulad-Abdelghani, M., Kimura, H., and Tora, L. (2012). H3K9 and H3K14 acetylation co-occur at many gene regulatory elements, while H3K14ac marks a subset of inactive inducible promoters in mouse embryonic stem cells. BMC Genomics *13*, 424.

Kasten, M., Szerlong, H., Erdjument-Bromage, H., Tempst, P., Werner, M., and Cairns, B.R. (2004). Tandem bromodomains in the chromatin remodeler RSC recognize acetylated histone H3 Lys14. EMBO J. *23*, 1348–1359.

Katsumoto, T., Aikawa, Y., Iwama, A., Ueda, S., Ichikawa, H., Ochiya, T., and Kitabayashi, I. (2006). MOZ is essential for maintenance of hematopoietic stem cells. Genes Dev. *20*, 1321–1330.

Kaufman, P.D., Kobayashi, R., Kessler, N., and Stillman, B. (1995). The p150 and p60 Subunits of Chromatin Assembly Factor I : A molecular link between newly synthesized histones and DNA replication. *81*, 1105–1114.

Kelly, T.J., Qin, S., Gottschling, D.E., and Parthun, M.R. (2000). Type B histone acetyltransferase Hat1p participates in telomeric silencing. Mol. Cell. Biol. *20*, 7051–7058.

Kimura, A., Umehara, T., and Horikoshi, M. (2002). Chromosomal gradient of histone acetylation established by Sas2p and Sir2p functions as a shield against gene silencing. Nat. Genet. *32*, 370–377.

Kojima, K., Kaneda, K., Yoshida, C., Dansako, H., Fujii, N., Yano, T., Shinagawa, K., Yasukawa, M., Fujita, S., and Tanimoto, M. (2003). A novel fusion variant of the MORF and CBP genes detected in therapy-related myelodysplastic syndrome with t(10;16)(q22;p13). Br. J. Haematol. *120*, 271–273.

Kueh, A.J., Dixon, M.P., Voss, A.K., and Thomas, T. (2011). HBO1 is required for H3K14 acetylation and normal transcriptional activity during embryonic development. Mol. Cell. Biol. *31*, 845–860.

Lalonde, M.E., Avvakumov, N., Glass, K.C., Joncas, F.H., Saksouk, N., Holliday, M., Paquet, E., Yan, K., Tong, Q., Klein, B.J., et al. (2013). Exchange of associated

factors directs a switch in HBO1 acetyltransferase histone tail specificity. Genes Dev. *27*, 2009–2024.

Lee, J.S., and Shilatifard, A. (2007). A site to remember: H3K36 methylation a mark for histone deacetylation. Mutat. Res. - Fundam. Mol. Mech. Mutagen. *618*, 130–134.

Li, Q., Zhou, H., Wurtele, H., Davies, B., Horazdovsky, B., Verreault, A., and Zhang, Z. (2008). Acetylation of histone H3 lysine 56 regulates replication-coupled nucleosome assembly. Cell *134*, 244–255.

Liang, J., Prouty, L., Williams, B.J., Dayton, M. a, and Blanchard, K.L. (1998). Acute mixed lineage leukemia with an inv(8)(p11q13) resulting in fusion of the genes for MOZ and TIF2. Blood *92*, 2118–2122.

Ma, X.J., Wu, J., Altheim, B. a, Schultz, M.C., and Grunstein, M. (1998). Deposition-related sites K5/K12 in histone H4 are not required for nucleosome deposition in yeast. Proc. Natl. Acad. Sci. U. S. A. *95*, 6693–6698.

Marks, P.A., and Xu, W.-S. (2009). Histone deacetylase inhibitors: Potential in cancer therapy. Expert Opin. Investig. Drugs *107*, 600–608.

Marvin, K.W., Yau, P., and Bradbury, E.M. (1990). Isolation and characterization of acetylated histones H3 and H4 and their assembly into nucleosomes. J. Biol. Chem. *265*, 19839–19847.

Marzluff, W.F., Gongidi, P., Woods, K.R., Jin, J., and Maltais, L.J. (2002). The human and mouse replication-dependent histone genes. Genomics *80*, 487–498.

Masumoto, H., Hawke, D., Kobayashi, R., and Verreault, A. (2005). A role for cell-cycle-regulated histone H3 lysine 56 acetylation in the DNA damage response. Nature *436*, 294–298.

Meijsing, S.H., and Ehrenhofer-Murray, A.E. (2001). The silencing complex SAS-I links histone acetylation to the assembly of repressed chromatin by CAF-I and Asf1 in Saccharomyces cerevisiae. Genes Dev. *15*, 3169–3182.

Mellone, B.G., Ball, L., Suka, N., Grunstein, M.R., Partridge, J.F., and Allshire, R.C. (2003). Centromere silencing and function in fission yeast is governed by the amino terminus of histone H3. Curr. Biol. *13*, 1748–1757.

Merson, T.D., Dixon, M.P., Collin, C., Rietze, R.L., Bartlett, P.F., Thomas, T., and Voss, A.K. (2006). The transcriptional coactivator Querkopf controls adult neurogenesis. J. Neurosci. *26*, 11359–11370.

Millar, C.B., and Grunstein, M. (2006). Genome-wide patterns of histone modifications in yeast. Nat. Rev. Mol. Cell Biol. *7*, 657–666.

Miotto, B., and Struhl, K. (2008). HBO1 histone acetylase is a coactivator of the replication licensing factor Cdt1. Genes Dev. *22*, 2633–2638.

Miotto, B., and Struhl, K. (2010). HBO1 histone acetylase activity is essential for DNA replication licensing and inhibited by Geminin. Mol. Cell *37*, 57–66.

Mishima, Y., Miyagi, S., Saraya, A., Negishi, M., Endoh, M., Endo, T.A., Toyoda, T., Shinga, J., Katsumoto, T., Chiba, T., et al. (2011). The Hbo1-Brd1/Brpf2 complex is responsible for global acetylation of H3K14 and required for fetal liver erythropoiesis. Blood *118*, 2443–2453.

Morgan, M.A., and Shilatifard, A. (2015). Chromatin signatures of cancer. Genes Dev. *29*, 238–249.

Nair, D.M., Ge, Z., Mersfelder, E.L., and Parthun, M.R. (2011). Genetic interactions between POB3 and the acetylation of newly synthesized histones. Curr. Genet. *57*, 271–286.

Nakayama, J., Rice, J.C., Strahl, B.D., Allis, C.D., and Grewal, S.I.S. (2001). Role of histone H3 lysine 9 methylation in epigenetic control of heterochromatin assembly. Science (80-.). *292*, 110–113.

Nielsen, P.R., Nietlispach, D., Mott, H.R., Callaghan, J., Bannister, A., Kouzarides, T., Murzin, A.G., Murzina, N. V, and Laue, E.D. (2002). Structure of the HP1 chromodomain bound to histone H3 methylated at lysine 9. Nature *416*, 103–107.

Nugent, R.L., Johnsson, A., Fleharty, B., Gogol, M., Xue-Franzén, Y., Seidel, C., Wright, A.P., and Forsburg, S.L. (2010). Expression profiling of S. pombe acetyltransferase mutants identifies redundant pathways of gene regulation. BMC Genomics *11*, 59.

Panagopoulos, I., Fioretos, T., Isaksson, M., Samuelsson, U., Billström, R., Strömbeck, B., Mitelman, F., and Johansson, B. (2001). Fusion of the MORF and CBP genes in acute myeloid leukemia with the t(10;16)(q22;p13). Hum. Mol. Genet. *10*, 395–404.

Parthun, M.R., Widom, J., and Gottschling, D.E. (1996). The major cytoplasmic histone acetyltransferase in yeast: Links to chromatin replication and histone metabolism. Cell *87*, 85–94.

Perez-Campo, F.M., Borrow, J., Kouskoff, V., and Lacaud, G. (2009). The histone acetyltransferase activity of monocytic leukemia zinc finger is critical for the proliferation of hematopoietic precursors. Blood *113*, 4866–4874.

Pokholok, D.K., Harbison, C.T., Levine, S., Cole, M., Hannett, N.M., Lee, T.I., Bell, G.W., Walker, K., Rolfe, P.A., Herbolsheimer, E., et al. (2005). Genome-wide map of nucleosome acetylation and methylation in yeast. Cell *122*, 517–527.

Poux, A.N., and Marmorstein, R. (2003). Molecular basis for Gcn5 / PCAF histone acetyltransferase selectivity for histone. Biochemistry *42*, 14366–14374.

Qin, S., and Parthun, M.R. (2002). Histone H3 and the histone acetyltransferase Hat1p contribute to DNA double-strand break repair. Mol. Cell. Biol. *22*, 8353–8365.

Reddy, B.D., Wang, Y., Niu, L., Higuchi, E.C., Marguerat, S.B., Bähler, J., Smith, G.R., and Jia, S. (2011). Elimination of a specific histone H3K14 acetyltransferase complex bypasses the RNAi pathway to regulate pericentric heterochromatin functions. Genes Dev. *25*, 214–219.

Sharma, G.G., So, S., Gupta, A., Kumar, R., Cayrou, C., Avvakumov, N., Bhadra, U., Pandita, R.K., Porteus, M.H., Chen, D.J., et al. (2010). MOF and histone H4 acetylation at lysine 16 are critical for DNA damage response and double-strand break repair. Mol. Cell. Biol. *30*, 3582–3595.

Sheikh, B.N., Dixon, M.P., Thomas, T., and Voss, A.K. (2012). Querkopf is a key marker of self-renewal and multipotency of adult neural stem cells. J. Cell Sci. *125*, 295–309.

Simo-Riudalbas, L., Perez-Salvia, M., Setien, F., Villanueva, A., Moutinho, C., Martinez-Cardus, A., Moran, S., Berdasco, M., Gomez, A., Vidal, E., et al. (2015). KAT6B is a tumor suppressor histone H3 lysine 23 acetyltransferase undergoing genomic loss in small cell lung cancer. Cancer Res. *75*, 3936–3944.

Sinha, I., Wiren, M., and Ekwall, K. (2006). Genome-wide patterns of histone modifications in fission yeast. Chromosom. Res. *14*, 95–105.

Sinha, I., Buchanan, L., Rönnerblad, M., Bonilla, C., Durand-Dubief, M., Shevchenko, A., Grunstein, M., Stewart, A. F., and Ekwall, K. (2010). Genome-wide mapping of histone modifications and mass spectrometry reveal H4 acetylation bias and H3K36 methylation at gene promoters in fission yeast. Epigenomics *2*, 377–393.

Smith, C.M., Gafken, P.R., Zhang, Z., Gottschling, D.E., Smith, J.B., and Smith, D.L. (2003). Mass spectrometric quantification of acetylation at specific lysines within the amino-terminal tail of histone H4. Anal. Biochem. *316*, 23–33.

Sobel, R.E., Cook, R.G., Perry, C.A., Annunziato, A.T., and Allis, C.D. (1995). Conservation of deposition-related acetylation sites in newly synthesized histones H3 and H4. Proc. Natl. Acad. Sci. U. S. A. *92*, 1237–1241.

Sridharan, R., Gonzales-Cope, M., Chronis, C., Bonora, G., McKee, R., Huang, C., Patel, S., Lopez, D., Mishra, N., Pellegrini, M., et al. (2013). Proteomic and genomic approaches reveal critical functions of H3K9 methylation and heterochromatin protein-1γ in reprogramming to pluripotency. Nat. Cell Biol. *15*, 872–882.

Suka, N., Suka, Y., Carmen, A.A., Wu, J., and Grunstein, M. (2001). Highly specific antibodies determine histone acetylation site usage in yeast heterochromatin and euchromatin. Mol. Cell *8*, 473–479.

Suka, N., Luo, K., and Grunstein, M. (2002). Sir2p and Sas2p opposingly regulate acetylation of yeast histone H4 lysine16 and spreading of heterochromatin. Nat. Genet. *32*, 378–383.

Taverna, S.D., Ilin, S., Rogers, R.S., Tanny, J.C., Lavender, H., Li, H., Baker, L., Boyle, J., Blair, L.P., Chait, B.T.T., et al. (2006). Yng1 PHD finger binding to H3 trimethylated at K4 promotes NuA3 HAT activity at K14 of H3 and transcription at a subset of targeted ORFs. Mol. Cell *24*, 785–796.

Taylor, G.C.A., Eskeland, R., Hekimoglu-Balkan, B., Pradeepa, M.M., and Bickmore, W.A. (2013). H4K16 acetylation marks active genes and enhancers of embryonic stem cells but does not alter chromatin compaction. Genome Res. *23*, 2053–2065.

Thomas, C.E., Kelleher, N.L., and Mizzen, C.A. (2006a). Mass spectrometric characterization of human histone H3: A bird's eye view. J.Proteome Res. *5*, 240–247.

Thomas, T., Voss, A.K., Chowdhury, K., and Gruss, P. (2000). Querkopf, a MYST family histone acetyltransferase, is required for normal cerebral cortex development. Development *127*, 2537–2548.

Thomas, T., Corcoran, L.M., Gugasyan, R., Dixon, M.P., Brodnicki, T., Nutt, S.L., Metcalf, D., and Voss, A.K. (2006b). Monocytic leukemia zinc finger protein is essential for the development of long-term reconstituting hematopoietic stem cells. 1175–1186.

Tsai, W.-W., Wang, Z., Yiu, T.T., Akdemir, K.C., Xia, W., Winter, S., Tsai, C.-Y., Shi, X., Schwarzer, D., Plunkett, W., et al. (2010). TRIM24 links a non-canonical histone signature to breast cancer. Nature *468*, 927–932.

Ullah, M., Pelletier, N., Xiao, L., Zhao, S.P., Wang, K., Degerny, C., Tahmasebi, S., Cayrou, C., Doyon, Y., Goh, S.-L.S.-L., et al. (2008). Molecular architecture of quartet MOZ/MORF histone acetyltransferase complexes. Mol. Cell. Biol. *28*, 6828–6843.

VanDemark, A.P., Kasten, M.M., Ferris, E., Heroux, A., Hill, C.P., and Cairns, B.R. (2007). Autoregulation of the Rsc4 tandem bromodomain by Gcn5 acetylation. Mol. Cell *27*, 817–828.

Verreault, A., Kaufman, P.D., Kobayashi, R., and Stillman, B. (1996). Nucleosome assembly by a complex of CAF-1 and acetylated histones H3/H4. Cell *87*, 95–104.

Verreault, A., Kaufman, P.D., Kobayashi, R., and Stillman, B. (1997). Nucleosomal DNA regulates the core-histone-binding subunit of the human Hat1 acetyltransferase. Curr. Biol. *8*, 96–108.

Wang, J., Reddy, B.D., and Jia, S. (2015). Rapid epigenetic adaptation to uncontrolled heterochromatin spreading. Elife *4*, 1–17.

Wang, Y., Kallgren, S.P., Reddy, B.D., Kuntz, K., López-Maury, L., Thompson, J., Watt, S., Chun, M., Hou, H., Shi, Y., et al. (2012). Histone H3 lysine 14 acetylation is required for activation of a DNA damage checkpoint in fission yeast. J. Biol. Chem. *287*, 4386–4393.

Wang, Z., Zang, C., Rosenfeld, J.A., Schones, D.E., Barski, A., Cuddapah, S., Cui, K., Roh, T.-Y., Peng, W., Zhang, M.Q., et al. (2008). Combinatorial patterns of histone acetylations and methylations in the human genome. Nat. Genet. *40*, 897–903.

West, A.C., and Johnstone, R.W. (2014). New and emerging HDAC inhibitors for cancer treatment. J Clin Invest. *124*, 30–39.

Wirén, M., Silverstein, R. a, Sinha, I., Walfridsson, J., Lee, H.-M., Laurenson, P., Pillus, L., Robyr, D., Grunstein, M., and Ekwall, K. (2005). Genomewide analysis of nucleosome density histone acetylation and HDAC function in fission yeast. EMBO J. *24*, 2906–2918.

Yamada, T., Fischle, W., Sugiyama, T., Allis, C.D., and Grewal, S.I.S. (2005). The nucleation and maintenance of heterochromatin by a histone deacetylase in fission yeast. Mol. Cell *20*, 173–185.

Yang, X.-J. (2004). The diverse superfamily of lysine acetyltransferases and their roles in leukemia and other diseases. Nucleic Acids Res. *32*, 959–976.

Yang, X.-J. (2015). MOZ and MORF acetyltransferases: Molecular interaction, animal development and human disease. Biochim. Biophys. Acta - Mol. Cell Res. *1853*, 1818–1826.

Young, N.L., DiMaggio, P.A., Plazas-Mayorca, M.D., Baliban, R.C., Floudas, C.A., and Garcia, B.A. (2009). High throughput characterization of combinatorial histone codes. Mol. Cell. Proteomics *8*, 2266–2284.